A Model Approach to Radioactive Waste Disposal at Sellafield

A thesis submitted for the degree of
Doctor of Philosophy

by

Christopher McKeown
B.Sc. Glasgow University

Department of Geology and Applied Geology
University of Glasgow

February 1997

Abstract

Sellafield in West Cumbria is the potential site of a repository for radioactive, Intermediate Level Waste (ILW). The proposed repository lies at 650 m beneath the ground surface to the west of the 1000 m uplands of the Lake District. The fractured Borrowdale Volcanic Group (BVG) host rock is overlain by a sequence of Carboniferous and Permo-Triassic sediments. Fresh, saline and brine groundwaters exist in the subsurface. Upward trending fluid pressure gradients have been measured in the area of the potential repository site. Steady-state, 2-D simulations of fluid flow were undertaken with the OILGEN code. Topographically driven flow dominates the regional hydrogeology. Subsurface fluid flow trended persistently upwards through the potential repository site. The dense brines to the west of the site promoted upward deflection of groundwaters. The groundwater flow rate through the potential repository site was dependent upon the hydraulic conductivity of the BVG. Calibration of the model was achieved by matching simulated subsurface pressures to those measured in-situ. Emergent repository fluids could reach the surface in 15,000 years. The measured BVG hydraulic conductivity is up to 1000 times too high to be simply declared safe.

Geochemical simulations, with Geochemist's Workbench™, showed natural BVG groundwaters display redox disequilibrium. The in-situ Eh is most probably +66 mV. Pyrite, absent from rock fractures, would not enforce a reducing -250 mV Eh. Steel barrels and alkaline cement are intended to geochemically retain 2.5×10^6 kg of uranium. Simulations of repository cement/BVG groundwater interactions produced pH ≈10 at 80°C but no change in the +66 mV Eh. Steel barrel interactions produced an alkaline fluid with Eh ≈ -500 mV. Uranium solubility in the high pH repository near field was as high as $10^{-2.7}$ M, regardless of steel interactions. Uranium solubility adjacent to the repository (pseudo near field) was controlled by Eh; ranging from 10^{-13} M in the presence of steel, to $10^{-2.7}$ M with no steel. Uranium retention is controlled only by steel barrel durability. Oxidising, natural BVG groundwater will enhance steel barrel destruction. Distant from repository (far field) uranium solubility was $10^{-5.4}$ M if Eh was as measured in-situ. Thermodynamic data variations affect the calculation of uranium solubility; uranium near field solubility can be as high as $10^{-1.4}$ M. Uranium solubilities in near-field high pH groundwater could be more than 600 times greater than the $10^{-5.5}$ M used by UK Nirex Ltd. in their safety case simulations.

The hydrogeological and hydrogeochemical modelling performed utilised data obtained from the most comprehensive, and expensive, groundwater investigations undertaken in the UK. The simulations have shown that, given the current understanding of the site's geology, hydrogeology and hydrochemistry, there is no scientifically sound reason for selecting Sellafield in Cumbria as the site to retain radioactive waste that will be lethal for millions of years.

Christopher McKeown, Ph.D. Thesis, 1997
Geology & Applied Geology, Glasgow University, Glasgow, G12 8QQ, UK
Tel: 44-(0)141-330-5469, Fax: 44-(0)141-330-4817

Thesis Declaration

The material presented in this thesis is the result of research carried out between October 1992 and February 1997 in the Department of Geology and Applied Geology, University of Glasgow, under the supervision of Dr. Stuart Haszeldine.

This thesis is based on my own independent research and any published or unpublished material I have used has been given full acknowledgement in the text.

Christopher McKeown

February 1997

I certify that Christopher McKeown has undertaken the bulk of the work involved in this thesis. Specifically, background geology, data collation and analysis, and computer modelling. I have assisted with advice and help of a general, technical, conceptual nature, as would be expected in the course of normal Ph.D supervision. Christopher McKeown has written the thesis himself, and is responsible for its content.

R.S. Haszeldine

For Lorraine

Acknowledgements

There are a great many people who have helped me from the start of this project. Without their help I would either never have started or chucked it all in long ago. I will begin by thanking the most important person in my life, my wife Lorraine, for managing not to kill me these past four years of struggle and toil. You kept me sane. Without your help and love I would have never have made it. I can't thank my Mum and Dad enough for giving so much of themselves over the past four years (and more !). Both they, and my family; David and Claire, James and Eleanor and big Sis Kathleen (not forgetting Allana, Jennifer, Natalie, Sarah, Stephen and Suzanne) have always given me support and understanding when it was (and wasn't) called for. The "In-Laws"; Mary, Pauline and Paul and Claire and Craig, and all the M's; Mark, Max, Mick and Mick are all thanked for never letting me get too down when things were going badly. Iain and Mike are also thanked for making travelling to Heriot-Watt bearable. A big TA goes to everyone in the Glasgow department who either helped me out over the course of the research project; Big John, Bob, Colin, Eddie, George B, George G, Jeanette, Jim G, Jim K, Mary, Pete and Rosemary, or knew when was the right time to go "dahn the boozah"; Abdulla, Andy C, Andy D, Cam, Clark, Clint, Carolyn, Dan, Fitchy, Gary, Gavin, Helen, Jeremy, John, Karen, Ken, Maggie, Mark O, Mark W, Orla, Simon, Susan and Thomas. A very special thanks go to Dave and Sharon Darby. Stuart Haszeldine had the idea for this project from the start, without his keen eye, swift mind and enthusiastic pursuit of science, I would have never have got this work off of the ground. The Greenpeace Environmental Trust, especially Sue, Helen and Bridget are thanked for their financial support and continued interest and zeal. There are also a great many people who have offered me help and advice regarding the direction of my research. From the Glasgow department I'd like to thank Allan, Mike and Tony for everything they have done for me. I am indebted to Gary Couples for help, advice, code development and always pointing out the right path. Thanks are also due to everyone who has advised me on the perils of using computers to simulate this crazy world in which we live in; Amy Berger and Craig Bethke (Illinois U), John Bunney (Heriot-Watt U), Carol Bruton (LLNL), Randy Cygan (SNL), Susan Duerden (HMIP), Grant Garven (Johns Hopkins U), Gordon Macleod (Newcastle U), Vala Ragnarsdottir (Bristol U), Phil Richardson (GDE), Ian Ridley (USGS), David Read (RMCE) and Eva Valsami-Jones (NHM). UK Nirex Ltd are also thanked for providing the data which has formed the basis of this research project.

Contents

Figures and tables

Chapter 4

No Figures

Chapter 5

Tables

Figures

Chapter 1 Introduction

1.1 Setting of research

By the year 2030 the United Kingdom will have generated almost 1,000,000 m^3 of radioactive waste. Sources range from defence activities, fuel reprocessing and operation and decommissioning of commercial reactors to medical and research laboratories (Nirex, 1992a). This waste is at present stored, pending the construction of the UK's first deep geological disposal facility, a so called repository.

The UK waste disposal organisation responsible for this is UK Nirex Ltd. It oversees the design, construction and management of a repository, and is currently undertaking performance and safety case assessments to investigate one candidate site for a repository near Sellafield. If these assessments are adequate then Nirex would apply for planning permission to develop a repository. If planning permission is granted the repository is projected to begin construction around 2001 and be operational for at least fifty years (Holmes, 1995). This thesis presents results of computer modelling of geological processes that have a direct effect on the safety assessment of the currently proposed repository site.

As this thesis brings together a variety of disciplines this introduction is intended to provide the reader with a general overview of the relevant information regarding the disposal of radioactive waste, i.e.; what, and how much waste is to be disposed of; what is the UK repository concept; what sites might be suitable; what is the preferred UK site; what is the geological and hydrogeological setting and what are the aims and layout of the thesis.

1.2 Radioactive waste forms

In the UK, radioactive wastes are subdivided into over 900 'streams' of distinct and different origin (Nirex, 1992a). The inventory is usually considered as Low, Intermediate and High level waste and can be classified as follows.

Low Level Waste (LLW)

LLW is defined as those waste streams with an activity content not exceeding $1.2x10^{10}$ Bq/tonne of beta (β) and gamma (γ) radioactivity (Nirex, 1992e). The Bequerel (Bq) is the measure of the 'activity' of radioactive material and is equal to one nucleus disintegrating every second (Chapman & McKinley, 1987). LLW streams total 728,000m^3, forming 74% of total conditioned waste volume to 2030 (Nirex, 1992a). Conditioning of LLW waste forms is done by supercompaction of

the materials to reduce their volumes by as much as 50%. Examples of LLW include general and laboratory wastes such as used protective clothing and redundant equipment that is contaminated with small amounts of radioactive material. Other examples include concrete, rubble, metal and soil from the demolition of buildings and other nuclear facilities (Nirex, 1992d).

Intermediate Level Waste (ILW)

ILW is a large number of waste streams with a radioactive content exceeding that of LLW, but with a lower radioactivity and heat output than High Level Waste (HLW) (Nirex, 1992e). ILW streams total 257,000 m^3, forming 26% of the total conditioned waste volume (Nirex, 1992a). Examples of ILW are the metal cladding of nuclear reactor fuel, reactor components, chemical process residues and used filters (Nirex, 1992d). This forms the majority of the wastes destined for subsurface disposal in the UK.

High Level Waste (HLW)

Intensely radioactive waste from the reprocessing of irradiated nuclear fuel, 94% of which is radioactive liquid from the nitric acid solution of fission products from fuel reprocessing (Nirex, 1992d). HLW waste streams are of relatively small volume (3,830m^3) (Nirex, 1992a) but contain over 95% of the total radioactivity in waste from the nuclear fuel cycle; $7.1x10^{20}$ Bequerels (Nirex, 1992e). HLW has a high heat output due to the energy from radioactive decay, and this heat (as much as 200°C) has to be taken into account when designing storage or disposal facilities (Chapman & McKinley, 1987; Nagra, 1995). None of this waste is currently destined for subsurface disposal by UK Nirex Ltd.

1.3 Deep disposal of radioactive waste

In the UK HLW is currently being vitrified (encapsulated in synthetic glass) and housed in surface stores to allow much of the activity to decay prior to final disposal. This waste is expected to remain in storage for a period of some 50 years after this conditioning (Nirex, 1992a). It is highly likely that the HLW will be disposed of in a deep repository but there is, at present, no HLW repository concept being developed (Miller *et al.*, 1994).

In common with disposal organisations overseas (Karlsson, 1995; McCombie, 1995), it is proposed by the British radioactive waste disposal organisation, UK Nirex Ltd., that the entire UK inventory of ILW and around 100,000m^3 of longer lived LLW will be disposed of in a deep, geological repository (Nirex, 1993d). The repository will be subject to regulatory guidelines (Holmes, 1995; Hooper, 1995)

such that for the period after closure of the disposal facility the radiological risk to the human population will be $1x10^{-6}$ per year (i.e. 1 in 1 million per year).

International radiological protection bodies' guidelines (International Commission on Radiological Protection, 1990) lay down that it should be shown to be unlikely that radionuclides released from a disposal facility would lead *at any time* to significant increases in the levels of radioactivity in the accessible environment (Hooper, 1995). Given that ILW contains a significant inventory of *very* long-lived and radioactive radionuclides (Table 1.1) (Nirex, 1992e; Royal Society, 1994), the disposal concept must provide adequate containment for up to 10^8 years.

1.3.1 Multi-barrier containment

To provide this long term safety UK Nirex Ltd. use a system of multi-barrier containment in their deep geological disposal concept (Fig. 1.1), (Holmes, 1995; Hooper, 1995). The man-made features, often referred to as the *near-field* barriers, are to consist of the waste immobilisation media; the steel or concrete packages; the vault structure and the cement based backfill material (Nirex, 1993d). These barriers are intended to provide a level of containment for the short term (hundreds of years) sufficient to allow the shorter lived radionuclides to decay to negligible levels of activity (Atkinson *et al.*, 1993) .

Although the physical integrity of these near-field barriers will rapidly decay as the repository becomes saturated with groundwater the use of steel and massive amounts of concrete in the structure should provide an alkaline and chemically reducing environment which *may* persist for thousands of years (Nirex, 1993d). {Alkaline fluids have high pH ; the negative log of the activity of the Hydrogen (H^+) ion. Reducing conditions have low *Eh* ; oxidation/reduction (Redox) potentials are generally represented by Eh; a measure of the oxidation state of a system equal, at 25°C, to 0.059 x pe; negative log of the activity of electrons in a system}.

This environment is intended to provide a chemical barrier by limiting the transport of the longer-lived, redox-sensitive, radionuclides (Atkinson *et al.*, 1993; Goldberg *et al.*, 1995; Nuclear Energy Agency, 1993). The concrete backfill is porous and of low mechanical strength to assist removal should a need arise to retrieve waste and is intended to retard radionuclide migration by sorption (Hooper, 1995); radionuclides removed from solution become bound to exposed surfaces either physically, chemically or electrostatically (Allard, 1982).

The so-called far-field barriers are provided naturally by the geological surroundings which separate the repository from the biosphere. By placing the wastes deep underground in rocks with little natural resource potential they should be isolated from human activities (Nirex, 1993d). The principal mechanisms for the inhibition of the movement of radionuclides by the groundwater pathway, are derived from the physical properties offered by the host environment (Chapman & McEwen, 1986) as characterised by:

- Thermal, seismic and glacial stability of host rock;
- Predictable groundwater flow paths, preferably long and resulting in progressive mixing with older, deeper waters or leading to discharge at sea;
- Very slow local and regional groundwater movements in an area with low regional hydraulic gradients;
- Favourable natural groundwater geochemistry; reducing (see above).

1.3.2 Site selection

In the UK, after a site selection process lasting three years, the five generic geological environments considered most suitable for disposal of radioactive waste (Fig. 1.2), (Chapman & McEwen, 1986) were narrowed to one; "Basement under sedimentary cover" (BUSC); (c in Fig. 1.2) subsequently Sellafield in Cumbria and Dounreay in Caithness were selected for further investigations. Initial boreholes and other geological and geophysical surveys were felt to indicate that the geology at both sites had the potential to meet the safety requirements for a deep repository.

In July 1991, UK Nirex Ltd. announced that it was to concentrate its further investigations at the Sellafield site (Chaplow, 1995). The proposed repository would be at a depth of about 650 metres below Ordnance Datum (m bOD) within rocks of the Borrowdale Volcanic Group (BVG; see section 1.4) (Holmes, 1995). This thesis is therefore solely concerned with aspects relating directly to the Sellafield site.

1.3.3 The Sellafield Site

The Sellafield Works of British Nuclear Fuels plc (BNFL) are located on the coastal plain of the western flank of the Lake District upland dome (Fig. 1.3a). The preferred design concept of UK Nirex Ltd. locates all the waste receipt facilities on the existing BNFL Sellafield site, the waste being conveyed via underground drifts to the disposal chambers (Nirex, 1989). The surface expression would be headworks providing ventilation and emergency exits via two shafts. These shafts are also intended to provide access for the proposed underground rock laboratory or Rock

Characterisation Facility (RCF) (Holmes, 1995). A public inquiry into the siting of the RCF was held in West Cumbria between September 1995 and February 1996.

UK Nirex Ltd. have proceeded with geological site investigations at three nested size scales ; Region (3,600 km^2), District (600 km^2) and Site (52 km^2) (Nirex, 1993d) (Fig. 1.3a). A Potential Repository Zone (PRZ) has been outlined adjacent to the A595, between the Sellafield Works and the Lake District National Park boundary (Fig. 1.3b). Geophysical surveys (on land and offshore), geological, remote sensing and hydrogeological surveys and the drilling, coring and logging of deep boreholes have been used in an attempt to develop an understanding of the depositional, structural and tectonic history of the Region (Michie & Bowden, 1994). Data have been used by UK Nirex Ltd. to provide a framework for the construction of computer models of:

- geosphere/biosphere interactions;
- safety performance assessments;
- seismic hazard assessment;
- rock engineering properties;
- hydrogeology and hydrochemistry.

Results from the above have been presented at public and semi-public technical meetings, published in UK Nirex Ltd. reports and summarised in various updates. All numerical data used in this thesis is sourced from such publications

1.4 Geological setting

As the geology of north-west England and adjacent parts of the East Irish Sea have been covered in detail elsewhere only a synopsis will be presented here. It is, however, necessary that the reader be aquainted at the outset with the present understanding of the stratigraphy, tectonism and fluid regimes in the Sellafield area.

1.4.1 Stratigraphy

The stratigraphy of the Region, i.e. west Cumbria, comprises three principal divisions (Millward, 1995), (Fig. 1.4);

- basement rocks of lower Palaeozoic age (c. 510-395 million years (Ma)), exposed in the uplands of the Lake District;
- a cover sequence of sedimentary rocks of Carboniferous age (c. 350 Ma) to Triassic (>210 Ma) age, in the coastal belt and offshore (within the East Irish Sea Basin).
- a variable thickness of poorly consolidated glacial and post- glacial sediments

Characterisation Facility (RCF) (Holmes, 1995). A public inquiry into the siting of the RCF was held in West Cumbria between September 1995 and February 1996.

UK Nirex Ltd. have proceeded with geological site investigations at three nested size scales ; Region (3,600 km^2), District (600 km^2) and Site (52 km^2) (Nirex, 1993d) (Fig. 1.3a). A Potential Repository Zone (PRZ) has been outlined adjacent to the A595, between the Sellafield Works and the Lake District National Park boundary (Fig. 1.3b). Geophysical surveys (on land and offshore), geological, remote sensing and hydrogeological surveys and the drilling, coring and logging of deep boreholes have been used in an attempt to develop an understanding of the depositional, structural and tectonic history of the Region (Michie & Bowden, 1994). Data have been used by UK Nirex Ltd. to provide a framework for the construction of computer models of:

- geosphere/biosphere interactions;
- safety performance assessments;
- seismic hazard assessment;
- rock engineering properties;
- hydrogeology and hydrochemistry.

Results from the above have been presented at public and semi-public technical meetings, published in UK Nirex Ltd. reports and summarised in various updates. All numerical data used in this thesis is sourced from such publications

1.4 Geological setting

As the geology of north-west England and adjacent parts of the East Irish Sea have been covered in detail elsewhere only a synopsis will be presented here. It is, however, necessary that the reader be aquainted at the outset with the present understanding of the stratigraphy, tectonism and fluid regimes in the Sellafield area.

1.4.1 Stratigraphy

The stratigraphy of the Region, i.e. west Cumbria, comprises three principal divisions (Millward, 1995), (Fig. 1.4);

- basement rocks of lower Palaeozoic age (c. 510-395 million years (Ma)), exposed in the uplands of the Lake District;
- a cover sequence of sedimentary rocks of Carboniferous age (c. 350 Ma) to Triassic (>210 Ma) age, in the coastal belt and offshore (within the East Irish Sea Basin).
- a variable thickness of poorly consolidated glacial and post- glacial sediments

Fig. 1.5 summarises the stratigraphy and outlines the unconformable relationship of the main lithological units. Fig. 1.6 shows a geological cross-section running WSW-ENE through the potential repository site, passing through site investigation boreholes 3 and 2, and close to boreholes 1, 10 and 4 (Fig 1.3b). This section was based on published data (Nirex, 1992b; Nirex, 1993b; Nirex, 1993d) and was extended both seaward and landward, using public geological and topographical information (Taylor *et al.*, 1971).

Lower Palaeozoic

In the Sellafield area, metamorphosed and deformed rocks of the Ordovician Borrowdale Volcanic Group (BVG), are overlain by a sedimentary cover sequence that dips and becomes progressively more varied in lithology, to the west (Millward, 1995), (Fig. 1.6).

Regionally the BVG exposed at the land surface comprises a lower, ~ 5 km thick unit of plateau lavas, (Petterson *et al.*, 1992) overlain by an upper, ~ 3 km thick unit of ignimbrites associated with caldera collapse (Branney *et al.*, 1988). Locally near Sellafield, the BVG has been shown to be dominated by pyroclastics (Millward *et al.*, 1994; Nirex, 1992b; Nirex, 1993b). In boreholes near and within the PRZ, the sequence almost entirely comprises welded tuffs, (Beddoe-Stephens & Phillips, 1993) with thicknesses exceeding 1140 m.

Regional seismic reflection interpretation suggests that the BVG may be up to 2 km thick beneath Sellafield (Nirex, 1993b). Volcanoclastic sedimentary rocks are prominent in boreholes to the north of the PRZ (Millward *et al.*, 1994), but with no lavas present this contrasts strongly with the basaltic and andesitic lava fields of the upland fells (Petterson *et al.*, 1992).

Carboniferous

Of the Carboniferous succession of limestones, sandstones and coals present in west Cumbria only the Dinantian Limestones occur below, and in close proximity to, the Sellafield site (Nirex, 1992b). Locally beneath Sellafield, these shallow marine, carbonate ramp limestones rest unconformably on the peneplained erosional surface of the BVG with an onshore maximum thickness of 300m recovered from boreholes north of Sellafield (Barclay *et al.*, 1994). The sequence feathers out by erosional thinning about 1 km east of the site (Fig. 1.6) Offshore seismic suggests progressive, basinward thickening to a maximum of around 4 km (Nirex, 1992b).

Permian

The basal unit of the Permian rocks, the coarse, poorly bedded, ~100m thick Brockram Breccia unconformably overlies the Carboniferous limestones to the south east of the Sellafield site, (Nirex, 1992b) but lies directly upon the BVG in the PRZ, with most clasts being of volcanoclastic origin (Nirex, 1993b; Strong *et al.*, 1994). Derived from local alluvial fans, (Jones & Ambrose, 1994) the Brockram is laterally extensive and interdigitates with the upper Permian St Bees Shales unit (Nirex, 1992b).

The St Bees Evaporite Formation comprises a complex sequence of dolomites and anhydrites, (Strong & Kemp, 1994) and was precipitated in a restricted hypersaline marine environment (Arthurton & Hemingway, 1972). Up to 50m thick in the St Bees area, the formation exceeds 200m offshore, particularly where the succession is dominated by halite (Nirex, 1992b) but pinches out towards the Lake District massif, (Fig. 1.6) (Millward, 1995).

The ~100m thick St Bees Shales Formation is, in part, a lateral equivalent of the St Bees Evaporites, (Strong *et al.*, 1994) forming a siliciclastic facies around the margins of an evaporite basin. Laminated and massive (blocky) facies, in addition to breccias of Brockram type, have been identified within the Formation (Nirex, 1993b). The distinctively red laminated facies consists of finely interbedded and interlaminated claystones, siltsones and fine quartz-arenites (Strong *et al.*, 1994). The St Bees Shale is not shown on Fig 1.6 as the Formation was not included in the original UK Nirex Ltd. section that was sourced to generate the figure.

Triassic

The base of the Triassic has traditionally been taken as the base of the Sherwood Sandstone Group (SSG) which is of Lower Triassic (Scythian) age (Warrington *et al.*, 1980). Recent work has identified a tripartite division of the SSG into St Bees Sandstone Formation (SBS), Calder Sandstone Formation (CS) and Ormskirk Sandstone Formation(OS) (Barnes *et al.*, 1994) (Fig. 1.6; OS not shown as the formation was not included in the original UK Nirex Ltd. section that was used to generate the figure and, onshore, the OS is a relatively small formation within the SSG). Over 1200 metres of SSG have been proved from boreholes beneath Sellafield although the full thickness of the OS is not present onshore in the Sellafield area (Jones & Ambrose, 1994).

Marked by a gradational boundary with the St Bees Shale Formation, the ~600m of the St Bees Sandstone Formation (SBS) comprises, at its base, a series of

interbedded sheetflood sandstones and mudstones occasionally containing lithic fragments derived from the BVG, (Strong *et al.*, 1994). Dominantly reddish brown in colour (Nirex, 1992b), these lithic, subarkosic, arenites grade up into a thick multi-storey sequence of very-fine to medium grained braidplain sandstones (Jones & Ambrose, 1994).

The sharp boundary between the SBS and the ~500m succession of overlying Calder Sandstone Formation (CS) is marked by a change from the generally fine grained SBS to coarser, more friable dark red sandstones with poorly cemented grains (Barnes *et al.*, 1994). Sedimentary facies analysis indicates that the CS was deposited under aeolian conditions, with a number of fluvial episodes at its top reworking the aeolian sand (Jones & Ambrose, 1994).

Forming the main reservoir for the offshore Morecambe Gas Field the thickness of the Ormskirk Sandstone (OS) declines from ~250m to ~140m towards the Lake District massif (Nirex, 1992b). Proved principally by seismic reflection data the boundary between the CS and OS is marked by the OS being finer grained than the CS and by a change in sedimentary facies from fluvial sandstone at the top of the CS to aeolian sandstone in the OS (Barnes *et al.*, 1994).

Quaternary

A discontinuous veneer of Quaternary sediments, up to 180m thick, masks the solid geology of the Region and are represented onshore by ~20m of superficial drift recovered from boreholes (Nirex, 1993b). Except in the uplands of the Lake District, only small areas are free of these 'Drift' deposits. The main deposits are tills, sands and gravels and clays of Devensian (Weichselian) age, laid down during the closing of the last glaciation (Nirex, 1992b). These are overlain by a variety of local deposits of peat, alluvium and lake deposits.

1.4.2 Structure

A detailed explanation of the structural history of the Sellafield Region is presented by other authors (Nirex, 1992c; Nirex, 1992g; Nirex, 1993a; Nirex, 1993c; Nirex, 1995a), only a brief synopsis is presented here. Structure within the BVG was initially syndepositionally controlled and is complicated by Ordovician and Silurian faulting and end-Silurian folding, faulting and deformation. The overall structure within the BVG is that of the western edge of a caldera but details remain unknown. Brittle fault structures dominate the sediments overlying the BVG.

The Sellafield Region (Fig. 1.3) is structurally divided by major faults into a system of extensional sedimentary basins and intervening blocks (Fig. 1.7), (Chadwick *et al.*, 1994). These structural features formed in latest Permian and early Triassic times as a complex series of extensional basins evolved on the north-west European shelf. The Permo-Triassic East Irish Sea Basin is bounded by the Keys and Lagman faults in the west and the Lake District Boundary Fault in the east (Fig. 1.7). The Lake District Boundary Fault juxtaposes the offshore Permo-Triassic East Irish Sea Basin sequence against the Carboniferous Limestones and Lower Palaeozoic strata of west Cumbria .

A series of, sub-parallel NW-SE trending faults, which dip steeply towards the SW, locally displace Carboniferous and Permo-Triassic sediments (Nirex, 1992b). A second set of faults, trending NW-SE/NE-SW, dipping towards the N are also present in the area but only displace strata of Carboniferous or older age. It is possible that Palaeozoic faults re-activated or influenced the distribution of the faults which displace the Permo-Triassic sediments (Nirex, 1993b).

It remains a matter of debate if faults were active within Quaternary time and at the present day. Features cited in favour of present activity are the linear coastline, shallow seismic evidence for faulting cutting sediments immediately offshore and the relative frequency of earthquakes (Haszeldine, 1996; Muir-Wood & Woo, 1992; Nirex, 1992c; Nirex, 1993b).

1.5 Hydrogeological setting

Due to the large body of work in publication dealing with the groundwater regimes around the potential repository site, (Black, 1995; Nirex, 1992b; Nirex, 1992f; Nirex, 1993b; Nirex, 1994; Nirex, 1995b) this section will only give a brief outline of the hydrogeology and hydrogeochemistry of the Sellafield area.

As outlined in section 1.4 there are a number of lithostratigraphic units in the area. These have distinct hydrogeological properties, i.e.; porosity; permeability; anisotropy; etc. These discrete parameters coupled with rock fractures, topographic drive from the Lakeland Fells and borehole measurements of groundwater pressure, chemistry and isotopic signatures all help build a picture of the tens of kilometres scale groundwater system in the Sellafield Site area.

The current UK Nirex Ltd. conceptual model (Fig. 1.8) illustrates that there are three distinct hydrological units (Black, 1995);

- Hills and Basement Regime; topographically driven water flow, relatively low flux, saline groundwater within fractured, faulted rocks of the BVG;

- Irish Sea Basin Regime; relatively low flux, hypersaline brines expelled from the East Irish Sea Basin occurring within fractured BVG, Carboniferous Limestones and Permo-Triassic cover rocks;

- Coastal Plain Regime; topographically driven water flow, high flux, fresh groundwaters within highly porous and permeable Triassic aquifer.

A more detailed explanation of the above conceptual model and an outline, exploration and discussion of the interplay between the hydrogeological regimes and implications for a safety case are given in Chapters 2, 3, 4 and 5.

1.6 Thesis rationale and objectives

As there is a large body of UK Nirex Ltd. work detailing the results of research into the suitability and robustness of the Sellafield site one question the reader of this thesis may raise is why bother? It is considered by the author that there is a need for *independent* research to be performed on such a complex (both scientifically and politically) issue as the deep disposal of radioactive waste. The aim of such site-specific research should not be who is right or who is wrong but to forward our understanding and find the *best* solution to the problem. With this in mind the objectives of this thesis are:

1 to undertake a detailed, independent computer modelling study of the flow and geochemistry of the groundwaters at the currently proposed site for the deep geological disposal of intermediate level radioactive waste. Published data are used to gain an insight into potential strengths and failings in the currently proposed models of subsurface groundwater conditions;

2 to use a computer modelling approach to delineate the controlling parameters of fluid movement in the far-field, PRZ and surface environments and to determine the sensitivity of this natural groundwater system to perturbations. Calculation of possible rates of groundwater return would allow elucidation of simple safety cases;

3 to determine the controls of groundwater chemistry by modelling geochemical fluid/rock interactions and redox states. Modelling the solubility of relevant radionuclides allows a simple safety case to be presented.

1.7 Outline of chapters

It is the intention of the author that individual chapters be presented as papers. To this end Chapters 3, 4, 5, and 6 can be viewed as individual bodies of work that in a holistic sense fit within a framework of a general study of the safety assessment of a proposed deep disposal site.

Chapter 2 The general concepts of site selection and appraisal undertaken world-wide are introduced. The hydrological and hydrogeological data available for the Sellafield Site, Region and District (see Fig. 1.3a) are outlined along with the data gathering techniques utilised in the site investigations.

Chapter 3 The conceptual model of the hydrogeology of the Sellafield region is reviewed. The mathematical and numerical formulations of the equations describing groundwater flow are presented. The use of such equations in the study of geological processes is briefly outlined. The mechanics of constructing mathematical models of fluid flow are introduced. A detailed explanation of the numerical formulation of the computer program used is given.

The use of such a modelling code to investigate the groundwater movement in the far-field of the Sellafield site is outlined. The modelling approach used is reviewed, appraised and justified. Results from sensitivity analysis are presented of variations in Sellafield groundwater salinity, rock unit hydrogeology and structure of individual rock units are presented. Graphical representations of hydraulic head and fluid velocity are used to illustrate the potential for movement of groundwater to, through and from the Potential Repository Zone (PRZ).

The possibility of validating the above models by comparison between calculated and predicted hydraulic head is explored. Suggestions are given as to the hydrogeological suitability of the proposed site. New work is presented on modelling particle movement as an aid in tracing the path and rate of groundwaters passing through the PRZ. A possible terrestrial discharge of groundwaters from the PRZ is outlined. Implications for a possible safety case are explored.

Chapter 4 The techniques utilised in the elucidation of data for use in the laboratory, computational and site experiments of the geochemical suitability of the

Sellafield site are presented. The difficulties in obtaining unpolluted samples are explained. The thermodynamic principals utilised by the geochemical modelling code used are outlined.

Chapter 5 presents new work on using geochemical reaction path codes to model the *in-situ* groundwater conditions at depth with respect to redox, pH, geochemical stability of host-rock minerals and the effect such processes might have on the solubility of the most significant radionuclides. Possible deficiencies in the current model of *in-situ* groundwater geochemistry are explored. The efficacy of engineered barriers in maintaining near-field geochemical conditions suitable for retention of radionuclides is investigated.

Chapter 6 introduces a synthesis of the results from previous chapters and outlines the conclusions that can be drawn. Potential further work is detailed and implications for the selection process of suitable sites for deep disposal of radioactive waste are drawn.

1.8 References

Allard, B.M. (1982) The geochemistry of actinides. *In:* (eds) *Geological disposal of radioactive waste. Geochemical processes.* Organisation for Economic Co-operation and Development, Paris, France, 49-68.

Arthurton, R.S. & Hemingway, J.E. (1972) The St Bees Evaporites- a carbonate-evaporite formation of Upper Permian age in West Cumberland, England. *Proceedings of the Yorkshire Geological Society*, **38**, 365-592.

Atkinson, A., Williams, S.J. & Wisbey, S.J. (1993) *NSARP reference document : the near field : January 1992.* Report No. **NSS/G117**, UK Nirex Ltd., Harwell, UK.

Barclay, W.J., Riley, N.J. & Strong, G.E. (1994) The Dinantian rocks of the Sellafield area, west Cumbria. *Proceedings of the Yorkshire Geological Society*, **50**, 37-49.

Barnes, R.P., Ambrose, K., Holliday, D.W. & Jones, N.S. (1994) Lithostratigraphical subdivision of the Triassic Sherwood Sandstone Group in west Cumbria. *Proceedings of the Yorkshire Geological Society*, **50**, 51-60.

Beddoe-Stephens, B. & Phillips, E.R. (1993) *The petrology of the Borrowdale Volcanic Group within Sellafield borehole No. 2.* Report No. **CC92S/193/CF-1-A**, British Geological Survey, Keyworth, UK.

Black, J.H. (1995) The hydrogeology of the Sellafield area, The geological disposal of radioactive waste, Royal Lancaster Hotel, London, IBC Technical Services Ltd, Gilmoora House, 57-61 Mortimer St., London.

Branney, M.J., Kokelaar, B.P & McConnell, B.J. (1988) Ordovician volcano-tectonics in the English Lake District. *Journal of the Geological Society, London*, **145**, 367-376.

Chadwick, R.A., Kirby, G.A. & Baily, H.E. (1994) The post-Triassic structural evolution of north-west England and adjacent parts of the East Irish Sea. *Proceedings of the Yorkshire Geological Society*, **50**, 99-102.

Chaplow, R. (1995) The investigations of the geology and hydrogeology at Sellafield, The geological disposal of radioactive waste, Royal Lancaster Hotel, London, IBC Technical Services Ltd, Gilmoora House, 57-61 Mortimer St., London.

Chapman, N.A. & McEwen, T.J. (1986) Geological environments for deep disposal of intermediate level wastes in the United Kingdom. *In:* (eds) *Siting, design and construction of underground repositories for radioactive wastes.* **IAEA-SM-289/37**, International Atomic Energy Authority, Vienna, Austria, 311-328.

Chapman, N.A. & McKinley, I.G. (1987) *The geological disposal of nuclear waste.* John Wiley & Sons, Chichester, 281 pp.

Goldberg, J.E., Gould, L.J., Heath, T.G., Thompson, A.M. & Tweed, C.J. (1995) *Development of a methodology for modelling the redox chemistry and predicting the redox potential of the near field of a cementitous radioactive waste repository.* Report No. **NSS/R398**, UK Nirex Ltd., Harwell, UK.

Haszeldine, R.S. (1996) Subsurface geology, geochemistry and water flow at a rock characterisation facility (RCF) at Longlands Farm. Proof of evidence. *In:* Haszeldine, R.S. & Smythe, D.K. (eds) *Radioactive Waste Disposal at Sellafield, UK. Site Selection, geological and engineering problems.* University of Glasgow, Glasgow, UK, 121-164.

Holmes, J. (1995) *Proof of Evidence. Science overview*. RCF Planning Enquiry, **PE/NRX/13**, UK Nirex Ltd., Harwell, UK, Cleator Moor, Cumbria, 40 pp.

Hooper, A. (1995) The Nirex repository concept, The geological disposal of radioactive waste, Royal Lancaster Hotel, London, IBC Technical Services Ltd, Gilmoora House, 57-61 Mortimer St., London.

International Commission on Radiological Protection. (1990) *Recomendations of the IRCP.* Report No. **60**, IRCP.

Jones, N.S. & Ambrose, K. (1994) Triassic sandy braidplain and aeolian sedimentation in the Sherwood Sandstone Group of the Sellafield area, west Cumbria. *Proceedings of the Yorkshire Geological Society*, **50**, 61-76.

Karlsson, F. (1995) The Swedish approach to near-field issues, The geological disposal of radioactive waste, Royal Lancaster Hotel, London, IBC Technical Services Ltd, Gilmoora House, 57-61 Mortimer St., London.

McCombie, C. (1995) International approaches to the organisation and execution of geological disposal programmes, The geological disposal of radioactive waste, Royal Lancaster Hotel, London, IBC Technical Services Ltd, Gilmoora House, 57-61 Mortimer St., London.

Michie, U.M. & Bowden, R.A. (1994) UK Nirex geological investigations at Sellafield. *Proceedings of the Yorkshire Geological Society*, **50**, 5-9.

Miller, W., Alexander, R., Chapman, N., McKinley, I. & Smellie, J. (1994) *Natural analogue studies in the geological disposal of radioactive wastes.* Report No. **NTB 93-03**, Nagra, Wettingen, Switzerland.

Millward, D. (1995) The geological environment of the Potential Repository Zone at Sellafield, Cumbria, The geological disposal of radioactive waste, Royal Lancaster Hotel, London, IBC Technical Services Ltd, Gilmoora House, 57-61 Mortimer St., London.

Millward, D., Beddoe-Stephens, B., Williamson, I.T., Young, S.R. & Petterson, M.G. (1994) Lithostratigraphy of a concealed caldera-related ignimbrite sequence within the Borrowdale Volcanic group of west Cumbria. *Proceedings of the Yorkshire Geological Society*, **50**, 25-36.

Muir-Wood, R. & Woo, G. (1992) *Tectonic hazards for nuclear waste repositories in the UK.* Report No. **HMIP/92/070**, Her Majesty's Inspectorate of Pollution, London, UK.

Nagra. (1995) *Bulletin : Disposal programme for high-level waste (HLW).* Report No. **25**, Nagra, Wettingen, Switzerland.

Nirex. (1989) *Deep repository project, preliminary environmental and radiological assessment and preliminary safety report.* Report No. **71**, UK Nirex Ltd., Harwell, UK.

Nirex. (1992a) *The 1991 UK radioactive waste inventory.* Report No. **284**, UK Nirex Ltd., Harwell, UK.

Nirex. (1992b) *The geology and hydrogeology of Sellafield.* Report No. **263**, UK Nirex Ltd., Harwell, UK.

Nirex. (1992c) *An interpretation of regional seismic reflection data offshore Sellafield.* Report No. **270**, UK Nirex Ltd., Harwell, UK.

Nirex. (1992d) *The physical and chemical characteristics of UK radioactive wastes.* Report No. **286**, UK Nirex Ltd., Harwell, UK.

Nirex. (1992e) *The radionuclide content of UK radioactive wastes.* Report No. **285**, UK Nirex Ltd., Harwell, UK.

Nirex. (1992f) *Sellafield hydrogeology. Report of the hydrogeology joint interpretation team.* Report No. **268**, UK Nirex Ltd., Harwell, UK.

Nirex. (1992g) *Structural geology of the Sellafield region. Report of the structural geology joint interpretation team.* Report No. **265**, UK Nirex Ltd., Harwell, UK.

Nirex. (1993a) *The geological structure of the Sellafield area: December 1993 update.* Report No. **520**, UK Nirex Ltd., Harwell, UK.

Nirex. (1993b) *The geology and hydrogeology of the Sellafield area: Interim assessment.* Report No. **524 (4 vols)**, UK Nirex Ltd., Harwell, UK.

Nirex. (1993c) *Jurassic to Neogene structural evolution of the Sellafield area: December 1993 update.* Report No. **518**, UK Nirex Ltd., Harwell, UK.

Nirex. (1993d) *Scientific update 1993 : Nirex deep waste repository project.* Report No. **525**, UK Nirex Ltd., Harwell, UK.

Nirex. (1994) *Regional hydrogeology and geochemistry in the Sellafield area. Phase 2.* Report No. **499**, UK Nirex Ltd., Harwell, UK.

Nirex. (1995a) *The 3D geological structure of the PRZ: summary report.* Report No. **S/95/005**, UK Nirex Ltd., Harwell, UK.

Nirex. (1995b) *The hydrochemistry of Sellafield, 1995 update.* Report No. **S/95/008**, UK Nirex Ltd., Harwell, UK.

Nuclear Energy Agency. (1993) *The status of near-field modelling*. Organisation for Economic Co-operation and Development, Paris, France, 289 pp.

Petterson, M.G., Beddoe-Stephens, B., Millward, D. & Johnson, E.W. (1992) A pre-caldera plateau-andesite field in the Borrowdale Volcanic Group of the English Lake District. *Journal of the Geological Society, London*, **149**, 889-906.

Royal Society. (1994) *Disposal of radioactive waste in deep repositories*. Report of a Royal Society study group, Royal Society, London, 194 pp.

Strong, G.E. & Kemp, S.J. (1994) *The petrographic, mineralogical and lithogeochemical characteristics of Permo-Triassic rocks from Sellafied BH2.* Report No. **CC93S/358/C-F-B-C**, British Geological Survey, Keyworth, UK.

Strong, G.E., Milodowski, A.E., Pearce, J.M., Kemp, S.J., Prior, S.V. & Morton, A.C. (1994) The petrology and diagenesis of Permo-Triassic rocks of the Sellafield area, Cumbria. *Proceedings of the Yorkshire Geological Society*, **50**, 77-89.

Taylor, B.J., Burgess, I.C., Land, D.H., Mills, D.A.C., Smith, D.B. & Warren, M.A. (1971) *Geology of Northern England.* HMSO, London, 121 pp.

Warrington, G., Audley-Charles, M.G., Elliot, R.E., Evans, W.B., Ivimey-cook, H.C., Kent, P.E., Robinson, P.L., Shotton, F.W. & Taylor, F.M. (1980) A correlation of Triassic rocks in the British Isles. *Special Publication of the Geological Society of London*, **13**.

Nuclide	1/2Life (y)	Mass	Act (Bq)	Mass (Kg)
H-3	1.20E+01	3	1.00E+17	2.72E-01
C-14	5.70E+03	14	2.30E+15	1.39E+01
Cl-36	3.00E+05	36	5.20E+12	4.25E+00
Ni-59	7.5E+04	59	1.20E+16	4.02E+03
Co-60	5.30E+00	60	5.70E+17	1.37E+01
Se-79	6.50E+04	79	1.60E+12	6.21E-01
Sr-90	2.90E+01	90	3.20E+17	6.32E+01
Zr-93	1.50E+06	93	3.40E+14	3.59E+03
Nb-94	2.00E+04	94	1.40E+17	1.99E+04
Tc-99	2.10E+05	99	1.70E+14	2.67E+02
Sn-126	1.00E+05	126	4.00E+12	3.81E+00
I-129	1.6E+07	129	9.20E+11	1.41E+02
Cs-135	2.3E+06	135	8.80E+12	2.07E+02
Cs-137	3.0E+01	137	9.30E+17	2.89E+02
Ra-226	1.60E+03	226	8.60E+12	2.35E-01
Th-230	7.70E+04	230	8.10E+10	1.09E-01
Th-232	1.40E+10	232	5.80E+10	1.43E+04
Pa-231	3.30E+04	231	1.90E+10	1.10E-02
U-234	2.4E+05	234	6.20E+13	2.63E+02
U-235	7.0E+08	235	1.50E+12	1.87E+04
U-238	4.5E+09	238	3.40E+13	2.75E+06
Np-237	2.10E+06	237	3.30E+13	1.24E+03
Pu-239	2.4E+04	239	1.10E+16	4.77E+03
Pu-240	6.5E+03	240	1.20E+16	1.42E+03
Pu-241	1.4E+01	241	3.00E+17	7.88E+01
Pu-242	3.8E+05	242	1.40E+13	9.64E+01
Am-241	4.3E+02	241	3.50E+16	2.76E+02
Am-243	7.4E+03	243	3.10E+13	4.20E+00

Table 1.1 Radionuclide content and mass of UK ILW and more active LLW at 2030 (Royal Society, 1994).

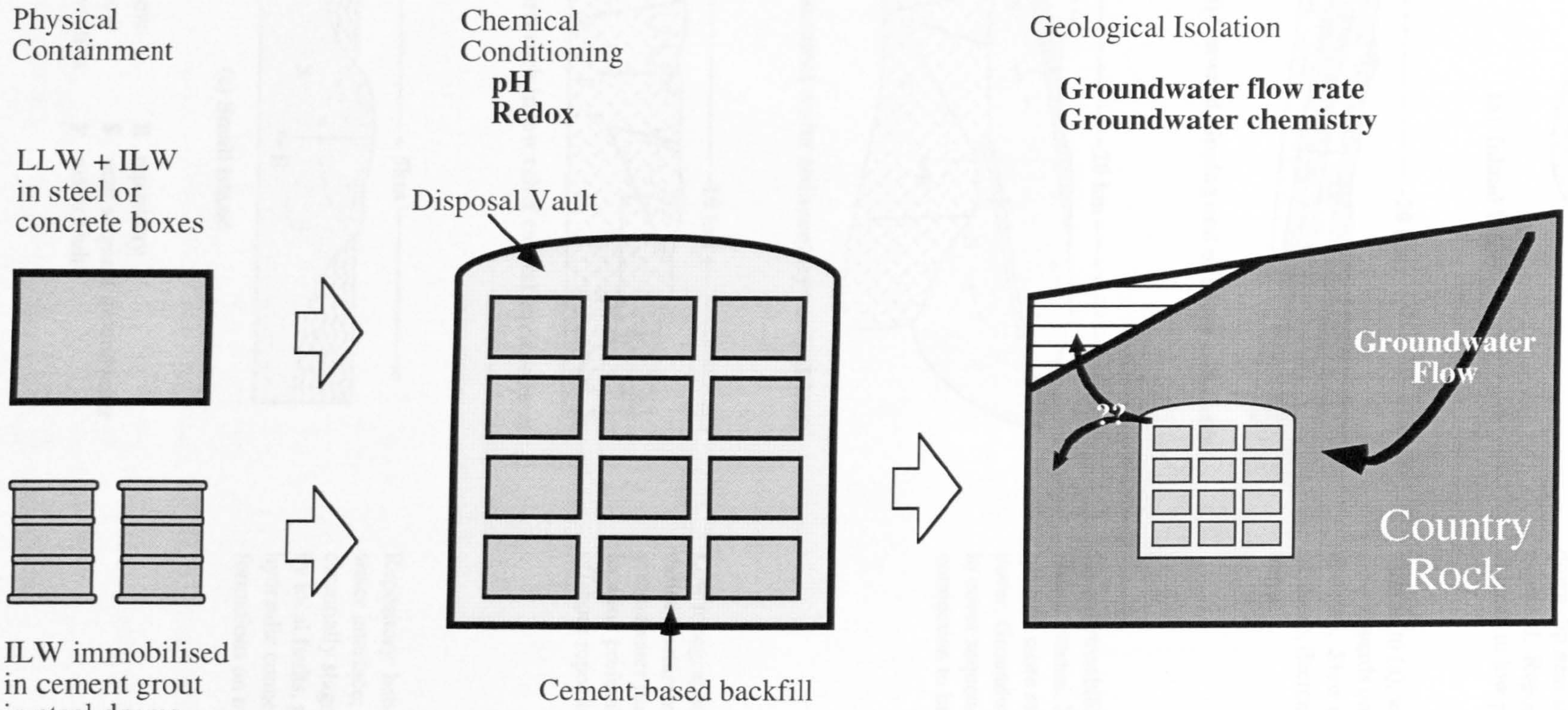

Fig. 1.1 **UK Nirex Ltd. multi-barrier repository concept. Near field engineered to provide physical and chemical barriers. Natural, far-field, containment provided by geological setting (after Holmes, 1995; Hooper, 1995).**

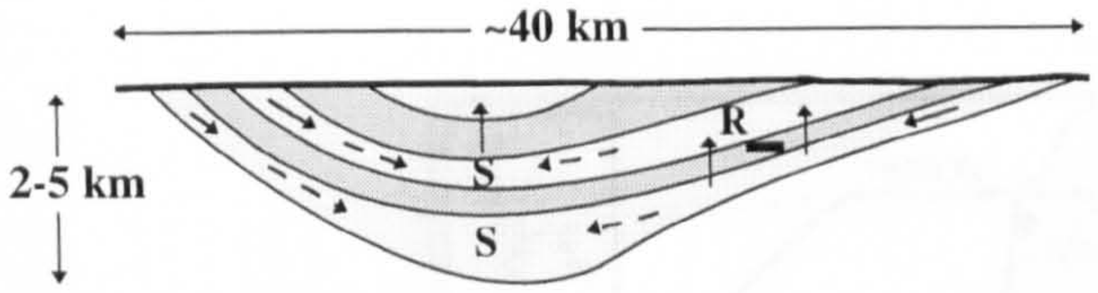

(a) Inland Basin

Sedimentary basins with many low permeability horizons. Regional groundwater flow down-dip in aquifer with minor vertical fluxes. Further down-dip near stagnant conditions expected. Repository located on limb of basin in low permeability unit.

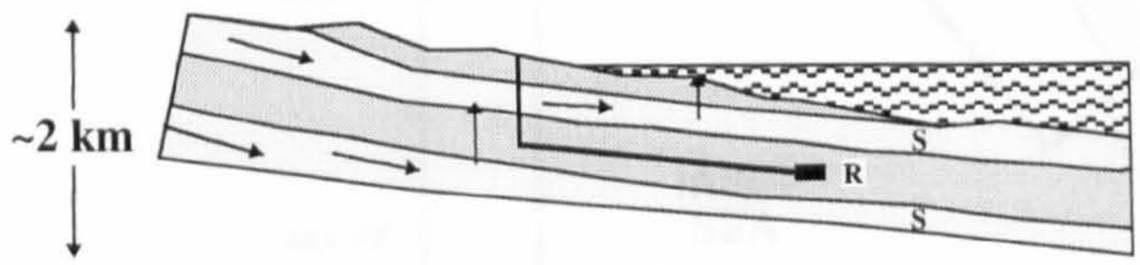

(b) Seaward dipping and offshore sediments

Similar to (a), with groundwater flow slow towards coast. Very slow fluxes at depth. Slow upward advection offshore, decreasing further from coast.

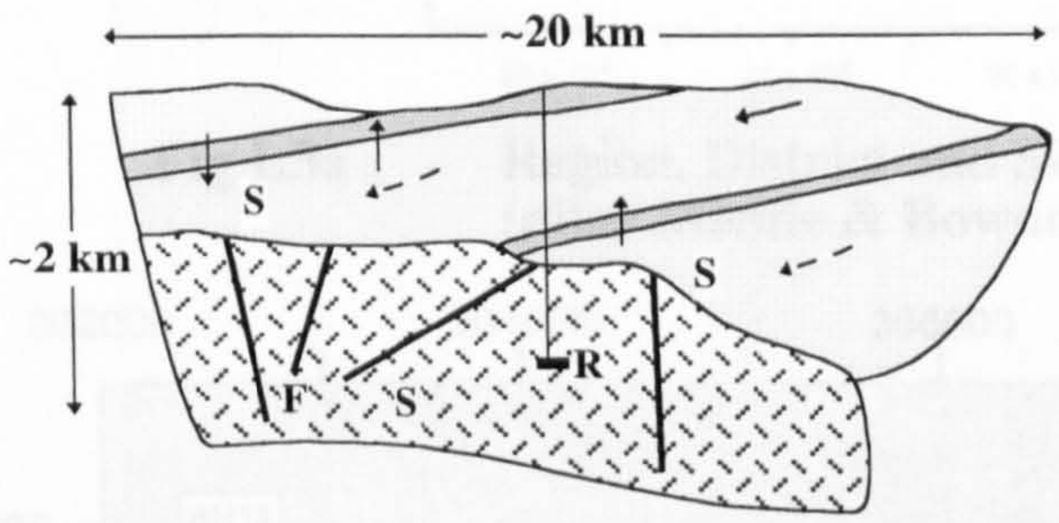

(c) Basement under sedimentary cover (BUSC)

Low permeability basement (shales, slates, volcaniclastics) occuring beneath more recent sedimentary cover. Groundwater flow dominantly in cover sequence, with little connection to basement.

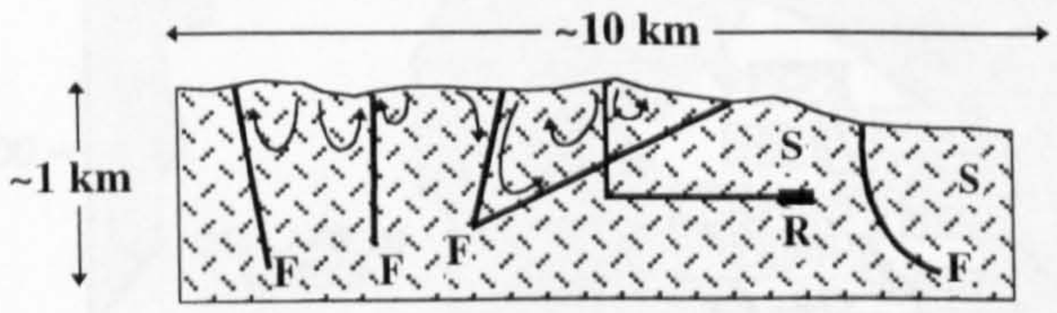

(d) Hard rock in low relief coastal environment

Low topographic drive. Frequent major fracture zones control groundwater flow systems. Coastal location preferable, to give access to offshore repository.

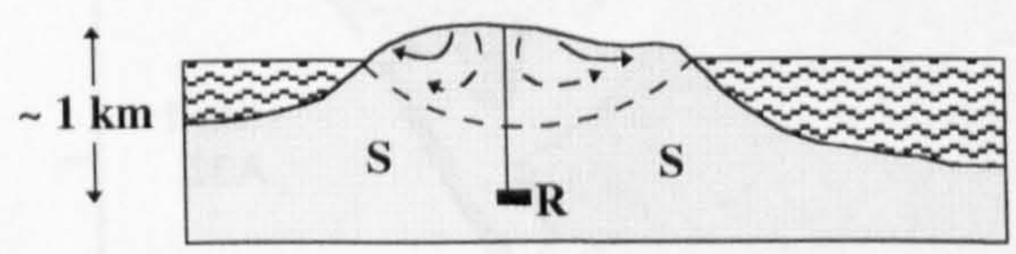

(e) Small island

Repository beneath sea water / fresh water interface; groundwater essentially stagnant. Design affected by local faults, proximity to shore and hydraulic connection to permeable formations on mainland.

major flow
minor flow
slow advection

R repository
S near stagnant groundwater
F major fault

Fig 1. 2 Geological environments considered most suitable for deep disposal of UK's long lived Intermediate Level Waste (after Chapman et al, 1986).

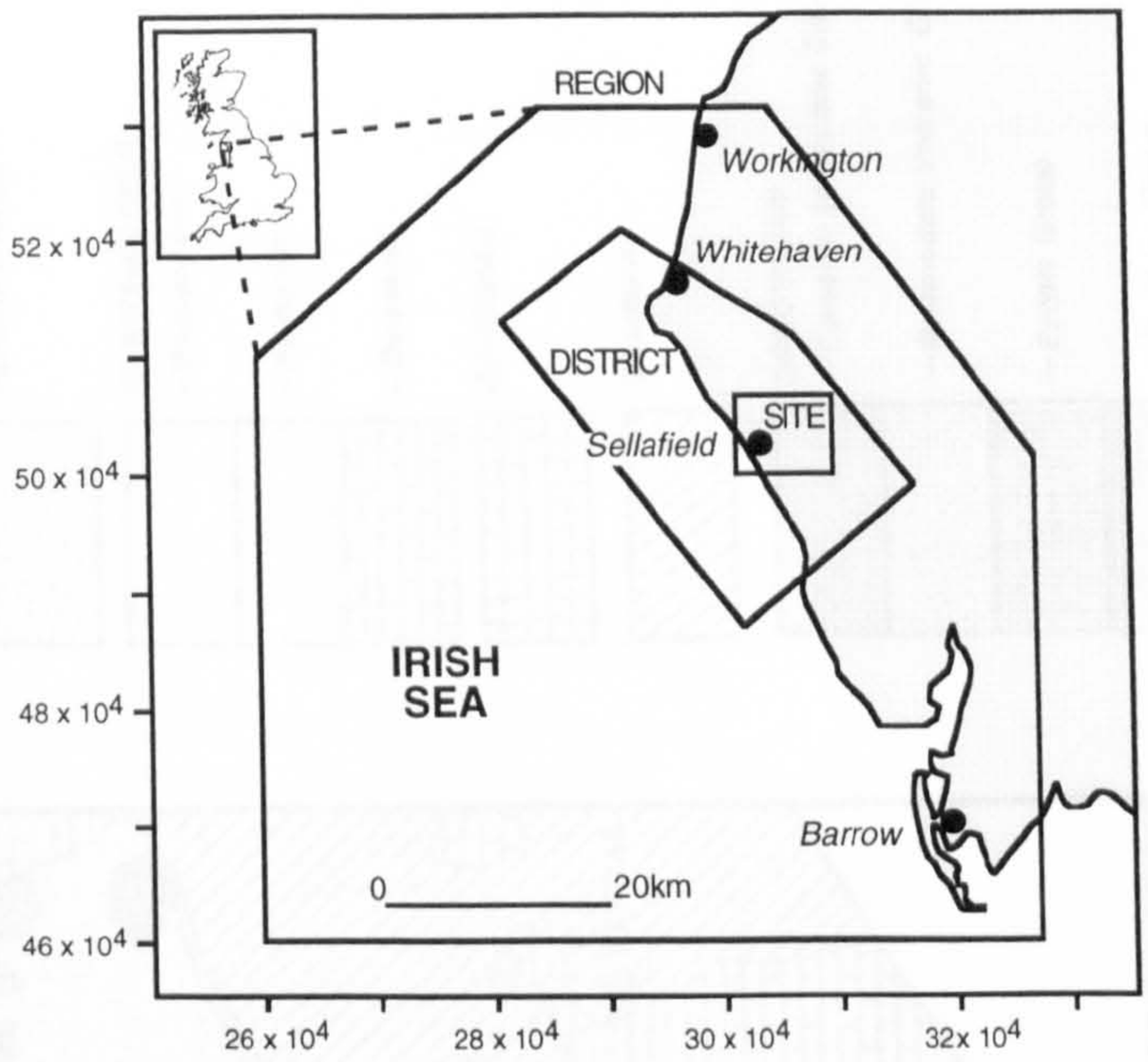

Fig 1.3a **Region, District and Site definitions (after Michie & Bowden, 1994).**

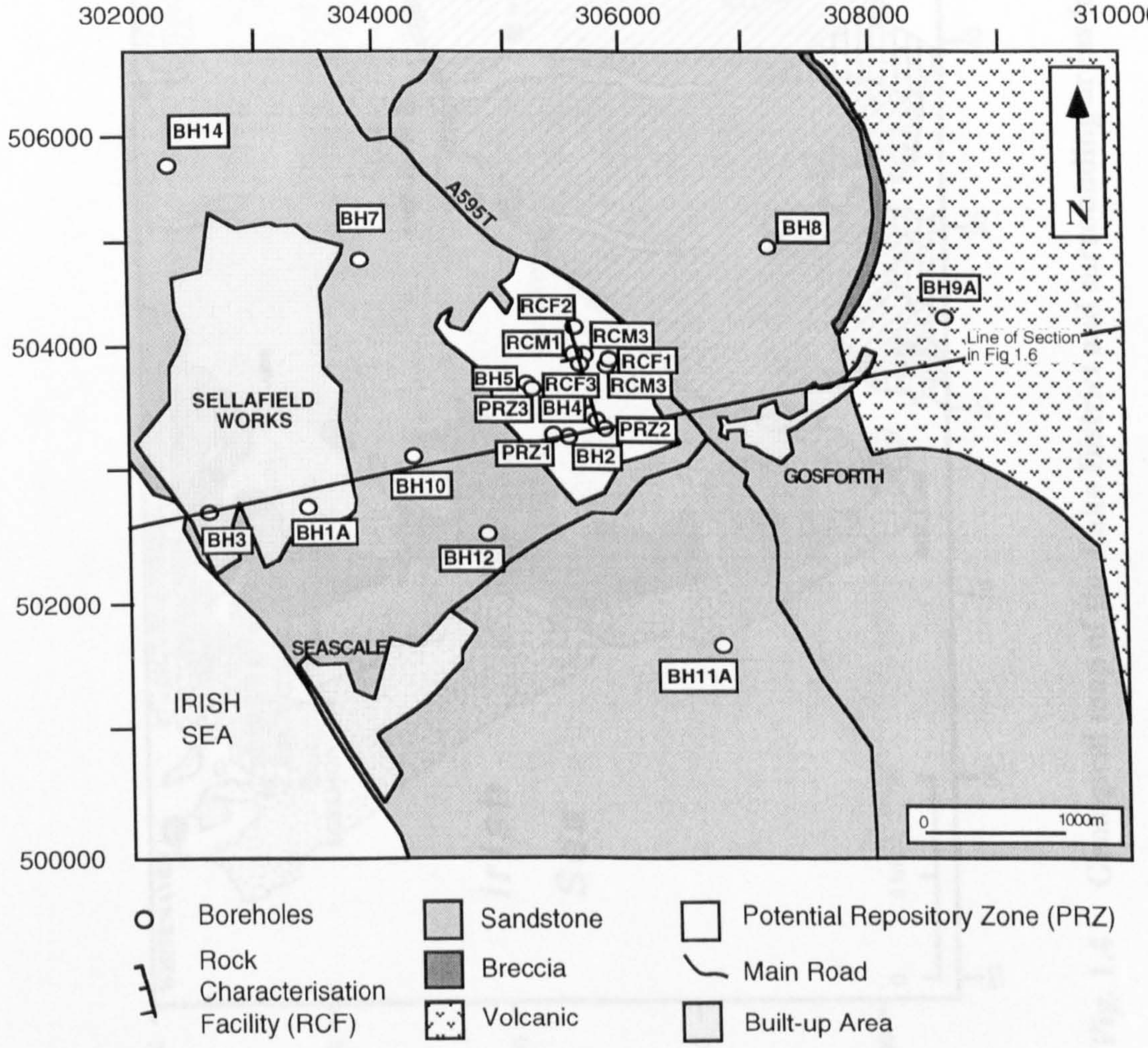

Fig 1.3b **Location of deep boreholes, the PRZ and RCF (after Michie & Bowden, 1994; Chaplow, 1995).**

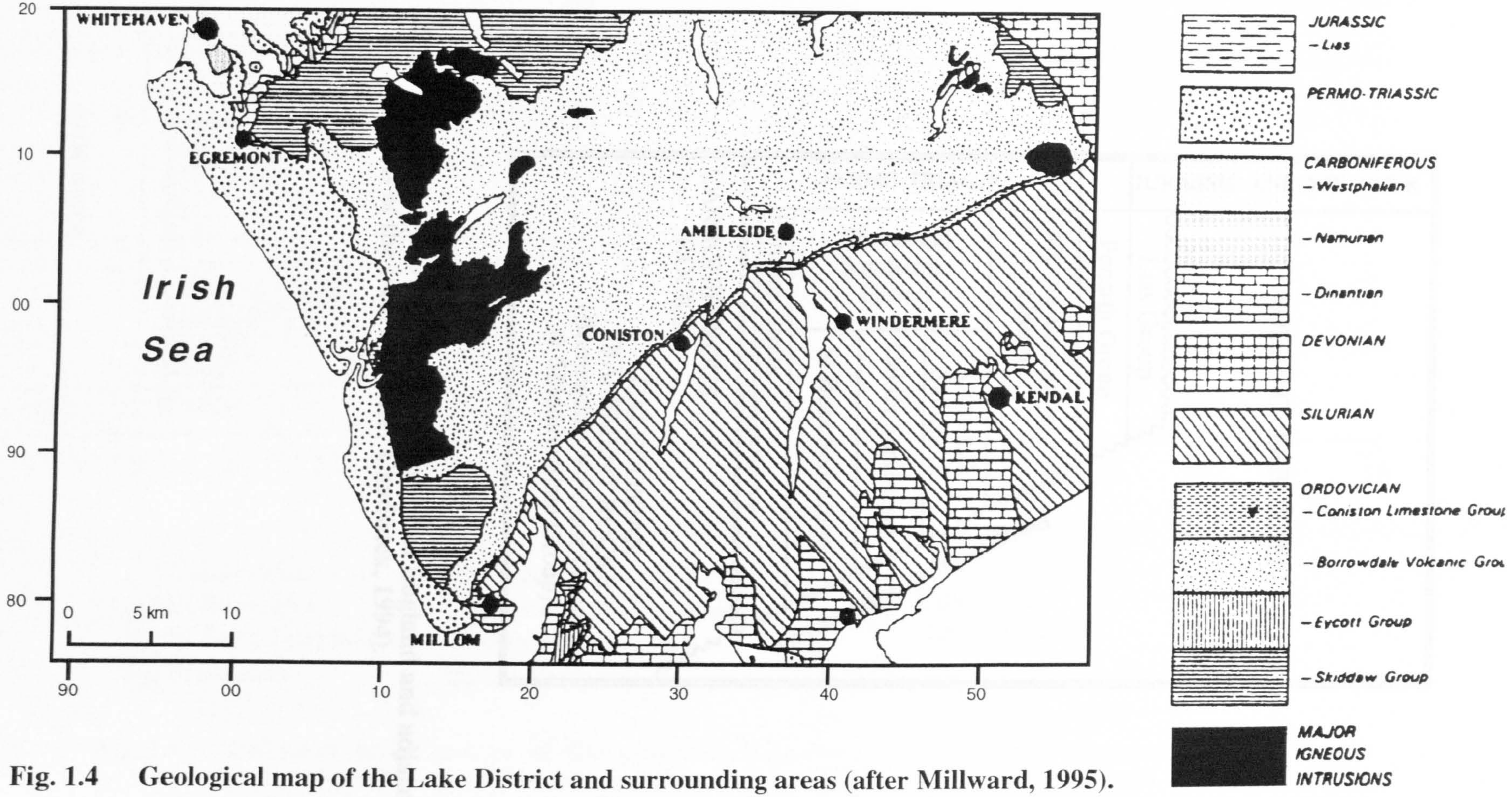

Fig. 1.4 Geological map of the Lake District and surrounding areas (after Millward, 1995).

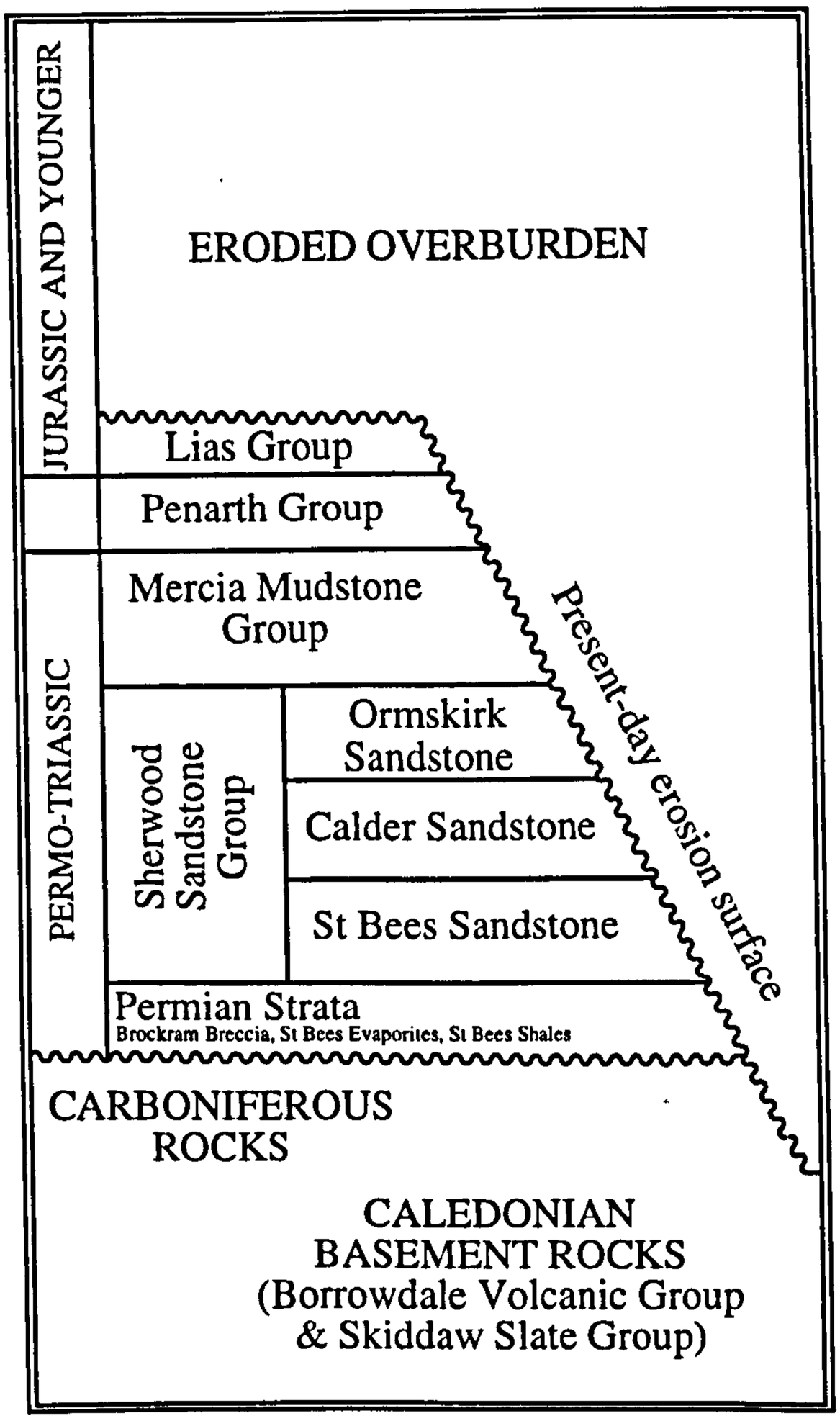

Fig 1.5 **Summary stratigraphy of north-west England and adjacent parts of the Irish Sea (after Chadwick, 1994).**

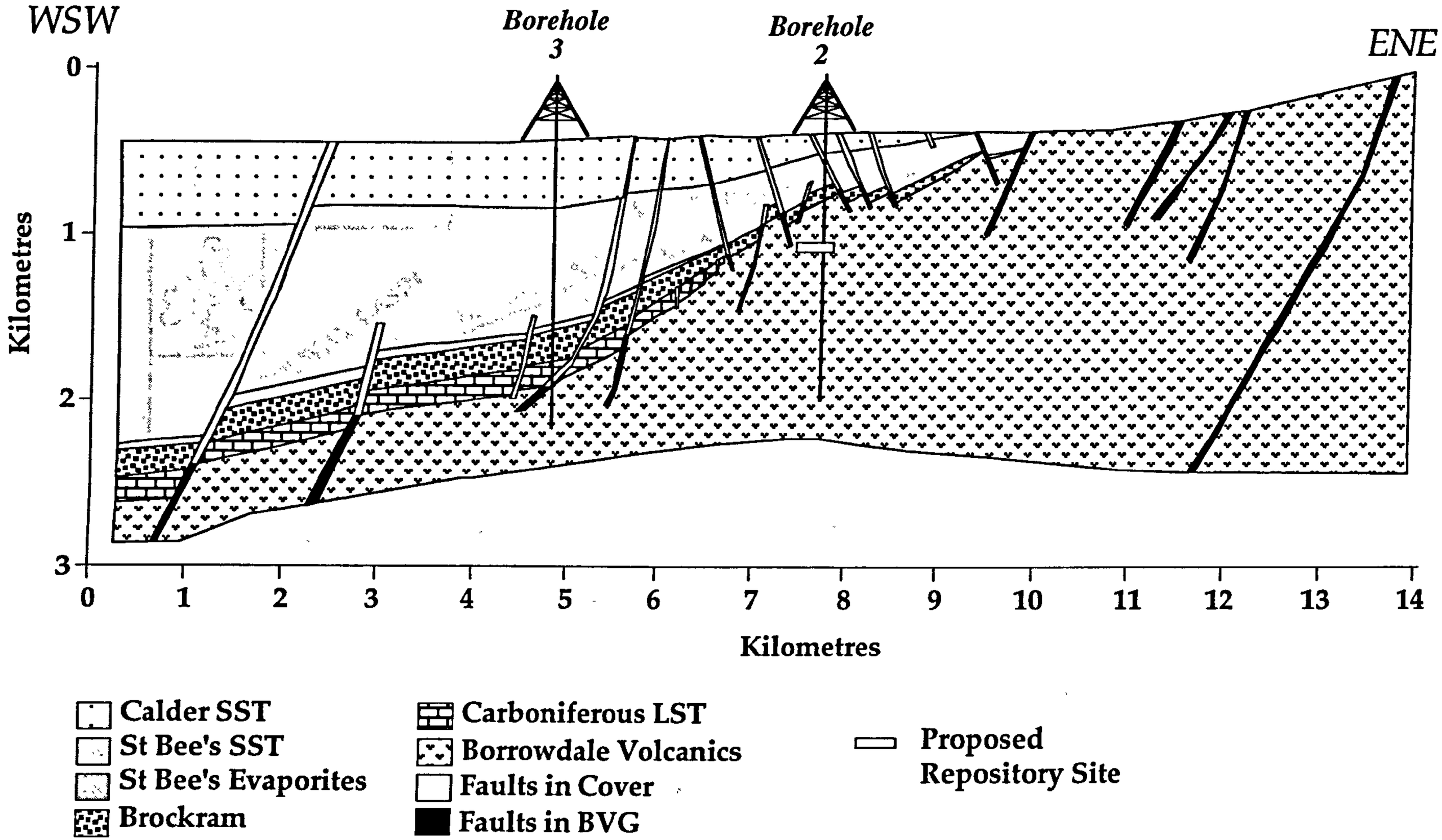

Fig. 1.6 Geological cross section of the proposed Repository site at 650m, compiled from published information (Nirex, 1992b; Nirex, 1993b; Nirex, 1993d) and extended W and E using publicly available geological information (Taylor et al 1971). Rocks of the Borrowdale Volcanic Group (BVG) rise to 1,000m elevation in the Lake District, and fall westwards to lie well below sea level. This elevation provides a topographical drive for meteoric water flow through any fracture or matrix conductivity in the BVG. Carboniferous to Triassic sediments onlap the BVG, and provide a series of matrix and fracture permeable aquifers.

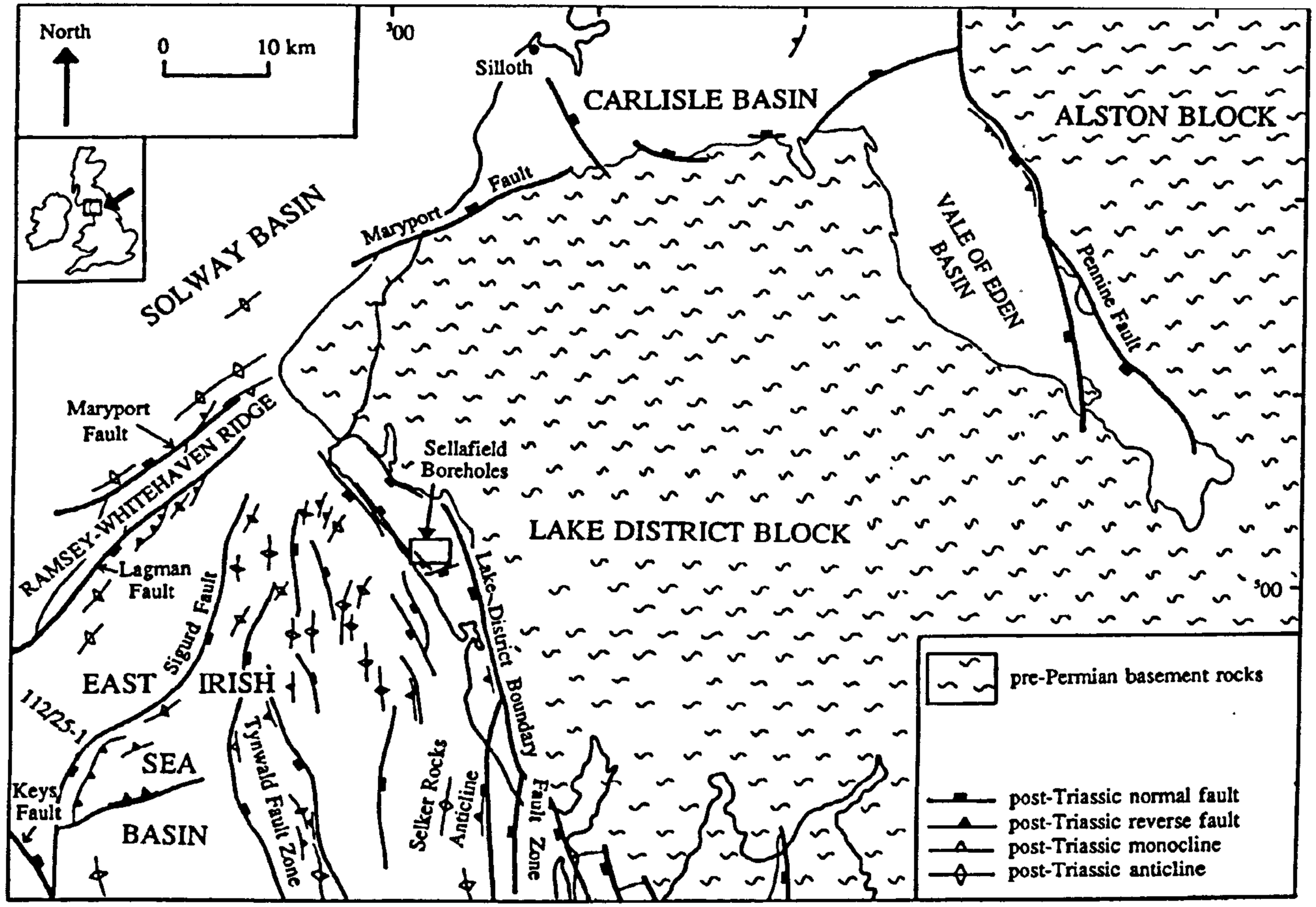

Fig. 1.7 **Simplified geological map showing putative post-Triassic structures (after Chadwick et al , 1994)**

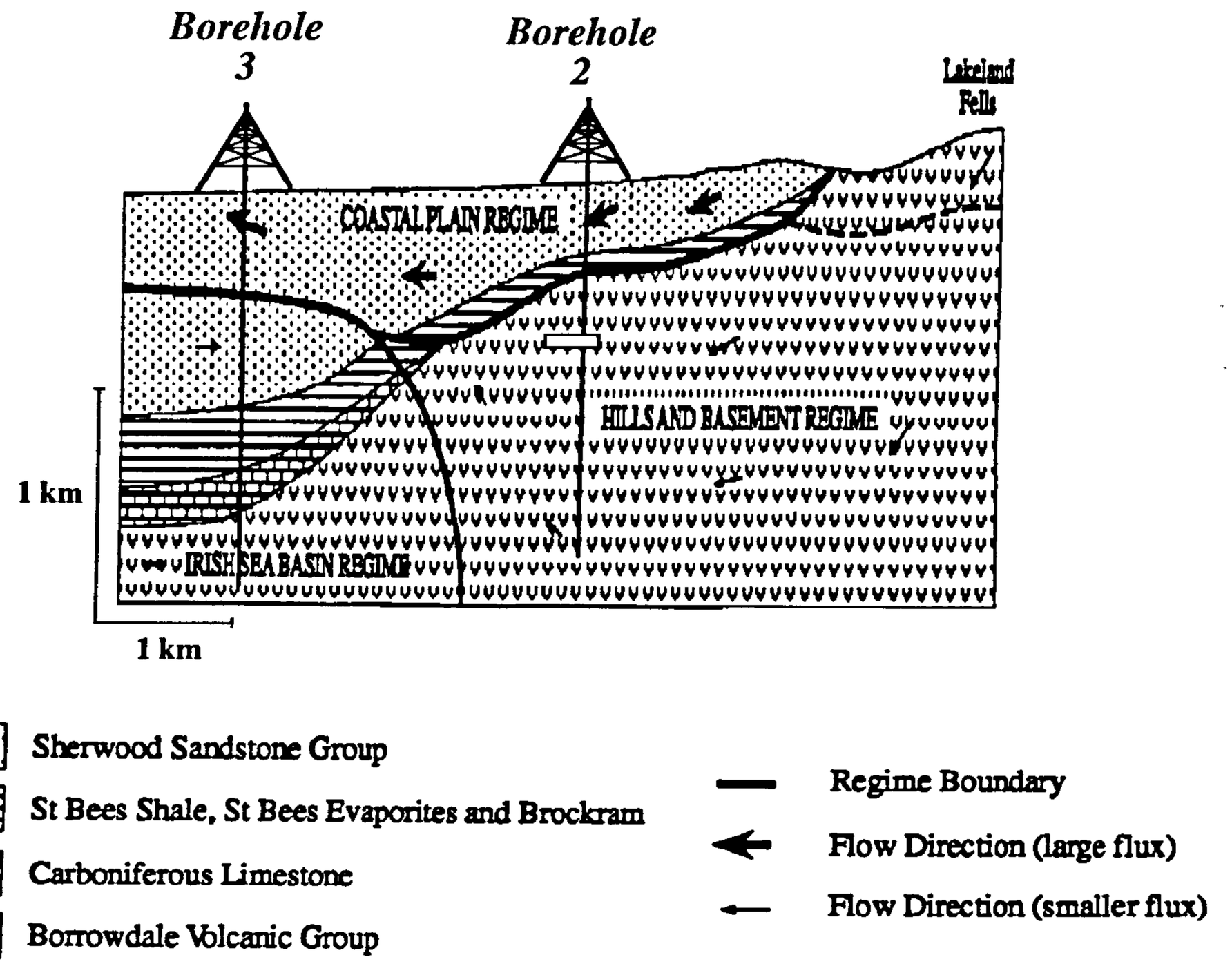

Fig 1.8 Cartoon showing the hydrogeological regimes of the Sellafield area (after (Black, 1995). The divisions coincide largely with the distribution of salinity. Groundwaters in the Irish Sea Basin regime are predominantly basin-derived brines; in the Hills and Basement Regime, saline; in the Coastal Plain Regime, fresh. Scale same as Fig. 1.6.

Chapter 2 Background to fluid flow modelling

2.1 Global context of the Sellafield repository

This small chapter is intended to place the UK approach to radioactive waste disposal in a global perspective and to describe the various field and laboratory techniques that can be used to elucidate the data required for constructing fluid flow models.

It is sometimes stated that other countries are already operating radioactive waste disposal programmes- by implication Britain is lagging behind, and should proceed rapidly with RCF and repository development at Sellafield. This is not a fair representation of the true picture. Part of the problem of comparison is that there are no international standard definitions of waste categories. In 1996, no country has a final repository operational for the mix of waste destined for the Sellafield repository. Britain has had a disposal site operating for radioactive waste since 1959, at Drigg in West Cumbria. This has already disposed of 750,000 m^3 of waste- albeit for LLW where radioactive half lives are typically less than 30 years, so that only 300 years of isolation are needed. In many respects Britain is ahead on the international waste disposal scene. The drive to go for deep disposal of ILW in Britain, is that this contains very long-lived radioactive elements, chiefly uranium, in the British mix of ILW. Many other countries exclude long-lived radionuclides from their definition of ILW.

The USA has had two repositories operating to receive LLW, remaining LLW is stored by different groups of co-operating states. Similar to British ILW is Trans Uranic Waste (TRU), military wastes of this nature are stored at 700m down in salt at Carlsbad New Mexico- this will probably become the first permanent ILW disposal site. Canada is currently storing waste with individual generators, but intends to construct a disposal site for LLW at Chalk River, Ontario. Belgium is currently storing all waste at the surface, but intends to construct a LLW disposal site in clay. France has been disposing of LLW at the surface since 1969, but has no ILW site. Spain operates a LLW disposal site at the surface in the El Cabril former uranium mine, since 1992. Japan has been operating a LLW disposal site at the surface since 1992 on the northern coast of Honshu.

Scandinavian countries have few glacial or sedimentary deposits at the surface to enable easy options on shallow burial, consequently their LLW disposals are in caverns excavated in hard rock. Sweden is operating the Forsmark shallow repository at 60m depth below the sea. This receives waste classified as LLW and

ILW in Sweden, of short-lived radioactive isotopes similar to that classified as LLW in the UK, and currently disposed of at the Drigg surface landfill site under UK regulations. Finland has excavated rock repositories for ILW at 100m beneath each nuclear site. Switzerland is currently storing all wastes, and has identified a candidate deep disposal site for LLW to be further assessed in mudrocks at Wellenberg. Germany is storing most waste near the site of production. The former GDR had disposed of some LLW and ILW in a former salt mine at Bartensleben, some additional LLW has been disposed here in 1994. Three sites of deep burial have been investigated since 1965 as repositories for LLW, ILW and HLW, but none are operational.

The role of Underground Rock Laboratories (URL) in assessing disposal sites for ILW or HLW varies between countries, and simplistic comparisons are not easy to make. However it is clear that the role of an RCF as envisaged in Britain is uncommon or unique. The British RCF is conceptually an integral part of assessing a particular site (rather than a generic setting), and the RCF also forms an integral part of a final repository. In Germany, an abandoned salt mine at Aase has been used since 1965 as an URL to investigate the properties of salt in general, but is not a preferred option as a repository. A repository site is being constructed 900m down in salt at Gorsleben, intended to become operational for LLW, ILW and HLW in 2008. An abandoned iron ore mine 800-1300m down at Konrad is overlain by clay, and has been under assessment since 1986 as a disposal site of LLW and ILW. In Canada, a generic URL has been under construction since 1986 at Whiteshell Lab, 500-1000m down within the Lac du Bonnet granite, Manitoba. It is not intended that this will be part of the disposal site- rather a means to assess generic methodology for other sites.

France may develop two URLs, to investigate candidate sites; in 2006 it may be decided that one of these could become a repository for ILW and HLW. Belgium does have a URL at Mol, 230m down in clay. This has operated since 1983; here there is the possibility that a final ILW and HLW repository may be constructed at the same site- but not commencing whilst experiments continue until 2030. Japan has examined fracture-flow at Kamaishi, and is developing a URL in sedimentary rocks at Horonobe on Hokkaido. This will not be part of a final disposal site which is not planned until 2040. Spain has no URL, and is still considering generic sites. Sweden has undertaken two URL projects. From 1980-1992, the international Nuclear Energy Agency URL was in the 400m deep abandoned iron mine at Stripa, and is now currently excavating a 450m deep URL at Aspo. Neither of these sites

are intended as the final repository. Finland has no URL, and is still investigating candidate LLW & HLW sites. Switzerland has had a 450m deep URL at Grimsel since 1984, this will not be a repository site. A further URL will be constructed near to the Wellenberg LLW candidate-repository site, but further work needs to be completed before use as a repository.

The USA has a pilot-plant military ILW repository in New Mexico at 700m in salt. A URL is presently operational in andesite lavas at Yucca Mountain in the Nevada desert. If characterisation is successful, then disposal of ILW and HLW could begin in 2010. No other ILW or HLW sites are being investigated; this appears to be the closest analogue to the current British approach. It can be seen that the RCF proposal in Britain is unique in choosing a deep repository site without 10, 20 or 30 years of prior generic investigation.

Many potential radwaste sites world-wide involve water flow through fractured rock, and as outlined in Chapter 1 the fractured nature of the BVG and the complicated nature of the subsurface geology of the Sellafield site make it fundamentally necessary that the hydrogeology and geology be fully understood before any construction of a repository begins. Thus the use of computer simulations of fluid movement becomes essential; in terms of repository siting, construction and safety case assessment.

2.2 Data required to construct fluid flow models

The movement of groundwater has been shown to play a major role in all geological processes (Garven, 1995). Studies into the disposal of material such as uranium in large quantities has many parallels with investigations into the formation of ore deposits (Raffensperger & Garven, 1995) and as a result there are many projects world-wide that use such deposits as so-called natural analogues (Miller *et al.*, 1994). But as the rocks in the Sellafield area are, in terms of the rock matrix, of low permeability the actual derivation of information pertinent to fluid flow modelling studies is made all the more difficult (Black, 1987) .

The construction of fluid flow models requires good quality input data; the model is only as good as the information that is "fed in" to the computer simulation code. It is important to note that the author did **not** gather such data, as the Sellafield site is a closed site, **all** data was collected by either UK Nirex Ltd. or their sub-contractors. This section is intended to illustrate the techniques utilised in the field and laboratory to provide the relevant good quality data required to generate flow models. As the rest of this thesis is set out as papers the methods and equations used

to calculate parameters such as permeability and hydraulic head are detailed in Chapter 3 and are dealt with only briefly in this section. Large scale geophysical techniques such as seismic reflection etc. are dealt with in a similar fashion; detailed explanations being reserved for boreholes and in-situ hydrogeological tests.

2.2.1 Large scale geophysical surveys

Fundamental to understanding the hydrogeology of the Sellafield site is the determination of the sub-surface geology (Chaplow, 1995; Michie & Bowden, 1994; Smythe, 1996). Since the Sellafield site is adjacent to the offshore East Irish Sea Basin oil and gas exploration area, data from large scale airborne magnetic and gravity surveys were already published for most of the Sellafield District (Michie & Bowden, 1994). Onshore and offshore gravity anomaly surveys were performed by UK Nirex Ltd. to complement data already available (Nirex, 1992a). Data derived by these methods are of a very large scale, determining the geometry of rock units and the faults and fractures that cross-cut them requires smaller scale detail. Such detail can be obtained by using seismic reflection techniques (Nirex, 1993).

The seismic reflection method is now the standard technique in the search for and exploitation of oil. It is now being applied to the search for suitable repository sites. As well as utilising previously available seismic reflection data UK Nirex Ltd. have also shot 2-D seismic lines offshore. By using the vibroseis technique, (Nirex, 1992a), in the area of the potential repository zone (PRZ) (Smythe, 1996), a 3-D seismic reflection trial of a small area within the PRZ has been undertaken but the results have yet to be made publicly available (University of Glasgow, 1994). One of the most important uses of geophysical surveys is the targeting of boreholes to determine more detail of the sub-surface geology. 2-D geophysical tomographic surveys between pairs of boreholes have also been undertaken in an effort to delineate the extent of faulting at the relatively small scale of tens to hundreds of metres (Nirex, 1994).

2.2.2 Boreholes

By 1995 there were a total of twenty two boreholes in the Sellafield area with a total of 25,712 m of drilling. The deepest borehole is 1,950 m deep and most of the drilling has been carried out to obtain continuous core of the rocks penetrated (Chaplow, 1995). The drilling mud used consisted of a freshwater based polymer laced with a LiCl tracer maintained at 1000 mg/l so that the degree of invasion could be assessed (Bath *et al.*, 1996). These cores have been photographed, logged and samples selected for routine and specialist characterisation in the lab. From each borehole drilled, both from the core and downhole geophysical logs (electric,

nuclear, sonic and calliper) (Chaplow, 1996) information is derived regarding the mineralogy and geochemistry, geotechnical, rock mechanics and geological properties, fracture geometry and characteristics, and engineering data (Michie & Bowden, 1994).

2.2.3 Hydrogeological testing

In essence the hydrogeological properties of a rock mass are a function of its voids, their shape, size, number and connectivity. The gross distribution of voids within a given rock unit determines the geometry of flow when tested and may be expressed in terms of parameters such as permeability or porosity; where porosity is simply the measure of the volume of voids within a rock, expressed as a percentage, and permeability is the ability of the rock to transmit fluid, often expressed in milli Darcies (mD) (or converted to hydraulic conductivity; measured in m/s) (de Marsily, 1986).

The derivation of the permeability and porosity of the rocks in the subsurface at Sellafield has progressed in two distinct modes; the laboratory analyses of core samples and the borehole hydrogeological testing programme (Nirex, 1993). The former provides data on the rock matrix properties at a smaller scale than those the latter provides on the rock mass.

Core tests

The effective porosity of cores has been derived by either Helium Gas Expansion (HGE) or Liquid Resaturation methods, the latter being the more commonly used. Permeability has been calculated for twice as many samples as porosity (Nirex, 1993) and was undertaken for the most part by the gas injection method. Core plugs were taken both parallel and perpendicular to the core to determine the horizontal and vertical permeability.

The gas permeabilities were measured by flowing pressurised nitrogen through samples at a constant flow rate (Nirex, 1992b) with the permeability expressed in mD. Since the lower limit to this method is 10^{-3} mD and the difference between gas and liquid permeability increases as the permeability decreases (Nirex, 1993) laboratory data obtained for low permeability rocks should be treated with caution. One of the most important reasons for measuring permeability on core samples is to provide a comparison between matrix permeability and larger scale rock mass permeability, determined from hydrogeological tests. In general matrix permeabilities are lower than mass permeabilities (Clauser, 1992; Neumann, 1990; Neuzil, 1986).

Borehole tests

During and after drilling of the boreholes there was a programme of testing to examine the hydrogeological properties of the formations intersected. The main aims were to give an indication of the variation of in-situ pressure with depth, to identify zones of groundwater flow and to obtain groundwater samples for geochemical analyses (Nirex, 1992a). To this end three basic test methodologies were applied during drilling; Environmental Pressure Measurements (EPM); Full Sector Tests (FST) and Discrete Extraction Tests (DET).

EPM

These tests are carried out at 50 m intervals during drilling. Once the drill string is withdrawn a packer is inflated to isolate the bottom 50m of the hole. Water is bailed from the test tubing, initiating 50 m of drawdown. The environmental pressure can then be derived from the recovery to this induced pressure disturbance (Sutton, 1996). The simplest fluid regime envisaged for the Sellafield site is that of radial flow in a homogenous porous medium but more complex regimes incorporating fractures can also be used (Nirex, 1992b). The simplest regime has been used in previous calculations of the rock mass permeability (Nirex, 1993).

Once the pressure is obtained the permeability can be calculated, taking into account the above assumed flow regime. Readers are referred to published work detailing the multiple steps involved in this process and the kind of software required (Nirex, 1992b). The environmental pressure can also be expressed as hydraulic head, where head is equivalent to the height above ordnance datum (OD) water would climb if allowed to rise up an open borehole. This conversion requires data on the density, temperature and salinity (derived from the Total Dissolved Solids (TDS) measured in-situ). As mentioned in section 2.3 the equations used to determine the permeability and hydraulic head are given in Chapter 3.

FST

These tests are carried out over each open section of borehole prior to casing installation or on borehole completion and are used to identify producing zones in the available section of borehole, certain of which could be then tested subsequently in more detail (Nirex, 1992b). Nitrogen gas injection is used to generate a much greater drawdown than that of the EPM: effectively 200 to 400 m in the open hole which induces flow. During the test a suite of wireline logs are run to measure temperature, fluid conductivity and this generated flow. These are then interpreted to identify inflow zones to the borehole (Sutton, 1996). After comparison of FST

results with preliminary core and fracture logs and wireline logs 4 or 5 zones of 10 to 20 m in length are selected for Discrete Extraction Testing (DET)

DET

The primary aim of these tests is to provide high quality groundwater samples from identifiable locations. Information derived from DET is essential to converting pressures to permeabilities and heads and in determining the in-situ hydrochemistry of the groundwater (Bath *et al.*, 1996). More detailed information regarding the hydrochemical tests performed are given in Chapter 4. Sample zones (generally individual fluid producing features) are isolated by a double packer system, straddling the interval of interest. Fluid is then abstracted by reverse circulation of nitrogen under very high drawdown conditions (up to 800 m).

The fluid samples are regularly monitored at the surface for LiCl contamination and when the flow in the test section is static, gas injection is stopped and a series of downhole pressure controlled groundwater samples collected (Sutton, 1996). Again the transient pressure recovery within the test section can be monitored and translated into head and permeability values for the rock immediately surrounding that test section (Nirex, 1992a).

Other hydrogeological tests

Other methods of sample collection include Drill Stem Tests (DST) and Swabbing Environmental Pressure Measurements (SEPMS). Since DETs appear to give the most comprehensive results readers are referred elsewhere for more details regarding these other tests (Bath *et al.*, 1996). Post-drilling DETs (PDDETs) are similar to DETs, except that a downhole pump is used to produce water from the test string, water samples can be collected downhole in wireline samplers or at the surface from the test string as it is removed from the borehole.

2.2.4 Synthesis of data for flow simulations

The seismic reflection profiles of the site area were used to determine the gross geological structure; and were used to produce the interpretative cross-section shown in Chapter 1. Subsequent seismic interpretation has produced many modifications to the geological understanding of the area (Nirex, 1993), but, in general, the main structural features remain the same (Nirex, 1995); with the dominant features being the upland BVG rocks of Lake District to the ENE of the site rising to around 500 m and descending to depth beneath and to the WSW of the site with the overlying onlapping thick succession of sediments dipping to the W and thinning to the E.

The pattern of regional boreholes in the area (1, 2, 3, 4, 5, 7, 10, 11, 12 and 14) have been drilled in two approximate lines; normal to the coast and parallel to the envisaged dominant direction of groundwater flow and the other approximately normal to the first line and parallel to the coast (Chaplow, 1996). Geochemical interpretations of sub-surface fluids produced the conceptual model outlined in Chapter 1 and this, coupled with the geological interpretations from the seismic and borehole data has provided the framework for the modelling presented in Chapter 3. The orientation of the cross-section used in the fluid flow modelling presented in this thesis is similar to that of the most recent, geologically realistic cross sections. These are generally believed to run parallel to the dominant direction of groundwater flow (Black & Brightman, 1996).

2.3 References

Bath, A.H., McCartney, R.A., Richards, H.G., Metcalfe, R. & Crawford, M.B. (1996) Groundwater chemistry of the Sellafield area: a preliminary investigation. *Quarterly Journal of Engineering Geology*, **29**, supplement 1, S39-S57.

Black, J.H. (1987) Flow and flow mechanisms in crystalline rock. *In:* Goff, J.C. & Williams, B.P.J. (eds) *Fluid flow in sedimentary basins and aquifers.* Geological Society Special Publication No. 34, London, 185-200.

Black, J.H. & Brightman, M.A. (1996) Conceptual model of hydrogeology of Sellafield. *Quarterly Journal of Engineering Geology*, **29**, supplement 1, S83-S93.

Chaplow, R. (1995) *Proof of Evidence. Geology and hydrogeology*. RCF Planning Enquiry, **PE/NRX/14**, UK Nirex Ltd., Harwell, UK, Cleator Moor, Cumbria, 72 pp.

Chaplow, R. (1996) The geology and hydrogeology of Sellafield. *Quarterly Journal of Engineering Geology*, **29**, supplement 1, S1-S12.

Clauser, C. (1992) Permeability of crystalline rocks. *Transactions American Geophysical Union*, **73**, 21, 233-238.

de Marsily, G. (1986) *Quantitative hydrogeology. Groundwater hydrology for engineers*. Academic Press Inc. (London) Ltd., London, 440 pp.

Garven, G. (1995) Continental-scale groundwater flow and geologic processes. *Annual Review in Earth and Planetary Sciences*, **23**, 89-117.

Michie, U.M. & Bowden, R.A. (1994) UK Nirex geological investigations at Sellafield. *Proceedings of the Yorkshire Geological Society*, **50**, 5-9.

Miller, W., Alexander, R., Chapman, N., McKinley, I. & Smellie, J. (1994) *Natural analogue studies in the geological disposal of radioactive wastes.* Report No. **NTB 93-03**, Nagra, Wettingen, Switzerland.

Neumann, S.P. (1990) Universal scaling of hydraulic conductivities and dispersivities in geologic media. *Water Resources Research*, **26**, 1749-1758.

Neuzil, C.E. (1986) Groundwater flow in low permeability environments. *Water Resources Research*, **22**, 8, 1163-1195.

Nirex. (1992a) *The geology and hydrogeology of Sellafield.* Report No. **263**, UK Nirex Ltd., Harwell, UK.

Nirex. (1992b) *Sellafield hydrogeology. Report of the hydrogeology joint interpretation team.* Report No. **268**, UK Nirex Ltd., Harwell, UK.

Nirex. (1993) *The geology and hydrogeology of the Sellafield area: Interim assessment.* Report No. **524 (4 vols)**, UK Nirex Ltd., Harwell, UK.

Nirex. (1994) *The 2-D interpretation of the tomogram data from the Rock Characterisation facility area, Sellafield.* Report No. **S/94/007**, UK Nirex Ltd., Harwell, UK.

Nirex. (1995) *The 3D geological structure of the PRZ: summary report.* Report No. **S/95/005**, UK Nirex Ltd., Harwell, UK.

Raffensperger, J.P. & Garven, G. (1995) The formation of unconformity-type uranium deposits. 1. Coupled groundwater flow and transport modeling. *American Journal of Science*, **295**, 581-636.

Smythe, D.K. (1996) The 3-D structural geology of the PRZ. Proof of Evidence. *In:* Haszeldine, R.S. & Smythe, D.K. (eds) *Radioactive Waste Disposal at Sellafield, UK. Site Selection, geological and engineering problems.* University of Glasgow, Glasgow, UK, 237-266.

Sutton, J.S. (1996) Hydrogeological testing in the Sellafield area. *Quarterly Journal of Engineering Geology*, **29**, supplement 1, S29-S38.

University of Glasgow. (1994) *3-D seismic reflection data aquisition report.* Report No. **622**, UK Nirex Ltd., Harwell, UK.

Chapter 3 Mathematical modelling of Sellafield groundwater flow

McKeown, C., Haszeldine, R.S. and Couples, G.D.

3.1 Abstract

Sellafield in West Cumbria has been selected as a potential site for the location of the UK's first underground repository for radioactive, Intermediate Level Waste (ILW). The proposed repository lies around 650 m beneath the ground surface within rocks of the Borrowdale Volcanic Group (BVG), a thick suite of SW dipping, fractured, folded and metamorphosed Ordovician meta-andesites and ignimbrites. These are overlain by an onlapping sequence of Carboniferous and Permo-Triassic sediments. In-situ borehole measurements show that upward trending fluid pressure gradients exist in the area of the potential repository site and that there are three distinct fluid types in the subsurface; fresh, saline and brine (at depth, to the west of the site). Simulations of fluid flow in the Sellafield region were undertaken with a 2-D, steady-state, coupled fluid and heat flow simulation code (OILGEN). In both simplified and geologically complex models, topographically driven flow dominated the regional hydrogeology. Fluids trended persistently upwards through the potential repository site. The dense brine to the west of the site promoted upward deflection of topographically driven groundwaters. The inclusion in hydrogeological models of faults and variably saline sub-surface fluids was essential to the accurate reproduction of regional hydraulic head variations. Sensitivity analyses of geological variables showed that the rate of groundwater flow through the potential repository site was dependent upon the hydraulic conductivity of the BVG, and was unaffected by the hydraulic conductivity of other hydrostratigraphic units. Calibration of the model was achieved by matching simulated subsurface pressures to those measured in-situ. Simulations performed with BVG hydraulic conductivity 100 times the base case median value provided the "best-fit" comparison between calculated equivalent freshwater head and that measured in-situ, regardless of the hydraulic conductivity of other hydrostratigraphic units. Transient mass transport simulations utilising the hydraulic conductivities of this "best fit" simulation showed that fluids passing through the potential repository site could reach the surface in 15,000 years. Simple safety case implications drawn from the results of the study showed that the measured BVG hydraulic conductivity must be less than 0.03 m/yr to be simply declared safe. Recent BVG hydraulic conductivity measurements show that the maximum BVG hydraulic conductivity is around 1000 times this safety limit.

3.2 Introduction

3.2.1 Background

Many substances, albeit in small doses, can cause potentially fatal illnesses in later life. This rationale can be applied to the removal of radioactive waste from the biosphere in which we live; there are untold dangers for future generations if radioactive material is disposed of carelessly (Chapman & McKinley, 1987).

The main question is, how can one safely dispose of such substances. The most commonly held theory is that the earth itself could provide the answer. (Of course one cannot simply throw such dangerous material into a hole in the ground !) Disposal of radioactive waste by isolation in caverns, constructed deep underground appears to be the best option at present. The cavern has to be prepared, developed and above all inherently geologically suitable for such disposal. Investigations are proceeding world-wide to develop deep, geologically safe, and robustly predictable repositories for the various classifications of radioactive waste. In the UK it is proposed that a suitable site exists to take all of the UK's Intermediate Level Waste (ILW) (Holmes, 1995). This site is 3 km to the east of the British Nuclear Fuels Ltd (BNFL) Sellafield reprocessing plant in West Cumbria, north-west England (Fig. 3.1 a, b).

As radioactive waste is toxic for many thousands and even millions of years it is difficult to predict what the earth will be like, both on and beneath the surface, far into the future. But such predictions must be made and are being made for the UK and other sites around the world. Since the earth's subsurface is almost universally saturated with water, its movement affects many geological processes (Cathles, 1990; Deming, 1994; Garven, 1995). The techniques developed for understanding the processes involved and reconstructing fluid movements in the past can be applied to predict fluid movement in the future. A common feature to all of the world-wide research projects into possible radioactive waste repositories is the use of complex computer simulations of groundwater movement. The computer codes used in such simulations are tools that can be used to predict future hydrogeological conditions, and how they might affect the integrity of a repository and ultimately the safety of the biosphere (Black, 1995; Karlsson, 1995; Langmuir, 1995; Nagra, 1995).

3.2.2 Geology, structure, hydrology and hydrogeology

When choosing a suitable repository site, the pattern and rate of underground water flow must be both predictable and safe for geologically long times into the future. The diverse geological factors affecting such predictions, and some of their difficulties of measurement and forecasting have been reviewed by others (Chapman, 1994). Fundamentally these problems relate to flow rates; which should be preferably long distance and slow duration and result in progressive mixing with older, deeper waters. Any discharge at sea should occur millions of years in the future. Thus it is essential that a repository be sited in an area of very slow local, and slow regional groundwater movements, i.e., in an area with low regional hydraulic gradients (Chapman & McEwen, 1986). Therefore it is necessary that a good understanding of both the geology and hydrogeology of a potential site be obtained before any such major structure is constructed.

3.2.2.1 Geology

Figure 3.2 shows a geological cross-section through the Sellafield area running WSW-ENE through the repository, passing through site investigation boreholes 3 and 2, and close to B/H 1, 10 and 4 (Fig. 3.1). This section was based on information available at the start of the research project (Nirex, 1992a; Nirex, 1993a; Nirex, 1993b) and has been extended both seaward and landward, using public geological and topographical information (Taylor *et al.*, 1971).

The Sellafield site is situated on the west flank of the Cumbrian Dome, between the high upland hills of the Lake District and the shore of the Irish Sea (Fig. 3.1). The ground elevation reaches 500 m within 15 km of the site and as much as 800 m 26 km away (RWMAC, 1994). The core of the dome is underlain by a thick succession (6000m regionally (Millward *et al.*, 1994)) of heavily fractured and folded Ordovician meta-andesites ignimbrites and tuffs collectively named the Borrowdale Volcanic Group (BVG) (Beddoe-Stephens & Phillips, 1993; Branney *et al.*, 1988; Millward, 1995). This succession of rocks has been tilted by later tectonism so that it is in the subsurface beneath the Sellafield site, although the BVG exposed at the surface forms many of the hills in the upland areas to the east (Petterson *et al.*, 1992).

The BVG is the intended host rock for the postulated repository which is planned to be located at least 650 mbOD within an area designated as the Potential Repository Zone (PRZ). This is adjacent to the A595, between the Sellafield Works and the Lake District National Park boundary (Fig. 3.1b). Overlying the Ordovician "basement" is a cover sequence (~ 400m at the site and ~ 1900 m regionally)

containing unconformity-bounded sequences of Carboniferous limestones and Permian/Triassic clastics and evaporites and (locally) breccias at the basement/cover contact (Millward, 1995).

3.2.2.2 Structure

The gross structural configuration of the post-Ordovician rock units is generally simple, with westerly dips of around 20° typifying these strata (Michie, 1996). However faults disrupt the continuity of the rock sequences (Fig. 3.2) and may be intimately involved in causing the westerly dips of the post-Ordovician strata. NW-SE trending faults dominate, dipping steeply towards the SW (Chadwick *et al.*, 1994). A second set of faults, trending NW-SE/NE-SW, dipping towards the N are also present in the area but only displace strata of Carboniferous or older age (Nirex, 1993a). It is a matter of debate if some faults were active during the Quaternary or even at the present day (Haszeldine, 1996).

3.2.2.3 Hydrology and hydrogeology

From the very extensive hydrogeological testing program initiated in the many Sellafield boreholes (Fig. 3.1b) a picture of the complexity of the hydrology of the subsurface has emerged. More details regarding the methods and results of such testing programs are given elsewhere (Chapter two), but fundamentally the measurement program can be split into two types; in-situ samples of pressure which are used to determine the hydraulic head in the subsurface (Sutton, 1996) and fluid extraction tests to determine the chemistry of groundwaters (Bath *et al.*, 1996).

One of the most intriguing and potentially significant features encountered in the hydrogeological interpretations of the Sellafield area are the high pressures (and thus heads) encountered at depth in many boreholes, including borehole 2, in the area. As this borehole passes through the PRZ this means that there is a natural tendency for groundwater to move upwards towards the surface, which would not be beneficial to the safety of a site containing radioactive waste.

The chemistry of the groundwaters is of obvious importance to hydrogeological studies as it can delineate the evolution of the groundwater system over time and be used to differentiate between distinct hydrological types in the sub-surface. The main way of doing this is by means of the salinity of the groundwaters. Discrete Extraction Tests (DETs) are used to determine the Total Dissolved Solids (TDS) dissolved in the solutions at depth. This can be expressed either as a simple amount in mg/l or as a % (in many cases expressed as NaCl equivalent), this salinity effects the density and viscosity of the groundwater and ultimately could influence the sub-

surface flows. There are three distinct fluid types in the area; fresh water, saline water (~ 2 %) and brines with salinity as much as 20 %. (Fig. 3.3).

3.3 Conceptual model

A conceptual model can be described as a hypothesis for how a system or process operates with this hypothesis then expressed quantitatively in the form of a mathematical model (Konikow & Bredehoeft, 1992). Generally, a hydrogeological conceptual model is composed of a set of assumptions that reduce the real problem to a simple description of the system (Bear & Verruijt, 1987). It must also define the processes important to that particular system, the parameters required to model these processes and the boundaries to the system. It provides the framework for the mathematical model and should be consistent with field and experimental data (Bear, 1972).

3.3.1 Existing conceptual models

The most recently published conceptual model based on publicly available salinity data and hydrogeological tests (see above) has indicated that there may be three distinct fluid regimes in the subsurface; a domain of fresh water; a near shore domain of saline waters; and a deep domain of highly saline brines (Fig. 3.4), (Black, 1995). A simple picture can be derived in that the topographically driven, high flux, fresh groundwaters are derived from modern recharge in the Cumbrian Hills to the east of the site which flows westward to discharge at the coast beneath the sea. The topographically driven, relatively low flux, saline groundwater within fractured, faulted rocks of the BVG represent connate pore fluids and/or exchange with the Irish Sea, and the relatively low flux or static hypersaline brines may be related to offshore dissolution of Triassic evaporites or brine expulsion from the East Irish Sea Basin.

In the case of the Sellafield area the most important process that has been identified is gravity driven groundwater flow moving in a generally SW direction (i.e. perpendicular to the coast) from the uplands of the Lake District through the PRZ and towards the Irish Sea (Black, 1995; Black & Brightman, 1996; Haszeldine & McKeown, 1995; Heathcote *et al.*, 1996; Littleboy, 1996; McKeown & Haszeldine, 1995). If the present view of the spatial locations of these fluid domains is correct, then the brines, being considerably more dense, may act as inhibitors to the flow of groundwaters.

3.3.2 Conceptual model used in this study

The model used in this study (Fig. 3.5) builds on the conceptual model outlined above. This was specifically intended to explore the possibility that there may be upward trending flow of groundwaters in the BVG beneath and through the PRZ, and the groundwater in the BVG may be affected by the salinity of fluids encountered, especially the brines encountered to the west.

As outlined in section 3.2.2 there are 3 distinct fluid types in the Sellafield area but when this study was initiated in 1993 the most sophisticated modelling that had been published had very little geological detail. This had only incorporated three hydrostratigraphic units, few faults and a uniformly freshwater groundwater (Nirex, 1992a). Thus the mathematical modelling envisaged for this study was required to encompass more geological detail, faults, and variations in groundwater salinity.

3.3.2.1 Hydrogeological units

The simulation code used in this study requires a fixed number of hydrostratigraphically distinct units. These units are the subdivisions of the rock mass into parts which have hydrogeological parameters that are sufficiently similar to merit the use of the term "unit" and parameters which are significantly different from the parameters of the other units that they can be distinguished.

With this in mind, and given the geological interpretations of the rock units (Chapter 1) the hydrostratigraphic units were identified (Table. 3.1a). The values reported in Table 3.1a are derived from published data (Michie, 1996; Nirex, 1992a; Nirex, 1993a; Nirex, 1995) and represent close to logarithmic median values for the range of hydraulic conductivity (or permeability) reported for the hydrostratigraphic units. As these data are some of the most up to date available it is important to note that the median values for the BVG, Calder Sst., St Bees Sst., and faults in both the cover sequence and the BVG are generally higher than those reported in older publications by the author (Haszeldine & McKeown, 1995; McKeown & Haszeldine, 1993; McKeown & Haszeldine, 1995). These utilised the data available at the time.

In simple terms the Calder and St Bees Ssts. are permeable and porous; the Brockram Breccia and St Bees Evaporites are impermeable and of low porosity; the Carboniferous Limestone is slightly more permeable and the BVG is of low to medium permeability and low porosity. The faults in both the cover and BVG are more permeable than the surrounding rock matrix with moderate porosity. These close to median values (Table 3.1a) will be termed the "base case" values in this

modelling study and are used as the basis for extended modelling over a range in values.

3.3.2.2 Fluid types

As mentioned there are distinct fluid types in the region therefore the simulations performed in this study were undertaken both with freshwater and with variably saline water of comparable position and salinity as that measured in-situ.

3.3.2.3 Boundary conditions

The modelling expression of boundary conditions to the numerical simulations is outlined in a later section (3.4.4) but it is useful to describe the likely boundaries to flow that might be incorporated into fluid flow simulations. As can be seen in Fig. 3.2 the eastern boundary of the cross section corresponds to the maximum height encountered in the area; very little is known about flows in these outcropping basement rocks thus it would be appropriate to assign a no flow boundary to the eastern vertical edge. A similar situation regarding data applies to the flows to west of the coast and, due to highly saline nature of these fluids (possibly becoming more saline further offshore (Nirex, 1995)), it would be appropriate to assign a no flow boundary to the western edge also.

This highly saline groundwater is likely to persist at greater depths than those attained in the present boreholes (which are up to 2 km). At depths beyond the bottom hole such highly saline, dense groundwater would be relatively immobile so again it would be appropriate to assign a no flow boundary to the base of the section. In modelling studies of groundwater flow it is common to assume that the water table is coincident with the land surface and that the water at this part of the boundary would be fresh (Garven, 1995), thus it would be acceptable to assign a boundary to the top surface that would allow flow to pass through it.

3.3.3 Relevance and specific aims of project

The geology of the Sellafield area is a variant of a long-recognised proposal for underground disposal of radioactive waste in crystalline rock beneath sediments (Bredehoeft & Maini, 1981). This implicitly relies upon the adequate present-day description and reliable forecasting of the subsurface hydrogeological conditions. The objective is to ensure a reliable and robust prediction of the date which radioactive water could return to the surface, far into the future. If it could be shown that the geology of the Sellafield site has predictable, deeply descending, long groundwater flow paths with very slow local and regional groundwater movements

and low regional hydraulic gradients then the site could be construed as showing good promise as a repository.

The geology and hydrogeological investigations of this Sellafield site are summarised elsewhere (Nirex, 1992a; Nirex, 1993a; Nirex, 1993b). Based on these investigations it is widely recognised that there is a possibility that the regional groundwater flow pathways surrounding the proposed repository could be directed upwards (ERM, 1993; Royal Society, 1994; RWMAC, 1994). However none of these studies had, when this work was first undertaken, published simulations to support their work, or attempted to quantify the flow rates and pathways involved. Subsequent studies have attempted to simulate such groundwater movement (Heathcote *et al.*, 1996; Nirex, 1995).

3.3.3.1 Aims of project

Absolute flow magnitudes cannot be proved, verified, or validated by single models (Konikow & Bredehoeft 1992, Oreskes et al 1994). However, there is conceptual value in producing pictorial representations of flow directions which persist in simulations spanning the measured range of present-day permeabilities, and value in producing a numerical safety target which can be compared to field measurements. Thus the aims of this study were;

- to develop simple numerical fluid flow models, without modelling complex geology to determine the essential important features of the regional groundwater flow regime;
- to expand upon these models and test the robustness of the flow concept and flow simulator;
- to develop geologically realistic numerical models where the relative importance of hydrogeological parameters can be scoped out;
- to perform sensitivity analyses on these more complex models to test the robustness of both the conceptual model and the flow simulator;
- to determine the hydrostratigraphic units controlling flow rate through a potential repository and determine the relative importance of other hydrostratigraphic units;
- to compare vertical pressure profiles predicted from the model, with those measured in-situ by making use of the concept of hydraulic head, this would determine if any of the simulations could account for the high pressure conditions encountered at depth in borehole 2;
- to determine the "best fit" simulation by means of such comparisons;

- to determine the sensitivity of the "best fit" simulations to variations in hydrogeological parameters;
- to use the results of the "best fit" comparison study to develop safety case assessments by utilising the tracking of fluids in the simulations;
- to develop conclusions from the above simulations that have relevance to the safety of the proposed repository site.

3.4 Mathematical model

The region of flow in the Sellafield area has been defined in the conceptual model as being dominated by topographically driven fluids in both the fractured crystalline rocks of the BVG and the more permeable cover sediments. Near static conditions may occur in the highly saline fluids of the so-called Irish Sea Basin regime. The vertical section running perpendicular to the coast shown in Fig. 3.2 was used as the basis for the mathematical model of the regional flow system.

The simulation of fluid flow through rocks is a subject of great complexity (Cathles, 1990; de Marsily, 1986; Deming, 1994). Flow between the pore space of rocks enables groundwater flow to be described using a porous medium continuum approach (Bear & Yehuda, 1990). The presence of fluid flow in fractures can add further complexity (Garven, 1995).

3.4.1 Modelling methods

In fractured rocks (such as those of the BVG at Sellafield), the interconnected fractures are considered to be the main passages for fluid flow, with the solid rock matrix considered to be almost impermeable (Domenico & Schwartz, 1990). This results in wide ranges in hydraulic conductivity, with fracture conductivity many orders of magnitude greater than that of the matrix (Brace, 1980; Clauser, 1992; Neumann, 1990). Modelling flow in such a fractured system is obviously problematic (de Marsily, 1987; Freeze & Cherry, 1979), however this can be achieved by;

- modelling the fluid transport through each fracture or network of discrete fractures (Moreno & Neretnieks, 1993);
- modelling the transport regime in the fractured mass as an equivalent porous and anisotropic continuum (Follin & Thunkin, 1994).

The problem with the first approach is that the fractures/fracture networks have to be extensively mapped with information regarding the hydraulic conductivity, connectivity and geometry exhaustively recorded (Garven, 1994) which for large scale regional modelling is obviously somewhat arduous, although some numerical

models use stochastic methods to generate statistical fracture networks (Long *et al.*, 1991).

3.4.1.1 Porous-medium approach

In the second approach the fractured medium is viewed essentially as a porous medium, the obvious advantage of this being that models of this type are well understood by a wide array of geoscientists and engineers and there are numerous implementations available (Domenico & Schwartz, 1990). The extent of porous aquifers and high density of fracturing in the crystalline rocks of the Sellafield area precludes the need to consider individual fractures within such a regional system. Beyond such practical matters, if the spacing of fractures or fracture zones is less than the scale of numerical discretisation, or grid size, in the model then the equivalent porous media approach is justifiable (Garven, 1994). The porous medium is a favoured approach for regional 2-D modelling of fluid movement and has been applied by others to the Sellafield site (Heathcote *et al.*, 1996; Nicholls, 1995; Nirex, 1995) (Fig. 3.6 & 3.7).

3.4.2 Mathematical formulation

3.4.2.1 Fluid flow

When dealing with regional groundwater flow it is common to treat the porous-media continuum mathematical model as steady-state (Garven & Freeze, 1984a). The equation for the conservation of mass for steady state flow of a single phase fluid of density ρ is written as;

$$\nabla \cdot (\rho q) = 0 \qquad 3.1$$

where q is the specific discharge vector (often termed the darcy velocity), commonly presented in ms^{-1} and ∇, the differential operation, defined by

$$\nabla = \frac{\partial}{\partial x}\bar{i} + \frac{\partial}{\partial z}\bar{k} \qquad 3.2$$

with $\bar{i}$ and $\bar{k}$ are the unit vectors in the x and z directions (Garven, 1989).

The specific discharge vector q is given by the general term of Darcy's Law; (Garven & Freeze, 1984a);

$$q = -\frac{k}{\mu}(\nabla p + \rho g \nabla Z) \qquad 3.3$$

where k is the intrinsic permeability tensor. The tensor in 2-D is a matrix of four coefficients, symmetrical with respect to the diagonal (de Marsily, 1986);

$$\mathrm{k} = \begin{vmatrix} k_{xx} & k_{xz} \\ k_{zx} & k_{zz} \end{vmatrix} \text{ with } k_{xz} = k_{zx} \qquad 3.4$$

μ is the fluid viscosity at ambient conditions, p is fluid pressure, g is the gravitational acceleration constant and Z is the elevation above a datum.

The Sellafield region is composed of fluids which differ in density (brine, saline and fresh water). Therefore it is necessary to define relative viscosity $\mu_r = \mu / \mu_0$. Also the relative fluid density $\rho_r = (\rho_0 - \rho) / \rho_0$ where μ_0 is the reference state viscosity, defined at the same temperature, pressure and salinity as the reference state density ρ_0. This permits the model to employ the concept of equivalent fresh-water hydraulic head, h (Bear, 1972);

$$\mathrm{h} = \frac{\mathrm{p}}{\rho_0 g} + Z \qquad 3.5$$

If the permeability tensor k is replaced by hydraulic conductivity tensor K, where

$$\mathrm{K} = \frac{\mathrm{k}\rho_0 g}{\mu_0} \qquad 3.6$$

then equation 3.3 can be modified to be suitable for solving problems in groundwater of variable density (Garven, 1995);

$$\mathrm{q} = -\mathrm{K}\mu_r(\nabla h + \rho_r \nabla \mathrm{Z}) = \mathrm{v}\phi \qquad 3.7$$

where v is the average linear velocity or seepage velocity and ϕ is the porosity.

3.4.2.2 Heat transport

As most regional geological processes involve conductive and convective heat transport (Cathles, 1990; Deming, 1994; Deming *et al.*, 1992; Garven, 1995) it is necessary to develop an expression describing the conservation of thermal energy. For the case of a saturated porous medium under steady-state conditions, the conservation of thermal energy can be expressed as;

$$\nabla \cdot [\mathrm{E}\nabla \mathrm{T}] - \rho \mathrm{c} \mathrm{q} \cdot \nabla \mathrm{T} = 0 \qquad 3.8$$

where E is the combined thermal conductivity-dispersion tensor (derived from the thermal conductivity, porosity and thermal dispersion of the material), c is the specific heat capacity of water and T is temperature (Garven & Freeze, 1984a).

3.4.2.3 Mass transport

The transport of mass must be treated as a transient phenomenon, (Garven & Freeze, 1984a), thus equation 3.1 can no longer be dealt with as steady-state and a new term has to be introduced to the right hand side ;

$$-\nabla \cdot (\rho q) = \rho S_s \frac{\partial h}{\partial t} \qquad 3.9$$

where S_s is the specific storage coefficient; defined as the volume of water released from a unit volume of rock for a unit decline in head : units of m^{-1} (Brassington, 1988) and t is time.

3.4.3 Numerical formulation

The partial differential equations describing fluid flow, heat transport and mass transport shown above can be solved by numerical techniques such as finite difference and finite element methods (Huyakorn & Pinder, 1983). Finite differences are restricted to simple meshes and are not well suited to solving the transport equation. Consequently the complex geology, faults, and thus irregular geometry of the Sellafield area, makes the finite element technique most suitable for solving the flow equations above (Kazda, 1990). The code selected for this modelling study, OILGEN, a coupled heat and fluid flow code, (Garven, 1989), utilises the finite element method to solve these, and other, equations for steady state flow and transient mass transport in 2-D.

This 2-D steady-state and transient code was formulated to study groundwater movement in large saturated sedimentary basins over geological timescales (Garven, 1989; Garven & Freeze, 1984a; Garven *et al.*, 1993). Although fluid flow in the subsurface is a 3-D phenomenon (de Marsily, 1986), the general flow regime in the Sellafield area is that of topographically driven groundwater moving perpendicularly towards the coast (as outlined in the above sections) therefore the use of a 2-D fluid flow simulator is justifiable. Similarly since the rocks of the Sellafield area are "fully" compacted the solution of the *flow* equation rather than the *transport* equation is permitted to be steady-state (Garven, 1995), i.e., conditions in the region have been constant for so long that the groundwater flow regime and temperature distribution have reached an invariant state (Bethke, 1993).

3.4.3.1 Set up of numerical model

The first step in the numerical formulation of the mathematical model is the discretisation of the physical system into a series of finite elements, connected at a discrete number of nodal points (Huyakorn & Pinder, 1983). This can be achieved by digitising a simplified representation of the geology in the form of a grid of quadrilaterals (Fig. 3.8) or by using a simple FORTRAN code to generate a uniform grid of quadrilaterals. These quadrilaterals are subdivided into a set of triangular elements defined by their nodal co-ordinates (Fig. 3.9) (Garven & Freeze, 1984a).

3.4.3.2 Implementation

In the OILGEN code the discretised 2-D section must not exceed 2500 quadrilateral elements and must not be made up of more than 9 distinct material types (Garven, pers comm.). Each element is composed of a material that may have distinct rock properties such as porosity and permeability. Hydrostratigraphic boundaries within the mesh have no special qualities, and flow simply crosses between elements of different porosity and hydraulic conductivity. Flow rates are constant over individual elements, but discontinuous across element boundaries (Garven *et al.*, 1993).

The OILGEN code allows a spatially variable fluid salinity profile to be assigned to the grid. This can be done by means of a salinity gradient expressed as a linear vertical gradient of % NaCl m^{-1} from a datum point measured in metres from the base of the section or as an arbitrary distribution based on field data (Garven & Freeze, 1984a). The inclusion of such a variable salinity fluid profile is a simplification in that the salinity is constant in space and time and is not a fully coupled density-flow solution (Nicholls, 1995).

3.4.3.3 Solution procedure

At the start of the simulation, once the discretised section is read into the program (Fig. 3.10) the code develops matrix expressions for each equation which are combined to form the global matrix that describes the entire system (Huyakorn & Pinder, 1983). Once the prescribed boundary conditions are included, the code utilises the Galerkin weighted average formulation (de Marsily, 1986; Mercer *et al.*, 1975) to solve the flow equation to calculate the steady-state hydraulic head distribution. The Darcy velocities in each triangular element are then calculated for each node (Equation 3.7).

The steady state heat equation (Equation 3.8) is then solved to determine the temperature variation in the grid, then these new values of pressure and temperature

and the specified salinity profile are used to calculate fluid densities and viscosities from the equations of state (Kestin *et al.*, 1981). Utilising gaussian elimination (Bear & Verruijt, 1987) the code then iterates these steps until convergence of temperature change reaches less than 1°C.

It is important to point out that although the variable salinity profile is fixed in space and time (see above) the density and viscosity of the grid may not be. These can vary significantly with variations in temperature, although the former is only significant when large thermal gradients are encountered (e.g. if the modelled system extended to 8 km deep, where temperatures are greater than 240°C). Variable salinity would cause density gradients that could be altered by influx of rapidly moving colder water or simply by the iteration of the code to converge to less than the necessary temperature change of 1°C mentioned above.

3.4.3.4 Transient mass transport

As outlined in section 3.4.1 the transport of mass (in this case mimicking dissolved radioactive "particles") is treated as a transient problem and once the steady-state velocity distribution is calculated and the equation of conservation of fluid mass observed, mass transport is simulated using a moving-particle random-walk method (Bear, 1972; LaBolle *et al.*, 1996). During a prescribed time step, chosen carefully to ensure that tracer particles do not move further than the length of a finite element cell in any given time step (Garven & Freeze, 1984a), each particle is *advected* according to the magnitude of average linear velocity of the fluid in the element with *hydrodynamic dispersion* simulated by the displacement of the particle position by the random walk method (Bear, 1972), where the displacement is calculated from an expression relating the assigned longitudinal and transverse dispersion coefficients, time steps and a randomly generated number in the range 0-1 (Garven, 1989).

This method assumes that no interaction of particles ("radionuclides") with surrounding rock occurs, but simply monitors the progress of several hundred "water particles" released from the Repository at an arbitrary Time = 0 (Garven, 1989). Such water could conceivably be carrying dissolved radionuclides (Metcalfe & Crawford, 1994; Nuclear Energy Agency, 1993; Pearson & Scholtis, 1993). These particles have the same density and temperature as the surrounding water, so that they are passive indicators of water flow paths and dispersion, and do not have any inherent buoyancy or capillarity effects (Garven & Freeze, 1984a).

3.4.4 Numerical simulations

As outlined in section 3.3.2 the hydrostratigraphic units are defined fundamentally on the basis of their porosity, ϕ (expressed as a %) and hydraulic conductivity, K, (m/yr). Values for these were derived from published data (Michie, 1996; Nirex, 1992a; Nirex, 1993a; Nirex, 1995) (Table 3.1a) and for the purpose of this study have been simplified to ignore any variations in conductivity due to water salinity. The geothermal heat flux at the base of all the models was constrained at 70 mW/m^2 with the temperature at the water table of 15°C.

Table 3.2 gives the values already outlined in Table 3.1a for the "base case" hydraulic conductivity of the hydrostratigraphic units as well as extended modelled range in hydraulic conductivity for the Calder Sandstone and BVG. The hydraulic conductivity of the St Bees Sandstone, St Bees Evaporites, Brockram Breccia, cover faults and faults in the BVG were not previously reported as having a large range (Nirex, 1989; Nirex, 1992a). Reports recently published (Nirex, 1993a; Nirex, 1995) have extended the range of BVG hydraulic conductivity. The reports also indicate the possibility that these other units have much wider ranges in hydraulic conductivity. The modelled values for these are reported in Table 3.2 as well as the other parameters that are required to solve the relevant equations of fluid flow, heat transport and mass transport.

These are; a) for the fluid flow equation, the ratio of horizontal to vertical hydraulic conductivity (anisotropy; K_h / K_v); b) for the heat transport equation, the thermal conductivity ($Wm°C^{-1}$) and c) for the mass transport equation the specific storage coefficient (m^{-1}) and longitudinal and transverse dispersivities (m) (see transient mass transport part of section 3.4.3).

Values for anisotropy are commonly derived from lab-based data (Nicholls, 1995) but as this is a regional study it was more appropriate to use field-based values that reflect this. Therefore anisotropy values were abstracted from the literature (Freeze & Cherry, 1979; Garven & Freeze, 1984a) and are typical for the generic rock types encountered in the Sellafield area. For example the well bedded evaporites are highly anisotropic K_h / K_v =100 and the BVG much less so, K_h / K_v = 5. The storage coefficients of confined rocks can vary by as much as three orders of magnitude up to 10^{-3} (Brassington, 1988) and values used in this study were similar to those published elsewhere (Garven, 1989).

The thermal conductivities of most rocks lie in the range 1-8 $Wm°C^{-1}$ (Raffensperger & Garven, 1995) with many compilations of such data published in

the literature (Andrews-Speed *et al.*, 1984; Deming, 1993; Deming *et al.*, 1992). The values used in this study are similar to these, and other values used in studies published elsewhere (Fleming, 1996; Garven, 1989; Garven & Freeze, 1984b; Raffensperger & Garven, 1995). Similarly the coefficients of lateral and longitudinal dispersion are based on published material and upon advice given to the author (Garven, pers. comm.).

Two groups of simulations were run, a geologically realistic discretisation and a simpler computer-generated one. The geologically realistic model used the cross section shown in Fig 3.2 as its basis. This section was converted to a series of rows and columns, forming a finite element mesh of 2,100 quadrilaterals (Fig 3.8). Eight material types were assigned to relevant elements in the grid so as to represent the geological section.

Putative boundary conditions of the conceptual model were outlined in section 3.3.2. The boundary conditions of the mathematical model obviously have to reflect these and are therefore constrained such that the lateral (vertical) ends of the model are no-flow boundaries for fluids, heat and mass transport; the base is a no flow boundary but a uniform heat flux is specified across it; the upper (land) surface is the water table and is isothermal and isobaric, so that flow can pass up or down through this. Topographically-derived head is the major driving force for flow, although density induced flows are also permitted (see section 3.4.3).

This is obviously a very complex section so before performing any modelling it was sensible to perform experiments with a much simpler model (Fig. 3.11). This simpler grid had the same number of rows and columns, lateral and vertical extent, elevation at the land surface (representing the water table) and boundary conditions as that outlined for the more complex, geologically accurate model but was intended to give an outline as to the most relevant and important factors that may be encountered in the later simulations.

3.4.5 Experimental technique

Groundwater models can be used for contrasting purposes. In one approach, the conceptual model, as illustrated in section 3.3 is assumed to be correct, and the simulations are conducted for the purpose of making specific predictions and/or calibrating parameters which cannot be conveniently measured. A different approach is to use simulations to explore the ramifications of the conceptual model, and based on the results, perhaps to adjust it, as well as to assess the sensitivity of any predictions to uncertainties in the values or input parameters (Lerche, 1990).

The modelling performed in this study falls into the latter category - the main aim being to better understand which aspects are most crucial towards assessing the safety of this site.

At this site, there are good data on rock stratigraphy and geometry. However, there are many poorly known factors, such as hydraulic conductivity anisotropy, fault conductivity, and particularly the regional-scale conductivity of the BVG away from the boreholes. It is known from borehole data that the BVG has a fracture conductivity some 10^2 greater than matrix conductivity (Nirex, 1992a; Nirex, 1993a; Nirex, 1993b) as do most crystalline rocks (Brace, 1980; Brace, 1984; Clauser, 1992; Neuzil, 1986) (Fig. 3.12). For the purposes of the modelling performed in this study, borehole measurements (Nirex, 1992a; Nirex, 1993a; Nirex, 1993b) indicate that fluid flow in the BVG is controlled by fractures, which have a spacing of 50-100m. This is at least one fracture per finite element of the meshes, so that this can be treated as a matrix conductivity, (Follin & Thunkin, 1994; Neumann, 1990).

The approach used in this study was one of sensitivity analysis (Lerche, 1990) by undertaking a series of experiments with the numerical model. Before each simulation, a numerical attribute of the model was varied and the code run to completion. If the result did not change significantly from the previous experiment then that particular attribute was deemed unimportant. If the result did change, then it would be vital to measure that attribute as accurately as possible in the *actual* geological setting.

3.5 Simple case modelling results

3.5.1 Outline and format of graphical flow plots

The intention of this "simplistic" modelling was to develop an understanding of the fluid flow system that may be encountered given the prescribed boundary conditions, hydraulic parameters, density of fluids and the spatial relationships of the defined hydrostratigraphic units. Another reason for performing this modelling is to provide a comparison with the more complex grid to delineate if the pattern and rate fluid flow were affected by the orientation, size and shape of the grid cells and to explore the robustness of both the numerical simulator and the models.

For the fluid flow simulations the groundwater flow rates and directions are depicted by arrows representing the vector of the average linear velocity (from Equation 3.7) of fluid within a particular element. The tail of the vector is located in the centre of the relevant element. Each vector is scaled relative to the length of the arrow shown at the top of each plot. An element of standardisation has been applied in that for

the sake of comparison between plots the arrows are scaled to either 2, 20 or 200 m/yr. Crosses indicate that flow is less than 1% of the maximum for that plot, so that water could still be moving, but relatively slowly.

OILGEN calculates the hydraulic head distribution taking into account the variation in density, temperature and viscosity. However in the grid OILGEN plots hydraulic head as equivalent freshwater head, i.e. the height above ground surface *fresh* water would rise to under the pressure at the specified depth. Plots of equivalent freshwater hydraulic head are contoured from the Ordnance Datum (OD), i.e. sea level, and have contours spaced at 20 m intervals. Contours of equivalent freshwater hydraulic head indicate the possible hydraulic gradients in a flow system, with water having the potential to move from areas of high to low head, given a suitable route.

Contoured salinity plots begin at freshwater and have a contour interval of 0.02, thus a contour line representing 0.16 equates to 16 % NaCl or 160,000 mg/l Total Dissolved Solids (TDS). Temperature contours start at the constrained surface temperature of 15°C and have a contour spacing of 5 °C.

3.5.2 Homogenous hydrostratigraphy

The model is entirely composed of the Borrowdale Volcanic Group (BVG) hydrostratigraphic material type (Fig. 3.13) with the base case hydraulic conductivity value of 1.20E-02 m/yr, $K_h / K_v = 5$ and thermal conductivity of 4 $Wm°C^{-1}$. There is no salinity gradient so the fluid is freshwater throughout.

The freshwater hydraulic head contours (Fig. 3.14) show a relatively simple pattern with vertical high head in the highland area and very little vertical variation between the break in slope and the coast, before a strong vertical gradient beneath the sea to the west. These contours indicate that there is low vertical hydraulic gradient in the central part of the figure. The groundwater velocity plot (Fig. 3.15) confirms this; showing the topographically driven groundwater descending from the hills (where the 0.25 m/yr maximum flow is) travelling horizontally before travelling upwards and discharging at the OD. The crosses in the western part of the model indicate that there is flow occurring but at less than 1 % of the maximum.

3.5.3 Heterogeneous hydrostratigraphy 1

3.5.3.1 BVG and sediments

The model has a thick sequence of Permo-Triassic sediments; the St Bees Sst (SBS) and Calder Sst (CS) onlapping the BVG; mimicking the real hydrostratigraphy (Fig. 3.16). There is no salinity gradient and all units have the base case values; BVG as

before, the Calder Sst. and St Bees Sst. having hydraulic conductivities of 3 and 1.5 m/yr respectively, $K_h / K_v = 10$ for both units, and thermal conductivity = 3.1 $Wm°C^{-1}$ for both units.

Fig. 3.17 shows the contoured freshwater hydraulic head, showing a similar pattern to before; again a strong topographic-derived vertical gradient in the upland areas, little vertical gradient in the central part, but in this simulation the contours are deflected at the boundary between the sediments and the BVG and the vertical gradient beneath the sea is less pronounced. This is confirmed by the velocity plot (Fig. 3.18) which shows that the maximum flow of 1.58 m/yr occurs in the Calder Sst. and the majority of flow is in the sediments, with lateral flow and discharge at the OD although there is again topographically driven flow in the BVG, again descending and laterally transferring.

3.5.4 Heterogeneous hydrostratigraphy II

3.5.4.1 BVG, sediments and low permeability units

Fig. 3.19 shows the hydrostratigraphy modelled in this more complex experiment. The permeable Calder Sst. and St Bees Sst. are almost completely separated from the BVG by a thin ~200 m layer of low permeability, anisotropic sediments, representing the St Bees Evaporites/Brockram (SBEB). The parameters for the other units are as before and again there is no salinity gradient. The hydraulic conductivity of the SBEB is 9.46E-04 m/yr with $K_h / K_v = 100$ and thermal conductivity = 4 $Wm°C^{-1}$.

Two separate runs were made with this modelling scenario. The BVG set at its median hydraulic conductivity of 1.20E-02 m/yr and the 1.2 m/yr higher value that Nirex (1992a) had previously equated to the highest measured value in boreholes in the Sellafield area (Haszeldine & McKeown, 1995; McKeown & Haszeldine, 1995); the modelling runs with higher permeability BVG highlight some interesting features that are "masked" in the median permeability runs.

3.5.4.2 Median permeability BVG

The freshwater hydraulic head contour plot (Fig. 3.20) shows a markedly different pattern to the previous modelling runs. The contours again show a topographically-derived gradient in the upland areas and little vertical gradient in the sediments but the contours are very close together in the SBEB suggesting high vertical gradients in this unit. This would be a sensible result as the permeability of this unit is so low that the pressure of fluid (and by definition the head) attempting to penetrate it would be increased. The junction between the St Bees Sst. and the BVG that is not

separated by the SBEB does not have tight contours in it, rather the contours indicate a possible diagonal transfer from the BVG to the sediments. This is confirmed by the velocity plot (Fig. 3.21) which shows that although the maximum flow is again in the Calder Sst. (1.58 m/yr) there is an upward trend to the groundwater path in the BVG once it has descended from the upland areas.

3.5.4.3 Higher permeability BVG

This feature of diagonally, upward-trending topographically-driven groundwater is also shown in Fig. 3.22 that has the BVG hydraulic conductivity set to 1.2 m/yr. There is again little vertical gradient in the sediments but the freshwater head contours are even more tightly packed in the SBEB unit. The trend for diagonal transfer is highlighted by the orientation of the contours at the sediment/BVG boundaries. The groundwater velocity plot (Fig. 3.23) again shows this well. The "masking" effect of the sediment/BVG permeability relationship is decreased by setting the BVG to 1.2 m/yr. This plot indicates that flow is descending at a maximum of 24.97 m/yr in the BVG, is unable to penetrate the low permeability SBEB and ascends to transfer into the sediments via the sediment/BVG interface. There is also some evidence of outflow (springs) near the base of the slope in the top surface BVG.

3.5.4.4 Variable salinity solution

As has been shown, the groundwaters in the Sellafield area are not of uniform salinity. Salinity varies considerably in both the horizontal and vertical directions. It is therefore imperative that the simulations can include such variations. As the code did not provide a fully-coupled density flow solution, the spatially varying groundwater density is modelled by prescribing fixed salinities to each node of the grid, which are then used to calculate densities (see implementation part of section 3.4.3). Fig. 3.24 shows the variation in salinity prescribed to the grid. This variation is broadly similar to that encountered at Sellafield in that there is a highly saline brine (up to 16 weight % NaCl equivalent) to the west with freshwater overlying moderately saline (2 weight % NaCl equivalent) to the east (Bath, 1995; Bath *et al.*, 1996; Black & Brightman, 1996) (Fig. 3.3, Fig. 3.4).

When the above setup (base case hydraulic conductivities plus high permeability BVG) was run with the inclusion of a variable salinity fluid the *equivalent* freshwater hydraulic head plot (Fig. 3.25) showed a marked difference to that of the freshwater solution (Fig. 3.22). There is now much greater head at depth beneath the sea to the west, indeed the head for the area around the brine is much greater than before. The contours are again tightly packed in the SBEB but they feather out

in the area of the brine allowing a maximum of nearly 200m head to be reached in the base of the brine area, and a higher head in the deep part of the central area.

The groundwater velocity plot (Fig. 3.26) shows that the maximum flow of 25 m/yr is again in the BVG with, again, some evidence of springs near the base of the slope. Although not apparent from the equivalent freshwater hydraulic head plot there is a convective "eddy" of groundwater recirculation at the base of the model at around 4 km in the x-axis, with possible deflection to the groundwater flow field that exaggerates the upward trend of the flow in the BVG. Since the head plot did not show the convective eddy this highlights that the code allows density induced flows that would not be predicted purely from topographic head and that it is not due to the no flow basal boundary.

3.5.5 Summary and conclusions from simple modelling

This simple modelling of both the base case and higher permeability BVG showed:

- BVG homogenous grid — topographic flow, transverse movement across section;
- BVG and sediments — topographic flow and flow in sediments;
- BVG, seds & SBEB — topographic flow, high head in SBEB and "diagonal" transfer into sediments, regardless of BVG permeability;
- Variable salinity — topographic flow, high head in SBEB, "diagonal" transfer into sediments, high head in brine area, high head at depth in central area, eddy and upward deflection of groundwater flow in BVG.

In conclusion, the simplistic modelling of groundwater flow showed that topographically-driven groundwater flow in the BVG occurred regardless of the inclusion of more permeable sediments, less permeable barriers or variable salinity. Indeed the presence of the last two actually increased head with the salinity variation having a marked effect on head in the areas affected by brine.

3.6 Scoping study of geologically realistic model

To further develop on the conclusions reached from the simplistic modelling base case and higher permeability BVG, runs were made with the geologically realistic finite element mesh described in section 3.4.4 and shown in Fig. 3.8. Three distinct simulations were run in this study to determine the relative importance of;

- the presence or absence of faults
- the inclusion of variable salinity groundwater
- anisotropy in the BVG

If an attribute was found to be important it was included in further modelling runs.

3.6.1 No faults

The first simulations were run with no faults (Fig. 3.27), i.e. the hydrostratigraphic units are simply offset and there are no columns of hydrogeologically distinct material. Apart from the absence of faults the geology is identical to that of the cross section shown in Fig. 3.2 which is similar to sections used in other modelling studies of Sellafield (Nirex, 1992a; Nirex, 1993a).

3.6.1.1 Median permeability BVG

This simulation has all the hydrostratigraphic units set to their median or "base case" values (Table 3.1a). The freshwater hydraulic head plot (Fig. 3.28) shows that the more realistic geological model produces a very similar head plot to that of the simple base case model outlined in section 3.5.4.2 (Fig. 3.20) although the differences in the geometry of the geological units causes some variation. The contours indicate a topographically-derived head gradient in the upland areas and little vertical gradient in the sediments with high head gradients in the low permeability St Bees Evaporites and Brockram Breccia.

Possible "diagonal transfer" is again highlighted by the head contours at the BVG/St Bees Sandstone junction. The velocity plot (Fig. 3.29) shows that although the maximum flow is in the Calder Sst. (4.04 m/yr) there is an upward trend to the groundwater path in the BVG once it has descended from the upland areas. This is an important result as the similarity in output of this and the simple base case (Fig. 3.20) indicates that the shape and size of the grid cells is not significant to the solution.

3.6.1.2 Higher permeability BVG

This similarity between the simple and more complex model is highlighted when the BVG hydraulic conductivity is set to 1.2 m/yr. As in section 3.5.4.3 (Fig. 3.22) the higher value for hydraulic conductivity in the BVG causes a more pronounced head gradient in the low permeability horizons (Fig. 3.30) with the maximum flow (13.95 m/yr) now occurring in the highlands of the BVG (Fig. 3.31) and more rapid topographically driven groundwater descending, then ascending to diagonally transfer into the sedimentary cover. The offset nature of the Brockram and BVG appears to have caused a concentration of fluid in the central part of the figure. Again, there are some springs at the break in slope.

It appears then that, in general terms, the pattern of head and groundwater velocity when "unfaulted" models are run with either a simple, uniformly spaced, computer-generated finite-element grid or a complex variably discretised grid are very similar and that the variations in grid cell size and shape is unimportant.

3.6.2 Faults

Although the head and flow calculated from the above complex models are useful, when compared to the observed freshwater head in the Sellafield area (Fig. 3.32) there are marked differences. This figure, although shorter in extent, is of similar scale to the groundwater flow models and shows that the freshwater head contours determined from pressures measured in the field are markedly different from that of the model without faults. This and the fact that it is well known that ALL of the rocks of the Sellafield area are heavily faulted (Michie, 1996; Millward, 1995; Millward *et al.*, 1994; Taylor *et al.*, 1971) meant that it was imperative that simulations were performed with faults included as distinct hydrogeological units (Fig. 3.33) rather than simply as "offsets".

3.6.2.1 Size scaling of fault permeabilities

An important parameter when modelling groundwater flow in faults is transmissivity *(T)*, defined, most simply when hydraulic conductivity (K) is isotropic, as :

$$T = Ke \qquad 3.10$$

where e is the width of the fault aperture (de Marsily, 1986; Huyakorn & Pinder, 1983). This relationship was used when modelling the effect of faults in the simulations. Faults were treated by modelling artificially wide quadrilaterals, but with correspondingly reduced conductivity. Consequently, as faults were isotropic in all simulations, the "effective" transmissivity is as it should be. For example a real fault 1m wide, 30 m/yr conductivity, is modelled as 100m wide, 0.3 m/yr hydraulic conductivity.

Preliminary simulations performed in the early stages of this study and previously published, (Haszeldine & McKeown, 1995; McKeown & Haszeldine, 1993; McKeown & Haszeldine, 1995) utilised values of hydraulic conductivity for faults in the sediments and BVG of 300 m/yr and 1 m/yr respectively. Recently published data indicated that a revision of these values was necessary. The 300 m/yr value for the faults in the sediments was derived as a log mean of published EPM and pumping tests (Nirex, 1993a). The inclusion of pump tests values may be spurious as only very productive faults were sampled (Nicholls, 1995). Therefore a high

value for the faults in sediments may not be representative of the average hydraulic conductivity of the majority of the faults, although the effects of very high hydraulic conductivity faults are dealt with in section 3.7.4.

The measured hydraulic conductivity values (Table 3.1a) used as "base case" for faults in the sediments and BVG, of 30 and 3 m/yr respectively are similar to values reported in other modelling studies (Heathcote *et al.*, 1996; Nicholls, 1995; Nirex, 1995). The faults in the OILGEN model shown here are, in general, some 100 times wider than those observed in the field (Nirex, 1993a) and a "base case" was therefore represented in these simulations by modelling faults as isotropic units with K = 0.3 and 0.03 m/yr for the faults in the cover and BVG respectively.

3.6.2.2 Median permeability BVG

The immediate result of the inclusion of faults is that for the complex model, when base case values are used (Fig. 3.33), the freshwater hydraulic head contours are markedly different (Fig 3.34) to the no fault simulation, and also different to the measured head. There is some offset of head contours across the faults, due to the difference in hydraulic conductivity of the BVG "matrix" and faults. The overall head contour pattern is now very similar to that shown in Fig. 3.17 where the grid was composed of base case BVG, sediments and no low permeable units. This indicates that the presence of faults allows fluid exchange across the low permeability St Bees Sst. and Brockram Breccia horizons, with very low vertical gradients in the central part of the figure and lateral transfer of fluids. Again this confirms that the cell shape and size is unimportant to the solution.

This, of course, seems reasonable, as shown in Fig. 3.35, the faults act as channels to fluid transfer between the topographically driven fluids in the BVG and the seaward discharging waters of the Calder Sst. (maximum flow in the faults of the Calder Sst. = 2.04 m/yr). Although there is a sharp diagonal upturn in the shape of the finite element grid (Fig. 3. 8) at around 9 km (in the x-axis) the velocity vectors remain horizontal. This shows that the orientation of the grid cells is relatively unimportant. Two flow regimes are becoming apparent, one in the BVG, with some upward cross connection to a separate, seaward-flow system in the Calder Sst..

3.6.2.3 Higher permeability BVG

The comparison between the observed, natural freshwater head contoured from measured pressure in boreholes (Fig. 3.32), and that calculated by the model is improved somewhat when the simulations are run with the hydraulic conductivity of the BVG set at 1.2 m/yr (Fig. 3.36). There is again some offset of head contours

across faults in the BVG. The higher head gradients in the central part of the plot, close to the thrust up block of Brockram Breccia (BB) are a better match, although there is a poor correlation at depth beneath the coast. The groundwater velocity plot (Fig. 3.37) shows topographically driven flow in the BVG, maximum flow rate of 14 m/yr in the BVG uplands with small springs at the break in slope. The BVG groundwater travels laterally, passing through the faults that cross the low permeability St Bees Sst. and Brockram Breccia and ascending into the St Bees Sst. and Calder Sst. before possible discharge at the OD.

3.6.2.4 Flow rate through repository

As well as determining the importance of faults to the flow path, the flow rate is of obvious concern when determining the relative safety of a proposed repository. With this is mind both the "no faults" and "faults" simulations were run over the entire modelled range of BVG hydraulic conductivity (Table 3.2). The OILGEN code produces numerical values that can be interrogated for particular nodes or elements of the mesh and thus the velocity of groundwater through the element that relates to the position of a putative repository (Fig. 3.38) can be extracted (Table 3.3).

The results presented in Table 3.3 show that there is very little difference between the "no faults" and "faults" cases for groundwater flow rate through the repository. The faults do affect the head pattern and the head gradients in the region and there is much borehole and geological evidence for their presence. Faults were therefore included in all subsequent runs with "real-world" hydraulic conductivities of 3 m/yr for cover faults and 0.03 m/yr for the BVG faults (unless stated otherwise). These are 100 times greater than the values used in the model. In effect these are equivalent to values used in other studies (Heathcote *et al.*, 1996; Nicholls, 1995; Nirex, 1995).

3.6.3 Variable salinity groundwater

As mentioned previously there is a highly variable salinity distribution in the Sellafield region, effectively three salinities are apparent; fresh, saline and brine. The position of the saline/brine interface and density variation (Fig. 3.39) is reasonably well established from field measurements in boreholes 1, 2, 3, 4, 5, 10 and 12 (Nirex, 1993a; Nirex, 1993b). So suitable values of salinity were calculated from total dissolved solid (TDS) calculations from Discrete Extraction Tests (DET) from boreholes 2 and 3. These were used to generate a spatially variable salinity profile that would be a reasonable salinity profile observed in the field (Fig. 3.40). This

does not have to match the published density variation profile exactly as this itself is interpolated and possibly inaccurate (Nicholls, 1995).

3.6.3.1 Median permeability BVG

As can be seen from the equivalent freshwater hydraulic head profile in Fig. 3.41, the inclusion of variable salinity, and thus density, causes a head profile closer to that determined from field observations; there are high hydraulic gradients in the BVG uplands, indicating a potential for topographically-driven descending groundwater; potential for diagonally-ascending fluid in the central part of the system; very high heads at depth in the brine area and again some offset of head contours across faults in the BVG.

The potential for discharge at the OD from fluids in the Calder Sst. is again apparent. When the velocity plot is considered (Fig. 3.42) there is some topographically driven groundwater in the BVG that appears to ascend into the central part of the figure and transfer, through faults in the Brockram Breccia and St Bees Evaporites, to the cover of Calder Sst. and St Bees Sst.. The maximum flow (2.04 m/yr) is in the Calder Sst. with groundwater transversely moving through the Calder Sst. and St Bees Sst. before discharging at the OD.

3.6.3.2 Higher permeability BVG

The higher permeability BVG simulation (Fig. 3.43) shows higher vertical heads in the central part of the figure where the contours cross the Brockram Breccia. Again there appears to be potential for topographically driven groundwater in the upland BVG, ascending and transversing the Brockram Breccia and St Bees Evaporites, with high heads again at depth in the area of the brine. The velocity plot (Fig. 3.44) conforms to the previous pattern, with maximum flow in the upland BVG (14.02 m/yr), small springs at the break in slope, gravity-driven descending groundwater travelling laterally into the central part of the region, ascending and passing through the faults that cross the low permeability St Bees Sst. and Brockram Breccia and ascending into the St Bees Sst. and Calder Sst. before possible discharge at the OD. The eddy outlined in the simple case (Fig. 3.26) is apparent in this simulation also, with some apparent deflection of velocity vectors and enhanced upward flow.

3.6.3.3 Flow rate through repository

Table 3.4 shows the results of comparing the no salinity gradient simulations with that of variable salinity models. Although the presence of the variable salinity fluid has little effect on the flow rates of fluid through the repository, it is more realistic to include such a variation as it is patently incorrect to simply treat the Sellafield area

as a purely freshwater environment. The inclusion of variations in salinity together with high permeability BVG, appears to produce equivalent freshwater head profiles that are closely similar to those calculated from in-situ pressures in boreholes.

3.6.4 Variations in BVG anisotropy

Anisotropy was examined by changing the BVG K_h / K_v value from 5, to 1. As can be seen in Figs. 3.45 and 3.46 this produced more exaggerated head and flow regimes with much greater flow in the upland area (maximum 30 m/yr), due to increased vertical hydraulic conductivity. This appears to be confined to the eastern part of the model, however, as the overall head contour pattern is similar to before. The main result is that flow through the repository was little affected (Table 3.5). This suggests that the direction and rate of flow in the BVG is not controlled by the shape of the finite element cells, and that the cross-sectional area of the BVG is so large that fracture orientation may have little importance in the real world. Subsequent simulations were assigned a BVG K_h / K_v value of 5.

3.6.5 Summary and conclusions from scoping study

The more complex modelling of both the base case and higher permeability BVG shows that when dealing with the hydraulic head profiles the inclusion of variable salinity fluid is essential in maintaining the match with head calculated from in-situ pressure; faults allow transfer of fluids across regionally extensive flow barriers and anisotropy had an effect on upland flow. These attributes do not appear to markedly affect the rate of groundwater flow through a potential repository volume.

3.7 Sensitivity analyses of Calder Sst. and BVG permeability ranges

As outlined in section 3.3.2 the original data used in the early stages of this study indicated that only two hydrostratigraphic units, the Calder Sandstone and the BVG, had substantial ranges in hydraulic conductivity. These two units are significant to the geological and radiological problem. The BVG needs to have low flow to retain radionuclides in the repository. The Calder Sandstone, being a rapidly flowing freshwater aquifer also plays a role in the safety case of the repository. The rapid flows have the possibility to dilute and disperse any release of radionuclides.

To this end these two units were modelled with the range of hydraulic conductivities shown in Table 3.2. The Calder Sst. (CS) was modelled with hydraulic conductivity of 3, 30 and 300 m/yr for the entire range of BVG hydraulic conductivity 1.20E-05 to 1.20E+01 m/yr. The BVG hydraulic conductivity of 1.2 m/yr used in previous parts of this study is still somewhat less than the maximum measured in the field in

the Sellafield area, as outlined in section 3.3.2(Michie, 1996; Nirex, 1993a). Therefore the modelled range is extended to 12 m/yr.

3.7.1 Calder Sandstone (CS)

To aid comparison, the figures used in the following section are arranged with the two head plots one after the other (similarly for the velocity plots). In these simulations all the hydrostratigraphic units are set to the base case values and the Calder Sst., is the only unit varied. Varying the Calder Sst. hydraulic conductivity from 3 m/yr (Fig. 3.47) to 300 m/yr (Fig. 3.48) has very little effect on the hydraulic head regime in the Calder Sst., and no effect on the head elsewhere in the region.

The difference becomes apparent when comparing velocity plots (Figs. 3.49 & 3.50). The maximum flow of 192 m/yr occurs in the Calder Sst. when its hydraulic conductivity is set at 300 m/yr. Once again the flow regime is defined by the topographic drive causing descent, transverse flow and ascent through faults in the low permeability units, then into the sediments. The eddy currents caused by the brine are again apparent. In the case of high permeability Calder Sst. the scale of the arrows makes this difficult to interpret. When all simulations of varying hydraulic conductivity of the Calder Sst. are plotted (Fig. 3.51) and tabulated (Table 3.6) varying the Calder Sst. hydraulic conductivity has no effect on the flow rate through the repository.

3.7.2 BVG

Again for these simulations the plots are arranged to aid comparison. All hydraulic conductivities are as the base case, except the Calder Sst. which is set at 30 m/yr, and the BVG varied from 1.20E-05 to 1.20E+01 m/yr. Fig. 3.52 shows the equivalent freshwater hydraulic head results of a simulation where the BVG is set to the base case value of 1.20E-02 m/yr, and in Fig. 3.53 the BVG is set to the maximum modelled of 12 m/yr. The most noticeable difference between the runs is the higher vertical gradients in the central-western part of Fig. 3.53. The higher head in the St Bees Evaporites, Brockram Breccia and Carboniferous limestone results from the large hydraulic conductivity contrast between the high permeability BVG and these low permeability units in the simulation with the BVG set to 12 m/yr.

When the velocity plots are compared, the maximum flow in the run with the BVG set to 1.20E-02 m/yr is 19.39 m/yr in the Calder Sandstone (Fig. 3.54) compared to 139.08 m/yr in the BVG for the maximum modelled flow rate (Fig. 3.55). The similar flow pattern observed in all of the runs is apparent in both simulations. The

topographic drive causing rapid descent, transverse flow and ascent through faults in the low permeability units, then flow upwards into the sediments. The eddy currents caused by the brine are again apparent.

The main difference between runs where the Calder Sst. hydraulic conductivity is increased and those runs where BVG hydraulic conductivity is increased is highlighted in Table 3.6. The log hydraulic conductivity v log repository flow rate is shown in Fig. 3.56. In these 21 experiments, flow rate through the repository is directly related to BVG hydraulic conductivity regardless of the Calder Sst hydraulic conductivity. The pattern of flow direction remains similar in all cases, with upward flow at the 650 -1,000 m bOD depth proposed for the repository.

3.7.3 Summary and conclusions from varying Calder Sst. and BVG

In a (fictional) homogenous system, the velocity of fluid through a porous medium should be linearly related to the permeability (given that other parameters remain constant). However, there may be no simple relationship between permeability and flow in a complex system within which there are considerable spatial differences in material properties.

Surprisingly there are simple, log linear relationships present in the simulations reported above. The fluid velocity through the BVG element representing the repository is dependent upon the hydraulic conductivity of the BVG but independent of the hydraulic conductivity of the Calder Sandstone. As these two hydrogeological units may be significant elements of the regional flow system, the observed relationship indicates that these units are hydrologically de-coupled. That is, their circulation patterns are controlled by essentially separate influx/outflux sites and their driving energies are separate.

The only contribution of the Calder Sandstone aquifer to the repository safety is the possible seaward transport, dilution and dispersion of any waters and radionuclides migrating upwards from the repository through the BVG. The pattern of flow through the repository is persistently upwards, through several decade values of BVG conductivity experiments. These flow patterns imply that water from the repository could eventually reach the surface as springs in the BVG outcrop, or by dispersion within the Calder Sandstone. Hence the proposed repository position would need to engineer against natural groundwater flow, rather than be assisted by it.

3.7.4 Sensitivity of other variables

As already mentioned the original modelling performed for this study was undertaken with the expectation that the Calder Sst. and BVG would have the widest range in values of hydraulic conductivity. In order to scope out the effects of variations in other units simulations were performed where

- St Bees Sst. hydraulic conductivity was varied over the range 1.5, 15 and 150 m/yr;
- Faults in the cover sequence were varied over the range 0.3, 3 and 30 m/yr (as mentioned above these over-wide faults simulate "real world" faults with actual hydraulic conductivities of 30, 300 and 3000 m/yr);
- Faults in the BVG were varied over the range 3.00E-04, 3.00E-02 and 3.00E+00 m/yr (as above simulating "real world" faults of 0.03, 3 and 300 m/yr);
- The low permeability St Bees Evaporites and Brockram Breccia modelled over the range 1.50E-03, 1.50E-01 & 1.50E+00 m/yr.

3.7.4.1 St Bees Sandstone

Table 3.7 and Fig. 3.57 show that varying the St Bees Sst. hydraulic conductivity for the entire range of BVG hydraulic conductivity has no effect on the flow rate through the repository. Thus the St Bees Sst. is unimportant with regard to flow rates but could still contribute to containing radionuclide leakage by dispersion and dilution, but this is uncertain and minor.

3.7.4.2 Faults, St Bees Evaporites and Brockram Breccia

In order to model the effect of varying the hydraulic conductivity of the cover faults, BVG faults, St Bees Evaporites and Brockram Breccia, the simulation where BVG hydraulic conductivity was set to 1.2 m/yr was run for the range of values outlined above. As can be seen in Table 3.8, the variation of these attributes had very little effect on the flow rate through the repository and can be thought of as unimportant as regards flow rates.

3.7.5 Comment on sensitivity analysis

The general flow pattern is extremely robust for all variables outlined in this section and is very similar to that of the simplistic modelling, i.e., topographically driven groundwater descending, advecting to the west, traversing low permeability units via faults and generally moving upwards to surface. This is assisted by deflection eddies, caused by density induced flows from areas of high salinity. Lateral movement of fluids in sediments has little effect on flow regime. The similarity between the complex geology models and simplistic models indicates that the shape

and size of the finite element cells is not relevant to either the flow rate or the flow path, nor indeed to the numerical solution of the flow and heat transport equations. This gives confidence in the OILGEN code.

3.8 Comparison of calculated and measured freshwater hydraulic head

3.8.1 Outline

It is always useful to compare the result of a modelling simulation to observational data. Naturally there are limits to the usefulness of this comparison if the model is specifically "tuned" to calibrate with the observed data, as there is always the possibility of getting the right answer for the wrong reasons. It has been maintained elsewhere (Black & Brightman, 1996; Heathcote *et al.*, 1996) that if there is a spatially varying solution density in either the vertical or horizontal plane no information on the potential for flow in the 1-D vertical plane can be derived from vertical plots of freshwater hydraulic head and the use of *environmental* head is required (Bachu, 1994; Lusczynski, 1961). However freshwater head is calculated from the pressure measured in situ and is therefore a true representation of the hydraulic head at a given point in the subsurface, i.e. the height above the ground surface *fresh* water would rise to if a route was available.

Since OILGEN, although calculating head taking into account variations in temperature, viscosity and more importantly density, represents head as equivalent freshwater head it is instructive to perform a comparison between calculated *equivalent freshwater head* and observed *freshwater* head in boreholes of the Sellafield area. *No* information regarding vertical head gradients is inferred from these comparisons. The position of boreholes 2 and 3 are shown in the cross-section used as the basis for the complex grid (Fig. 3.2) The OILGEN code can generate an output file that has equivalent freshwater hydraulic head values in any chosen vertical 1-D section.

3.8.2 Measured head plots

The observed freshwater head plots (Figs. 3.58- 3.65) were derived from published data (Nirex, 1992b) and represent spot results from Environmental Pressure Measurement (EPM) tests. Note that the head values have been portrayed with respect to Ordnance Datum (OD). This takes into account the land topography vertically above the borehole. Dealing with the measured freshwater hydraulic head in borehole 2 first (Fig. 3.58) it is apparent that there is a distinct increase in head with depth, with a maximum of around 150 m at the base of the borehole 2. The step-wise increase in head, punctuated at 350 and 600 m bOD is interrupted by a distinct drop in head between 800 and 1200 m bOD. Borehole 3 (Fig. 3.59) has a

generally low head (< 50 m) down to 800 m bOD, below this depth the head increases to a maximum of around 150 m at the bottom hole.

3.8.3 Varying the BVG hydraulic conductivity

The earlier sections have illustrated that the BVG is the most important unit in the modelling simulations. Head comparisons were performed for borehole 2 and 3 where all the units are set to their base case values and the BVG is varied from the base case value of 0.012 m/yr to 0.12 & 1.2 m/yr (Fig. 3.58). There is a step-wise component in the head increase in borehole 2. None of the simulations could match the variation in head between 800 and 1200 m bOD. However, it has been reported that the BVG becomes more heterogeneous below 800 m bOD (Nirex, 1993a) and since the BVG was treated as a homogenous material in this study it is unlikely that a good fit throughout will be made to measured head. The important zones are 0 - 700 m and the average trend continued to 1150 - 1500 m.

As the target depth of the repository is 650 m bOD it is significant that the simulation with the BVG hydraulic conductivity set at 1.2 m/yr has the best match to observed head in borehole 2 down to 700 m bOD (Fig. 3.58). This simulation also provides a fair, but not perfect, match to the deeper head data; 1150 - 1500 m. Other modelling studies of groundwater flow in the Sellafield area (Heathcote *et al.*, 1996; Nicholls, 1995; Nirex, 1993a; Nirex, 1993b; Nirex, 1995) have been unable to reproduce the relatively high heads at depth in the BVG.

The same range in BVG hydraulic conductivities are used to compare equivalent freshwater hydraulic head calculated from the model and head measured in-situ in borehole 3 (Fig. 3.59). There is little difference between the simulations down to 750 m bOD but the better fit at depth is again for the simulation where the BVG is set to 1.2 m/yr.

3.8.4 Faults, St Bees evaporites and Brockram Breccia

Simulations were performed to test if variations in the hydraulic conductivity of the St Bees Evaporites, Brockram Breccia and faults in the cover and BVG had an effect on comparisons between observed head in boreholes 2 and 3 and that calculated with the model. Comparisons were made where the BVG is set to 1.2 m/yr and the other units set to their base case values before variations were made in their hydraulic conductivity.

3.8.4.1 Brockram Breccia and St Bees Evaporites

When the hydraulic conductivity of these low permeability units is increased by 100 and then by 1000 times there is a slight decrease in predicted head down to 700 m bOD in borehole 2 (Fig. 3.60) for the highest permeabilities. Likewise the calculated head at 1400 m also decreases slightly. As this is only a variation of around 5-10 metres this is not significant. The match to measured head in borehole 3 is unaffected (Fig. 3.61). The hydraulic conductivity of these units do not greatly affect the head calibration.

3.8.4.2 BVG faults

Faults in the BVG were varied over the range 3.00E-04, 3.00E-02 and 3.00E+00 m/yr. As outlined above this simulates "real world" faults with hydraulic conductivity of as much as 300 m/yr. As this is more than an order of magnitude greater than fault permeabilities used in similar studies (Nicholls, 1995) it is interesting to note that such a variation has a negligible affect on the calculated head in both boreholes 2 and 3 (Figs. 3.62 and 3.63). Thus the permeability of the faults in the BVG has no major effect on the head calibration.

3.8.4.3 Cover faults

In contrast, the results of varying the hydraulic conductivity of the cover faults over the range 0.3, 3 and 30 m/yr does have an effect on the match between freshwater head measured in-situ and that calculated from the model. In borehole 2 the match down to 700 m bOD is poor for the simulations where the hydraulic conductivity of the cover faults is set to 3 m/yr and even poorer when set to 30 m/yr (Fig. 3.64). When the hydraulic conductivity of the faults is set to 3 m/yr this equates to 300 m/yr and 30 m/yr equates to 3 km/yr (an unlikely, extreme value). It is therefore hardly surprising that such highly permeable faults disrupt the flow system so much that the calibration with head breaks down. Simulations were also performed (not shown) with the hydraulic faults set to 0.03 m/yr (equivalent to a "real world" 3 m/yr). This caused a very minor increase in the predicted head down to 700 m bOD. This breakdown in the calibration of calculated head with observed head is reflected in the progressively poorer comparison with heads in borehole 3 (Fig. 3.65).

3.8.5 Summary and conclusions from head calibration

The comparison of in-situ freshwater head with that calculated from the numerical model indicates that the best fit simulations are those where the BVG hydraulic conductivity is set to 1.2 m/yr, and that the variations in low permeability horizons, faults in the BVG and (within reasonable limits) the cover faults, have very little

effect on the good fit produced. This calibration provides the basis for transient mass transport simulations.

3.9 Transient mass transport modelling

3.9.1 Set up of transient mass transport simulations

The use of OILGEN to simulate transient mass transport has been outlined in section 3.4. This feature of the code was used to provide a visual guide to the degree of physical containment the BVG and overlying sediments may afford. Any effects of enhanced flow due to thermal buoyancy of water from a warm repository, or vertical leakoff of H_2, CH_4 and CO_2 gases generated from the repository are ignored (Chapman, 1994). The particles have zero mass and once the steady state flow field is established, a number of particles are released from a specific point and tracked through time across the model. Since they have the same buoyancy of the ambient fluid they are passive indicators of the groundwater flow path and indicate the actual time repository fluids would take to reach the surface.

The simulations were run with the BVG set to the best match 1.2 m/yr hydraulic conductivity (outlined above). Fluid flow through porous media, or through fractures, usually moves preferentially along the highest conductivity conduits, rather than uniformly through the whole anisotropic medium. Consequently, this "average" modelling will tend to under-estimate maximum flow rates. The code is run iteratively to achieve the tracking simulations, with a time step of just 3 years for each iteration. This ensures that a tracer particle does not jump between finite element cells. 500 tracking particles were "released" at one time. Values of storage coefficient, and longitudinal and transverse dispersivity are given in Table 3.2.

3.9.1.1 Particle tracking model of best fit head-calibration

As can be seen in Fig. 3.66, the best-fit head calibration model produced a simulation where water from the repository zone could reach the surface within 15,000 yr. Breakthrough of water from the BVG to overlying sediments occurs predominantly via the major fault zone to the west of the repository (equivalent to fault F1 in earlier published reports (Nirex, 1992a)).

3.9.1.2 BVG set to base case value

As shown in Fig 3.67, it is apparent that a lower conductivity for the BVG resulted in much longer containment of water. Repository water does not even leave the BVG until 50,000 yr after release (not shown), and takes 200,000 yr to reach the surface, having moved laterally through the St Bees Sst. and into the Calder Sst. before discharging onto the present-day sea bed. There is a possibility that flow

might not reach the sea-bed at all if the section were extended and the no-flow boundary at the western edge was relaxed.

3.9.1.3 High permeability Calder Sst.

Fig. 3.68 shows the result of a simulation where the Calder Sst is set to 30 m/yr and the BVG 1.2 m/yr. There is lateral movement of the particles before they are discharged onto the sea bed after only 186,000 years. This indicates that it is, again, the hydraulic conductivity of the BVG that crucially controls the mass transport rate in the area.

3.9.2 Summary and conclusions from particle tracking

The regional BVG hydraulic conductivity is crucial. It is difficult to measure or estimate regional BVG hydraulic conductivity in connected fractures with sufficient certainty (Nirex, 1993a). Consequently, at this repository site, containment of radionuclides would depend upon the estimated certainty of chemical blocking from engineered barriers, or by chemical retardation from rock-water interaction. Any increase in BVG vertical conductivity, either from engineering the Repository or from gas leakoff from the waste (Chapman, 1994) would have a critically bad effect.

It is particularly instructive to contrast these deterministic results of the particle tracking experiments with the very different results obtained from probabilistic modelling published elsewhere (RWMAC, 1994). The Nirex model suggests that flow of water from the Repository will ascend into the fresh meteoric water in Carboniferous-Triassic sediments, and will then descend westwards into the higher density brines of the Irish Sea "brine plug". However modelling shown here contradicts this theory. Different models with different assumptions produce different results, perhaps illustrating a lack of descriptive and predictive confidence.

3.10 Safety case implications

A simple safety case calculation can be made from the graphic expression of the relationship between water flow to BVG hydraulic conductivity (Fig 3.69). Assuming that it is unacceptable for water from the repository, at 650 m bOD, to return to the surface within 10,000 yr, the flow rate would need to be less than 6.50E-02 m/yr to be acceptable. Using Fig. 3.69, this flow rate equates to a regional BVG hydraulic conductivity of 3.16E-02 m/yr. If measured BVG hydraulic conductivities exceeds this value, the hydrogeological safety of a 650m Repository could be doubted.

Superimposed on Fig. 3.69 are the range of BVG hydraulic conductivities measured in boreholes at 400-1,900m bOD (Nirex, 1993a; Nirex, 1993b). It is apparent that measured values are around 1000 times too large to be simply declared "safe". Only one connective fracture is needed to supply a radioactive warm spring to the surface, so that modelling the statistical distribution of fractures is unlikely to give sufficient confidence that a conductive fracture can be excluded (Nirex 1993a). Further site investigation work needs to be directed towards establishing the long term water flow rates in these locally measured fractures, so obtaining a more reliable assessment of regional BVG connectivity.

Stable isotopic and noble gas data on present day waters in these B/H (Nirex 1993a) suggests that some BVG water may have recharged during a glaciation. This raises the possibility that the extra loading, topographical head and fracturing provided by an ice sheet could have induced much more rapid and extensive flows in the recent geological past, and could do so again in the geologically short term future.

3.11 Summary & conclusions

3.11.1 Summary

The general geology, hydrology and hydrogeology of the Sellafield site was reviewed. A suitable cross section forming the basis of the study was constructed and a possible conceptual model elucidated. Possible boundary conditions for such a conceptual model were outlined and the median or base case values for the hydraulic conductivity and porosity of the main hydrostratigraphic units presented. The specific aims and relevance of the study were delineated.

The mathematical formulations required to solve the partial differential equations of steady state flow, and heat transport and transient mass transport were detailed and the suitable numerical methods of solving them explained. The appropriate method for this study, a finite element approach to solving the relevant equations describing a continuous porous medium and the solution procedure utilised by the code selected for the study was explained. The experimental technique of sensitivity analysis was elucidated.

The results of simulations of fluid flow, using a simple modelling grid of varying heterogeneity, showed that the regional flow regime was dominated by topographically driven flow that could ascend from low permeability basement rocks into the overlying sedimentary cover. The addition of low permeability units complicated the flow regime, inhibiting regional transfer of fluids and causing high

hydraulic heads. Highly saline deep groundwaters could possibly deflect descending less saline water.

A scoping study of a more geologically realistic model indicated that, although unimportant to actual flow rates through a potential repository, the inclusion of faults and variably saline fluid profile were essential to better understand the possible flow paths. Their inclusion offered a better comparison between measured freshwater hydraulic head and that calculated by the code. The variation of anisotropy of fractures in the basement, although increasing vertical flow, had no effect on repository flow rates, indicating that fracture orientation may not be important. In all cases upward flowing water passed through the potential repository site.

The sensitivity of flow rate through the repository to variations in the hydraulic conductivity of the basement and aquifer indicated that the permeability of the basement host rock for the repository directly controlled the flux through the potential site, whilst the aquifer had no effect. These units were thus described as being decoupled. The flow rates through the repository were unaffected by variations in the hydraulic conductivity of low permeability units and faults in the cover and basement. Good implications were drawn regarding the mathematically robust nature of the OILGEN code and the uniformly upward trending fluids.

Comparisons between in-situ measurements and calculated equivalent freshwater head showed that high heads at depth in the potential repository site could be best matched when the BVG basement was assigned high permeability. The high permeability simulations also provided better a better "fit" to observed head in highly saline areas. The variation of hydraulic conductivity of low permeability units and faults in the basement had no significant effect on the good fit. Setting cover faults to unrealistically high permeabilities was shown to decrease the good quality of the fit.

The simulation of transient mass transport, to represent movement of radioactive material, indicated that the variation of basement permeability, by as little as two orders of magnitude, can affect the rate of fluid material reaching the surface markedly. When the basement is set to the higher permeability, the return rate to the surface is relatively rapid. A simplistic safety case showed that the measured range in hydraulic conductivity of the basement rocks is far to high to be considered as assisting containment of waste.

3.11.1.1 Other modelling studies

Numerical models are intrinsically simplifications of natural systems. As an example this chapter has used a 2D representation for an inherently 3D system. It could be maintained that there are other potentially significant simplifications in the model described here: the fixed salinity profile, and the choice of boundary conditions. This section considers these possibilities and used uses results from other studies as a comparison. As mentioned in section 3.4.3.3, the simulations performed in this chapter utilised a numerical model where the salinity distribution is fixed in space (and time). The boundary conditions were such that the vertical ends and base were no-flow boundaries and the upper surface allowed fluid to pass up or down through it (see section 3.4.4). Also, since the model is steady state it must be considered to represent a "snapshot" of a present day groundwater system that is not experiencing rapid change.

Other modelling studies focused on Sellafield (Heathcote *et al.*, 1996; Nirex, 1995), whilst adopting a similar 2D equivalent porous medium approach (see section 3.4.1.1), utilised different modelling codes and different approaches relating to salinity and boundary conditions. It is useful to examine the results of these simulations to determine the significance of these parameters. The Heathcote *et al.* (1996) simulations were performed via the coupled salinity and groundwater flow code SUTRA (Voss, 1984). This hybrid finite element/finite difference code was used to construct a geologically simplified model very similar in extent to that shown in Fig. 3.2. The model was then used to calculate pseudo-steady state conditions for salinity and fluid flow. The boundary conditions were such that the top boundary had a fixed head (water table onshore and seabed+hydrostatic offshore) and the bottom and eastern boundaries were no flow. The western boundary was located far offshore in an effort to reduce its direct influence in the onshore flow regime. It was assigned pressure and salinity values based on the onshore borehole 3. For initial conditions all elements down to -400 m were assigned seawater NaCl concentration, below which salinity increased to six times seawater. The simulation was run for 10^8 years so that dynamic equilibrium was achieved.

Values of permeability derived from early petrophysical estimates (1992 values: BVG hydraulic conductivity ranging from 10^{-3} to 10^{-1} m/yr), and the inclusion of permeable faults were used in the Heathcote *et al.* simulations of flow and salt redistribution. Although their over-simplified models did not allow accurate calibration between calculated and observed heads it was apparent that groundwater

flow in the central and eastern parts of their model were similar to those calculated in this chapter; western moving, topographically driven fluids with a strong upward component in the area of the PRZ. However, the flows in the western brine region were markedly different to those described earlier in this chapter, and indicated that there was a strong landward component representing brine intrusion or possible brine expulsion from offshore basins. The simulations also calculated that the majority of the flow would be in the permeable Calder and St Bees Sandstone units, although this is unsurprising given the low hydraulic conductivity assigned to the BVG.

Similar flow patterns were reflected in a later (although the Heathcote *et al.* study was published in 1996 the simulations were performed in 1992) more detailed fluid flow study (Nirex, 1995). Using a much more complex finite element model (Fig. 3.7) UK Nirex Ltd. simulated coupled salinity and groundwater flow via the finite element NAMMU code. The study also incorporated more up to date information relating to inter- and intra-formational permeability variations (especially those within the BVG), and incorporated the upscaled effects of fracture and fault zones by means of the transmissivity multiplier approach outlined in section 3.6.2.1. The source of the deep brines was suggested to be from thick halites within the Mercia Mudstone Group (Nirex, 1993), which does not outcrop onshore in the Sellafield district but is known to form cap rocks in Southern East Irish Sea Basin gas fields. Similar boundary conditions to those of the SUTRA model were assigned: no flow eastern and basal boundary, a flow-through top surface and a specified variable salinity at the western boundary that takes into account both the measured salinity concentrations in onshore boreholes and the location of the Mercia Mudstone group offshore.

Steady state calculations of coupled groundwater flow and mass transport of dissolved salts were carried out for base case permeabilities incorporating the above variations in hydrostratigraphy, BVG permeability and the inclusion of fault and fracture zones. Salinity distribution was calculated as being broadly similar to that of the SUTRA model detailed above. As before the groundwater flow field has a downward component in the eastern inland part of the model which changes to a strong upward component in the vicinity of the PRZ. There is again a very strong landward component of density driven flow in the western brine part of the model. Pathline calculations indicated that water emanating from the repository breaches the BVG relatively rapidly (tens of thousand of years), enters the covering sediments and, in general, discharges offshore. However, NAMMU transport simulations

performed elsewhere (Nicholls, 1995) showed that fluids from the repository may reach the surface onshore, even if the bulk of groundwater discharge is offshore. Even if this were not the case, it is questionable whether polluting a potable water aquifer and using it do dilute and disperse radioactive material would be an acceptable practise.

These independent simulation results have a potential significance in that they reinforce the general outcome of the simulations undertaken as part of this thesis: upwards movement of groundwater in the area of the PRZ. They are also significant in that they illustrate a failing of the OILGEN code in not being able to simulate the movement of salt in solution. OILGEN's prediction that descending fresher water might interact with the deep brines to produce "eddies" (e.g. Fig. 3.26) could be an artefact of the codes' limitations. It would be more useful in future research to alter the OILGEN code to allow coupled flow of groundwater and dissolved solutes. However, it is equally correct to state that there are still uncertainties relating to the deep brines; their source, the timing of their formation, and how long they will remain in their current location. Therefore the assumption that the salinity variations at the western boundary are as measured at the present day onshore might possibly be incorrect and the models of Heathcote *et al.* and Nirex may also be questioned.

Thus, differing assumptions regarding the boundary conditions and method of modelling salinity distribution could have an effect on the interpretation of the regional fluid flow regimes at Sellafield. However, in terms of the movement of water from a potential repository towards the surface there would appear to be little difference between the predictions made in this thesis and those described by others.

3.11.2 Conclusions

- A successful attempt has been made to determine the controls of regional groundwater flow in the Sellafield area and to develop both simplistic and geologically realistic models of fluid movement.

- The fluid flow simulation code provides a mathematically robust indication of the movement directions of groundwater. Even the simplistic simulations show water flow to be topographically driven and upward trending in the central (Repository) area of the region.

- The anisotropy of the BVG and hydraulic conductivity of the St Bees Sst, St Bees Evaporites, Brockram Breccia, cover faults and faults in the BVG are unimportant relating to repository flow rates, but the inclusion of faults and variable salinity are essential.

- The geologically complex simulations produce similar results to those of the more simplistic modelling. This indicates that the shape and size of the finite element cells is not relevant to either the flow rate or the flow path, nor, indeed to the numerical solution of the flow and heat transport equations, lending confidence in the OILGEN code.

- Two decoupled, but connected, aquifer systems exist:- in the Calder Sst. and in the BVG. Comparison of measured and calculated freshwater hydraulic head indicates that the best fit simulation is one where the BVG hydraulic conductivity is 1.2 m/yr.

- This best fit is not affected by variations in hydraulic conductivity of low permeability units, faults in the BVG or, within reason, faults in the cover sequence. When the permeablities of the overlying sediments are set to their median, or "base case" values there is a good fit between measured and calculated freshwater hydraulic head.

- Newer measured data of BVG hydraulic conductivity shows that some rates of the BVG can be 1000 times too permeable to be acceptable. Flow rates through the repository are around 1.7 m/yr.

- The proposed repository at 650 m bOD is in a poor position where flow directions in the BVG are towards the surface, and will need to be counteracted.

- Simulated tracking of water particles released from the repository zone shows that radionuclides could return to the surface within 15,000 years, if regional hydraulic conductivity of the BVG is equivalent to 1.2 m/yr. This assumes that no chemical retardation occurs within the engineered repository, or within the overlying rock.

Acknowledgements

Chris McKeown was funded by the Greenpeace Environmental Trust. The OILGEN code was kindly provided by Grant Garven. UK Nirex Ltd. are thanked for providing data. JD Bredehoeft is thanked for a helpful review.

3.12 References

Andrews-Speed, C.P., Oxburgh, E.R. & Cooper, B.A. (1984) Temperature and depth-dependent heat-flow in Western North Sea. *Bulletin of the American Association of Petroleum Geologists*, **68**, 11, 1764-1781.

Bachu, S. (1994) Flow of variable-density formation water in deep sloping aquifers: reviews of methods of representation with case studies. *Journal of Hydrology*, **164**, 19-38.

Bath, A. (1995) Groundwater geochemistry in the potential repository zone and surrounding rocks at Sellafield, The geological disposal of radioactive waste, Royal Lancaster Hotel, London, IBC Technical Services Ltd, Gilmoora House, 57-61 Mortimer St., London.

Bath, A.H., McCartney, R.A., Richards, H.G., Metcalfe, R. & Crawford, M.B. (1996) Groundwater chemistry of the Sellafield area: a preliminary investigation. *Quarterly Journal of Engineering Geology*, **29**, supplement 1, S39-S57.

Bear, J. (1972) *Dynamics of fluids in porous media*. Environmental science series, American Elsevier, New York, 764 pp.

Bear, J. & Verruijt, A. (1987) *Modeling groundwater flow and pollution*. Theory and applications of transport in porous media, Kluwer Academic Publishers, Dordecht, 414 pp.

Bear, J. & Yehuda, B. (1990) *Introduction to modeling of transport phenomena in porous media*. Theory and applications of transport in porous media, Kluwer Academic Publishers, Dordecht, 553 pp.

Beddoe-Stephens, B. & Phillips, E.R. (1993) *The petrology of the Borrowdale Volcanic Group within Sellafield borehole No. 2.* Report No. **CC92S/193/CF-1-A**, British Geological Survey, Keyworth, UK.

Bethke, C.M. (1993) *Basin modeling with Basin2. A guide to using Basin2, B2plot, B2video and B2view*. University of Illinois, Urbana-Champaign, USA, 225 pp.

Black, J.H. (1995) The hydrogeology of the Sellafield area, The geological disposal of radioactive waste, Royal Lancaster Hotel, London, IBC Technical Services Ltd, Gilmoora House, 57-61 Mortimer St., London.

Black, J.H. & Brightman, M.A. (1996) Conceptual model of hydrogeology of Sellafield. *Quarterly Journal of Engineering Geology*, **29**, supplement 1, S83-S93.

Brace, W.F. (1980) Permeability of crystalline and argillaceous rocks. *International Journal of Rock Mechanics, Mineral Science & Geomechanics Abstracts*, **17**, 241-251.

Brace, W.F. (1984) Permeability of crystalline rocks : new in-situ measurements. *Journal of Geophysical Research*, **89**, B6, 4327-4330.

Branney, M.J., Kokelaar, B.P & McConnell, B.J. (1988) Ordovician volcano-tectonics in the English Lake District. *Journal of the Geological Society, London*, **145**, 367-376.

Brassington, R. (1988) *Field hydrogeology*. Professional Handbook Series, Open University Press, Milton Keynes, 175 pp.

Bredehoeft, J.D. & Maini, T. (1981) Strategy for radioactive waste disposal in crystalline rocks. *Science*, **213**, 293-296.

Cathles, L.M. III. (1990) Scales and effects of fluid flow in the upper crust. *Science*, **248**, 323-329.

Chadwick, R.A., Kirby, G.A. & Baily, H.E. (1994) The post-Triassic structural evolution of north-west England and adjacent parts of the East Irish Sea. *Proceedings of the Yorkshire Geological Society*, **50**, 99-102.

Chapman, N.A. (1994) The geologist's dilemma: predicting the future behaviour of buried radioactive wastes. *Terra Nova*, **6**, 5-19.

Chapman, N.A. & McEwen, T.J. (1986) Geological environments for deep disposal of intermediate level wastes in the United Kingdom. *In:* (eds) *Siting, design and construction of underground repositories for radioactive wastes.* **IAEA-SM-289/37**, International Atomic Energy Authority, Vienna, Austria, 311-328.

Chapman, N.A. & McKinley, I.G. (1987) *The geological disposal of nuclear waste.* John Wiley & Sons, Chichester, 281 pp.

Clauser, C. (1992) Permeability of crystalline rocks. *Transactions American Geophysical Union*, **73**, 21, 233-238.

de Marsily, G. (1986) *Quantitative hydrogeology. Groundwater hydrology for engineers.* Academic Press Inc. (London) Ltd., London, 440 pp.

de Marsily, G. (1987) An overview of coupled processes with emphasis on geohydrology. *In:* (eds) *Coupled processes associated with nuclear waste repositories.* Academic Press Inc., 27-37.

Deming, D. (1993) Regional permeability estimates from investigations of coupled heat and groundwater flow, North Slope of Alaska. *Journal of Geophysical Research*, **98**, B9, 16271-16286.

Deming, D. (1994) Fluid flow and heat transport in the upper continental crust. *In:* Parnell, J. (eds) *Geofluids: origin, migration and evolution of fluids in sedimentary basins.* Geological Society Special Publication No. 78, London, 27-42.

Deming, D., Sass, J.H., Lachenbruch, A.H. & De Rito, R.F. (1992) Heat flow and subsurface temperature as evidence for basin-scale groundwater flow, North Slope Alaska. *Bulletin of the Geological Society of America*, **104**, 528-542.

Domenico, P.A. & Schwartz, F.W. (1990) *Physical and chemical hydrogeology.* John Wiley & Sons, New York, 824 pp.

ERM. (1993) *Summary of radioactive waste disposal policy and environmental issues affecting Cumbria.* Report No. **ITA/9**, Environmental Resources Management.

Fleming, C.G. (1996) Modern day temperature fields, Central Graben, North Sea; Investigation of conduction and fluid advection, Ph.D. Thesis, University of Glasgow.

Follin, S. & Thunkin, R. (1994) On the use of continuum approximations for regional modeling of groundwater flow in crystalline rocks. *Advances in Water Resources*, **17**, 133-14.

Freeze, R.A. & Cherry, J.A. (1979) *Groundwater*. Prentice-Hall, Englewood Cliffs, N.J., 604 pp.

Garven, G. (1989) A hydrogeologic model for the formation of the giant oil sands deposits of the Western Canadian sedimentary basin. *American Journal of Science*, **289**, 105-166.

Garven, G. (1994) Genesis of stratabound ore deposits in the midcontinent basins of North America. 1. The role of regional groundwater flow - a reply. *American Journal of Science*, **294**, 760-765.

Garven, G. (1995) Continental-scale groundwater flow and geologic processes. *Annual Review in Earth and Planetary Sciences*, **23**, 89-117.

Garven, G. & Freeze, R.A. (1984a) Theoretical analysis of the role of groundwater flow in the genesis of stratabound ore deposits. 1. Mathematical and numerical model. *American Journal of Science*, **284**, 1085-1124.

Garven, G. & Freeze, R.A. (1984b) Theoretical analysis of the role of groundwater flow in the genesis of stratabound ore deposits. 2. Quantitative results. *American Journal of Science*, **284**, 1125-1174.

Garven, G., Ge, S., Person, MA. & Sverjensky, D.A. (1993) Genesis of stratabound ore deposits in the midcontinent basins of North America. 1. The role of regional groundwater flow. *American Journal of Science*, **293**, 497-568.

Haszeldine, R.S. (1996) Subsurface geology, geochemistry and water flow at a rock characterisation facility (RCF) at Longlands Farm. Proof of evidence. *In:* Haszeldine, R.S. & Smythe, D.K. (eds) *Radioactive Waste Disposal at Sellafield, UK. Site Selection, geological and engineering problems.* University of Glasgow, Glasgow, UK, 121-164.

Haszeldine, R.S. & McKeown, C. (1995) A model approach to radioactive waste disposal at Sellafield. *Terra Nova*, **7**, 1, 87-96.

Heathcote, J.A., Jones, M.A. & Herbert, A.W. (1996) Modelling groundwater flow in the Sellafield area. *Quarterly Journal of Engineering Geology*, **29**, supplement 1, S59-S81.

Holmes, J. (1995) *Proof of Evidence. Science overview*. RCF Planning Enquiry, **PE/NRX/13**, UK Nirex Ltd., Harwell, UK, Cleator Moor, Cumbria, 40 pp.

Huyakorn, P.S. & Pinder, G.F. (1983) *Computational methods in subsurface flow*. Academic Press Inc., London, 473 pp.

Karlsson, F. (1995) The Swedish approach to near-field issues, The geological disposal of radioactive waste, Royal Lancaster Hotel, London, IBC Technical Services Ltd, Gilmoora House, 57-61 Mortimer St., London.

Kazda, I. (1990) *Finite element techniques in groundwater flow studies with applications in hydraulic and geotechnical engineering*. Elsevier, Amsterdam, 313 pp.

Kestin, J., Khalifa, H.E. & Correia, R.J. (1981) Tables of the dynamic and kinematic viscosity of aqueous NaCl solutions in the temperature range 20-150°C and the pressure range of 0.1-35 MPa. *Journal Physical Chemical Reference Data*, **10**, 71-87.

Konikow, L.F. & Bredehoeft, J.D. (1992) Goundwater models cannot be validated. *Advances in Water Resources*, **15**, 75-83.

LaBolle, E.M., Fogg, G.E. & Tompson, A.F.B. (1996) Randon-walk simulation of transport in heterogeneous porous media: Local mass-conservation problem and conservation methods. *Water Resources Research*, **32**, 3, 583-593.

Langmuir, D. (1995) Nuclear waste management in the United States, The geological disposal of radioactive waste, Royal Lancaster Hotel, London, IBC Technical Services Ltd, Gilmoora House, 57-61 Mortimer St., London.

Lerche, I. (1990) *Basin analysis - quantitive methods, volume 1*. Academic Press Inc., San Diego, 562 pp.

Littleboy, A. (1996) The geology and hydrogeology of the Sellafield area: development of the way forward. *Quarterly Journal of Engineering Geology*, **29**, supplement 1, S95-S104.

Long, J.C.S., Karasaki, K., Davey, A., Peterson, J., Landsfeld, M, Kemeny, J. & Martel, S. (1991) An inverse approach to the construction of fracture hydrology models conditioned by geophysical data. An example from the validation exercises at the Stripa Mine. *International Journal of Rock Mechanics, Mineral Science & Geomechanics Abstracts*, **28**, 2/3, 121-142.

Lusczynski, N.J. (1961) Head and flow of ground water of variable density. *Journal of Geophysical Research*, **66**, 12, 4247-4256.

McKeown, C. & Haszeldine, R.S. (1993) *A Model approach to waste disposal. Progress report for Greenpeace Environmental Trust.* Report No. **1**, University of Glasgow.

McKeown, C. & Haszeldine, R.S. (1995) Modelling groundwater flow and chemistry in the proposed repository zone, The geological disposal of radioactive waste, Royal Lancaster Hotel, London, IBC Technical Services Ltd, Gilmoora House, 57-61 Mortimer St., London.

Mercer, J.W., Pinder, G.F. & Donaldson, I.G. (1975) A galerkin-finite element analysis of the hydrothermal system at Wairakei, New Zealand. *Journal of Geophysical Research*, **80**, 17, 2608-2621.

Metcalfe, R. & Crawford, M.B. (1994) *Models of water/rock interactions in the Borrowdale Volcanic Group within the potential repository zone at Sellafield.* Report No. **WE/94/26C**, British Geological Survey, Keyworth, UK, Keyworth, UK.

Michie, U. (1996) The geological framework of the Sellafield area and its relationship to hydrogeology. *Quarterly Journal of Engineering Geology*, **29**, supplement 1, S13-S27.

Millward, D. (1995) The geological environment of the Potential Repository Zone at Sellafield, Cumbria, The geological disposal of radioactive waste, Royal Lancaster Hotel, London, IBC Technical Services Ltd, Gilmoora House, 57-61 Mortimer St., London.

Millward, D., Beddoe-Stephens, B., Williamson, I.T., Young, S.R. & Petterson, M.G. (1994) Lithostratigraphy of a concealed caldera-related ignimbrite sequence within the Borrowdale Volcanic group of west Cumbria. *Proceedings of the Yorkshire Geological Society*, **50**, 25-36.

Moreno, L. & Neretnieks, I. (1993) Fluid flow and solute transport in a network of channels. *Journal of Contaminant Hydrology*, **14**, 163-192.

Nagra. (1995) *Bulletin : Disposal programme for high-level waste (HLW).* Report No. **25**, Nagra, Wettingen, Switzerland.

Neumann, S.P. (1990) Universal scaling of hydraulic conductivities and dispersivities in geologic media. *Water Resources Research*, **26**, 1749-1758.

Neuzil, C.E. (1986) Groundwater flow in low permeability environments. *Water Resources Research*, **22**, 8, 1163-1195.

Nicholls, D.B. (1995) *Hydrogeological modelling of the Sellafield site, Vols I & II - Text and Appendices.* Report No. **TR-Z2-7**, Her Majesty's Inspectorate of Pollution, London, UK.

Nirex. (1989) *Deep repository project, preliminary environmental and radiological assessment and preliminary safety report.* Report No. **71**, UK Nirex Ltd., Harwell, UK.

Nirex. (1992a) *The geology and hydrogeology of Sellafield.* Report No. **263**, UK Nirex Ltd., Harwell, UK.

Nirex. (1992b) *Sellafield hydrogeology. Report of the hydrogeology joint interpretation team.* Report No. **268**, UK Nirex Ltd., Harwell, UK.

Nirex. (1993a) *The geology and hydrogeology of the Sellafield area: Interim assessment.* Report No. **524 (4 vols)**, UK Nirex Ltd., Harwell, UK.

Nirex. (1993b) *Scientific update 1993 : Nirex deep waste repository project.* Report No. **525**, UK Nirex Ltd., Harwell, UK.

Nirex. (1995) *Nirex 95: A Preliminary analysis of the groundwater pathway for a deep repository at Sellafield.* Report No. **S/95/012 (3vols)**, UK Nirex Ltd., Harwell, UK.

Nuclear Energy Agency. (1993) *The status of near-field modelling*. Organisation for Economic Co-operation and Development, Paris, France, 289 pp.

Pearson, F.J. & Scholtis, A. (1993) *Chemistry of reference waters of the crysalline basement of northern Switzerland for safety assessment studies.* Report No. **NTB 93-07**, Nagra, Wettingen, Switzerland.

Petterson, M.G., Beddoe-Stephens, B., Millward, D. & Johnson, E.W. (1992) A pre-caldera plateau-andesite field in the Borrowdale Volcanic Group of the English Lake District. *Journal of the Geological Society, London*, **149**, 889-906.

Raffensperger, J.P. & Garven, G. (1995) The formation of unconformity-type uranium deposits. 1. Coupled groundwater flow and transport modeling. *American Journal of Science*, **295**, 581-636.

Royal Society. (1994) *Disposal of radioactive waste in deep repositories*. Report of a Royal Society study group, Royal Society, London, 194 pp.

RWMAC. (1994) *Fourteenth annual report of the radioactive waste management advisory committee.* Report No. **14**, HMSO, London.

Sutton, J.S. (1996) Hydrogeological testing in the Sellafield area. *Quarterly Journal of Engineering Geology*, **29**, supplement 1, S29-S38.

Taylor, B.J., Burgess, I.C., Land, D.H., Mills, D.A.C., Smith, D.B. & Warren, M.A. (1971) *Geology of Northern England*. HMSO, London, 121 pp.

Voss, C.I. (1984) *A finite element simulation model for saturated-unsaturated, fluid density dependent ground water flow with energy transport or chemically reactive single species solute transport.* Report No. US Geological Survey, Reston, VA, USA.

Hydrostratigraphic Unit	Hydraulic conductivity, K m/yr	$Log_{10}K$ m/yr	Porosity %
Calder Sandstone (CS)	3.00E+00	+0.48	20
St Bees Sandstone (SBS)	1.50E+00	+0.18	10
St Bees Evaporites (SBE)	1.60E-03	- 2.80	1
Brockram Breccia (BB)	9.40E-04	-3.03	10
Carb. Limestone (CL)	1.50E-01	-0.82	1
BVG	1.20E-02	-1.92	1
Cover faults (CF)	3.00E+01	+1.48	5
BVG faults (BVG F)	3.00E+00	+0.48	2

Table 3.1a Values of hydraulic conductivity and porosity used as base case for modelling study. Values derived from logarithmic median values taken from published reports (Michie, 1996; Nirex, 1992a; Nirex, 1993a; Nirex, 1995). Sensitivity analyses performed in this study investigated hydraulic conductivity ranges at least as large as those observed in the field, i.e., as much as 10^4 above and below these median values (Table 3.2 - 3.8).

Hydrostratigraphic Unit	Hydraulic conductivity m/yr	$Log_{10}K$ m/yr	Porosity %
Calder Sandstone (CS)	3.00E+00 - 3.00E+02	+0.48 - +2.48	20
St Bees Sandstone (SBS)	4.20E-01	-0.38	12
St Bees Evaporites (SBE)	1.60E-03	- 2.80	1
Brockram Breccia (BB)	9.46E-04	-3.02	8
Carb. Limestone (CL)	1.50E-01	-0.82	1
BVG	1.20E-04 - 1.20E+00	-1.92-+0.08	1
Cover faults (CF)	3.42E+02	+2.53	20
BVG faults (BVG F)	1.30E+00	+0.11	20

Table 3.1b Older values used in previous modelling studies (Haszeldine & McKeown, 1995; McKeown & Haszeldine, 1993; McKeown & Haszeldine, 1995) derived from published reports (Nirex, 1992a; Nirex, 1993a).

30 m/yr (log_{10} = 1.48) = 10^{-6} m/s = 100 mD

Unit	Modelled Base Case K (m/yr)	Extended modelled range in K	K_h/K_v	(ϕ) %	Storage Co-eff (m^{-1})	Thermal Cond ($Wm^{\circ}C^{-1}$)	disper-sivity x (m)	disper-sivity z (m)
CS	3	3, 30, 300	1.00E+01	20	1.00E-04	3.1	10.0	1.0
SBS	1.5	1.5, 15, 150	1.00E+01	10	1.00E-04	3.1	1.0	0.1
SBE	1.60E-03	1.00E-03, 1.00E-01, 1.00E+00	1.00E+02	1	1.00E-06	4.0	1.0	0.1
BB	9.46E-04	1.00E-03, 1.00E-01, 1.00E+00	1.00E+02	10	1.00E-04	3.1	1.0	0.1
CL	1.50E-01	N/A	5.00E+01	1	1.00E-04	3.1	1.0	0.1
BVG	1.20E-02	1.20E-05, 1.20E-04, 1.20E-03 1.20E-02, 1.20E-01, 1.20E+00 1.20E+01	5.00E+00	1	1.00E-06	4.0	1.0	0.1
CF	3 *	0.3, 3, 30 *	1.00E+00	5	1.00E-04	3.1	1.0	0.1
BVGF	0.03 *	0.0003, 0.03, 3 *	1.00E+00	2	1.00E-04	3.1	1.0	0.1

Table 3.2 Hydrogeological parameters for distinct hydrostratigraphic units used in groundwater flow models. All values are derived from published reports and literature (Freeze & Cherry, 1979; Fleming, 1996; Garven & Freeze, 1984a; Garven & Freeze, 1984b; Garven, 1989; Michie, 1996; Nirex, 1992a; Nirex, 1993a; Nirex, 1995; Raffensperger & Garven, 1995). Other thermal parameters are that the surface temperature is 15 °C and the geothermal heat flux at the base of all the models was constrained at 70 mW/m^2. Abbreviations derived from Table 3.1a.

*** = modelled fault hydraulic conductivity ~ 0.01 of value simulated due to excessive width of faults in model (see text for explanation)**

· **In the following tables the average linear velocity results (in italics) are in m/yr.**

Input		Results	
No	BVG K (myr^{-1}.)	No faults	Faults
0a	1.20E-05	*3.60E-05*	*2.76E-05*
1a	1.20E-04	*3.48E-04*	*2.73E-04*
2a	1.20E-03	*2.66E-03*	*2.70E-03*
3a	1.20E-02	*9.67E-03*	*2.67E-02*
4a	1.20E-01	*7.27E-02*	*2.40E-01*
5a	1.20E+00	*5.97E-01*	*1.62E+00*
6a	1.20E+01	*3.93E+00*	*4.15E+00*

Table 3.3 Average linear velocity of groundwater through cell representing repository volume presented in italics. Scoping study results for all models with or without faults. The presence of faults caused slightly increased flow for higher BVG hydraulic conductivity runs.

Input		Results	
No	BVG K (myr^{-1}.)	No salt	Salt
0a	1.20E-05	*2.76E-05*	*2.75E-05*
1a	1.20E-04	*2.73E-04*	*2.74E-04*
2a	1.20E-03	*2.70E-03*	*2.73E-03*
3a	1.20E-02	*2.67E-02*	*2.68E-02*
4a	1.20E-01	*2.40E-01*	*2.41E-01*
5a	1.20E+00	*1.62E+00*	*1.68E+00*
6a	1.20E+01	*4.15E+00*	*5.31E+00*

Table 3.4 Average linear velocity of groundwater through cell representing repository volume presented in italics. Scoping study results for all models with or without variable density groundwater. The presence of variable density fluid did not cause marked increase in flow through repository but the path of water was affected (see text).

Input		Results	
No	BVG K (myr^{-1}.)	BVG K_h/K_v =5	BVG K_h/K_v = 1
0b	1.20E-05	*2.75E-05*	*3.18E-05*
1b	1.20E-04	*2.74E-04*	*3.15E-04*
2b	1.20E-03	*2.73E-03*	*3.14E-03*
3b	1.20E-02	*2.68E-02*	*3.07E-02*
4b	1.20E-01	*2.41E-01*	*2.61E-01*
5b	1.20E+00	*1.68E+00*	*1.54E+00*
6b	1.20E+01	*5.31E+00*	*4.58E+00*

Table 3.5 Scoping study results for all models when BVG anisotropy varied from 5 to 1. The order of magnitude flow remains the same but the flow rate when BVG anisotropy = 1 is slightly greater. The path of flow through repository is not greatly affected. Average linear velocity of groundwater through cell representing repository volume are presented in italics.

Input		Results		
No	BVG K (myr^{-1}.)	Calder Sst K $3.0 \times 10^{+00}$	Calder Sst K $3.0 \times 10^{+01}$	Calder Sst K $3.0 \times 10^{+02}$
0	1.20E-05	*2.75E-05*	*2.74E-05*	*2.69E-05*
1	1.20E-04	*2.74E-04*	*2.73E-04*	*2.68E-04*
2	1.20E-03	*2.73E-03*	*2.72E-03*	*2.68E-03*
3	1.20E-02	*2.68E-02*	*2.67E-02*	*2.63E-02*
4	1.20E-01	*2.41E-01*	*2.41E-01*	*2.37E-01*
5	1.20E+00	*1.68E+00*	*1.72E+00*	*1.70E+00*
6	1.20E+01	*5.31E+00*	*5.74E+00*	*5.71E+00*

Table 3.6 Results for all models when BVG and Calder Sst hydraulic conductivity varied. Varying Calder Sst hydraulic conductivity has very little effect on average linear velocity of groundwater through cell representing repository volume. Varying the BVG hydraulic conductivity has a direct effect on this rate. Average linear velocity of groundwater through repository volume presented in italics.

Input		Results		
No	BVG K (myr^{-1}.)	Case A St Bees K 1.5 m/yr	Case E St Bees K 15 m/yr	Case F St Bees K 150 m/yr
0	1.20E-05	*2.75E-05*	*2.76E-05*	*2.77E-05*
1	1.20E-04	*2.74E-04*	*2.76E-04*	*2.76E-04*
2	1.20E-03	*2.73E-03*	*2.75E-03*	*2.75E-03*
3	1.20E-02	*2.68E-02*	*2.72E-02*	*2.71E-02*
4	1.20E-01	*2.41E-01*	*2.51E-01*	*2.52E-01*
5	1.20E+00	*1.68E+00*	*1.95E+00*	*1.99E+00*
6	1.20E+01	*5.31E+00*	*8.50E+00*	*9.29E+00*

Table 3.7 Results for all models when BVG and St Bees Sst hydraulic conductivity varied. Varying St Bees Sst hydraulic conductivity has very little effect on average linear velocity of groundwater through the cell representing repository volume. Varying the BVG hydraulic conductivity has a direct effect on this rate. Average linear velocity of groundwater through repository volume presented in italics.

Input	Result	Input	Result	Input	Result
BVG faults K (myr^{-1}.)	m/yr	Cover faults K (myr^{-1}.)	m/yr	Evap + Brock K (myr^{-1}.)	m/yr
3.00E-04	*1.47E+00*	0.3	*1.68E+00*	1.50E-03	*1.68E+00*
3.00E-02	*1.68E+00*	3.0	*2.00E+00*	1.50E-01	*1.72E+00*
3.00E+00	*2.06E+00*	30.0	*2.44E+00*	1.50E+00	*1.82E+00*

Table 3.8 Results for all models when ;

- **BVG fault hydraulic conductivity varied : Only small increase on flow rate through repository.**
- **Cover fault hydraulic conductivity varied. Increase in flow rate through repository but still same order of magnitude.**
- **Low permeability horizons : St Bees Evaporites and Brockram Breccia hydraulic condctivity varied. Very minor effect on flow rate through repository.**

Average linear velocity of groundwater through repository volume presented in italics.

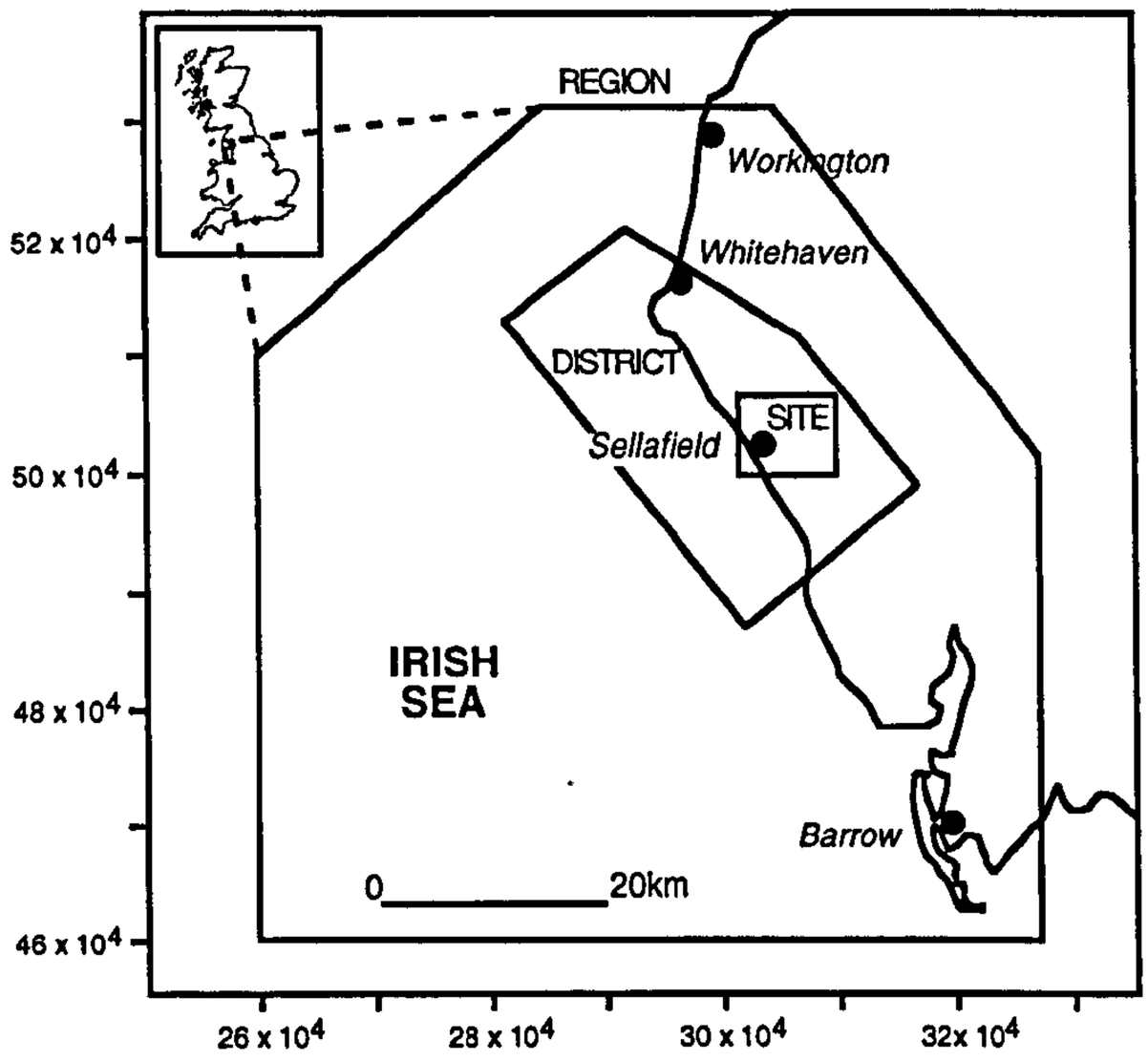

Fig. 3.1a Region, District and Site definitions (after Michie & Bowden, 1994).

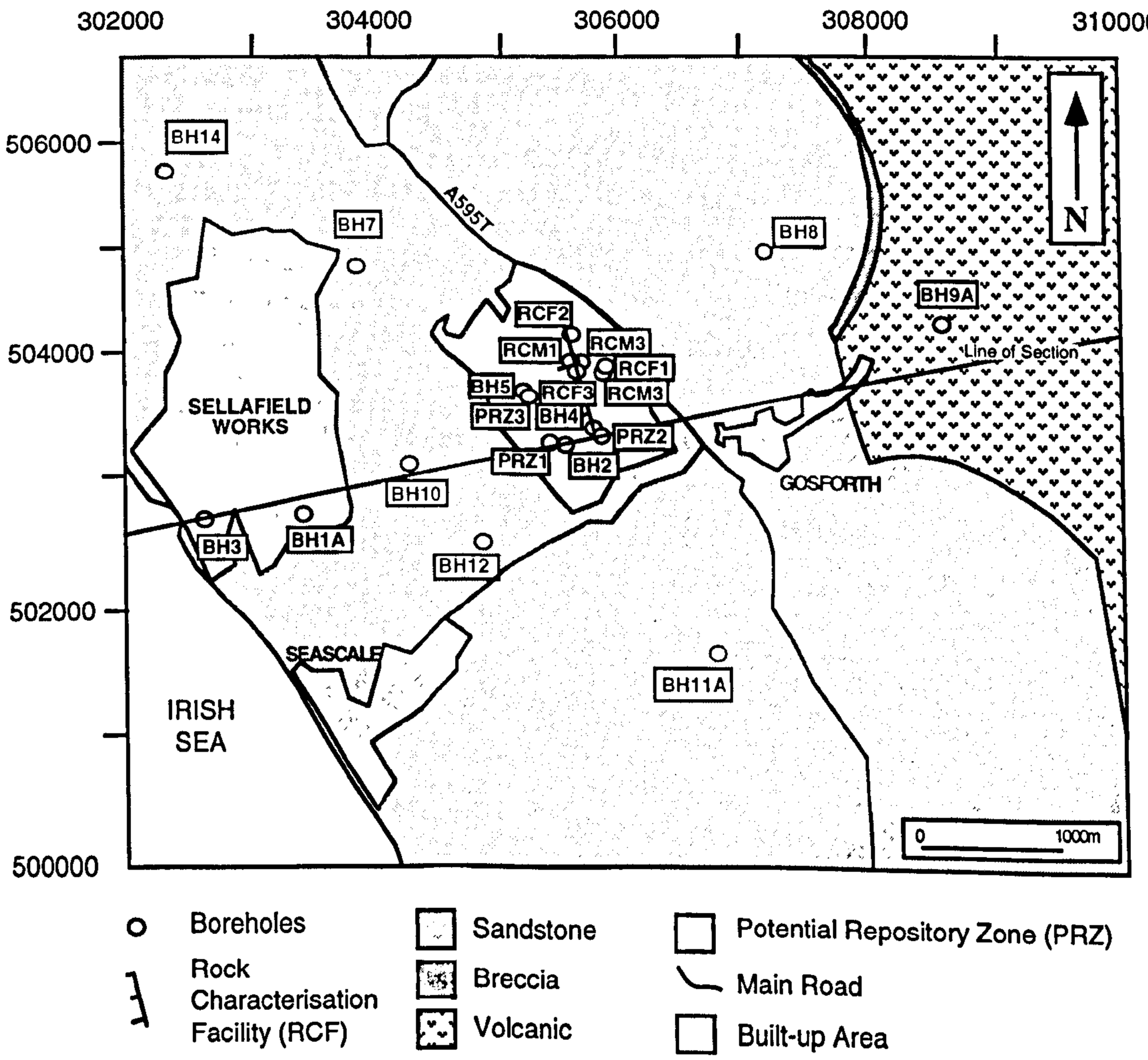

Fig. 3.1b Location of deep boreholes, the PRZ and RCF (after Michie & Bowden, 1994; Chaplow, 1995).

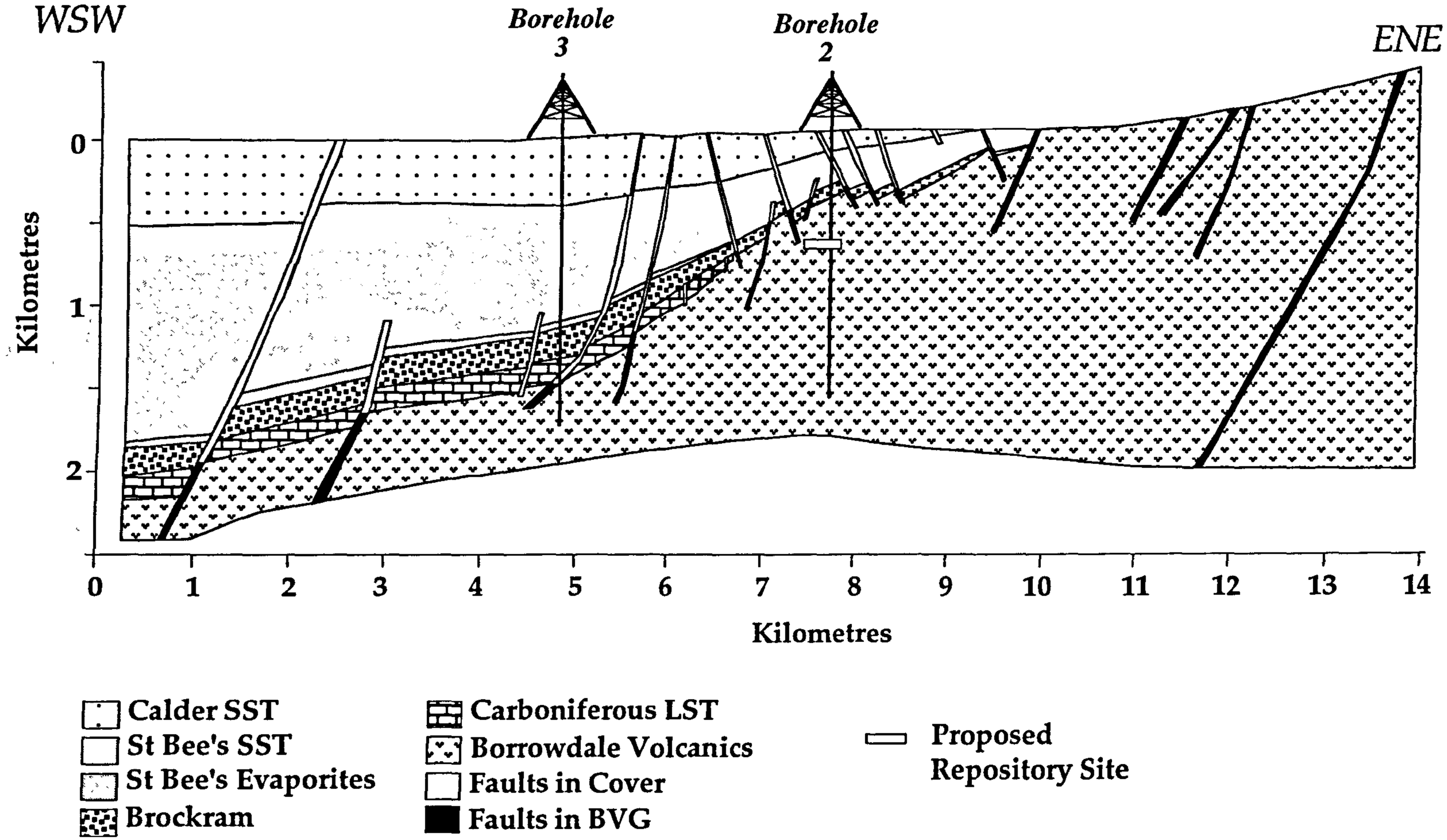

Fig. 3.2 Geological cross section of the proposed Repository site at 650m, compiled from published information (Nirex, 1992b; Nirex, 1993b; Nirex, 1993d) and extended W and E using publicly available geological information (Taylor et al 1971). Rocks of the Borrowdale Volcanic Group (BVG) rise to 1,000m elevation in the Lake District, and fall westwards to lie well below sea level. This elevation provides a topographical drive for meteoric water flow through any fracture or matrix conductivity in the BVG. Carboniferous to Triassic sediments onlap the BVG, and provide a series of matrix and fracture permeable aquifers.

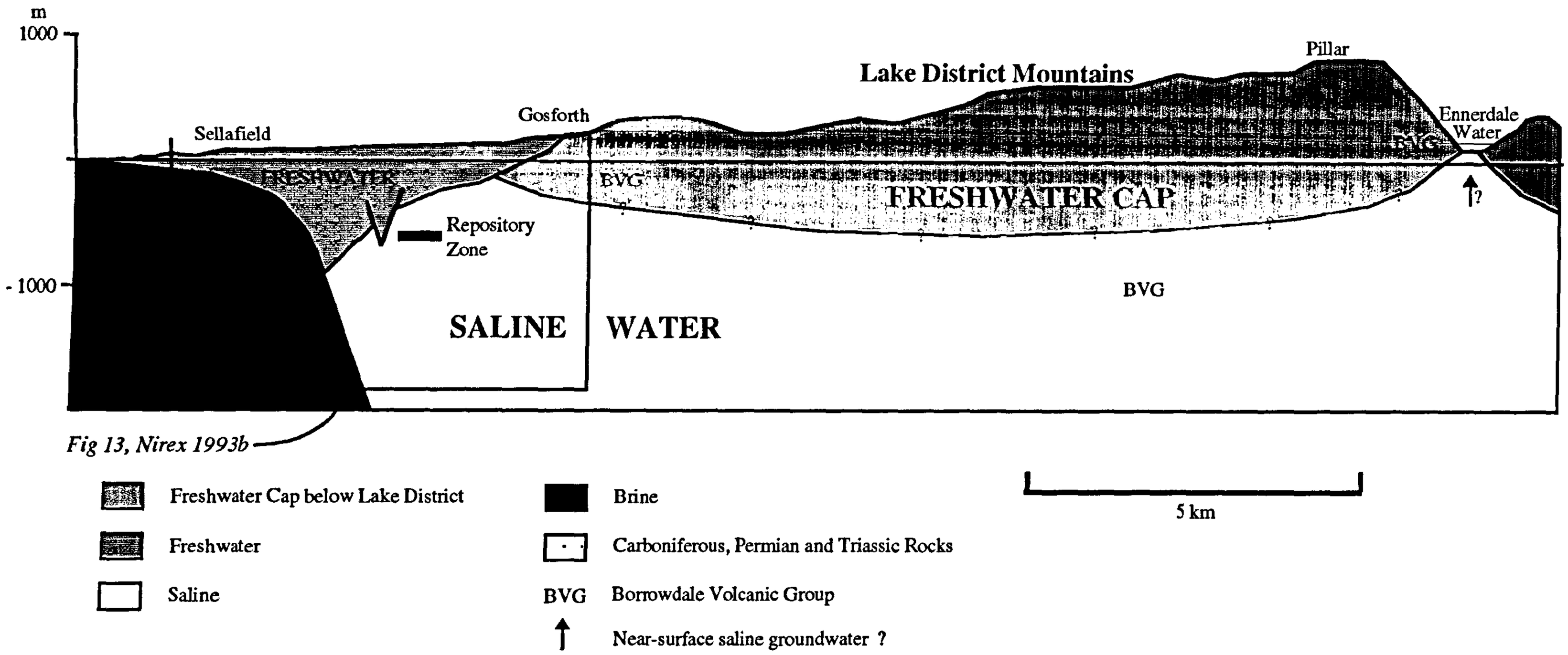

Fig. 3.3 Distinct fluid types in the Lake District (after RWMAC, 1994)

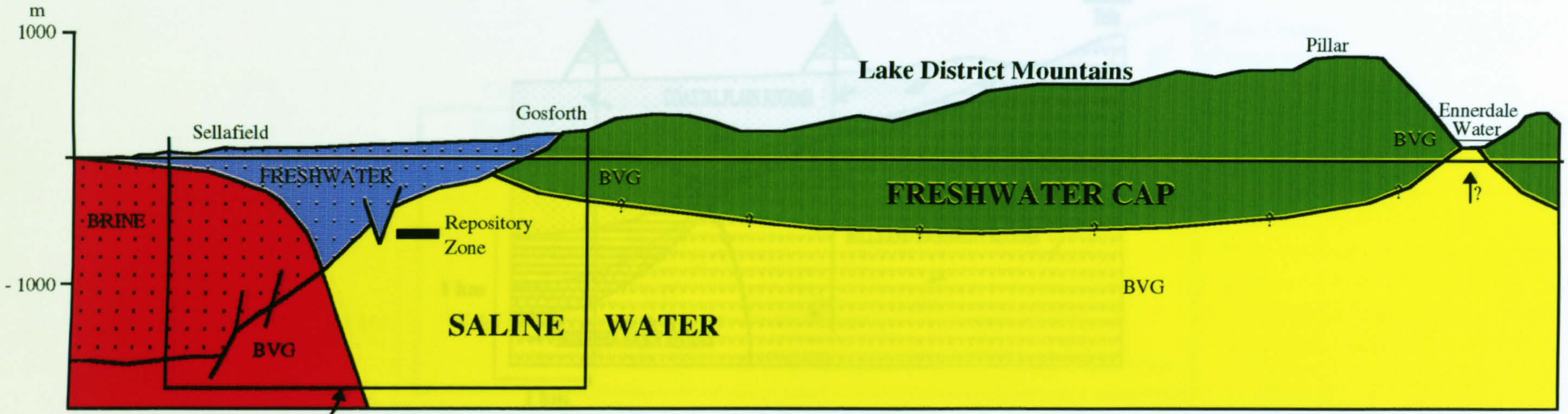

Fig. 3.3 Distinct fluid types in the Lake District (after RWMAC, 1994)

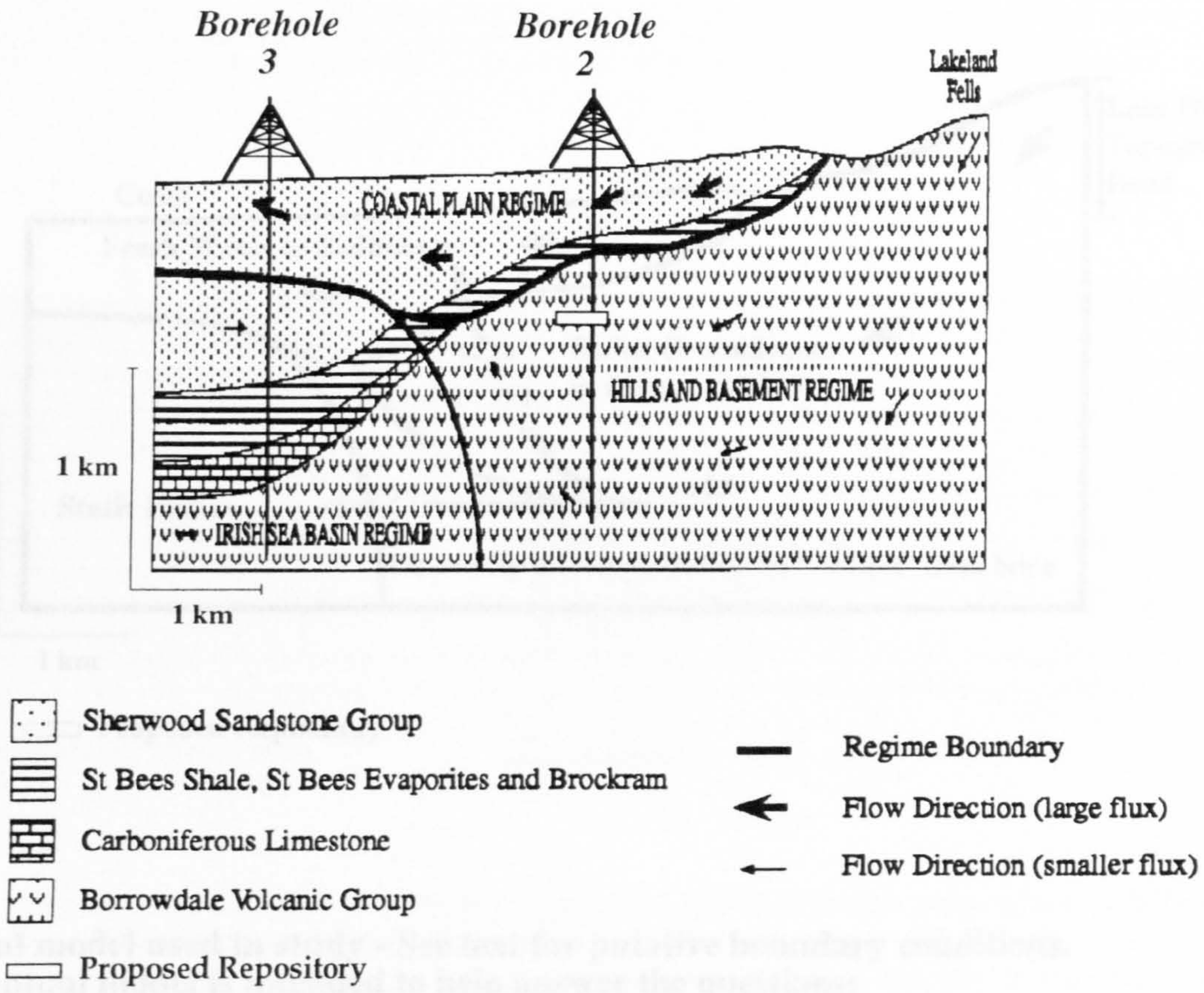

Fig. 3.4 Nirex conceptual model of the hydrogeology of the Sellafield area (after Black, 1995). The divisions coincide largely with the distribution of salinity Groundwaters in the Irish Sea Basin regime are predominantly basin-derived brines; in the Hills and Basement Regime, saline; in the Coastal Plain Regime, fresh. Scale same as Fig. 3.2.

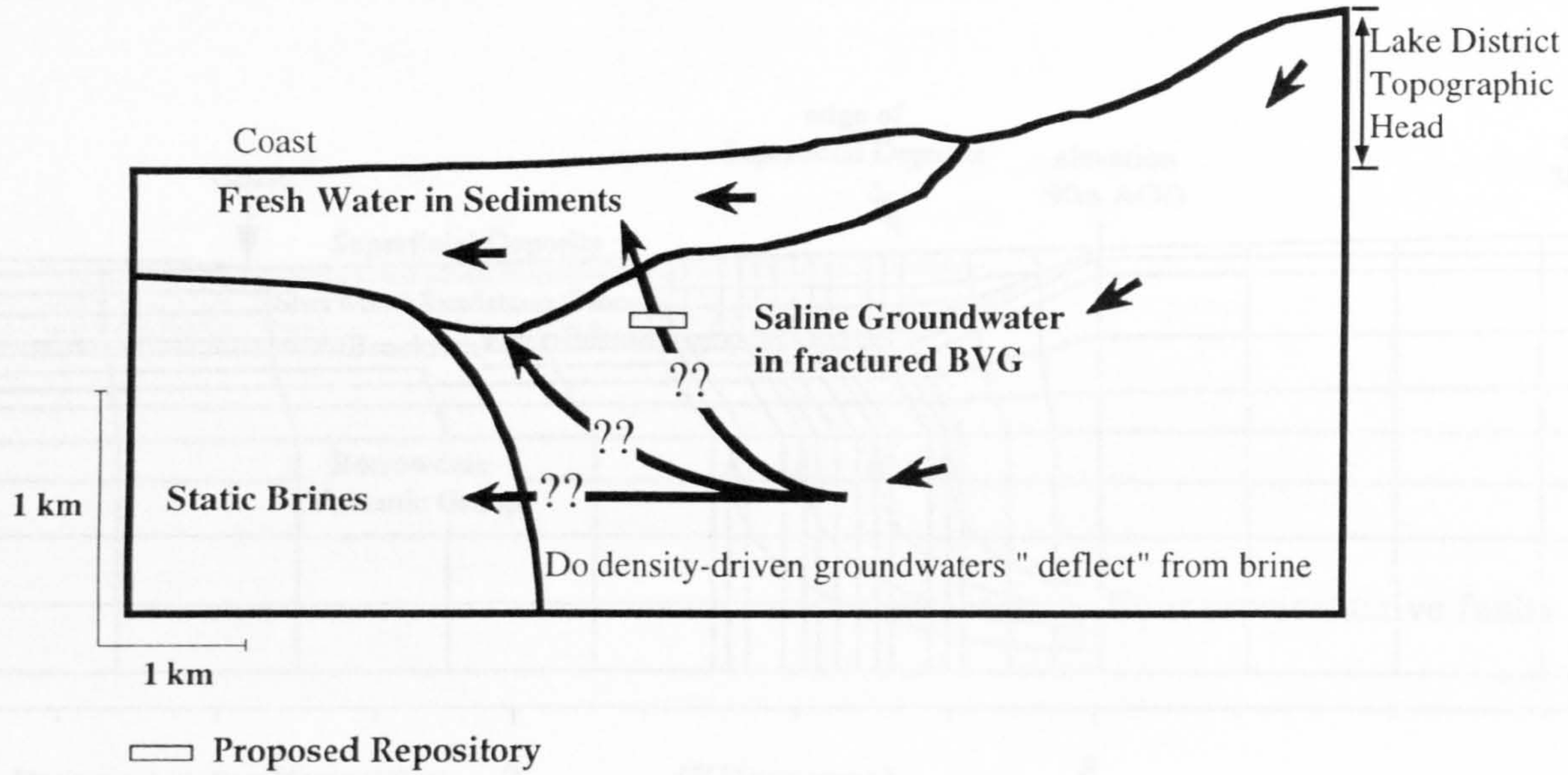

Fig. 3.5 Conceptual model used in study - See text for putative boundary conditions. The conceptual model is intended to help answer the questions;

What effect do static brines have on groundwater flow ?
How rapid is fluid flow in the BVG ?
Does flow travel upwards to surface via the PRZ ?

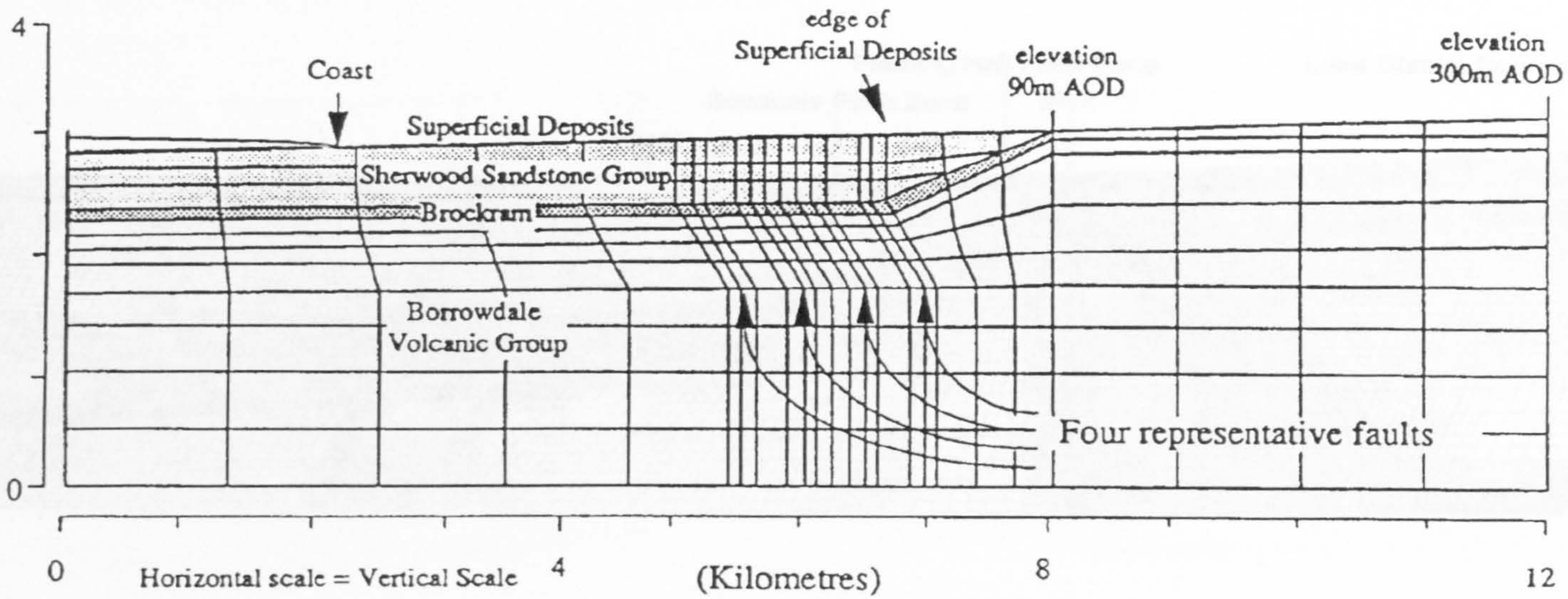

Fig. 3.6 **At the start of this research project the above was the only other published mathematical model of groundwater flow at the Sellafield site. The finite element mesh has 273 elements, there are only four faults and no variable density groundwater: all fresh water (after Nirex, 1992a).**

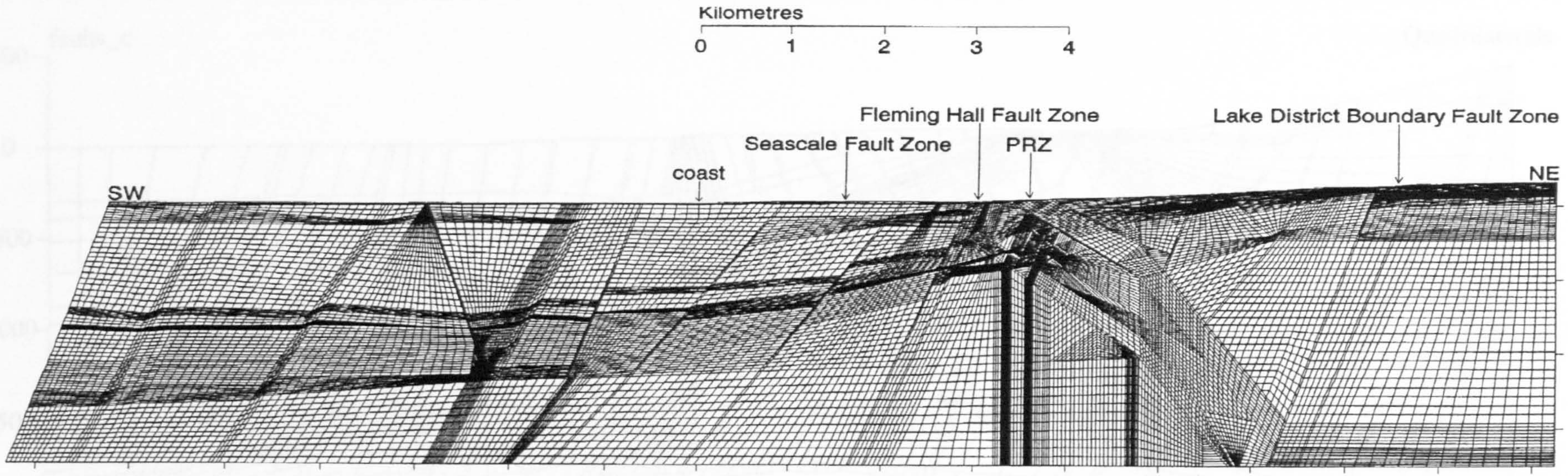

Fig. 3.7 **Nirex Finite Element grid used for groundwater flow modelling (vertical scale = horizontal scale) (after Nirex, 1995).**

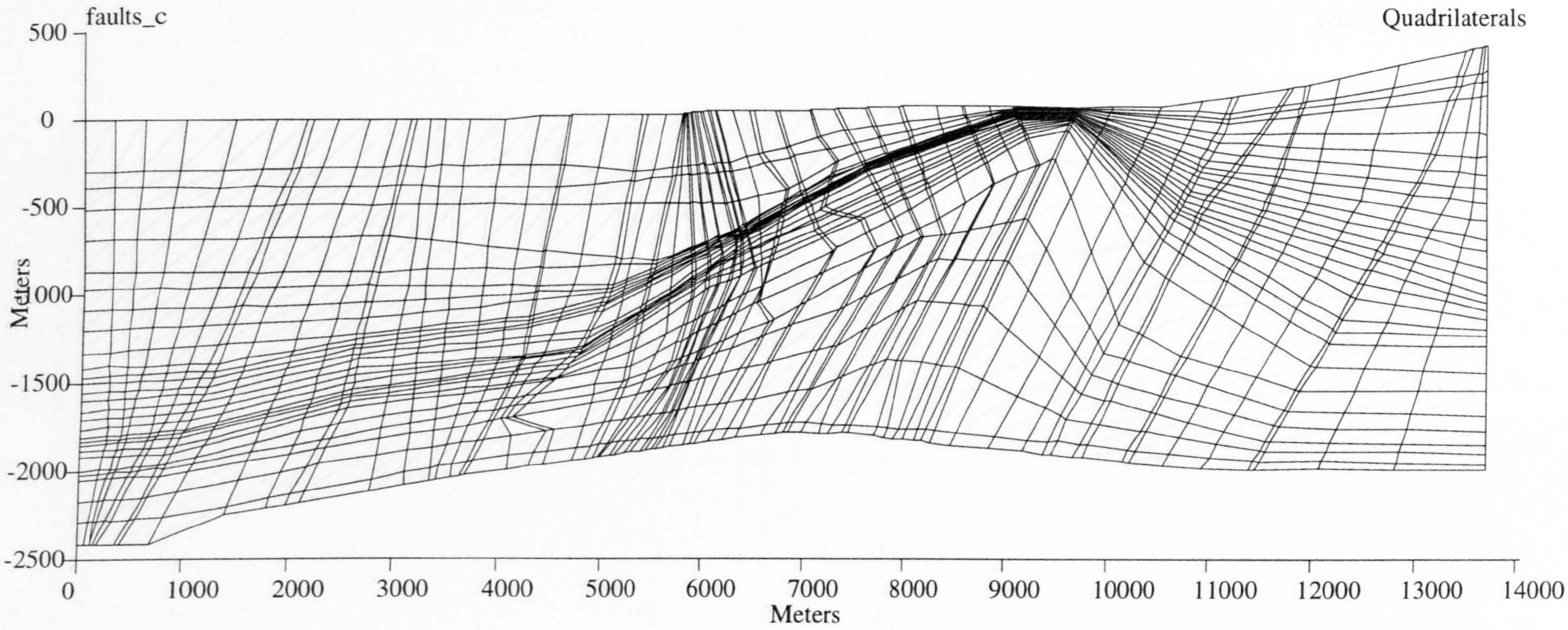

Fig. 3.8 Finite element mesh derived from Fig. 3.2 used in OILGEN code for simulating fluid flow. Each element can have discrete physical properties. Each lithology is represented by a distinct hydrogeological unit, with particular porosity and hydraulic conductivity. There are no barriers to flow between elements.

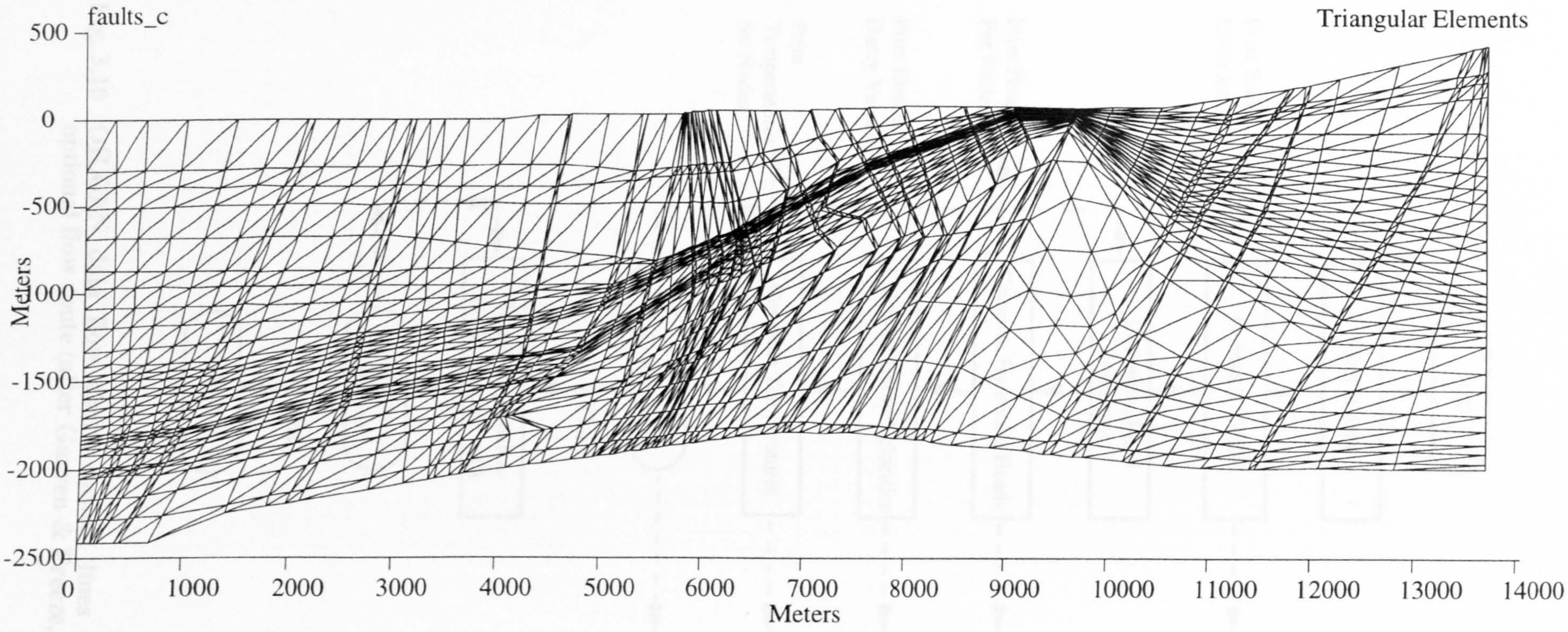

Fig. 3.9 Triangular element mesh used to solve coupled fluid flow and heat transport equations. Quadrilateral mesh (Fig. 3.8) used to track particles in transient mass transport simulations.

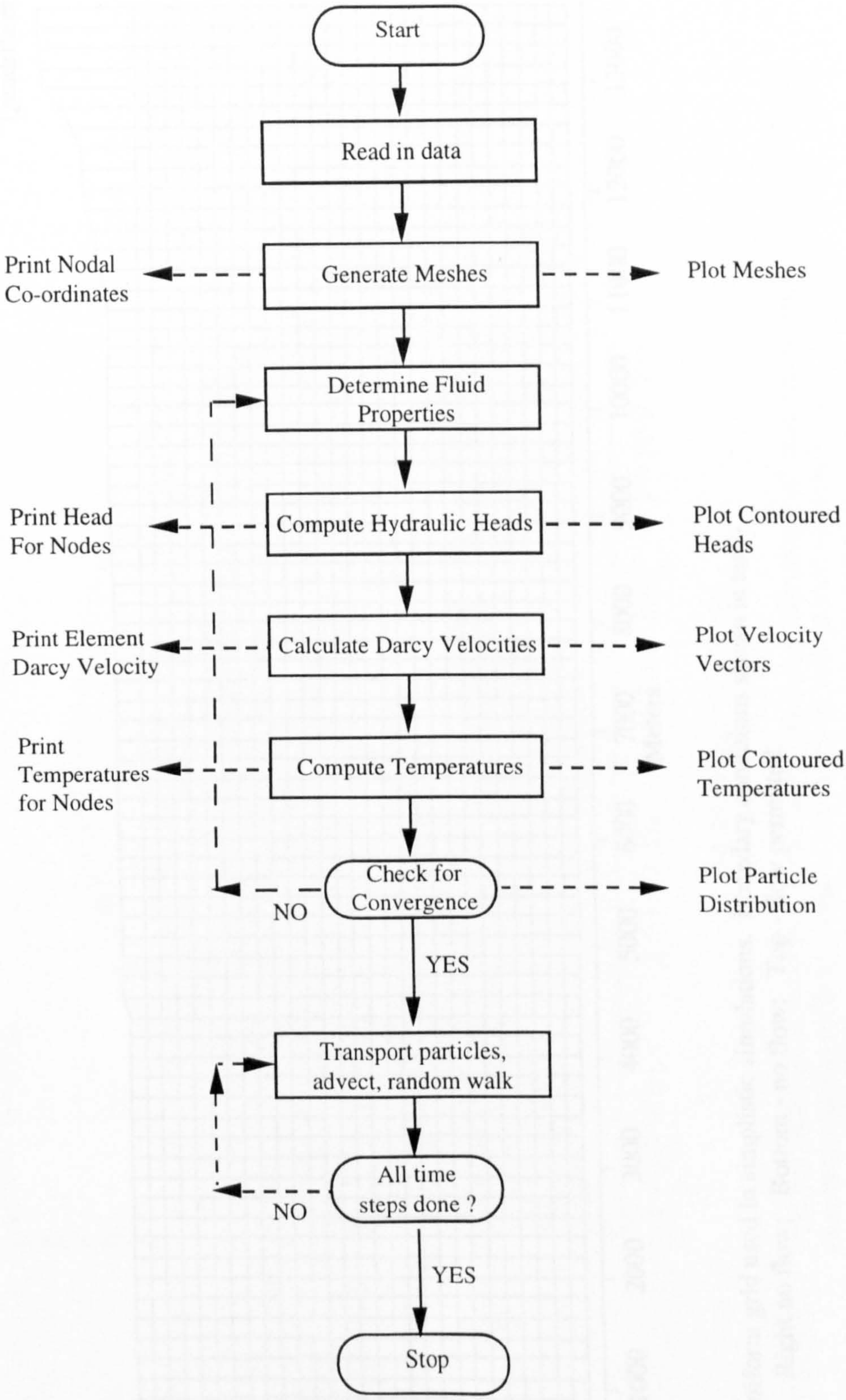

Fig. 3.10 OILGEN data flow chart, dashed lines indicate an optional flow route (after Garven & Freeze, 1984).

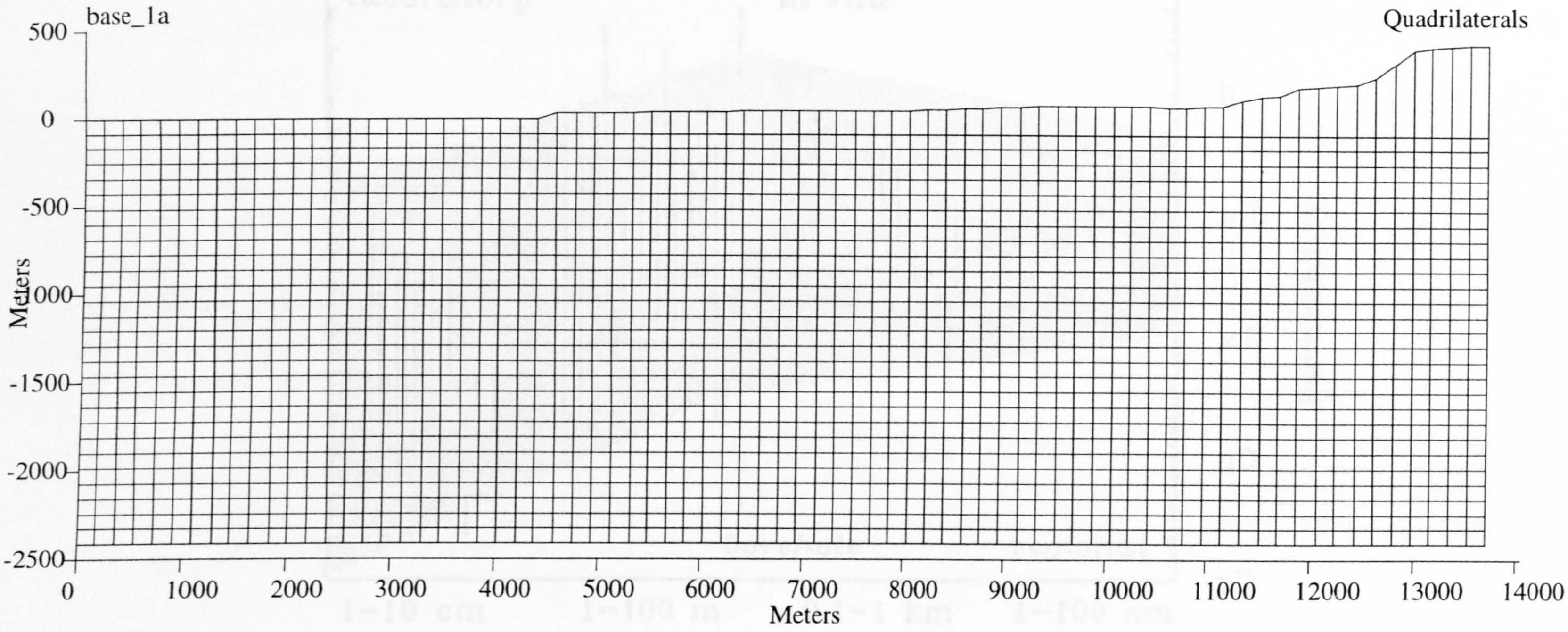

Fig. 3.11 Uniform grid used in simplistic simulations. Boundary conditions shown in text - Left - no flow; Right no flow; Bottom - no flow; Top - flow permitted.

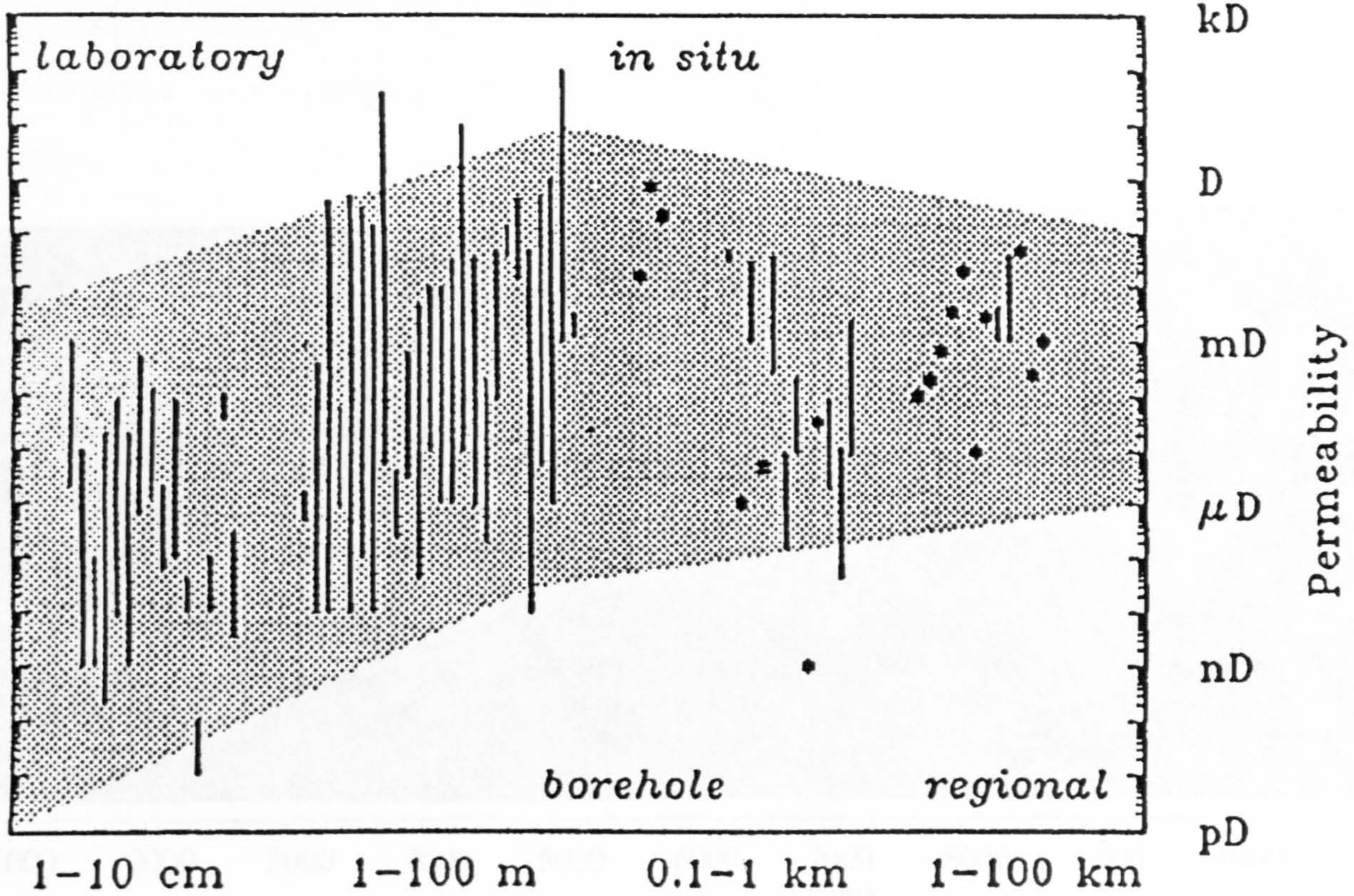

Fig. 3.12 **Permeability of crystalline rocks and characteristic scale of measurements: Bars mark the maximum permeabilty range when several values are reported, stars represent single values (Clauser 1992). The shaded region is Clauser's personal view of the data trend.**

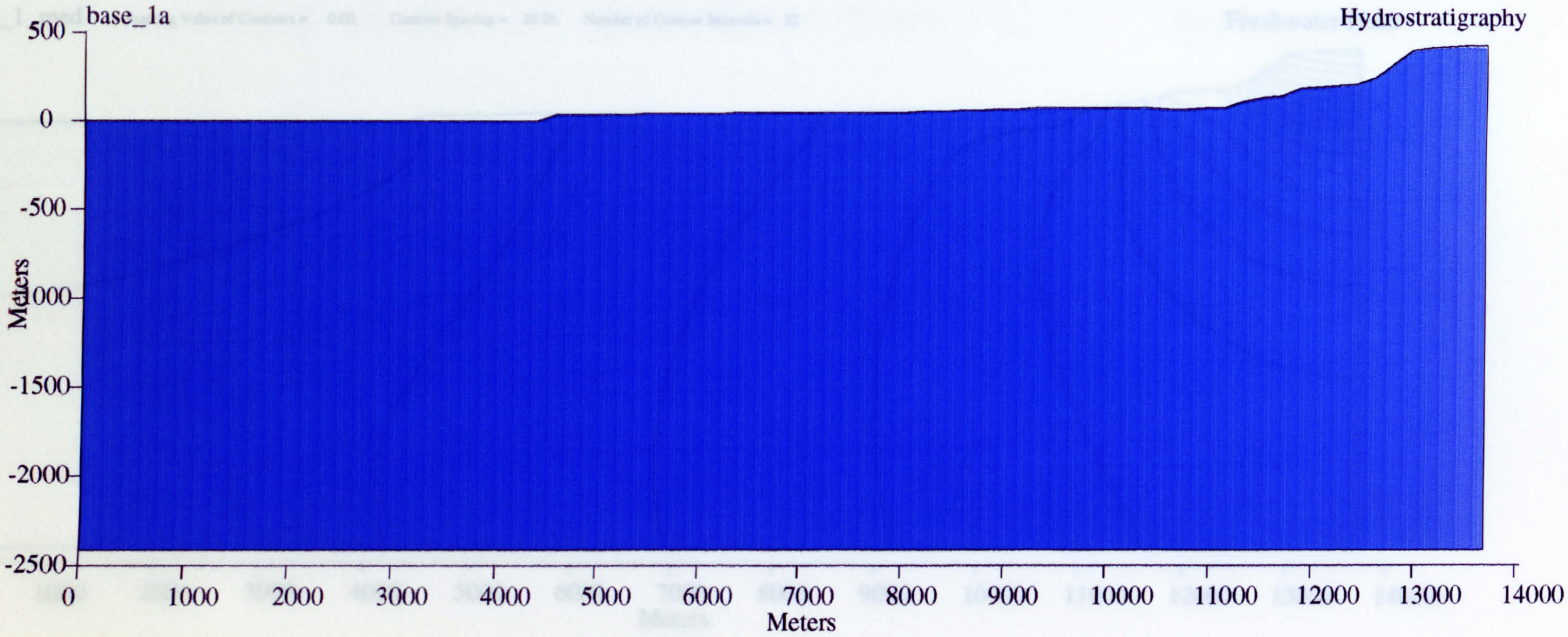

Fig. 3.13 Uniform grid composed of BVG (turquoise).

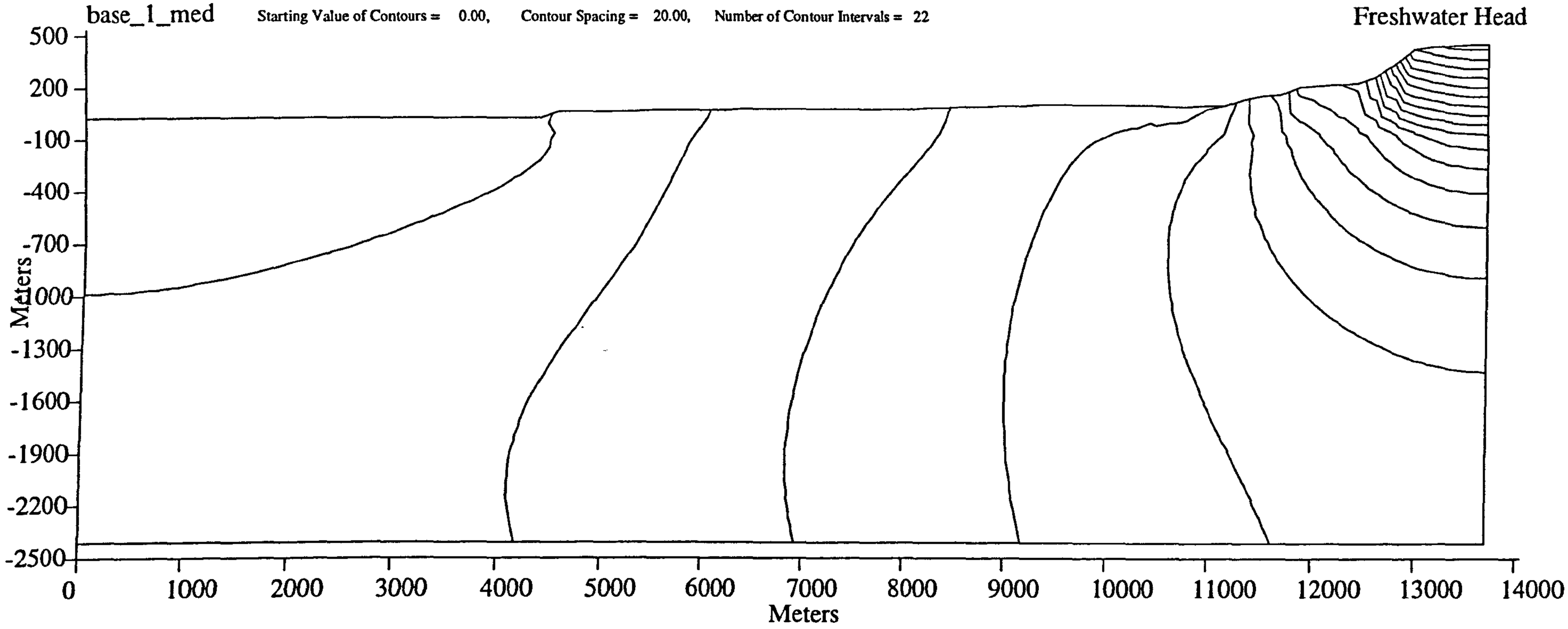

Fig. 3.14. Plot of equivalent freshwater hydraulic head calculated with uniform grid (Fig. 3.13). Horizontal hydraulic conductivity of the BVG set to base case value of 1.20E-02 m/yr.

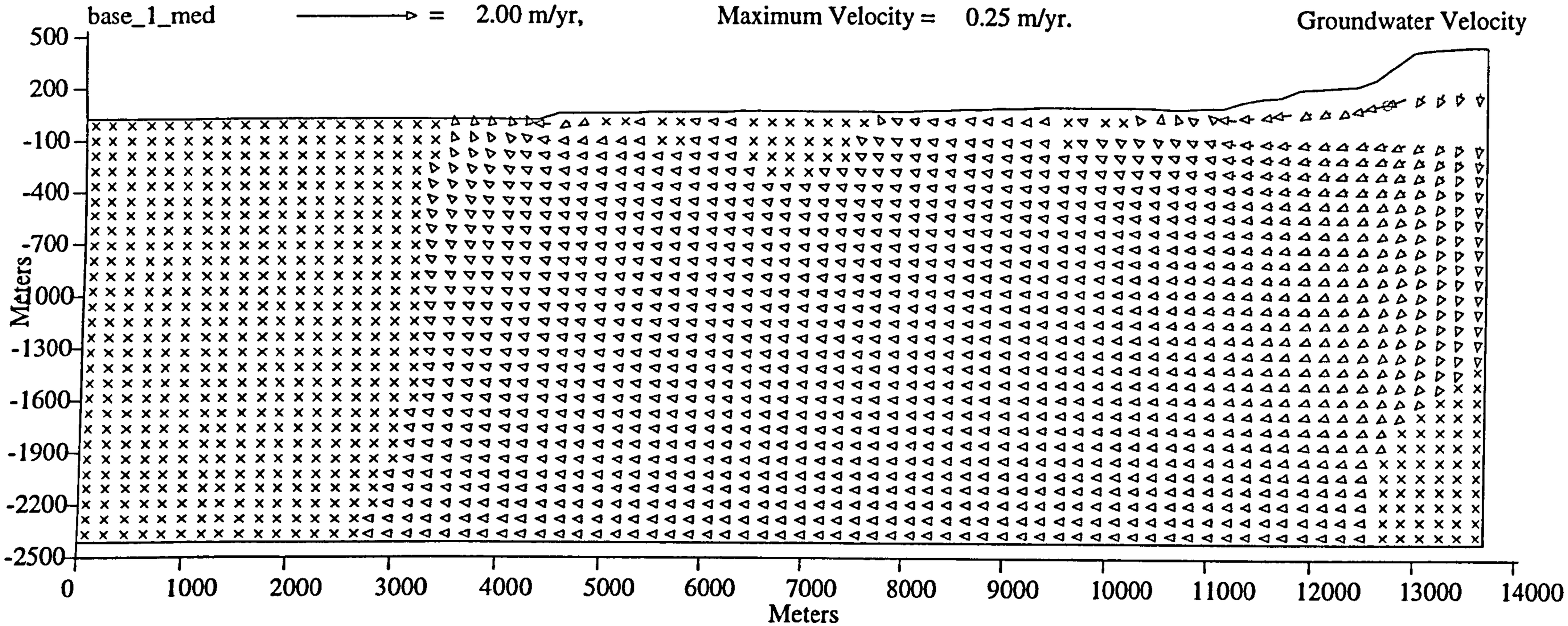

Fig. 3.15 Groundwater flow plot displaying average linear velocities calculated with uniform grid. Conditions as Fig. 3.14. Flow topographically driven and discharges at OD. Crosses represent flow that is less than 1% of maximum.

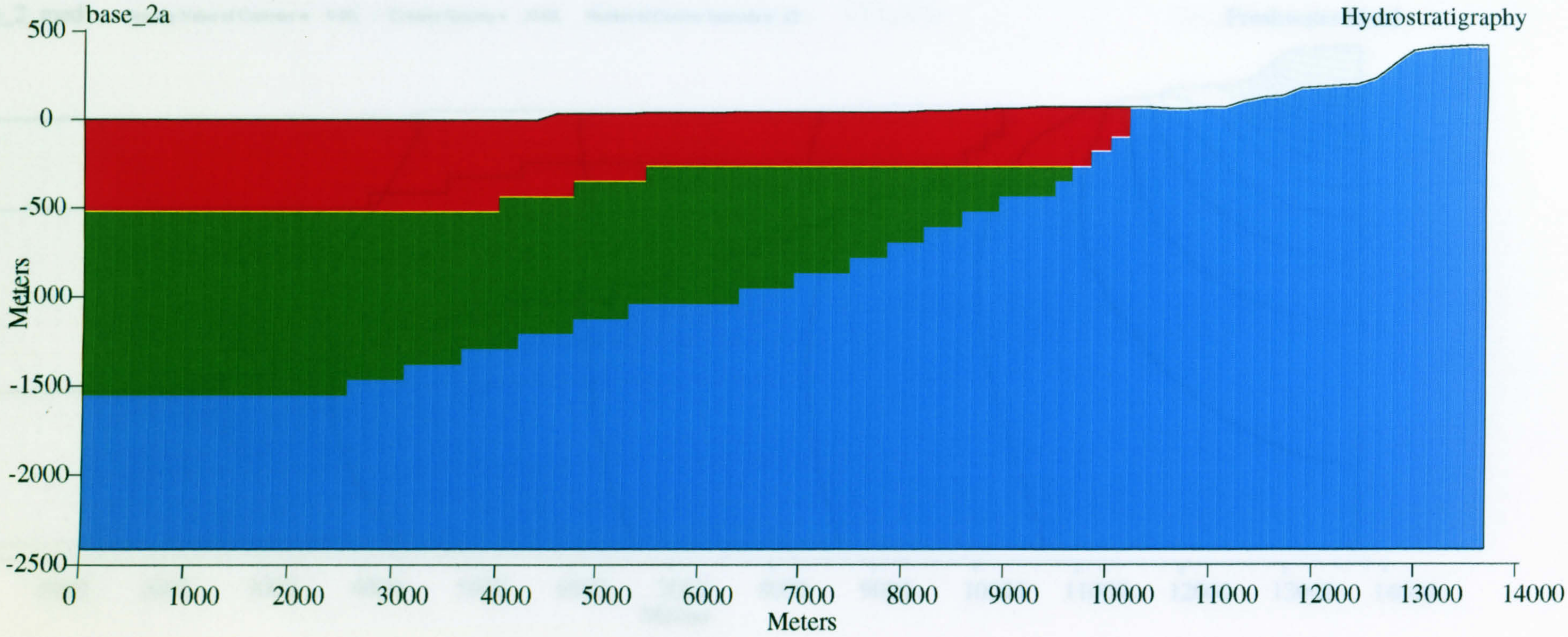

Fig. 3.16 Heterogeneous grid composed of Calder Sst. (red); St Bees Sst. (green) and BVG (turquoise). Base case hydraulic conductivities (horizontal); Calder Sst. = 3.00 m/yr; St Bees Sst. = 1.50 m/yr; BVG = 1.20E-02 m/yr. Boundary conditions as Fig. 3.11.

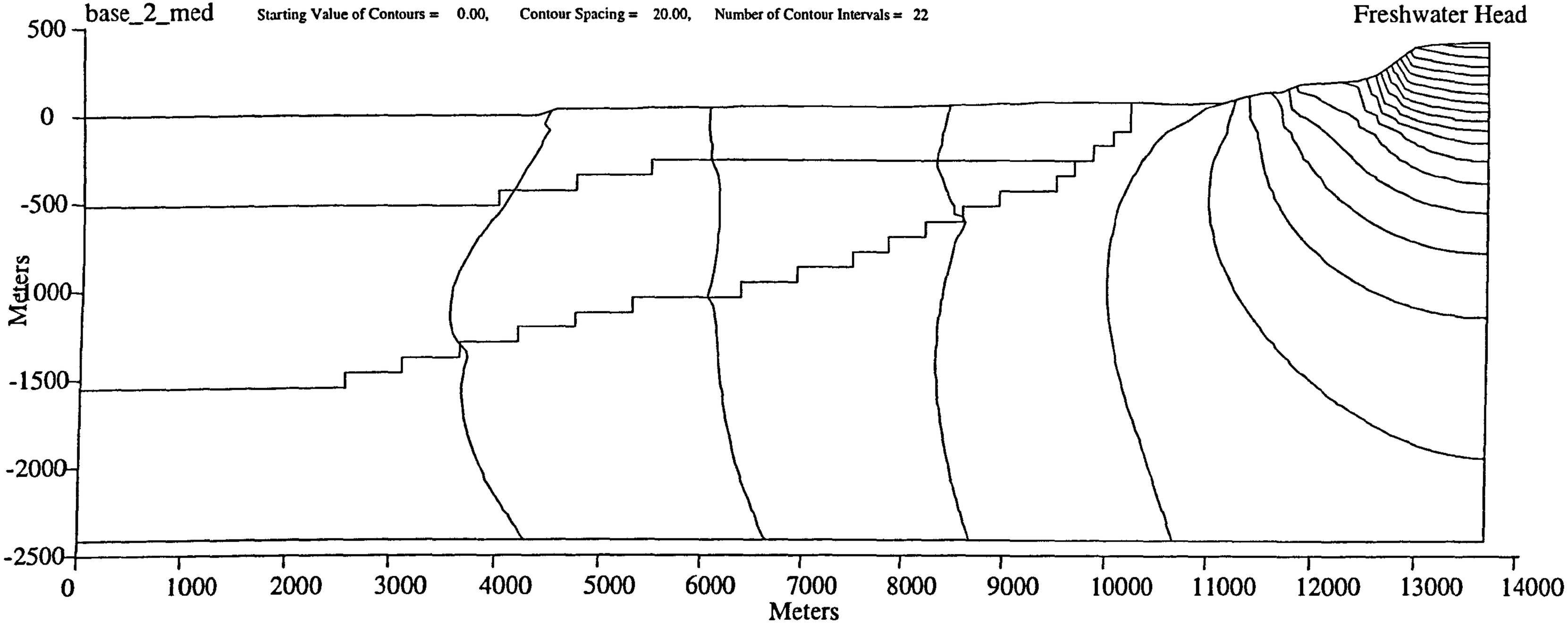

Fig. 3.17 Plot of equivalent freshwater hydraulic head calculated with heterogeneous grid (Fig. 3.16). Hydraulic conductivities as Fig. 3.16. Head contours are deflected across the boundary of St Bees Sst. and BVG. Low vertical hydraulic gradients in central part of grid.

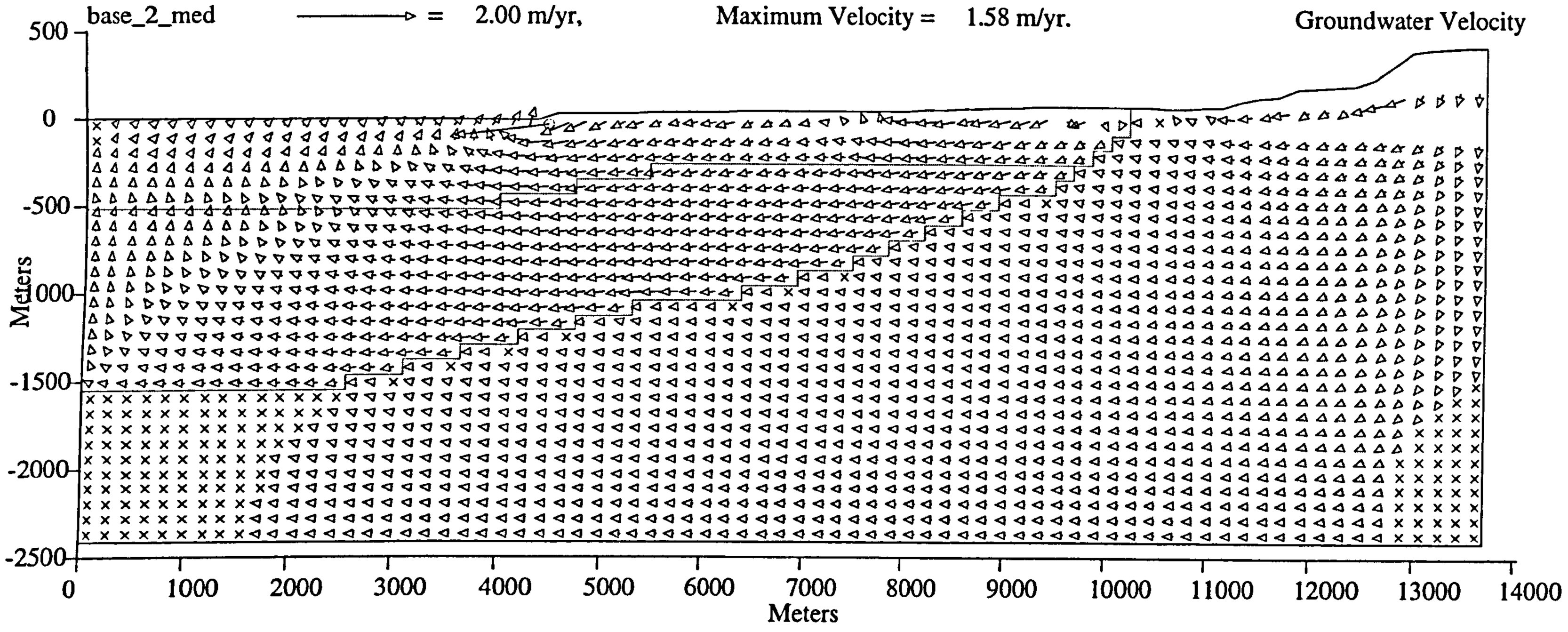

Fig. 3.18 Groundwater flow plot displaying average linear velocities calculated with heterogeneous grid (Fig. 3.16). Hydraulic conductivities as Fig. 3.16. Maximum flow in Calder Sst., some flow in BVG. Deep flow pattern similar to Fig. 3.15, i.e. topographically driven.

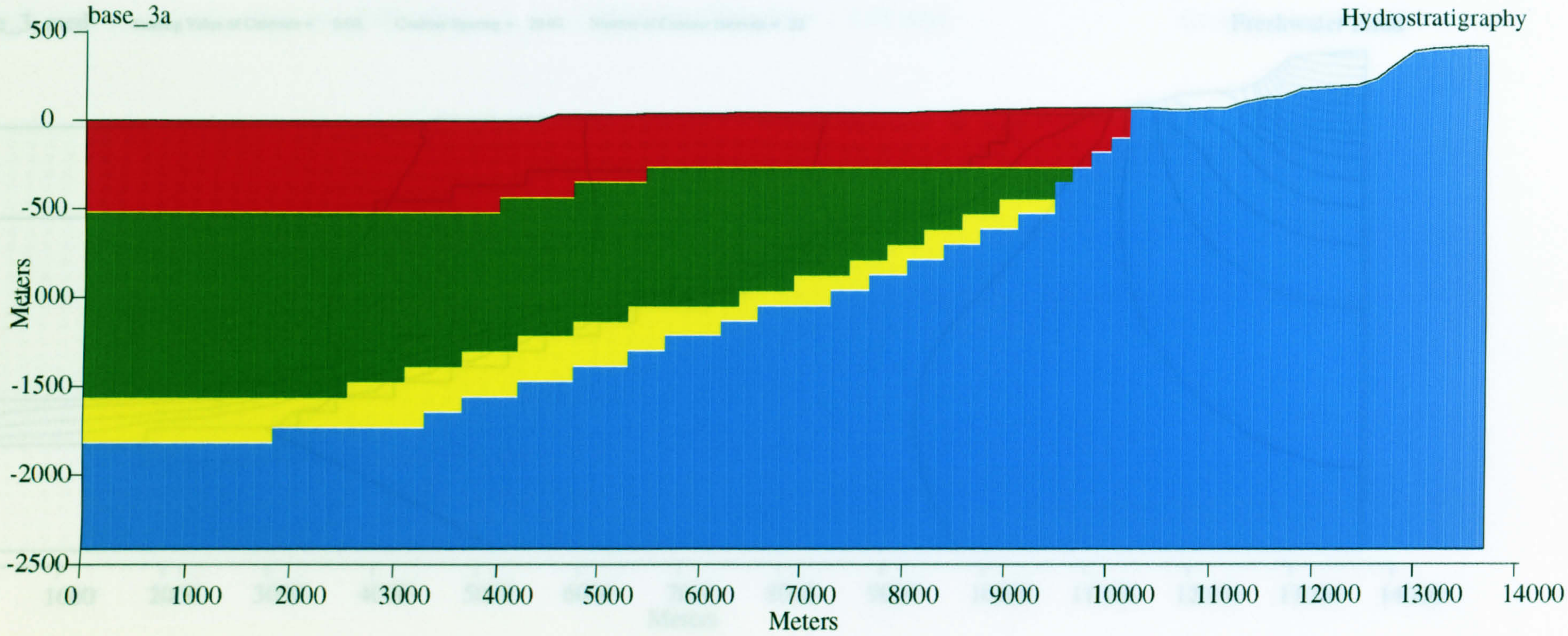

Fig. 3.19 Heterogeneous grid composed of Calder Sst. (red); St Bees Sst. (green) St Bees Evaporites / Brockram Breccia (yellow) and BVG (turquoise). Base case hydraulic conductivities (horizontal); Calder Sst. = 3.00 m/yr; St Bees Sst. = 1.50 m/yr; St Bees Evaporites / Brockram Breccia = 9.50E-04 m/yr; BVG = 1.20E-02 m/yr. Boundary conditions as Fig. 3.11.

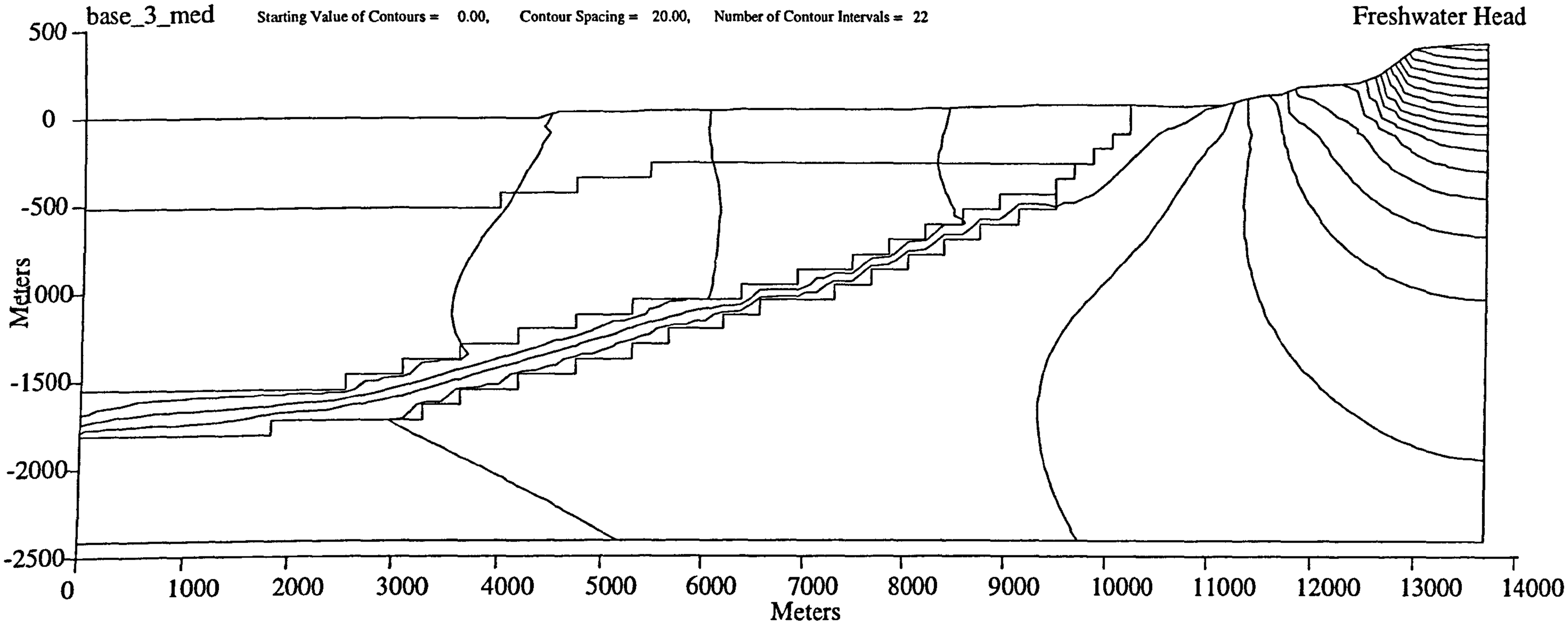

Fig. 3.20 Plot of equivalent freshwater hydraulic head calculated with heterogeneous grid (Fig. 3.19). Hydraulic conductivities as Fig. 3.19. Head contours compressed in St Bees Evaporites / Brockram Breccia. High hydraulic head gradients in vertical plane.

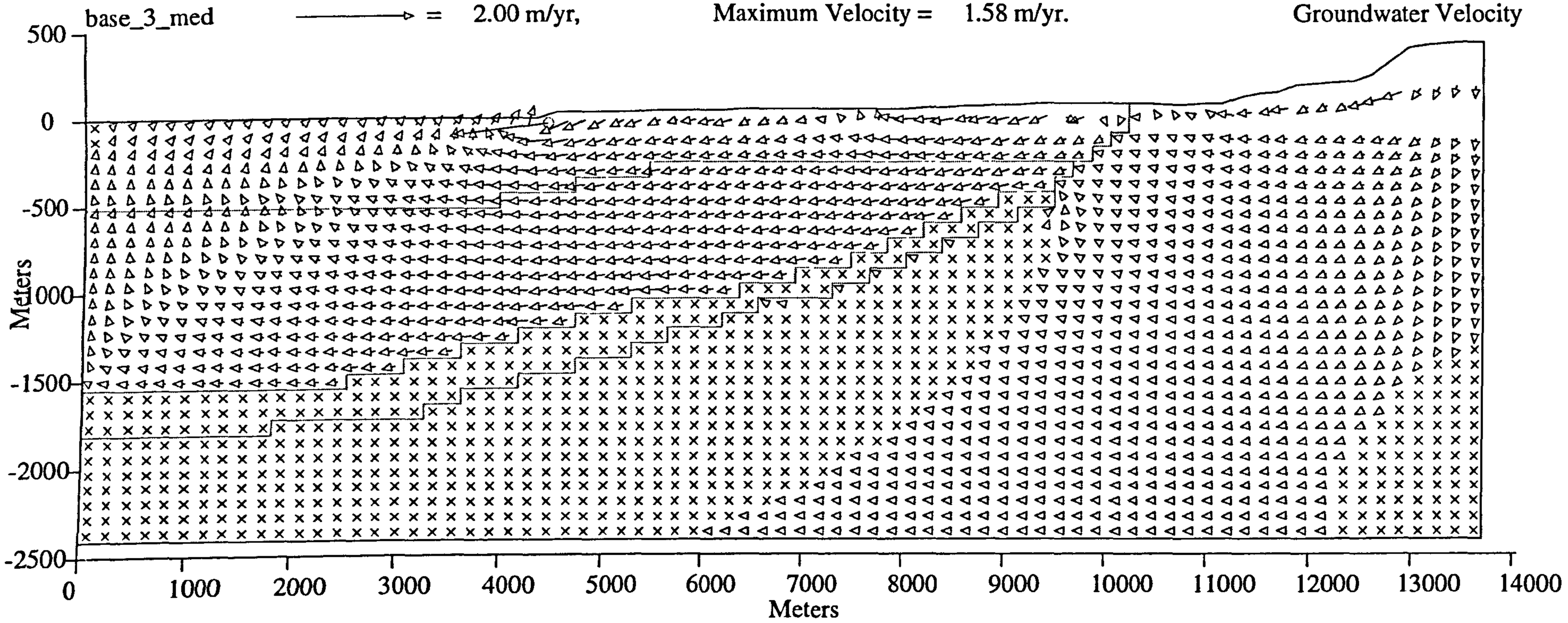

Fig. 3.21 Groundwater flow plot displaying average linear velocities calculated with heterogeneous grid (Fig. 3.19). Hydraulic conductivities as Fig. 3.19. Maximum flow in Calder Sst., some flow in BVG. Deep flow pattern similar to Fig. 3.15, i.e. topographically driven. Groundwater flows diagonally into cover sediments.

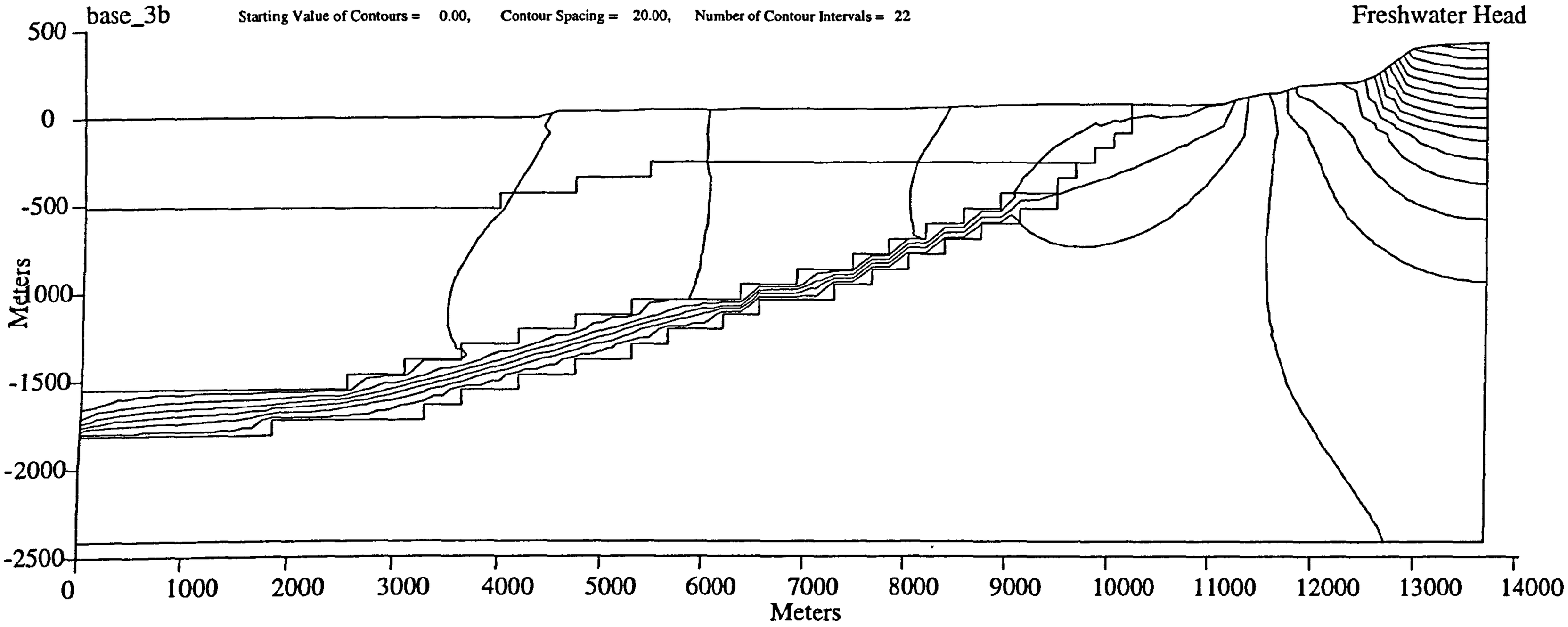

Fig. 3.22 Plot of equivalent freshwater hydraulic head calculated with heterogeneous grid (Fig. 3.19). Horizontal hydraulic conductivity of BVG set to 1.20E+00 m/yr. Hydraulic conductivities for other units as in Fig. 3.19. Head contours more compressed in St Bees Evaporites / Brockram Breccia. Higher hydraulic head gradients in vertical plane than Fig. 3.21.

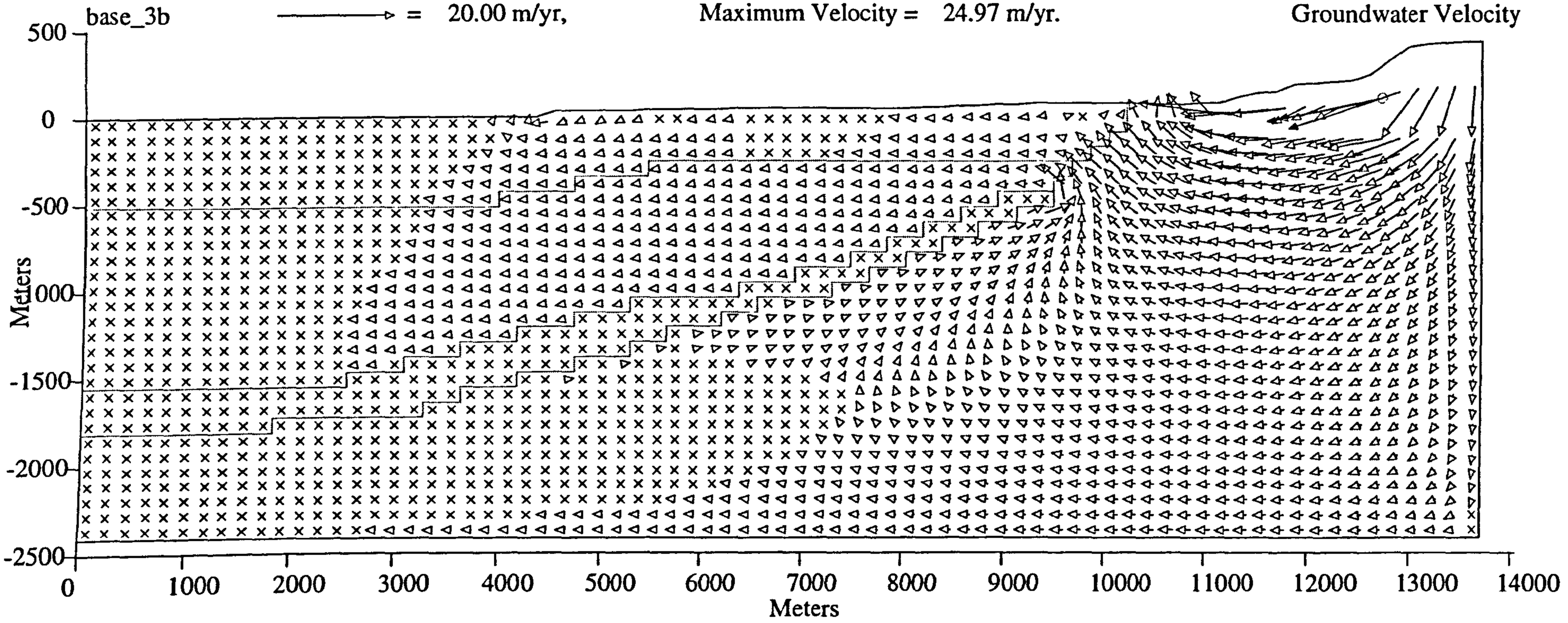

Fig. 3.23 Groundwater flow plot displaying average linear velocities calculated with heterogeneous grid (Fig. 3.19). Horizontal hydraulic conductivity of BVG set to 1.20E+00 m/yr. Hydraulic conductivities for other units as in Fig. 3.19. Maximum flow in BVG. Dominantly topographically driven flow. Strong diagonal transfer into cover sediments. Some springs at base of slope.

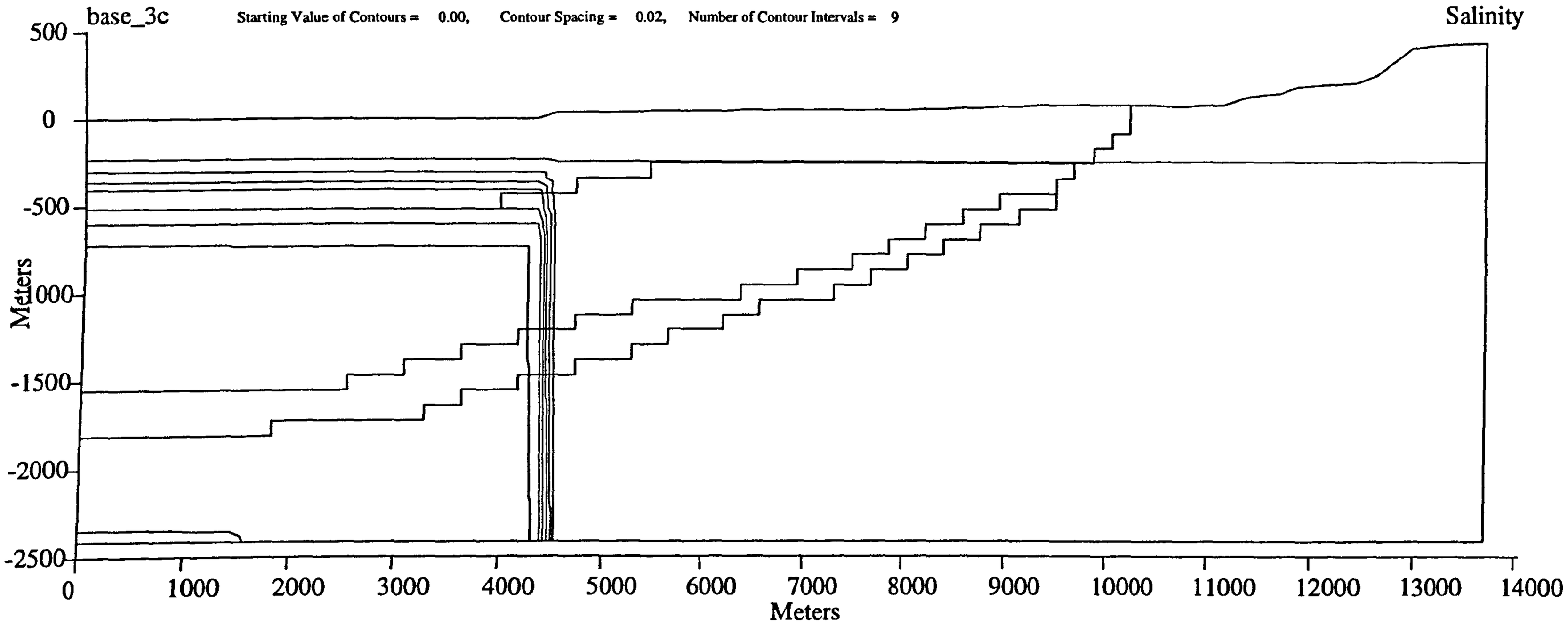

Fig. 3.24 Salinity profile imposed on simple grid. Deep western part has maximum salinity = 16 %; Salinity in central area = 2 %; fresh water down to 250 m.

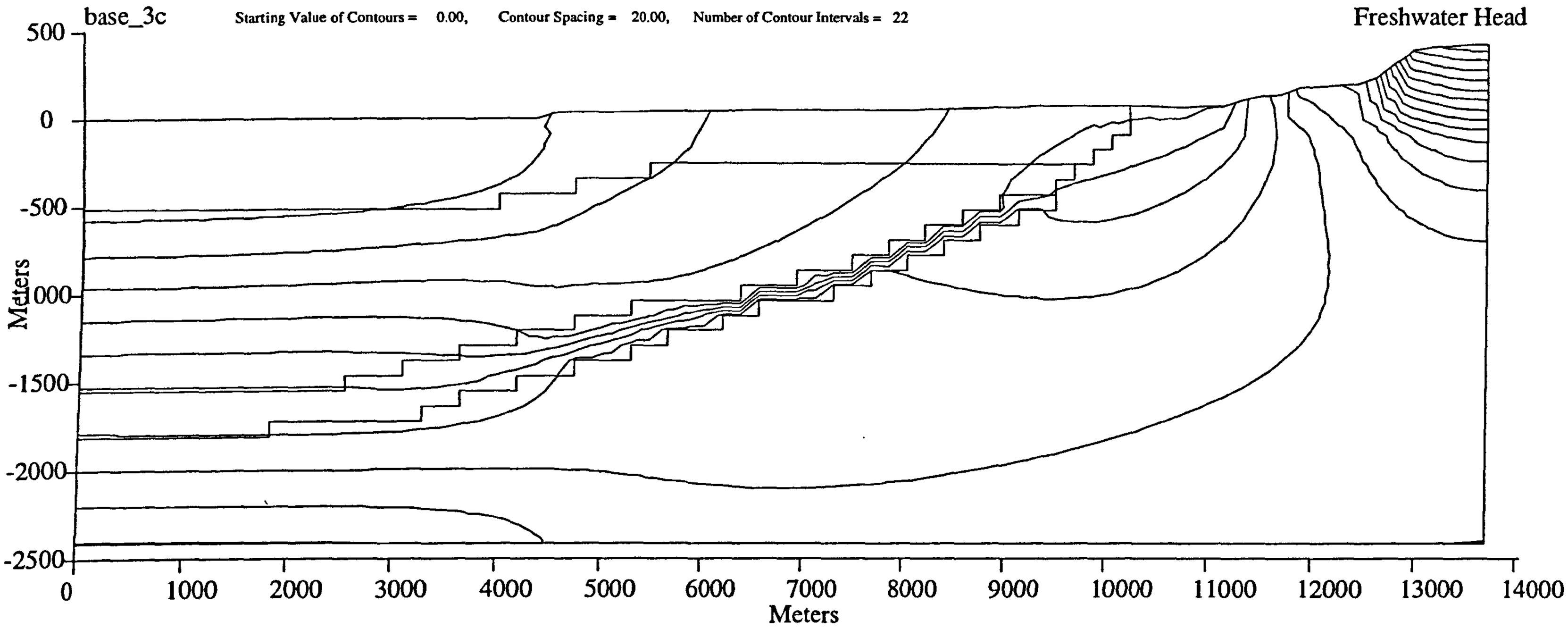

Fig. 3.25 Plot of equivalent freshwater hydraulic head calculated with heterogeneous grid (Fig. 3.19). Horizontal hydraulic conductivity of BVG set to 1.20E+00 m/yr . Imposed variable salinity profile as that of Fig. 3.24 . Hydraulic conductivities for other units as in Fig. 3.19. Strong vertical hydraulic gradients in western area of 16 % salinity. High hydraulic gradient in St Bees Evaporites / Brockram Breccia. Evidence for topographically driven flow in BVG.

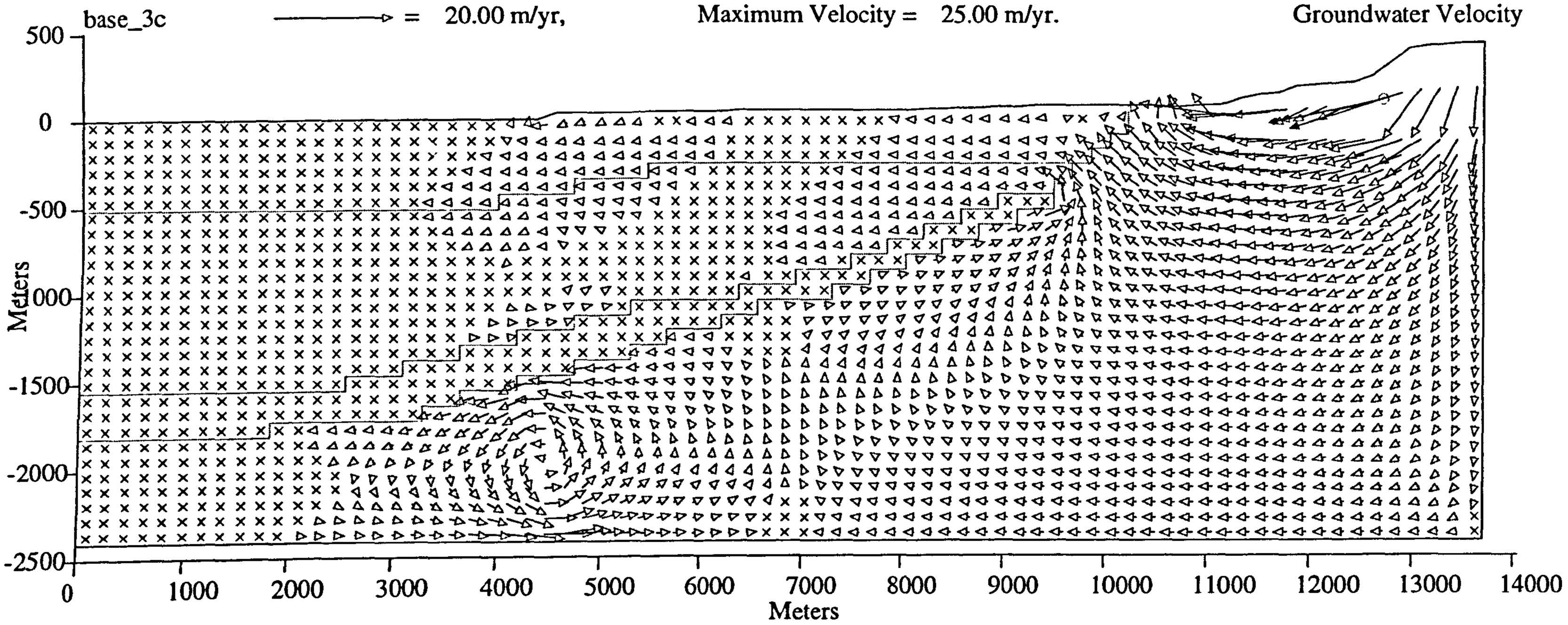

Fig. 3.26 Groundwater flow plot displaying average linear velocities calculated with heterogeneous grid (Fig. 3.19). Horizontal hydraulic conductivity of BVG set to 1.20E+00 m/yr. Imposed variable salinity profile as that of Fig. 3.24 . Hydraulic conductivities for other units as in Fig. 3.19. Groundwater flow at depth in area of brine develops convective "eddies". Possibly due to interface of topographically driven saline fluid meeting eastern "flowing" brine. Maximum flow in BVG. Dominantly topographically driven flow. Strong diagonal transfer into cover sediments.

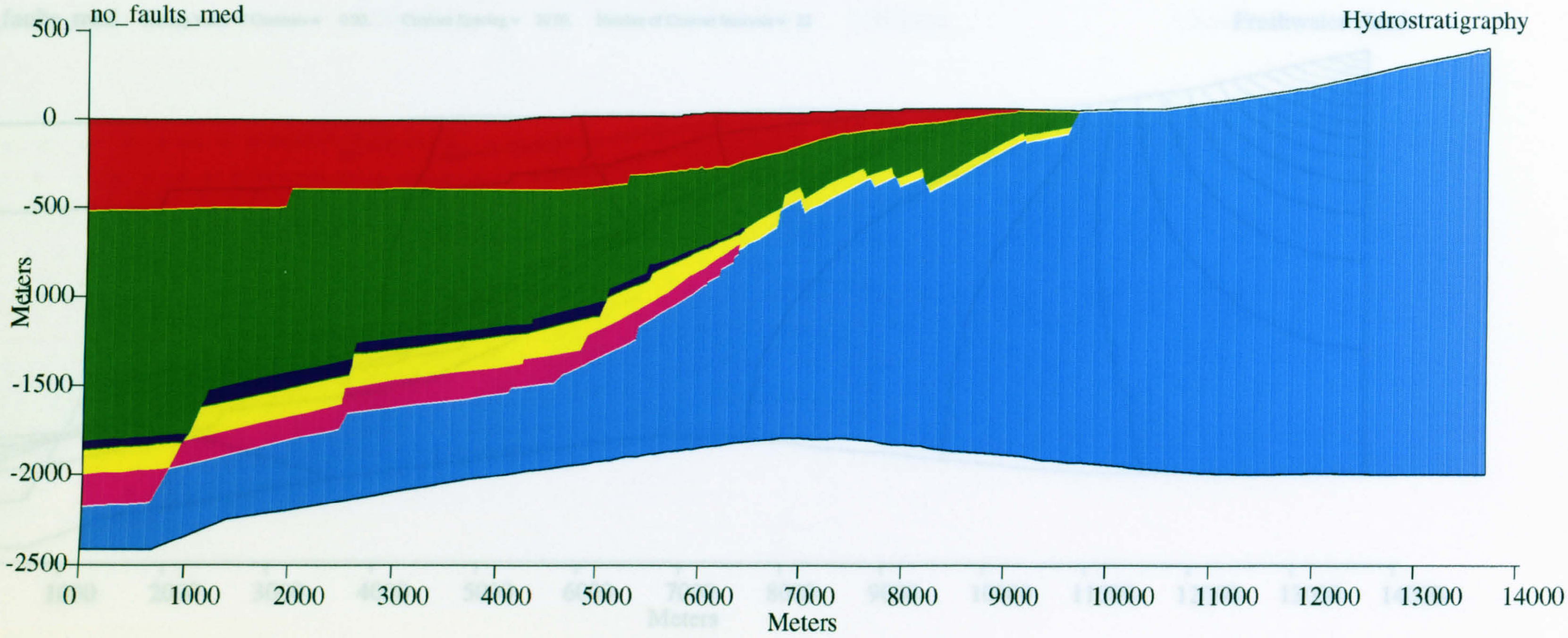

Fig. 3.27 Complex geology grid based on cross section shown in Fig. 3.2. No faults; hydrostratigraphic units simply offset. Calder Sst. (red); St Bees Sst. (green); St Bees Evaporites (purple); Brockram Breccia (yellow); Carboniferous Limestone (pink) and BVG (turquoise). Boundary conditions as those of simple models (Figs. 3.11, 3.16 & 3.19); Left - no flow; Right no flow; Bottom - no flow; Top - flow permitted.

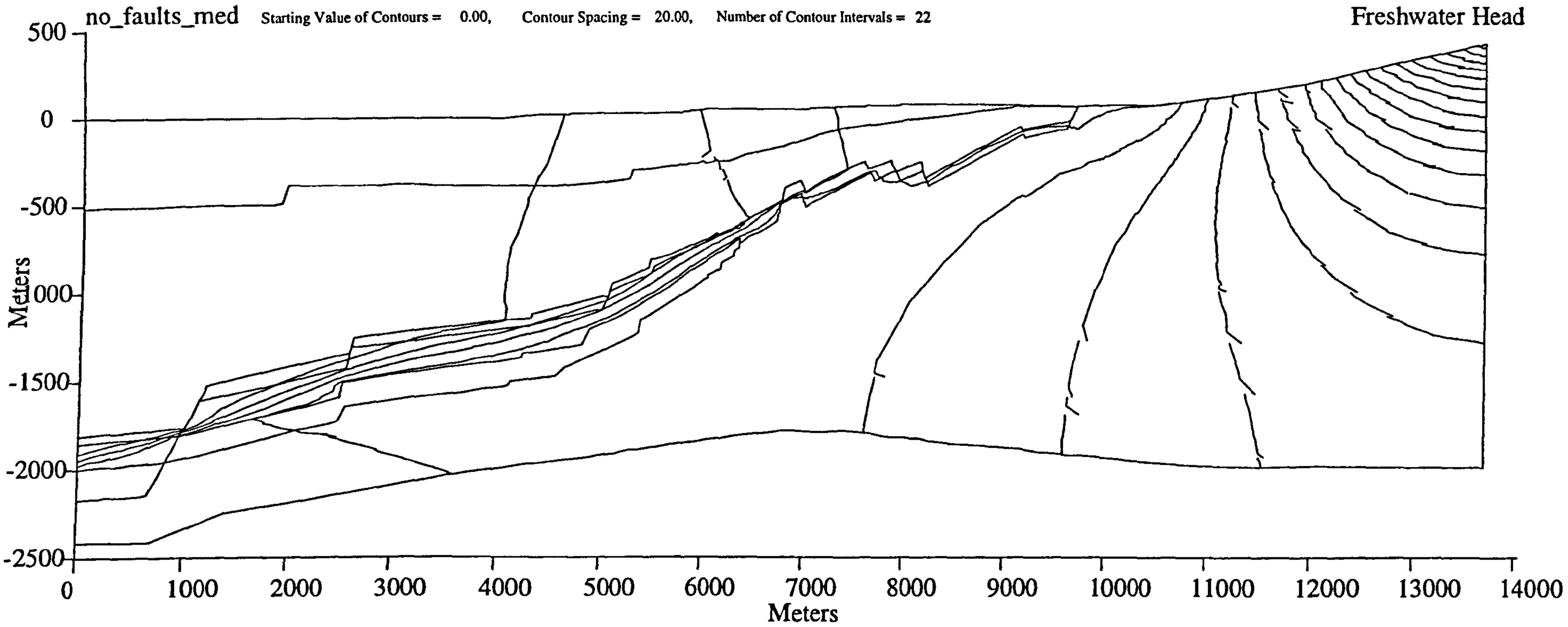

Fig. 3.28 Plot of equivalent freshwater hydraulic head calculated with complex grid (Fig. 3.27). Base case hydraulic conductivities (horizontal); Calder Sst. = 3.00 m/yr; St Bees Sst. = 1.50 m/yr; St Bees Evaporites = 1.60E-03 m/yr; Brockram Breccia = 9.50E-04 m/yr;. Carboniferous Limestone = 1.50E-01 m/yr; BVG = 1.20E-02 m/yr. Similar head profile to simple grid (Fig. 3.20). Head contours compressed in St Bees Evaporites and Brockram Breccia suggesting high hydraulic head gradients in vertical plane. Evidence for topographically driven flow in BVG.

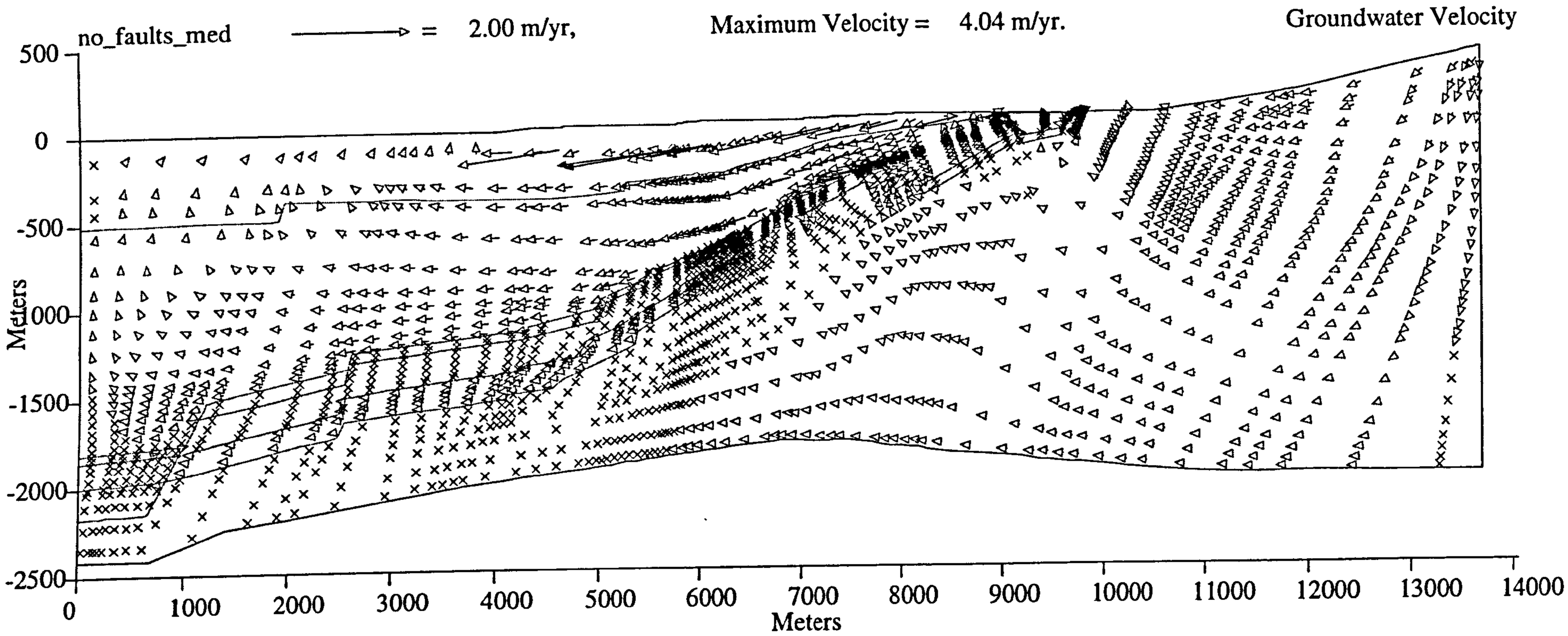

Fig. 3.29 Groundwater flow plot displaying average linear velocities calculated with complex grid (Fig. 3.27). Horizontal hydraulic conductivity as those of Fig. 3.28. Maximum flow in Calder Sst., some topographically driven flow in BVG. This is a similar result to that of Fig. 3.20 with a simple grid. This shows that the flow pathways within the BVG do not depend on the shape and size of the grid cells.

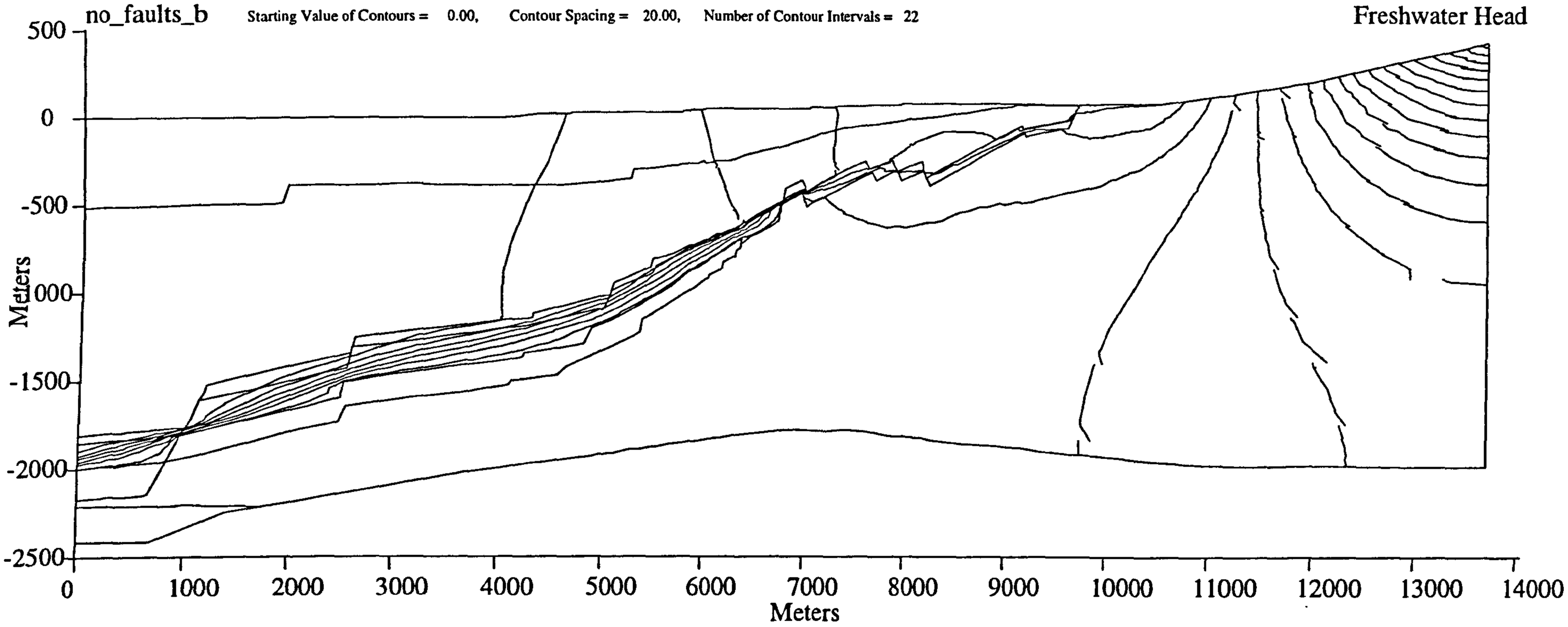

Fig. 3.30 Plot of equivalent freshwater hydraulic head calculated with complex grid (Fig. 3.27). Horizontal hydraulic conductivity of BVG set to 1.20E+00 m/yr. Hydraulic conductivities for other units set to base case (~ median) values, as in Fig. 3.28. Head contours more compressed in St Bees Evaporites & Brockram Breccia. Higher hydraulic head gradients in vertical plane than Fig. 3.28.

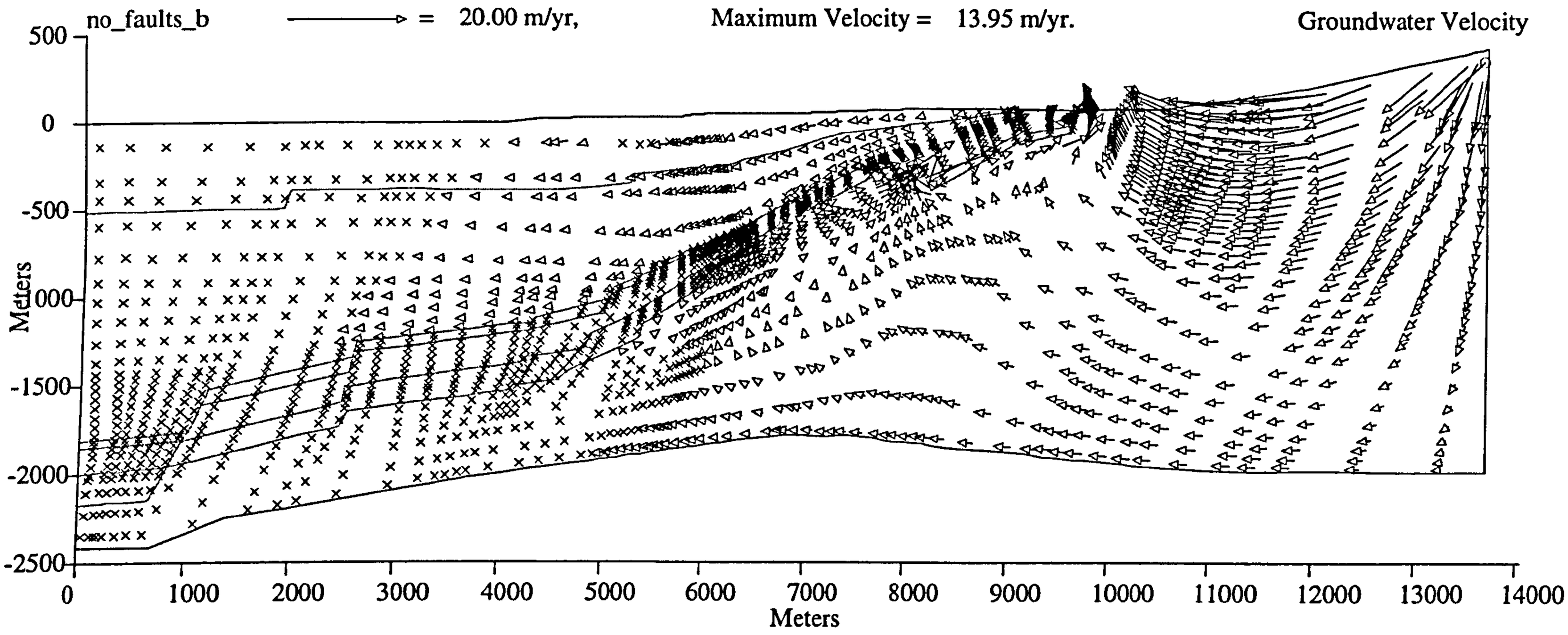

Fig. 3.31 Groundwater flow plot displaying average linear velocities calculated with complex grid (Fig. 3.27). Horizontal hydraulic conductivity of BVG set to 1.20E+00 m/yr. Hydraulic conductivities for other units as in Fig. 3.28. Maximum flow in BVG. Dominantly topographically driven flow. Strong diagonal transfer into cover sediments. Some springs at base of slope.

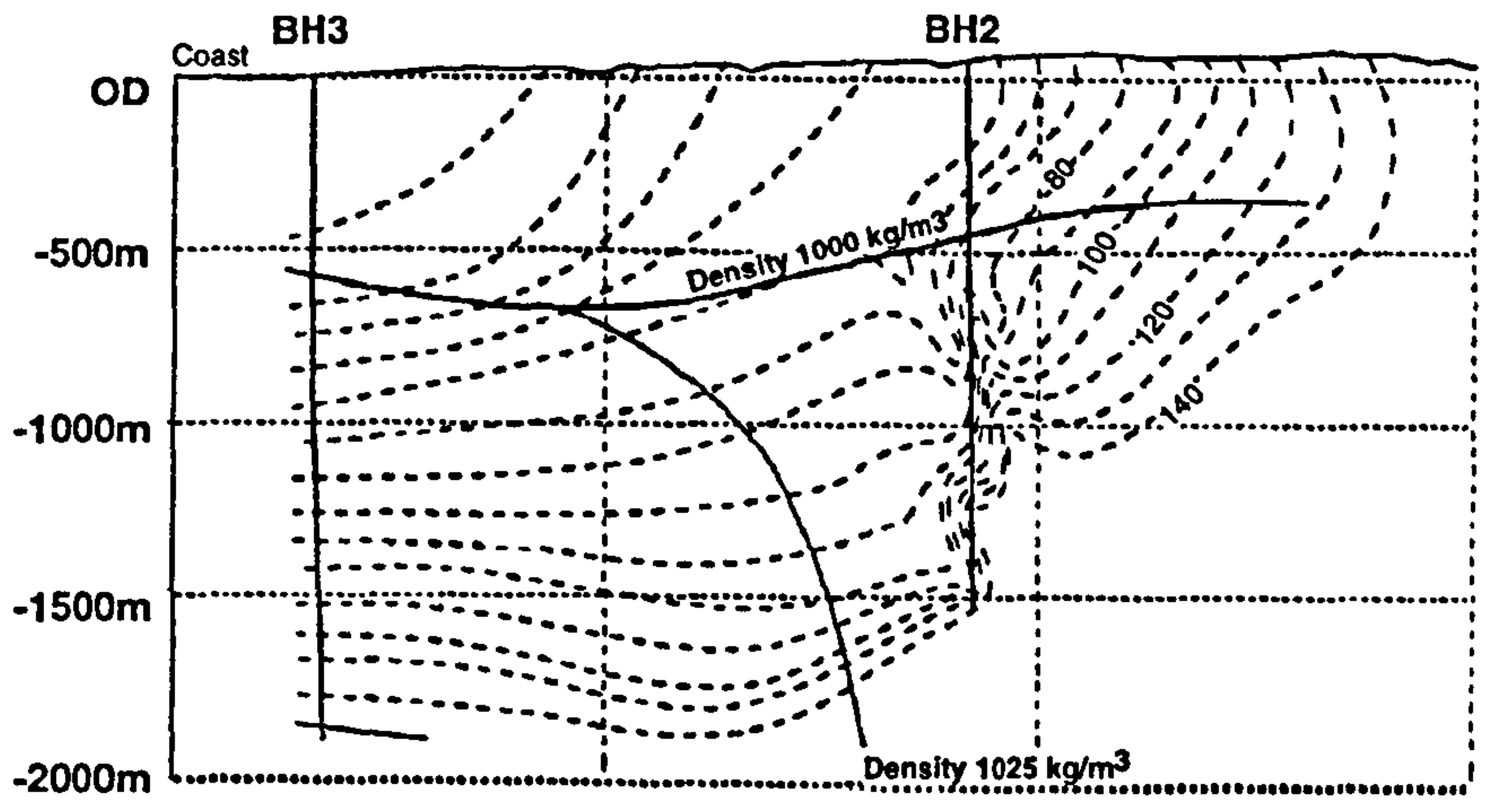

Fig. 3.32 West-east cross section showing variations in freshwater head (after Black, J.H. & Brightman, M.A., 1996). Scale same as groundwater flow models.

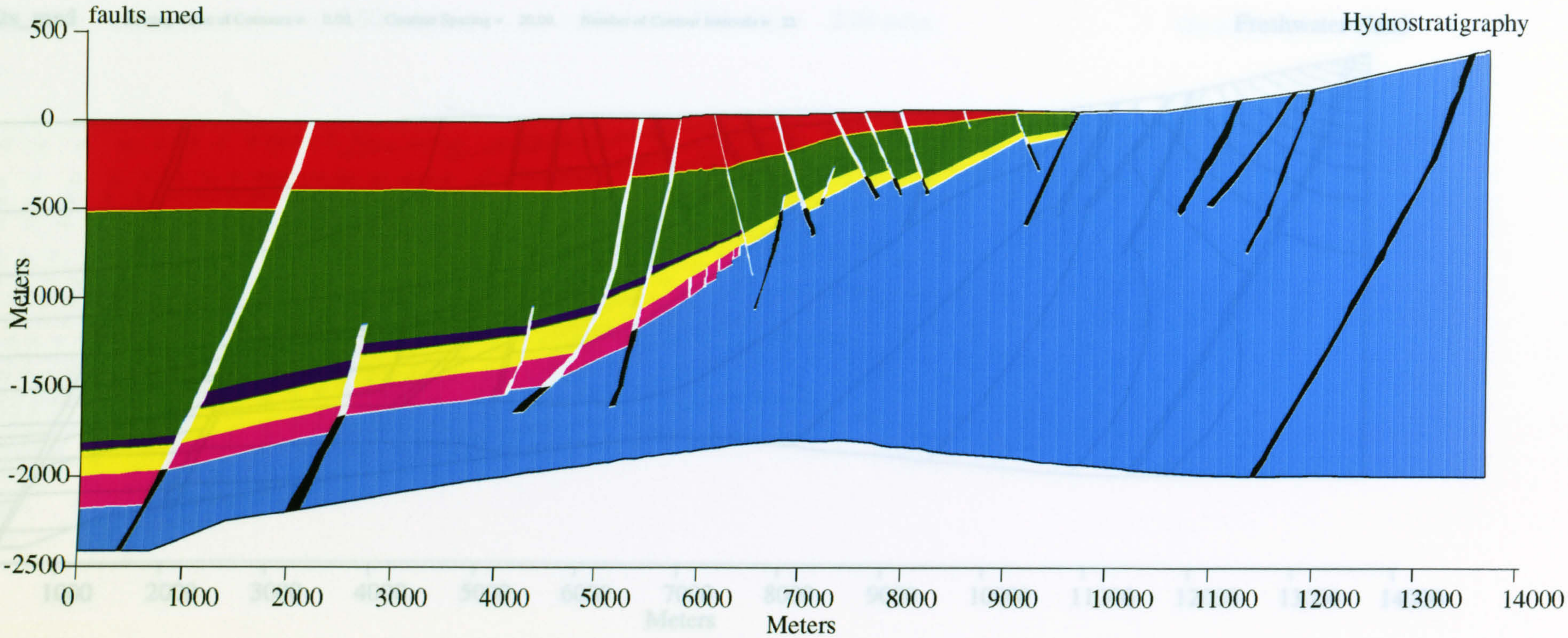

Fig. 3.33 Complex geology grid based on cross section shown in Fig. 3.2. Faults represented by overwide single columns of material (see text). Calder Sst. (red); St Bees Sst. (green); St Bees Evaporites (purple); Brockram Breccia (yellow); Carboniferous Limestone (pink); BVG (turquoise); cover faults (white); BVG faults (black). Boundary conditions as those of Fig. 3.27.

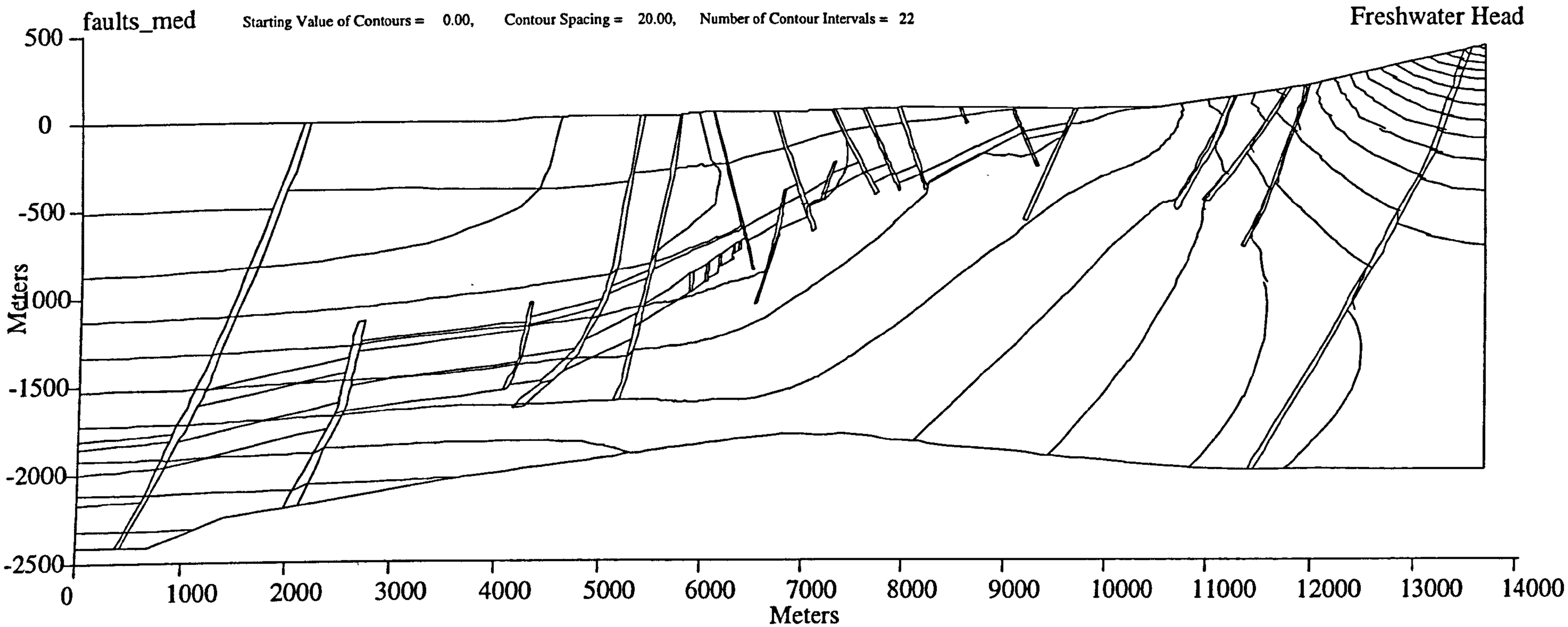

Fig. 3.34 Plot of equivalent freshwater hydraulic head calculated with complex grid (Fig. 3.33). Base case hydraulic conductivities (horizontal); Calder Sst. = 3.00 m/yr; St Bees Sst. = 1.50 m/yr; St Bees Evaporites = 1.60E-03 m/yr; Brockram Breccia = 9.50E-04 m/yr; Carboniferous Limestone = 1.50E-01 m/yr; BVG = 1.20E-02 m/yr. "Real world" hydraulic conductivities of cover faults and BVG faults = 30 m/yr and 3 m/yr respectively. Simulated hydraulic conductivities = 0.3 m/yr and 0.03 m/yr respectively (see text). Head profile markedly different to that observed in field (Fig. 3.32). Faults cause offset to hydraulic head. No vertical hydraulic gradients in central region of grid.

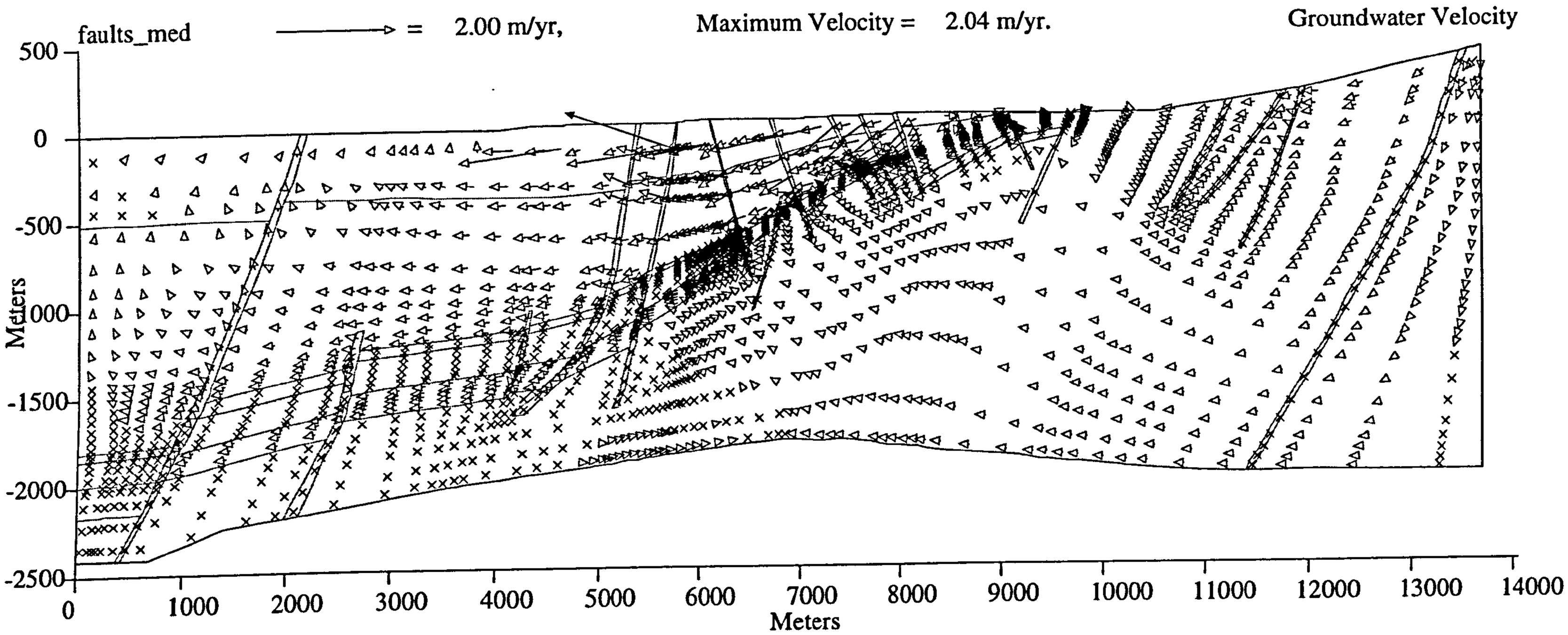

Fig. 3.35 Groundwater flow plot displaying average linear velocities calculated with complex grid (Fig. 3.33). Horizontal hydraulic conductivity as those of Fig. 3.34. Maximum flow in Calder Sst., some topographically driven flow in BVG.

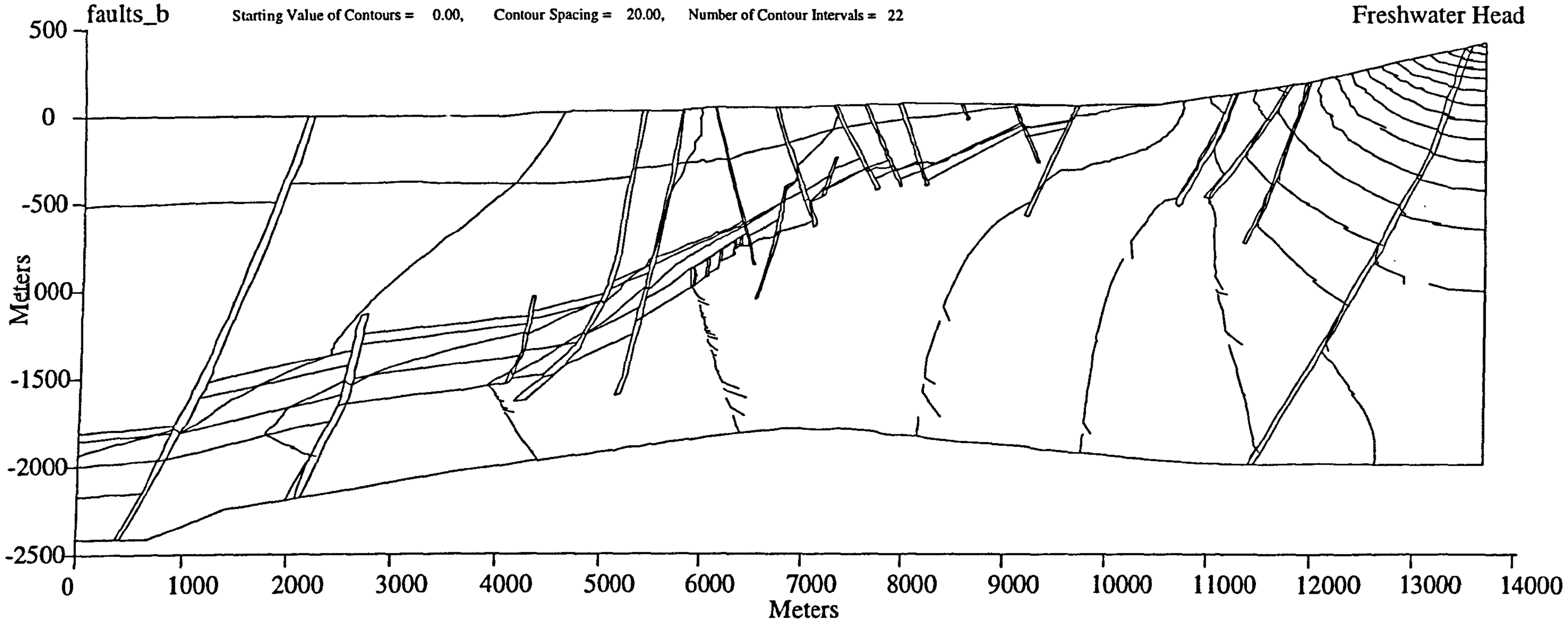

Fig. 3.36 Plot of equivalent freshwater hydraulic head calculated with complex grid (Fig. 3.33). Horizontal hydraulic conductivity of BVG set to 1.20E+00 m/yr. Hydraulic conductivities for other units set to base case values, as in Fig. 3.34. Slightly higher hydraulic head gradients in vertical plane of central region than Fig. 3.34. Evidence for topographically driven flow in BVG.

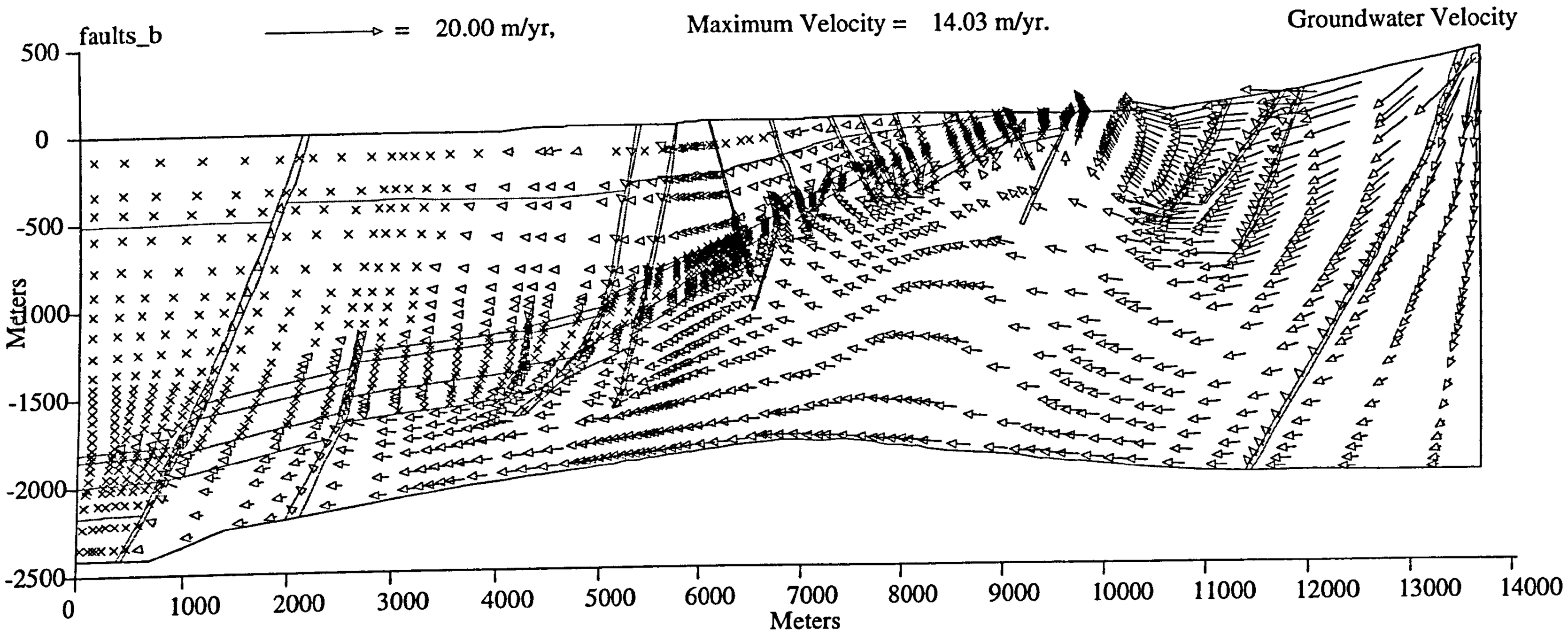

Fig. 3.37 Groundwater flow plot displaying average linear velocities calculated with complex grid (Fig. 3.33). Horizontal hydraulic conductivity of BVG set to 1.20E+00 m/yr. Hydraulic conductivities for other units as in Fig. 3.34. Maximum flow in BVG. Dominantly topographically driven flow. Strong diagonal transfer into cover sediments via faults in St Bees Evaporites and Brockram Breccia. Some springs at base of slope.

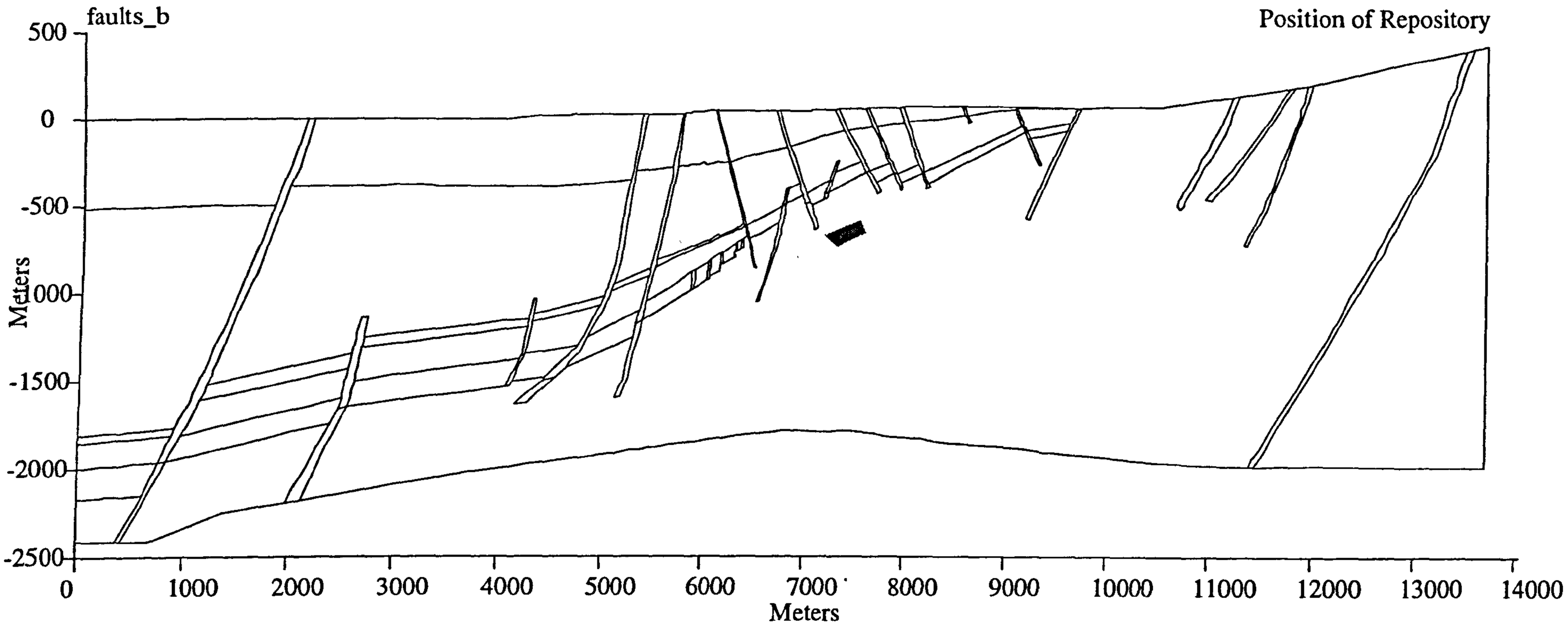

Fig. 3.38 Repository location. The absolute value of the average linear velocity for a specific element can be computed by calculating the mean resultant vector of the horizontal and vertical fluid velocity components.

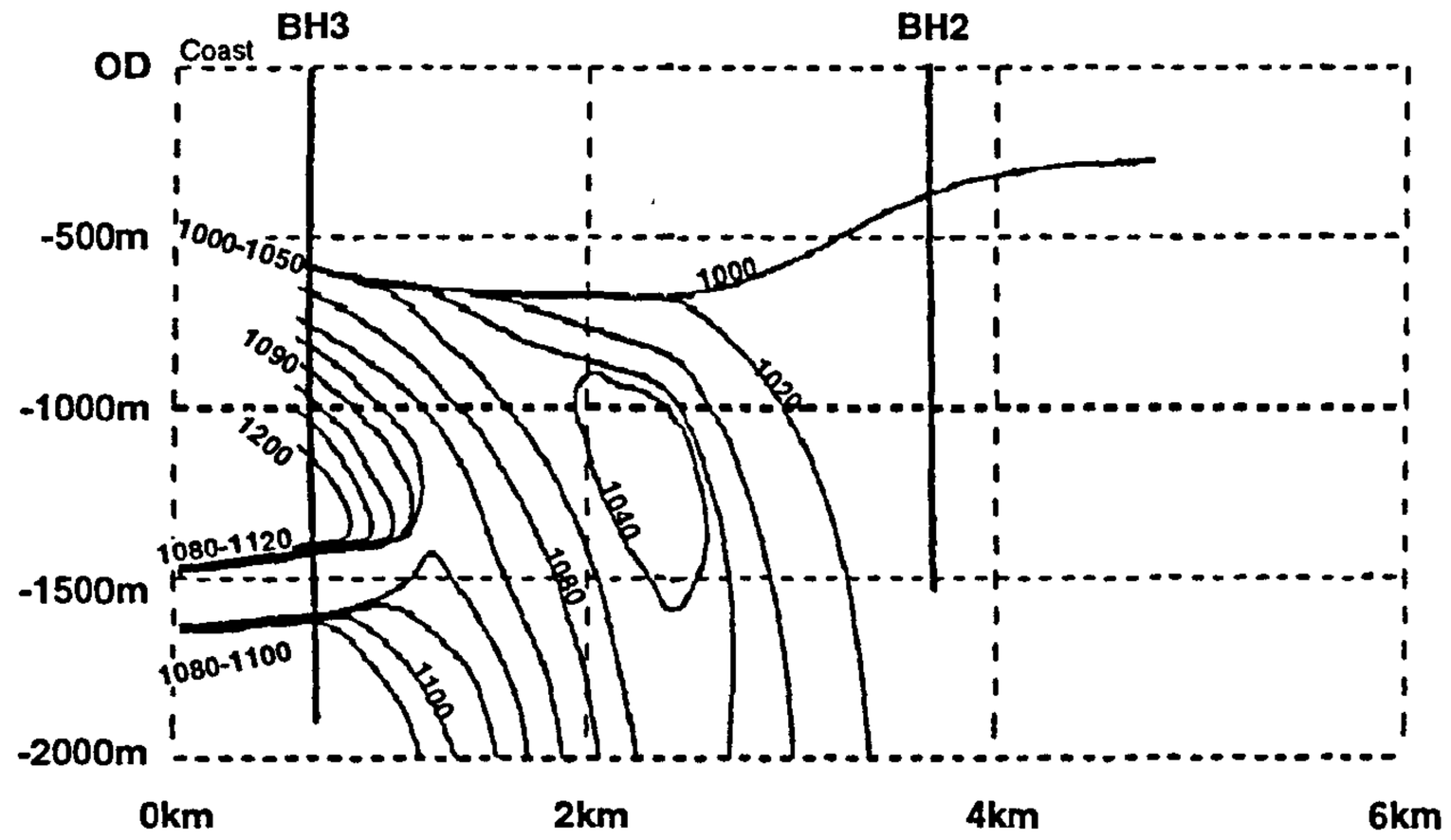

Fig. 3.39 **West-east cross section showing variations in groundwater density (after Black, J.H. & Brightman, M.A., 1996). Scale same as groundwater flow models.**

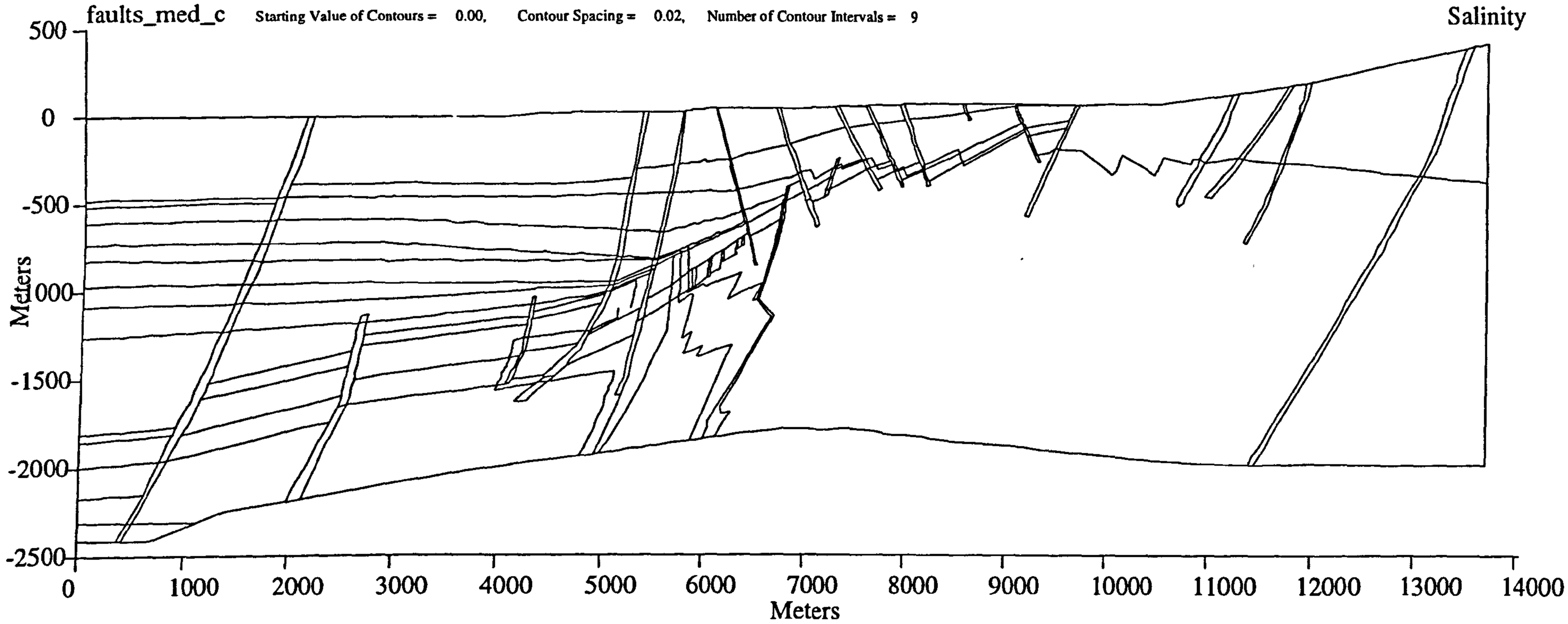

Fig. 3.40 Salinity profile imposed on complex grid. Data derived from published information (Nirex, 1993a; Nirex, 1993b). Deep western part has maximum salinity = 16 %; Salinity in central area = 2 %; fresh water down to 500 m. Contour spacing = 2 %.

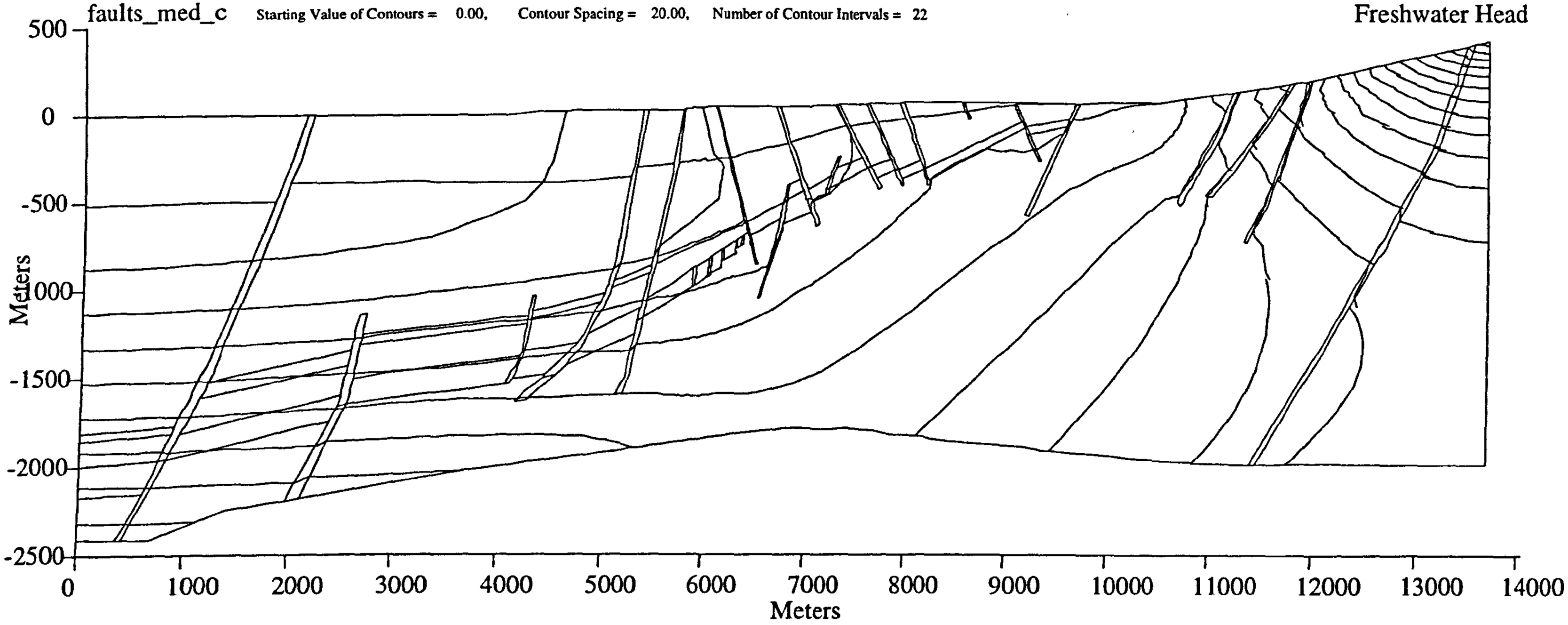

Fig. 3.41 Plot of equivalent freshwater hydraulic head calculated with complex grid (Fig. 3.33). Imposed salinity profile as that of Fig. 3.40. Hydraulic conductivities as in Fig. 3.34. Head gradients similar to those observed (Fig. 3.32). High vertical gradients in western area of 16 % salinity. Potential for diagonal flow in central region of high hydraulic gradient. Evidence for topographically driven flow in BVG.

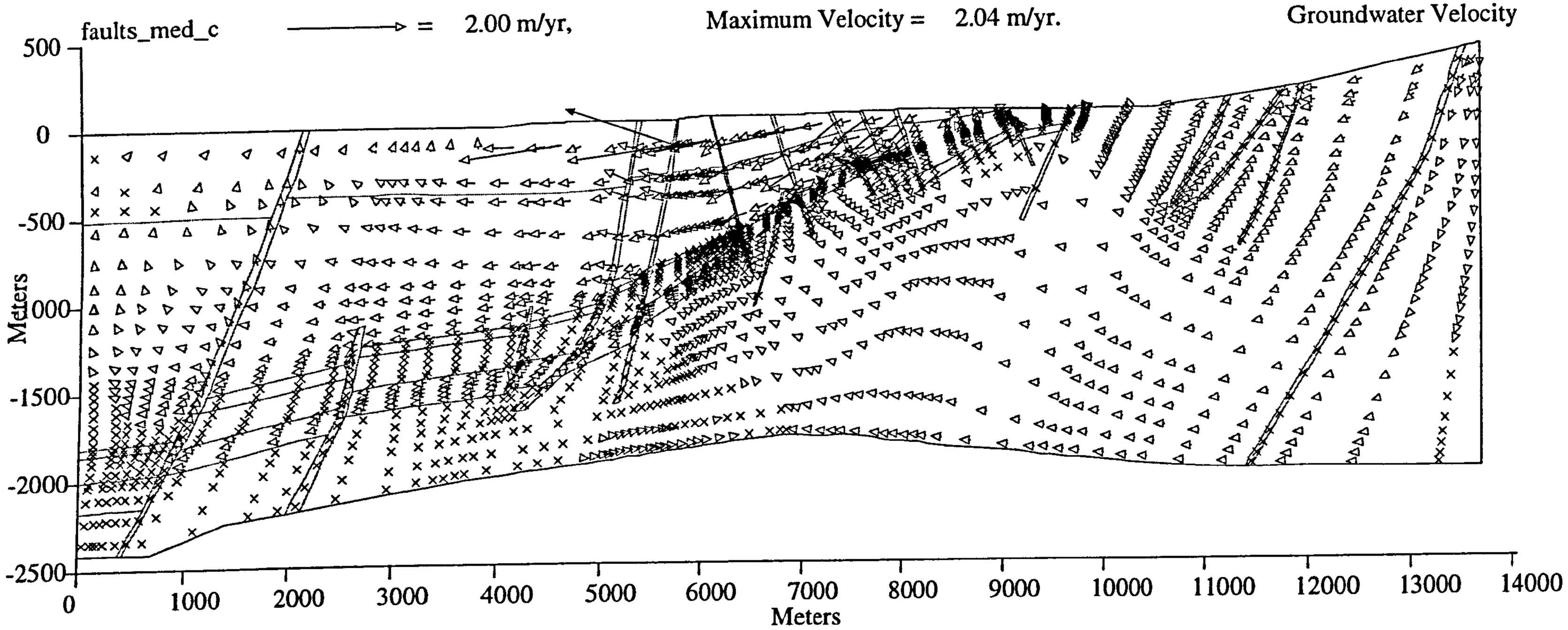

Fig. 3.42 Groundwater flow plot displaying average linear velocities calculated with complex grid (Fig. 3.33). Imposed salinity profile as that of Fig. 3.40. Hydraulic conductivities set to base case values, as in Fig. 3.34. Maximum flow in Calder Sst., some topographically driven flow in BVG with upward trending flow in central region of grid.

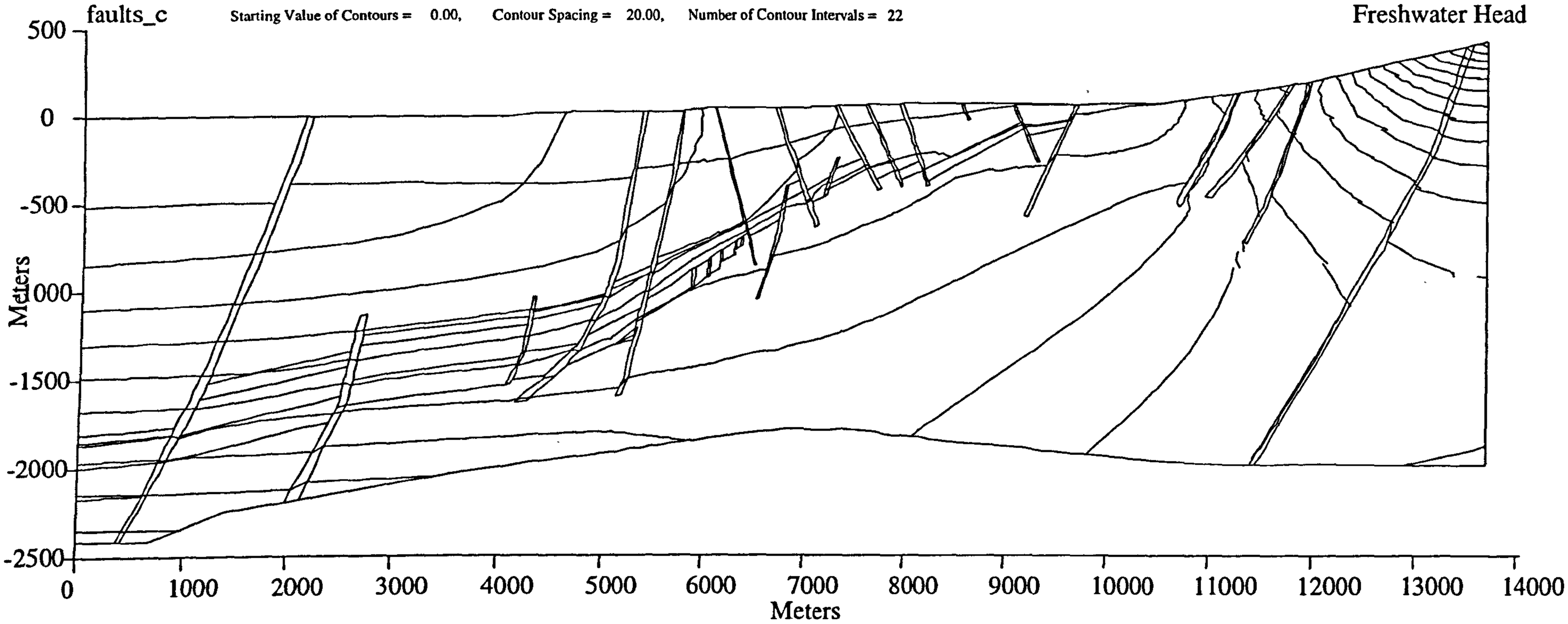

Fig. 3.43 Plot of equivalent freshwater hydraulic head calculated with complex grid (Fig. 3.33). Imposed salinity profile as that of Fig. 3.40. Horizontal hydraulic conductivity of BVG set to 1.20E+00 m/yr. Hydraulic conductivities for other units and faults set to base case values, as in Fig. 3.34. Head gradients very similar to those observed in field investigations (Fig. 3.32). High vertical gradients in western area of 16 % salinity. Potential for diagonal flow in central region of high hydraulic gradient. Evidence for topographically driven flow in BVG.

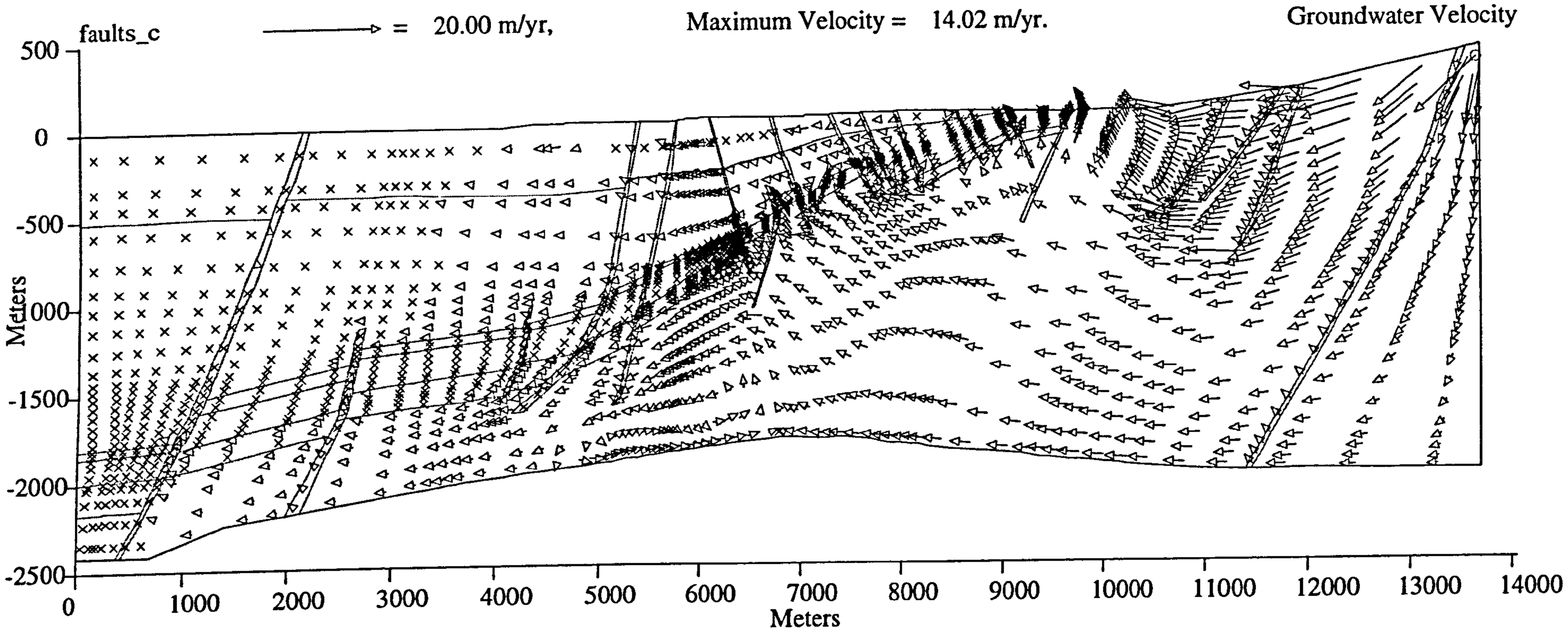

Fig. 3.44 Groundwater flow plot displaying average linear velocities calculated with complex grid (Fig. 3.33). Imposed salinity profile as that of Fig. 3.40. Horizontal hydraulic conductivity of BVG set to 1.20E+00 m/yr. Hydraulic conductivities for other units as in Fig. 3.34. Groundwater flow at depth in area of brine develops convective "eddies". Possibly due to interface of topographically driven saline fluid meeting eastern "flowing" brine. Maximum flow in BVG. Dominantly topographically driven flow. Strong diagonal transfer into cover sediments. Some springs at base of slope.

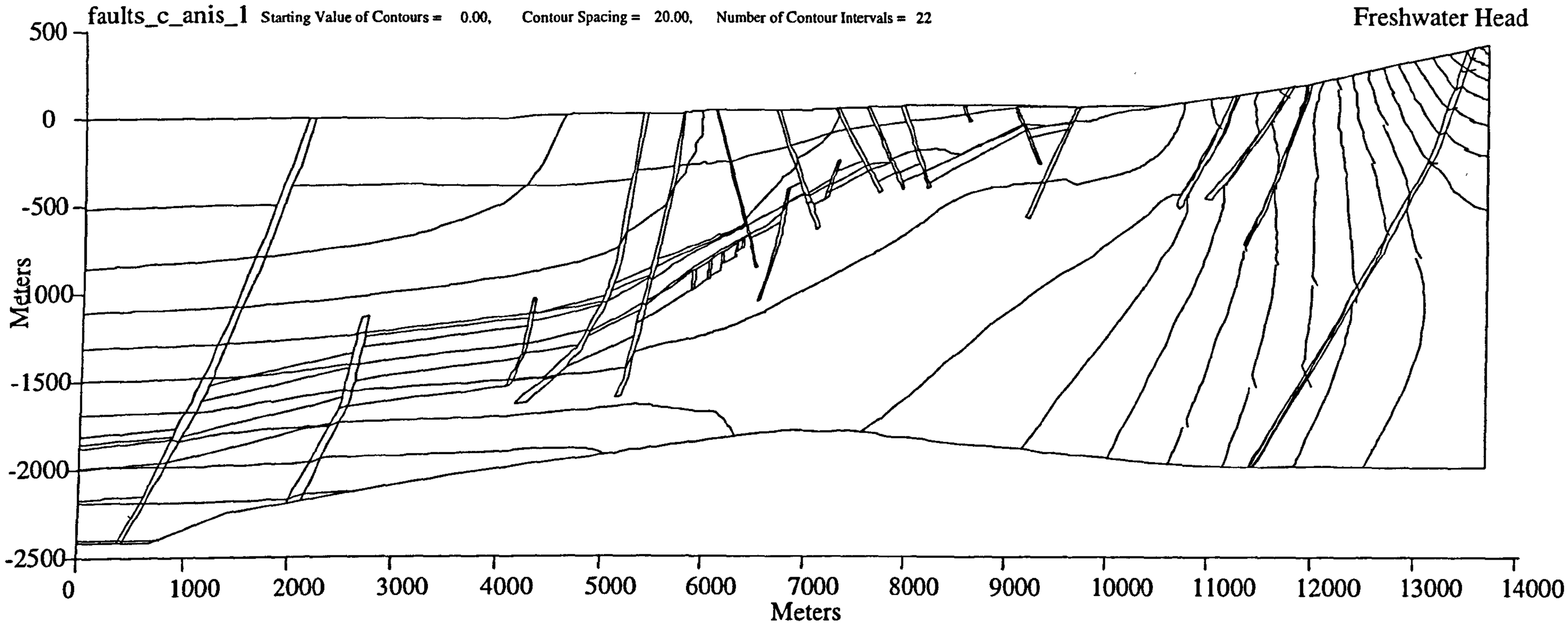

Fig. 3.45 Plot of equivalent freshwater hydraulic head calculated with complex grid (Fig. 3.41). Anisotropy of BVG changed to 1. All other conditions as in Fig. 3.43. Head profile indicates higher hydraulic gradients in BVG compared to Fig. 3.43. Head gradients very similar to those observed (Fig. 3.32). High vertical gradients in western area of 16 % salinity. Potential for diagonal flow in central region of high hydraulic gradient. Evidence for topographically driven flow in BVG.

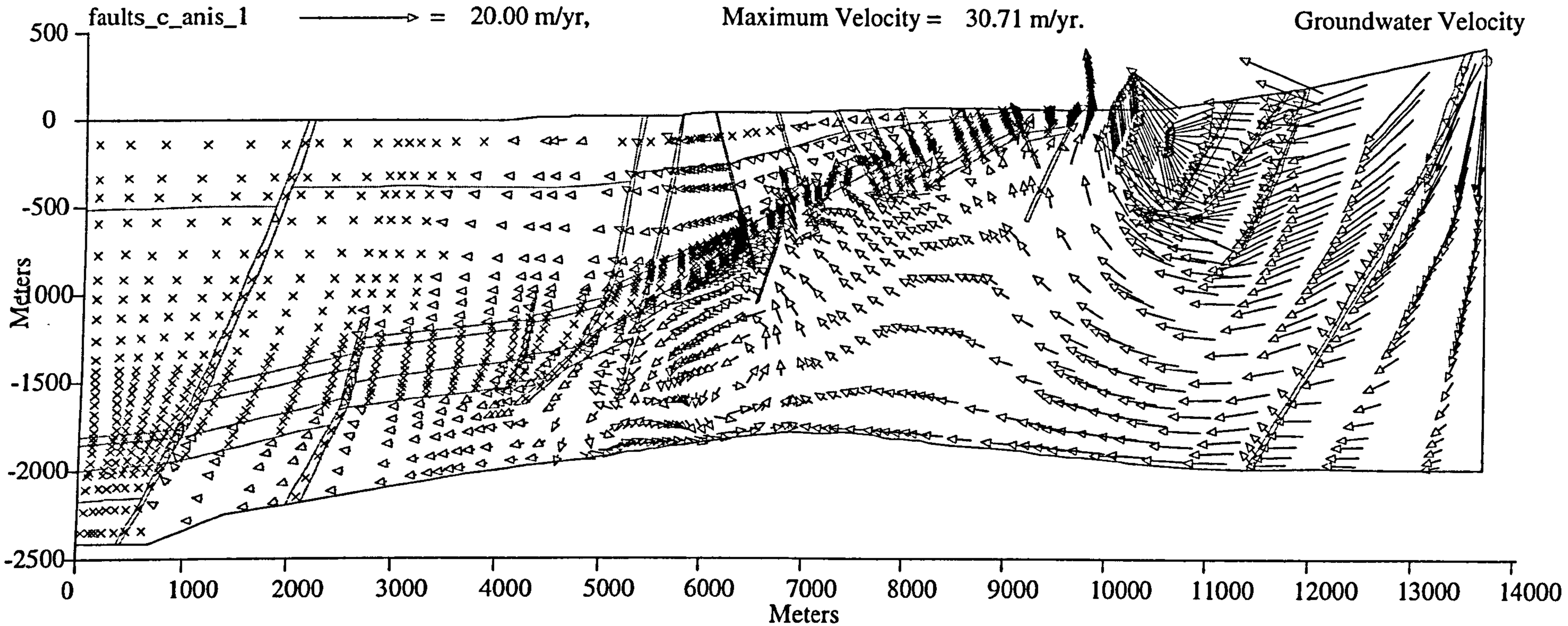

Fig. 3.46 Groundwater flow plot displaying average linear velocities calculated with complex grid (Fig. 3.33). Anisotropy of BVG changed to 1. All other conditions as in Fig. 3.44. Similar flow pattern to Fig. 3.44 although greater flow in BVG.

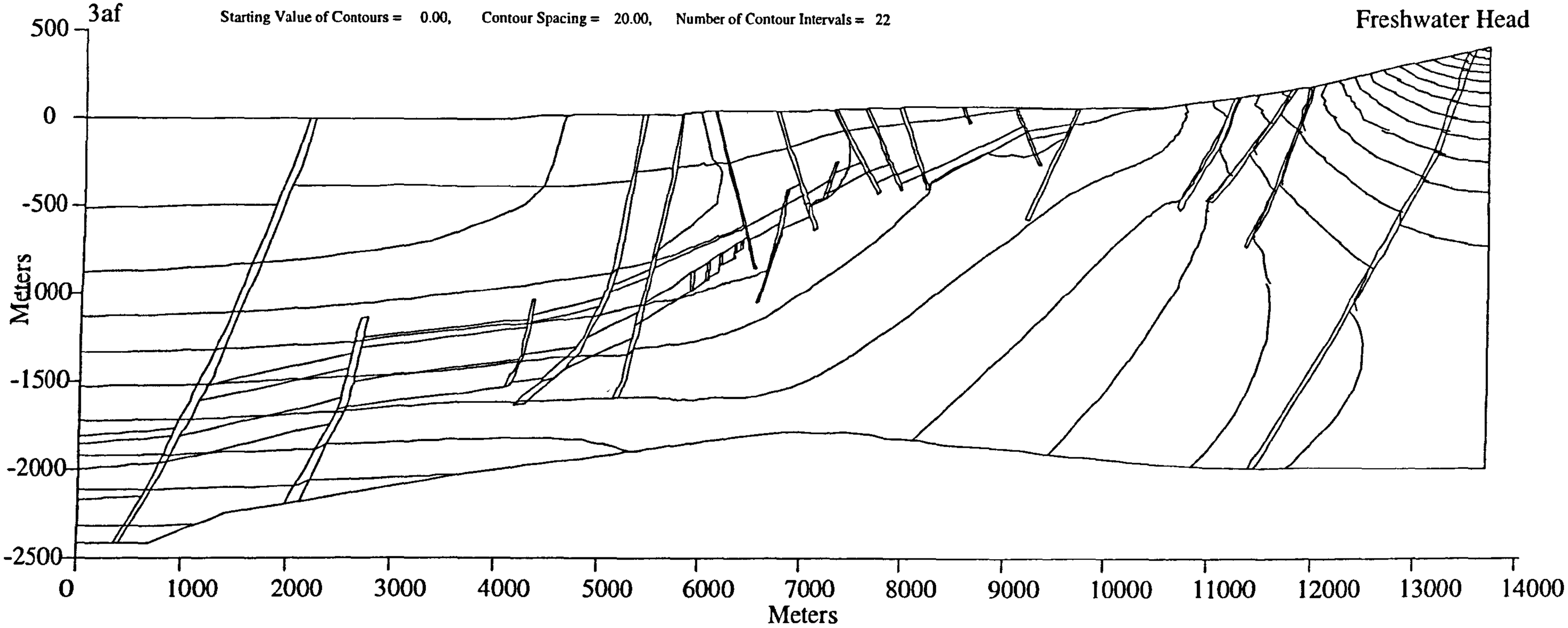

Fig. 3.47 Plot of equivalent freshwater hydraulic head calculated with complex grid (Fig. 3.33) showing result of simulation to test importance of Calder Sst. hydraulic conductivity to flow rate through repository. Base case hydraulic conductivities (horizontal); Calder Sst. = 3.00 m/yr; St Bees Sst. = 1.50 m/yr; St Bees Evaporites = 1.60E-03 m/yr; Brockram Breccia = 9.50E-04 m/yr; Carboniferous Limestone = 1.50E-01 m/yr; BVG = 1.20E-02 m/yr. "Real world" hydraulic conductivities of cover faults and BVG faults = 30 m/yr and 3 m/yr respectively. Simulated hydraulic conductivities = 0.3 m/yr and 0.03 m/yr respectively (see text). Head gradients very similar to those observed (Fig. 3.32). High vertical gradients in western area of 16 % salinity. Potential for diagonal flow in central region.

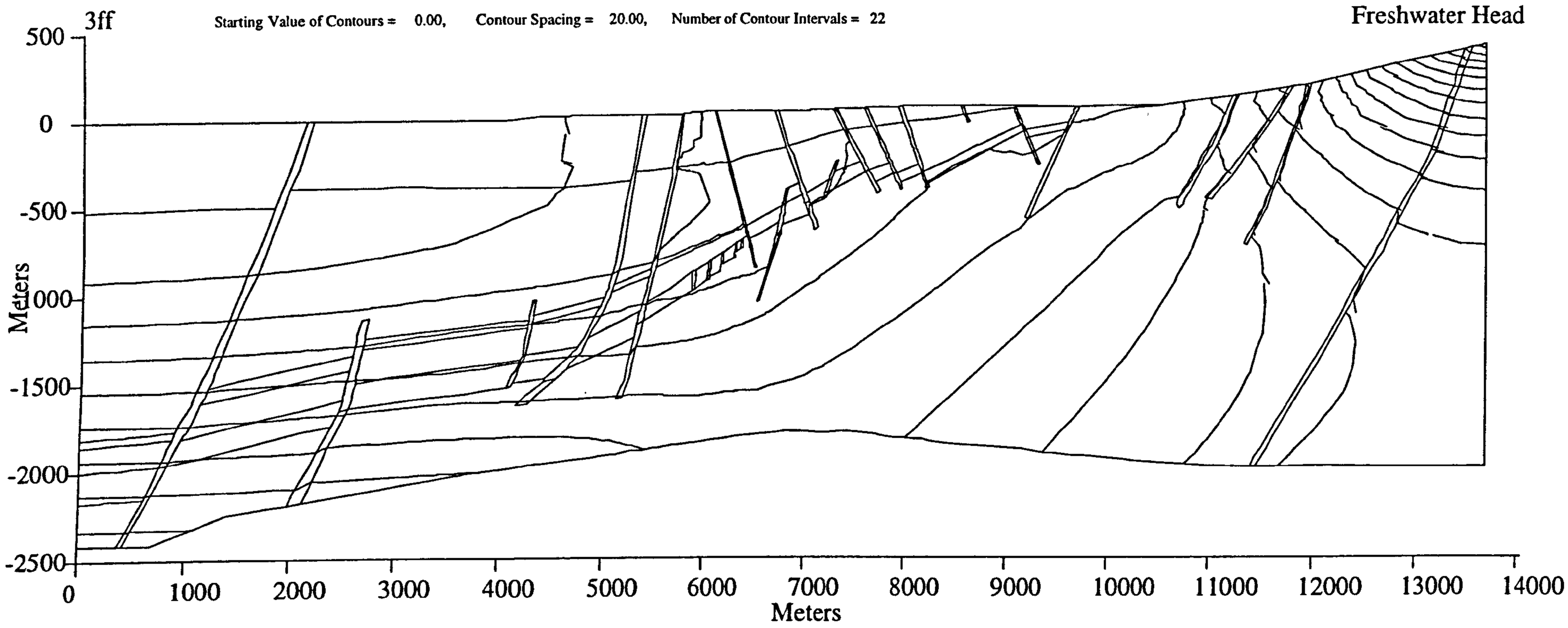

Fig. 3.48 Plot of equivalent freshwater hydraulic head calculated with complex grid (Fig. 3.33) showing result of simulation to test importance of Calder Sst. hydraulic conductivity to flow rate through repository. Calder Sst. = 300 m/yr, all other hydraulic conductivities as in Fig. 3.47. Very similar head profile to Fig. 3.47. Slight variation in head profile in Calder Sst. Head gradients still generally similar to those observed (Fig. 3.32). High vertical gradients in western area of 16 % salinity. Potential for diagonal flow in central region of high hydraulic gradient. Evidence for topographically driven flow in BVG.

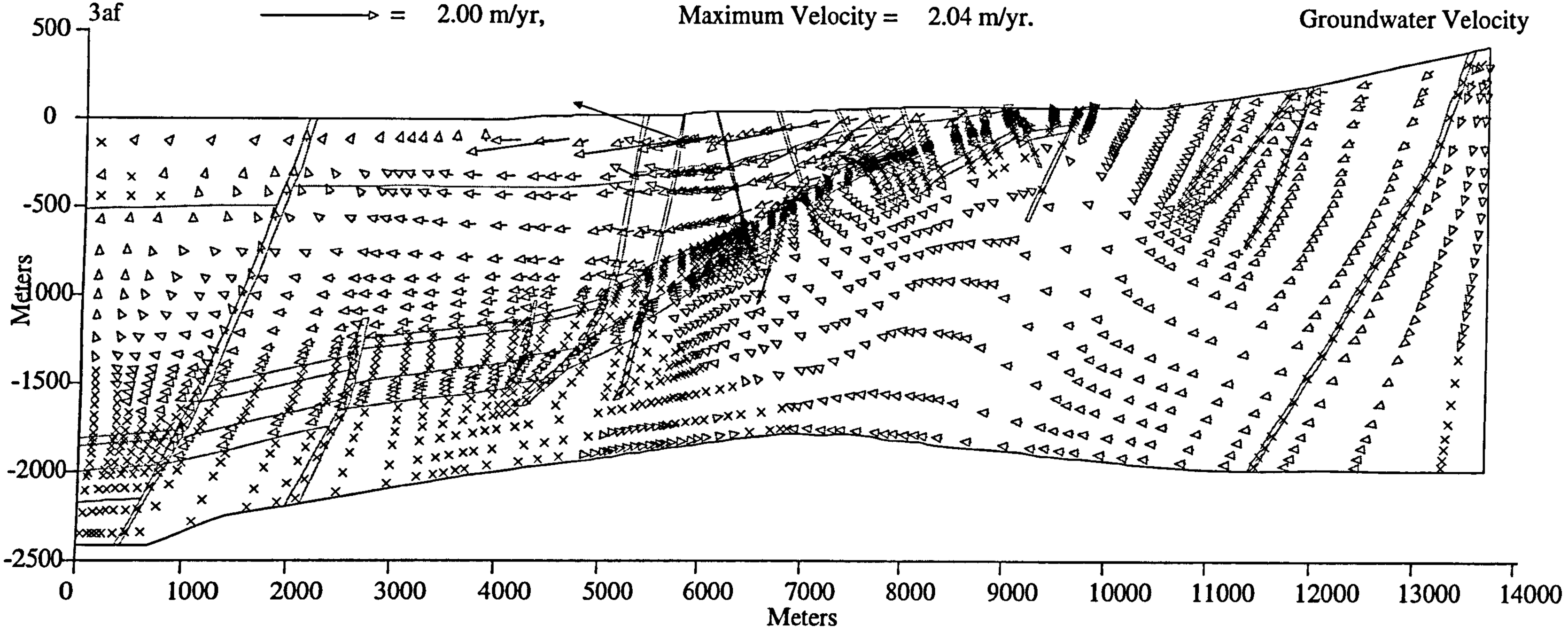

Fig. 3.49 Groundwater flow plot displaying average linear velocities calculated with complex grid (Fig. 3.33) showing result of simulation to test importance of Calder Sst. hydraulic conductivity to flow rate through repository. All parameters as Fig. 3.47; Calder Sst. = 3.00 m/yr. Maximum flow in Calder Sst. Topographically driven flow in BVG..

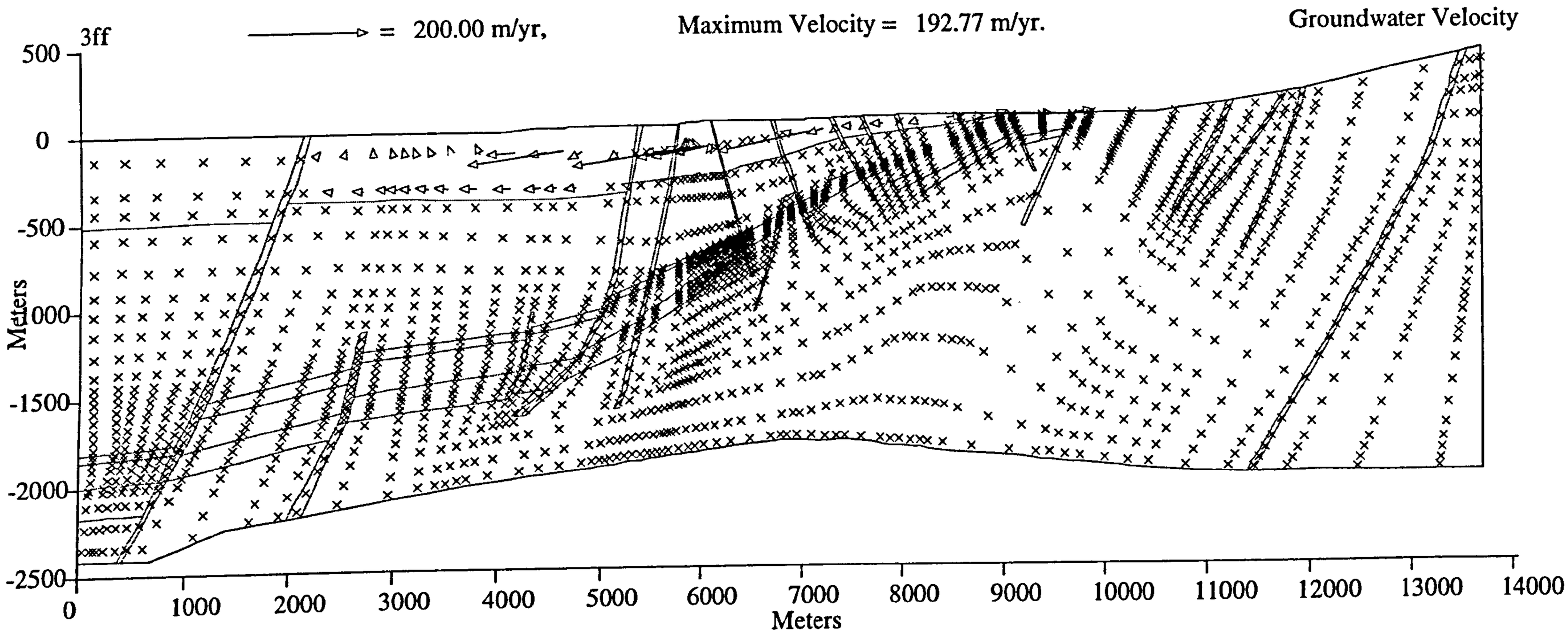

Fig. 3.50 Groundwater flow plot displaying average linear velocities calculated with complex grid (Fig. 3.33) showing result of simulation to test importance of Calder Sst. hydraulic conductivity to flow rate through repository. All parameters as Fig. 3.48. Maximum flow in Calder Sst. masks all other flow features.

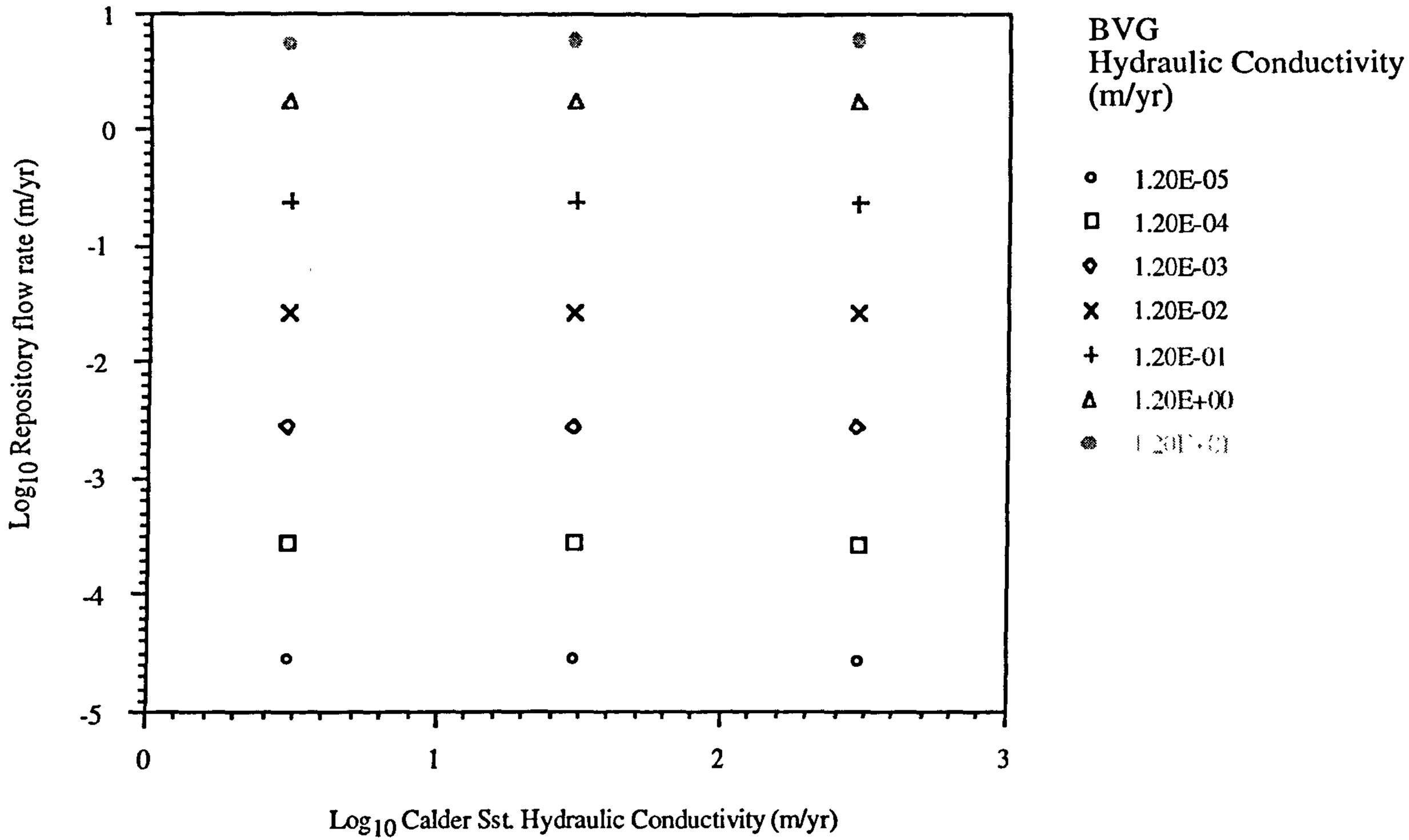

Fig. 3.51 **Graph of log_{10} calculated repository flow rate v log_{10} Calder Sst. hydraulic conductivity. Results from varying BVG hydraulic conductivity over six orders of magnitude also shown. Varying the Calder Sst. hydraulic conductivity has no effect on calculated flow rate through repository.**

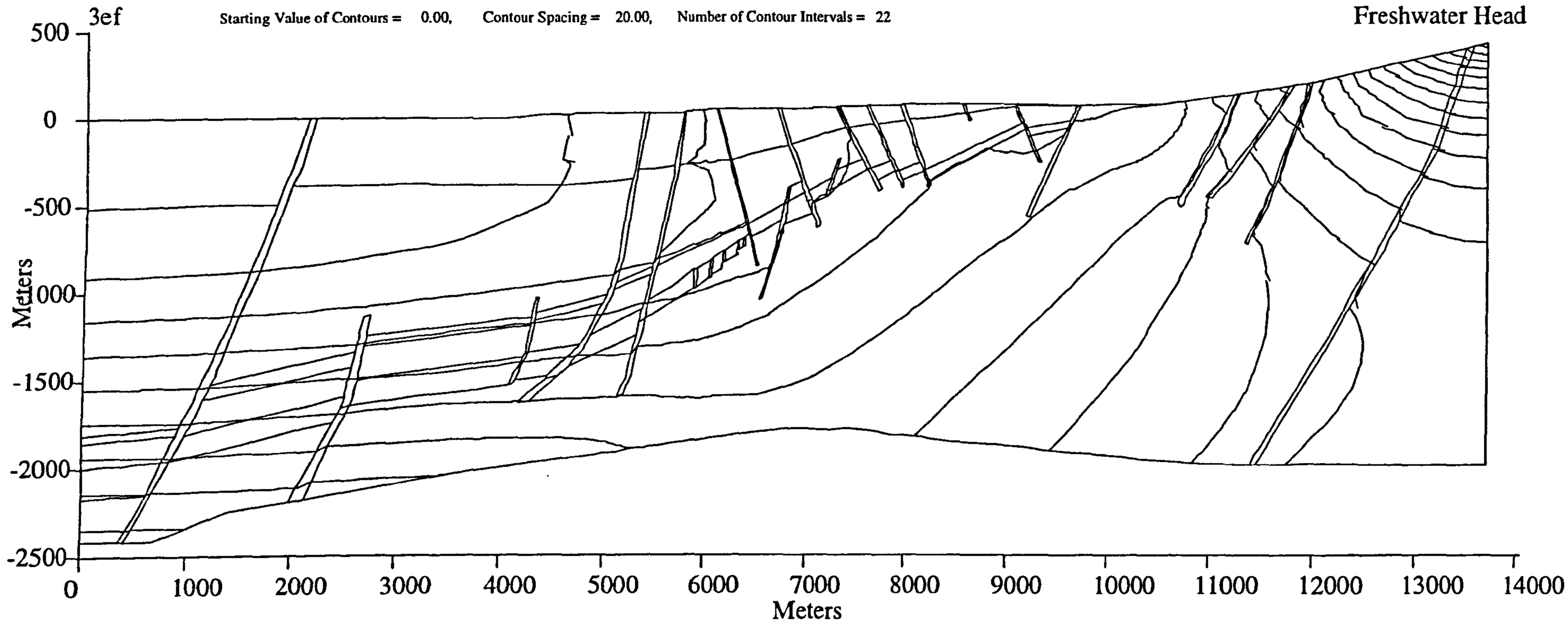

Fig. 3.52 Plot of equivalent freshwater hydraulic head calculated with complex grid (Fig. 3.33) showing result of simulation to test importance of BVG hydraulic conductivity to flow rate through repository. Hydraulic conductivities (horizontal); Calder Sst. = 30.0 m/yr; BVG = base case value of 1.20E-02 m/yr. All other conditions are base case, as in Fig. 3.47. Head gradients similar to those observed (Fig. 3.32). High vertical gradients in western area of 16 % salinity. Potential for diagonal flow in central region of high hydraulic gradient. Evidence for topographically driven flow in BVG.

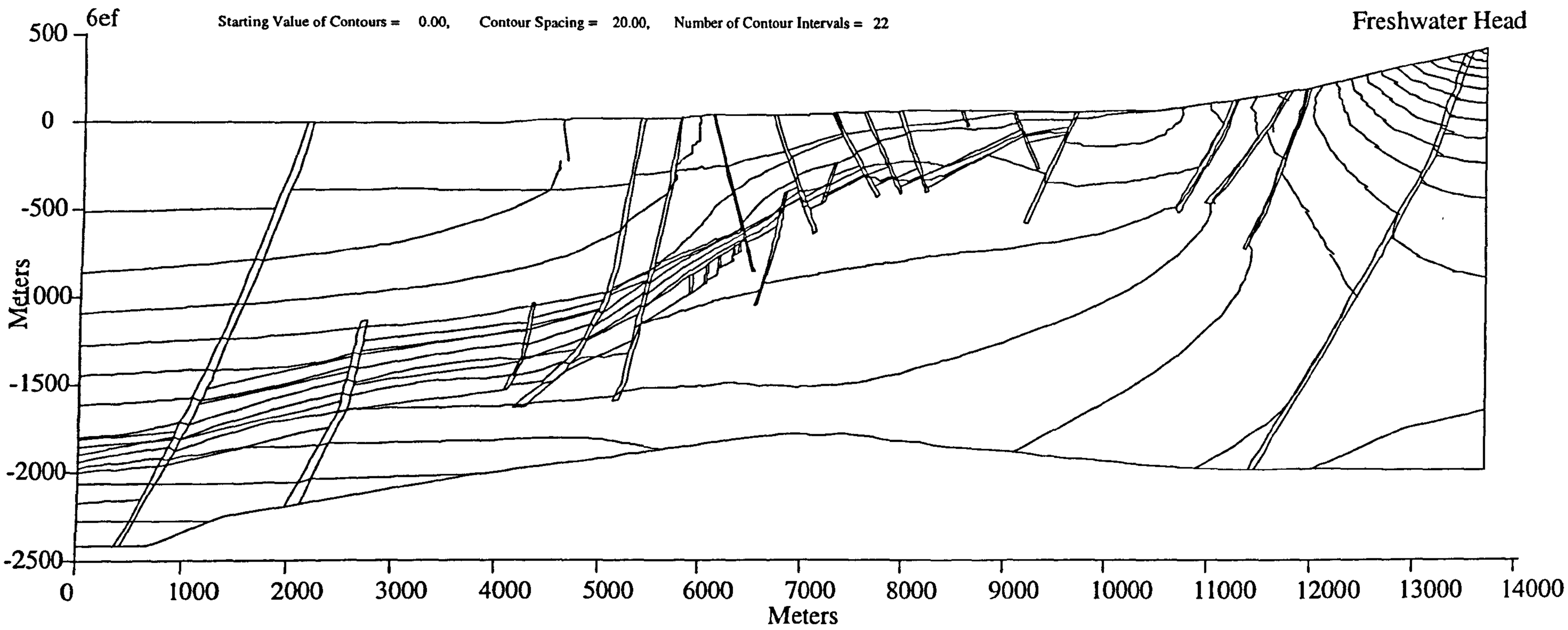

Fig. 3.53 Plot of equivalent freshwater hydraulic head calculated with complex grid (Fig. 3.33) showing result of simulation to test importance of BVG hydraulic conductivity to flow rate through repository. Hydraulic conductivities (horizontal); Calder Sst. = 30.0 m/yr; BVG = 1.20E+01 m/yr (maximum modelled). All other conditions are base case, as in Fig. 3.47. Head in central and western brine region much greater than Fig. 3.52.

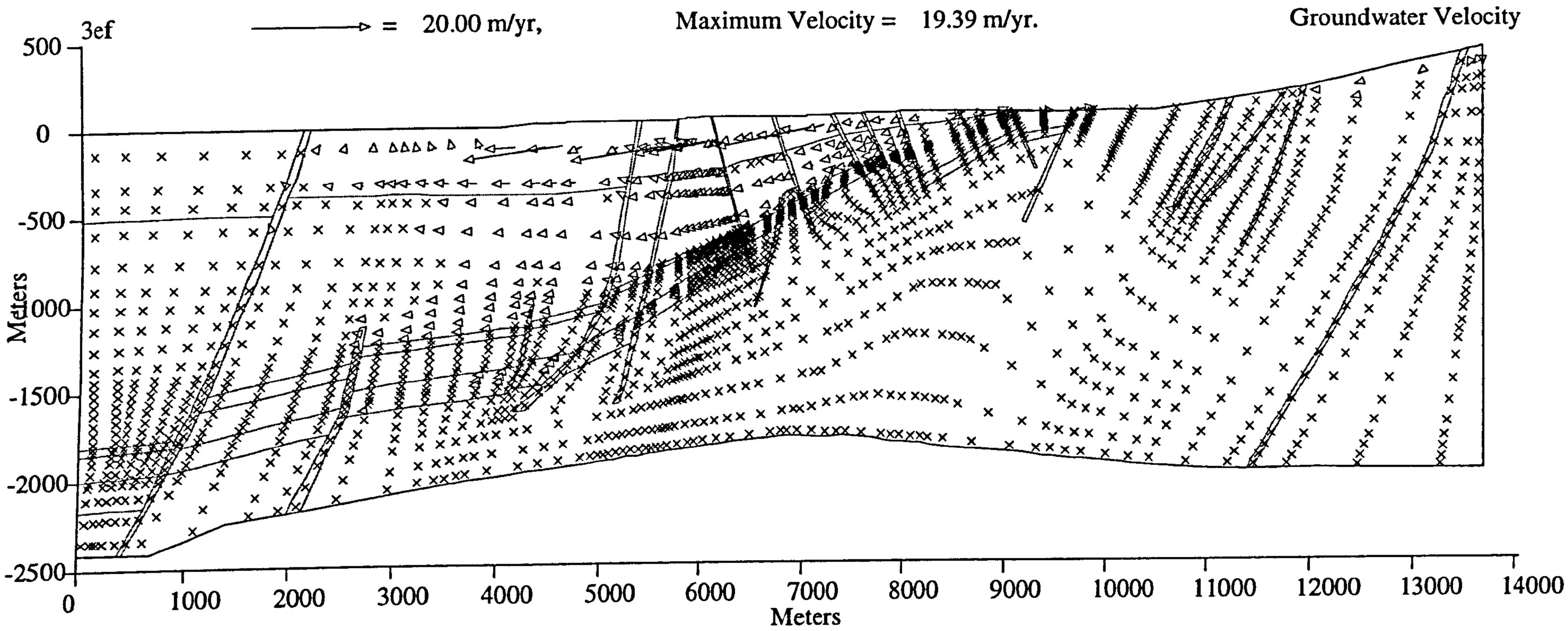

Fig. 3.54 Groundwater flow plot displaying average linear velocities calculated with complex grid (Fig. 3.33) showing result of simulation to test importance of BVG hydraulic conductivity to flow rate through repository. All parameters as Fig. 3.52; Calder Sst. = 30.0 m/yr; BVG = 1.20E-02 m/yr. Maximum flow in Calder Sst., possible topographically driven flow in BVG.

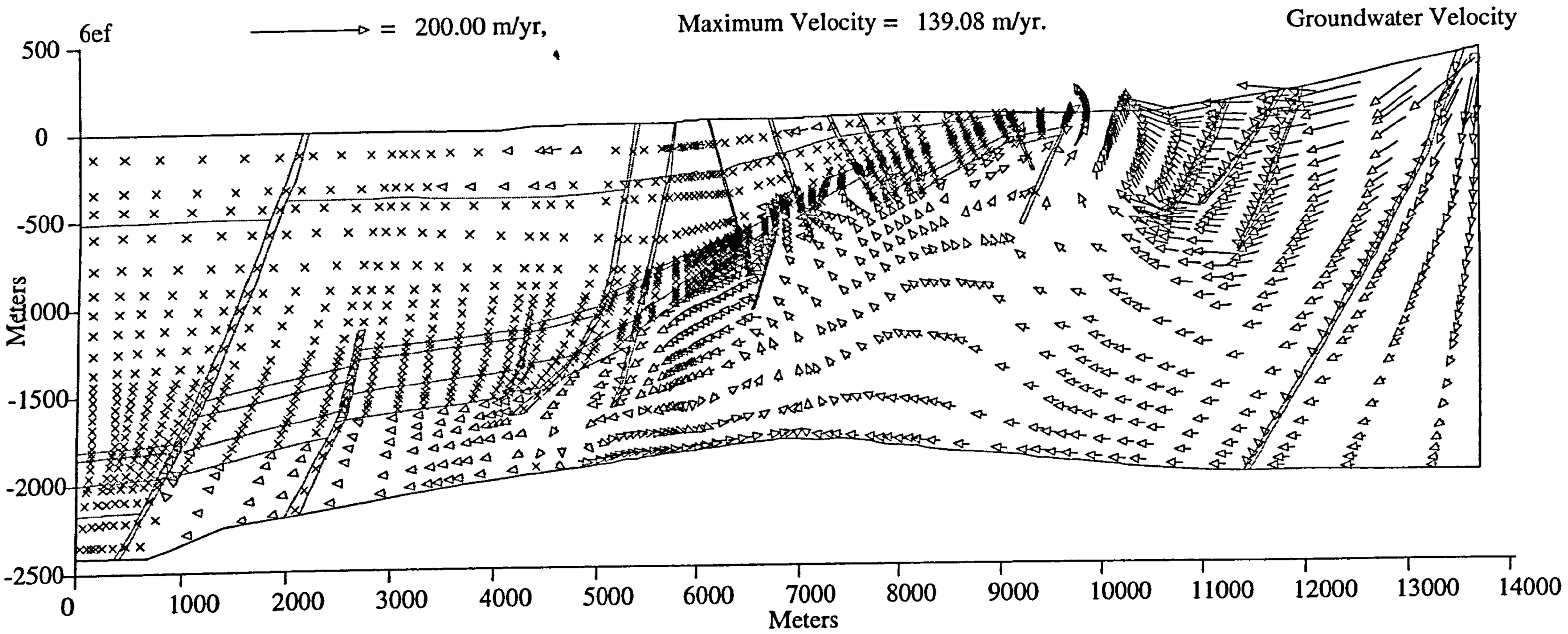

Fig. 3.55 Groundwater flow plot displaying average linear velocities calculated with complex grid (Fig. 3.33) showing result of simulation to test importance of BVG hydraulic conductivity to flow rate through repository. All parameters as Fig. 3.52; Calder Sst. = 30.0 m/yr; BVG = 1.20E+01 m/yr (maximum modelled). Groundwater flow at depth in area of brine develops convective "eddies". Possibly due to interface of topographically driven saline fluid meeting eastern "flowing" brine. Maximum flow in BVG. Dominantly topographically driven flow. Strong diagonal transfer into cover sediments. Springs at base of slope.

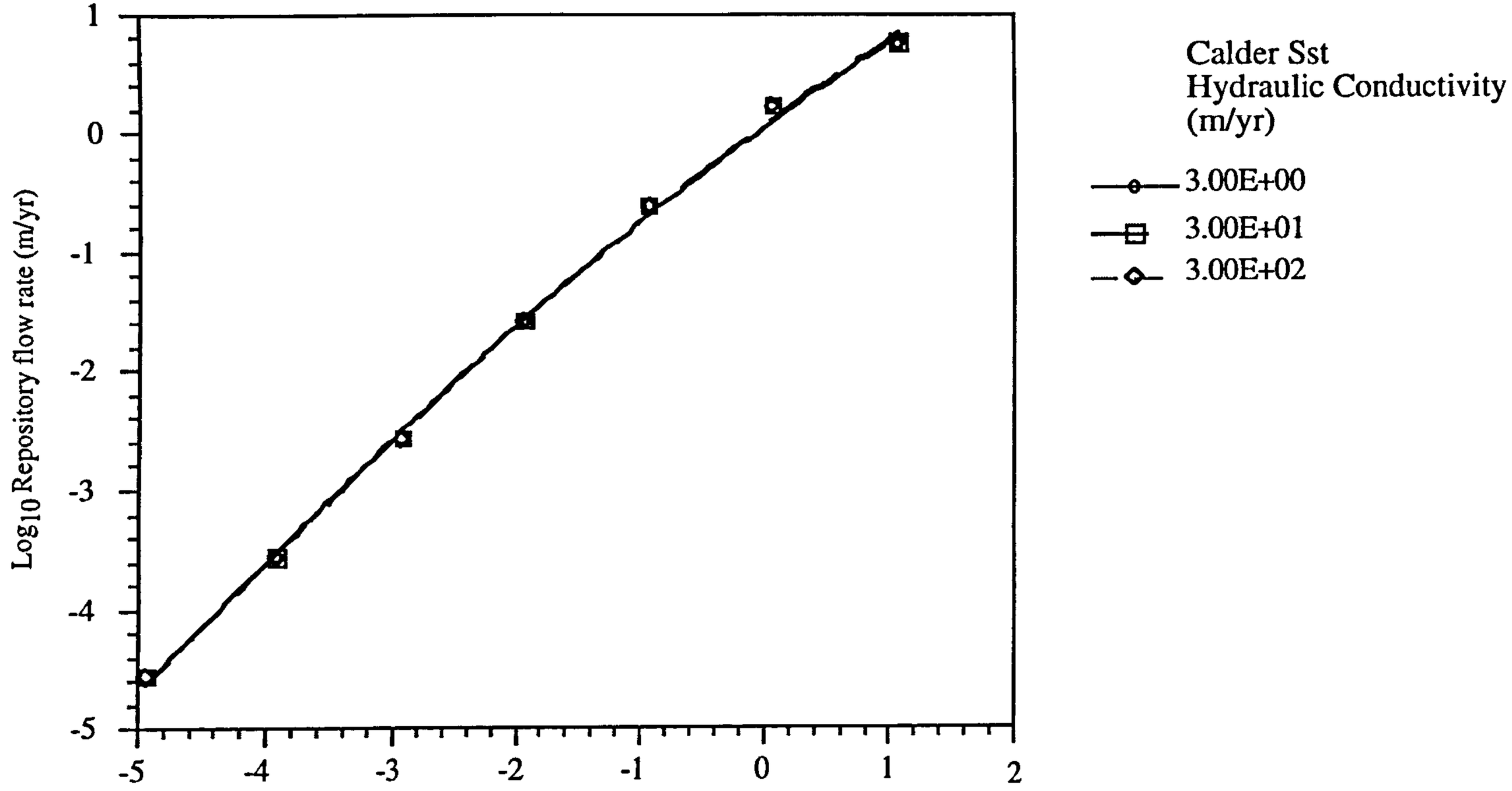

Fig. 3.56 **Graph of log_{10} calculated repository flow rate v log_{10} BVG hydraulic conductivity. Results from varying Calder Sst. hydraulic conductivity superimposed. BVG hydraulic conductivity has direct affect on flow rate through repository regardless of hydraulic conductivity of Calder Sst., indicating that these units are hydrologically decoupled.**

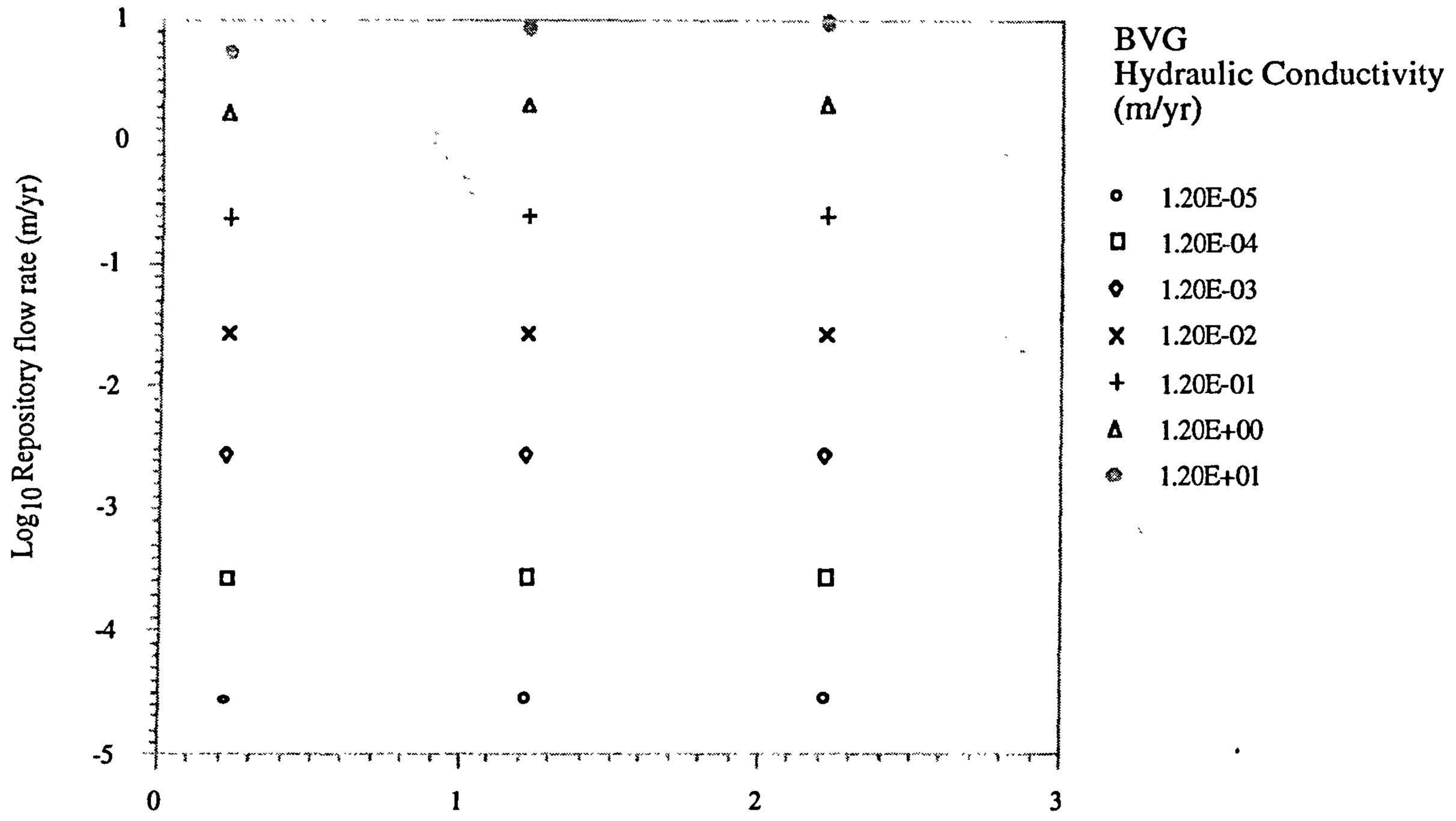

Fig. 3.57 **Graph of log_{10} calculated repository flow rate v log_{10} St Bees Sst. hydraulic conductivity. Results from varying BVG hydraulic conductivity over six orders of magnitude also shown. Varying the St Bees Sst. hydraulic conductivity has no effect on calculated flow rate through repository.**

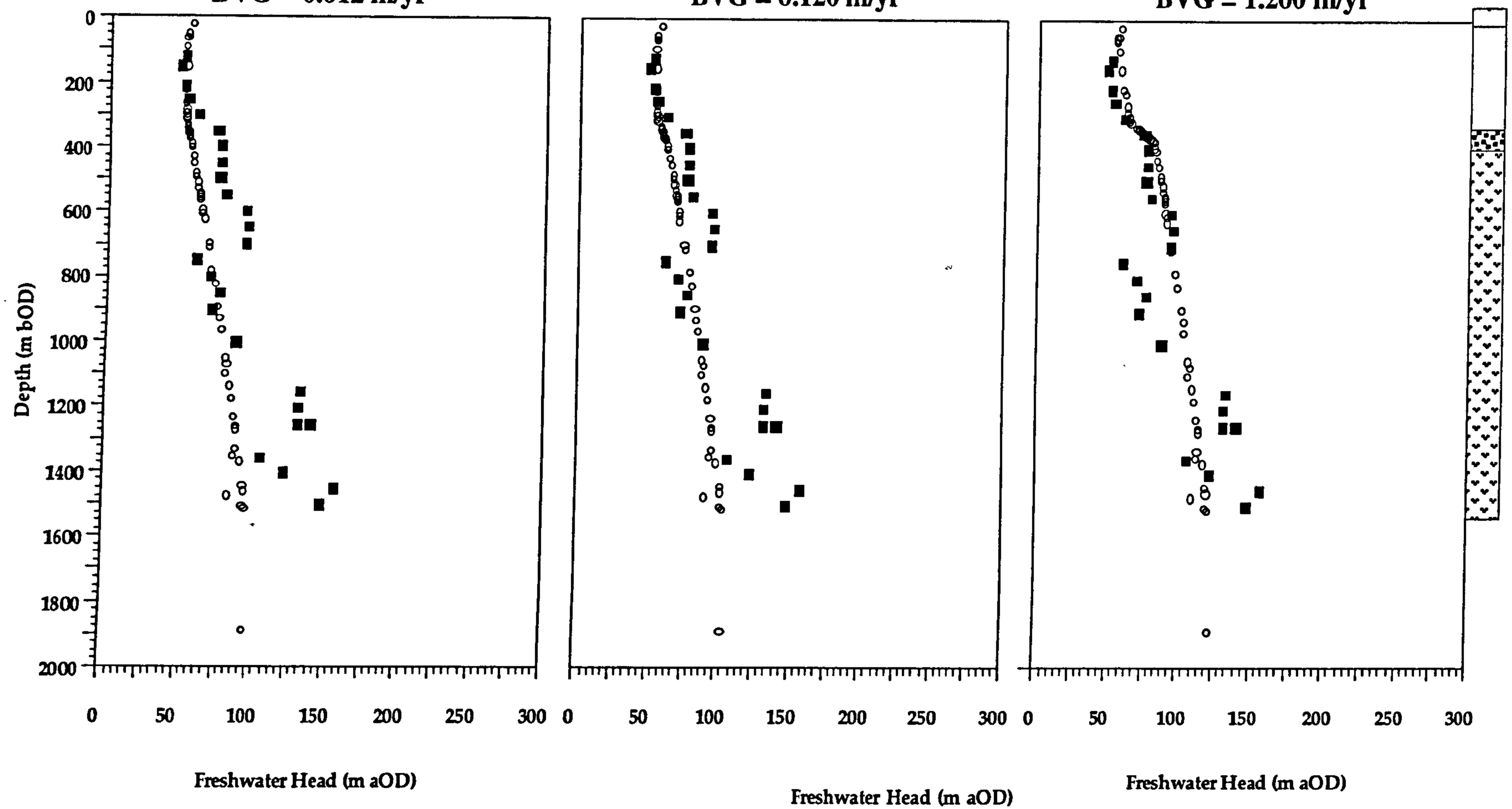

Fig. 3.58 **Comparison between measured and calculated freshwater head in Sellafield BH2.**
All parameters as those of base case (see Table 3.1a and text). BVG hydraulic conductivity ranges from 1.20E-02 to 1.2 m/yr. Increasing BVG hydraulic conductivity gives better match with measured freshwater head.

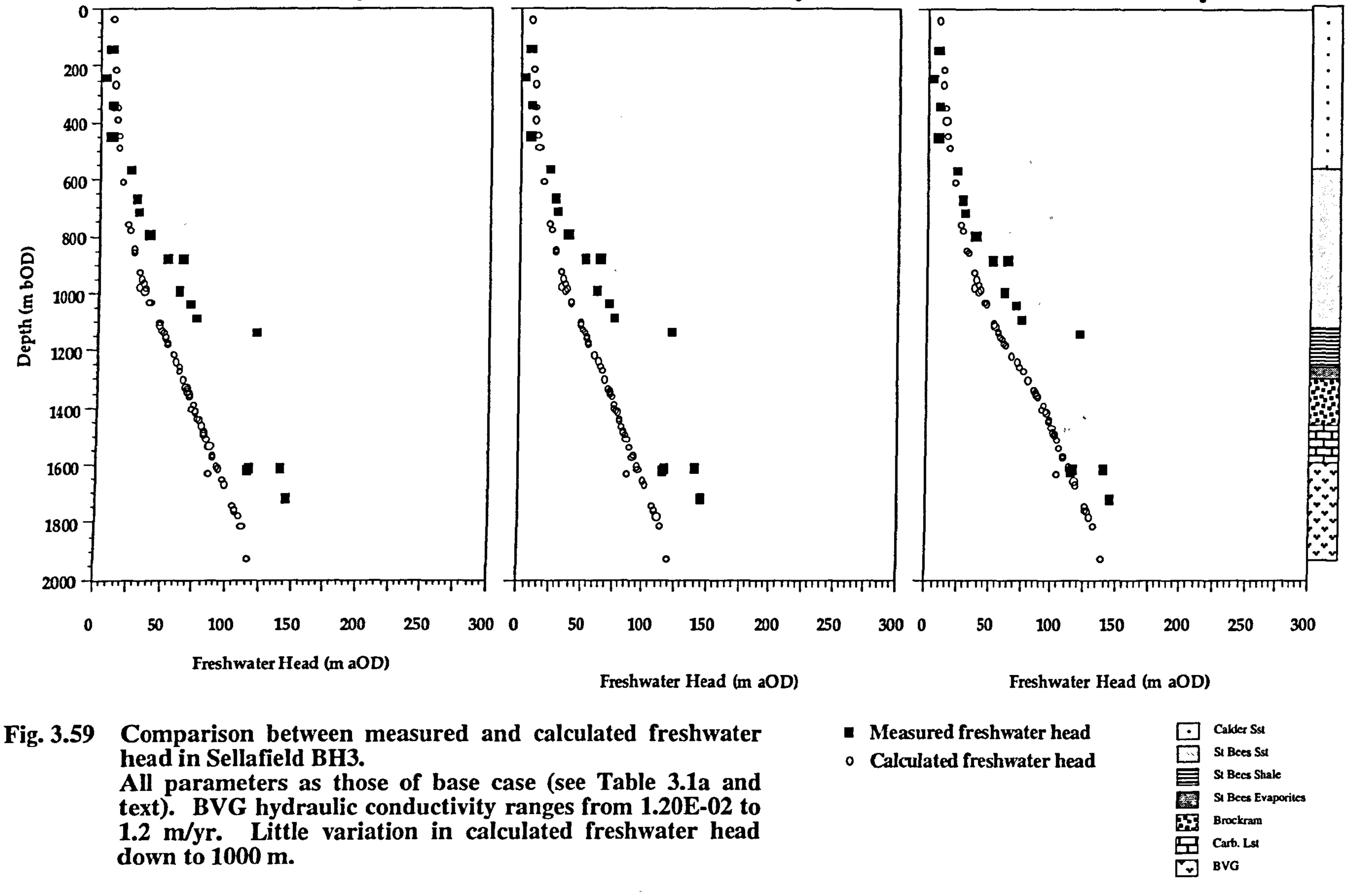

Fig. 3.59 Comparison between measured and calculated freshwater head in Sellafield BH3.
All parameters as those of base case (see Table 3.1a and text). BVG hydraulic conductivity ranges from 1.20E-02 to 1.2 m/yr. Little variation in calculated freshwater head down to 1000 m.

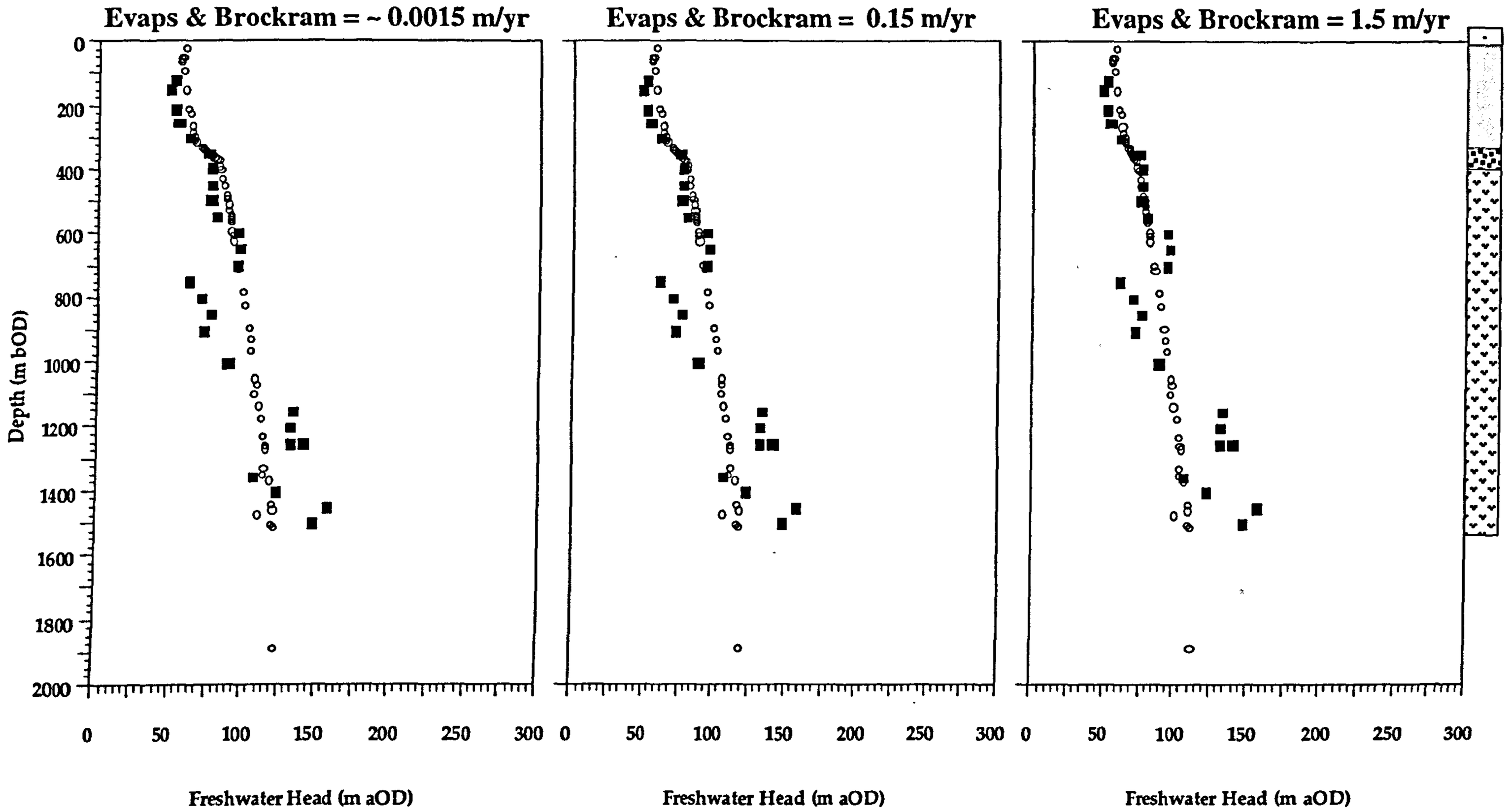

Fig. 3.60 Comparison between measured and calculated freshwater head in Sellafield BH2.
BVG hydraulic conductivity set to 1.2 m/yr. St Bees Evaporites and Brockram Breccia hydraulic conductivity increased by 100 and 1000 times. Other parameters as those of base case (see Table 3.1a and text). Calculated freshwater head decreases below 600 m when both increased.

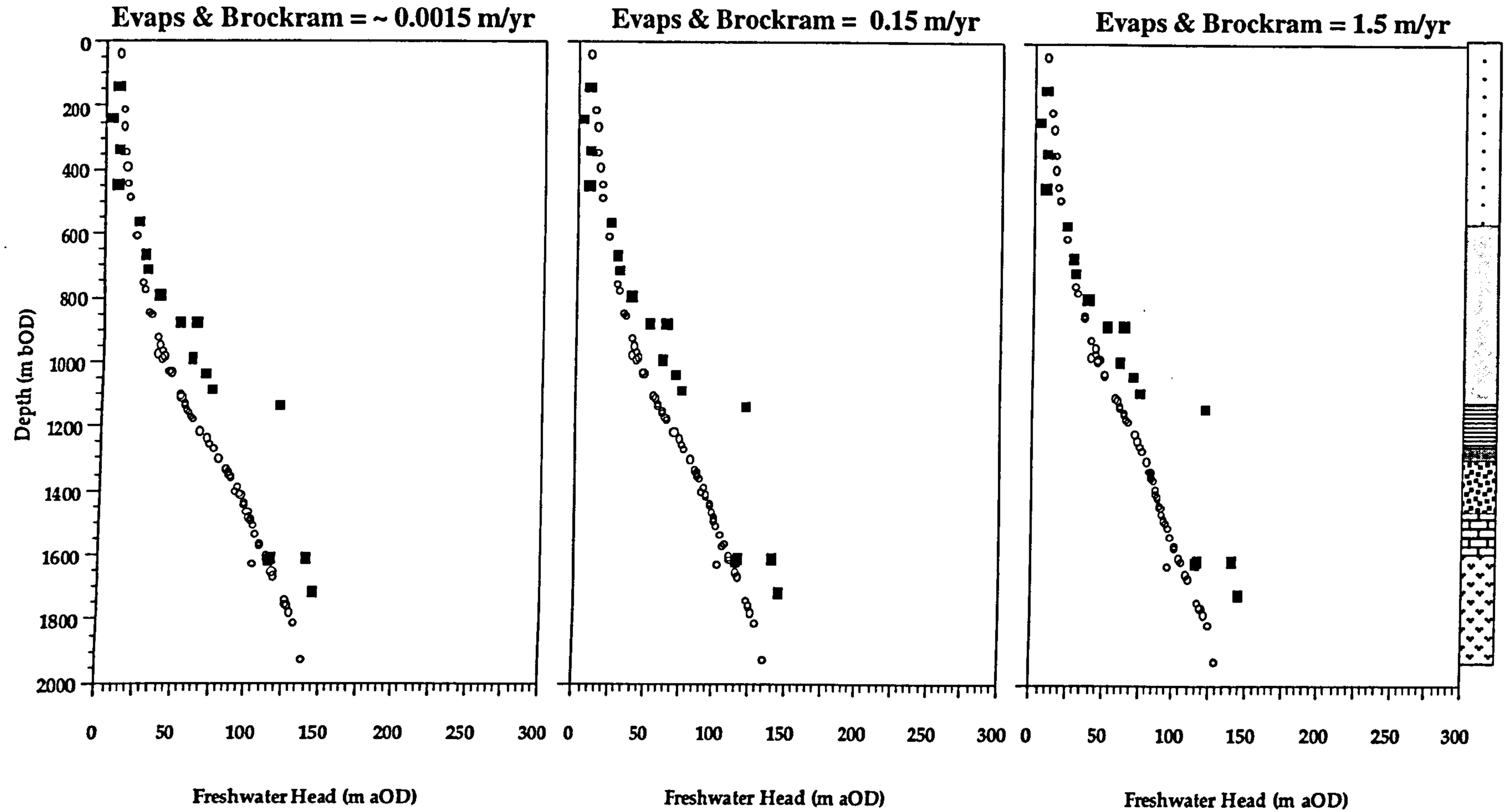

Fig. 3.61 **Comparison between measured and calculated freshwater head in Sellafield BH3.**
BVG hydraulic conductivity set to 1.2 m/yr. St Bees Evaporites and Brockram Breccia hydraulic conductivity increased by 100 and 1000 times. Other parameters as those of base case (see Table 3.1a and text). Calculated freshwater head unaffected when both increased.

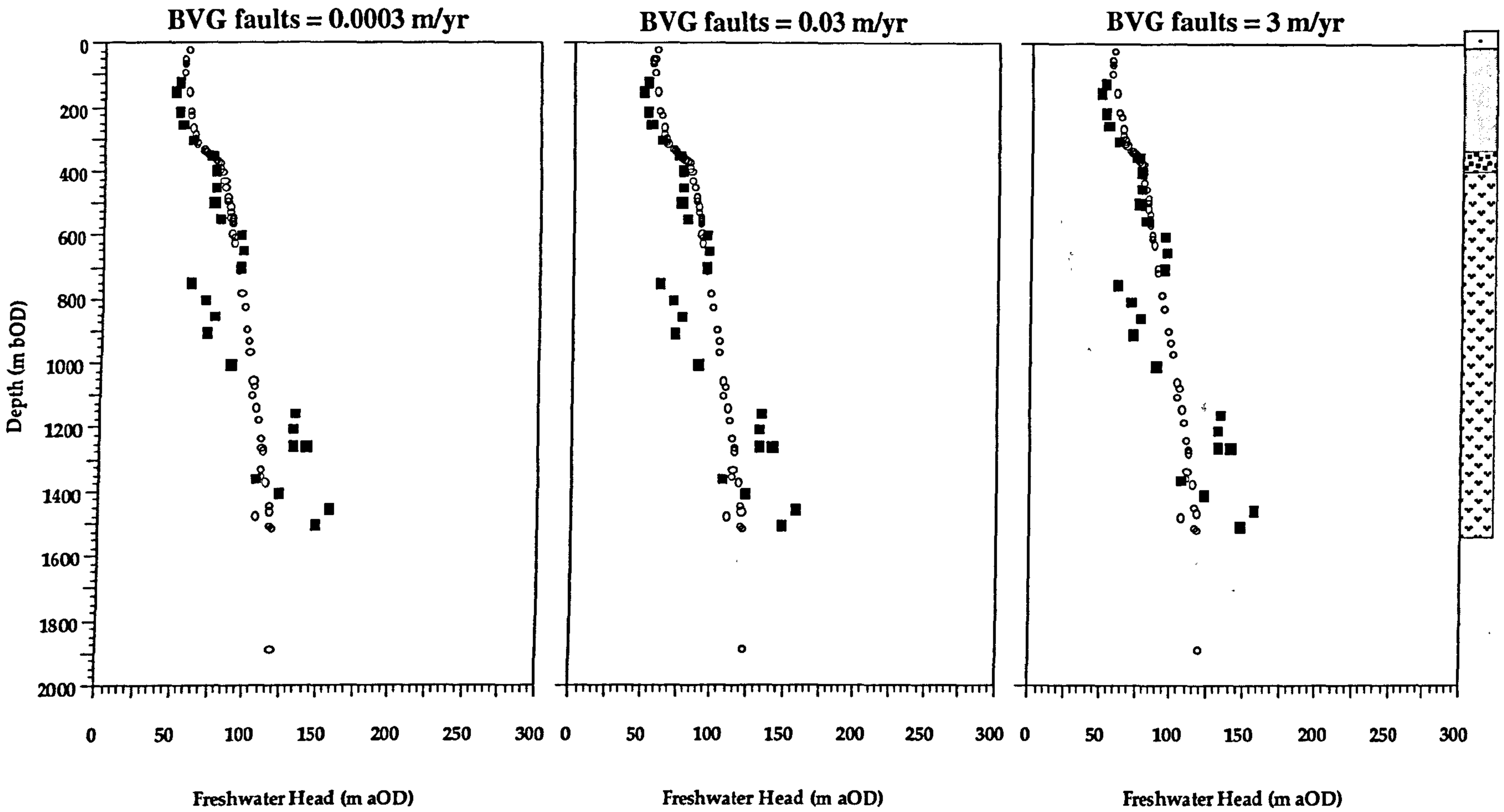

Fig. 3.62 **Comparison between measured and calculated freshwater head in Sellafield BH2.**
BVG hydraulic conductivity set to 1.2 m/yr. Other parameters as those of base case (see Table 3.1a and text). BVG faults hydraulic conductivity ranges from 0.0003 to 3 m/yr. BVG faults hydraulic conductivity variation has no effect on calculated freshwater head.

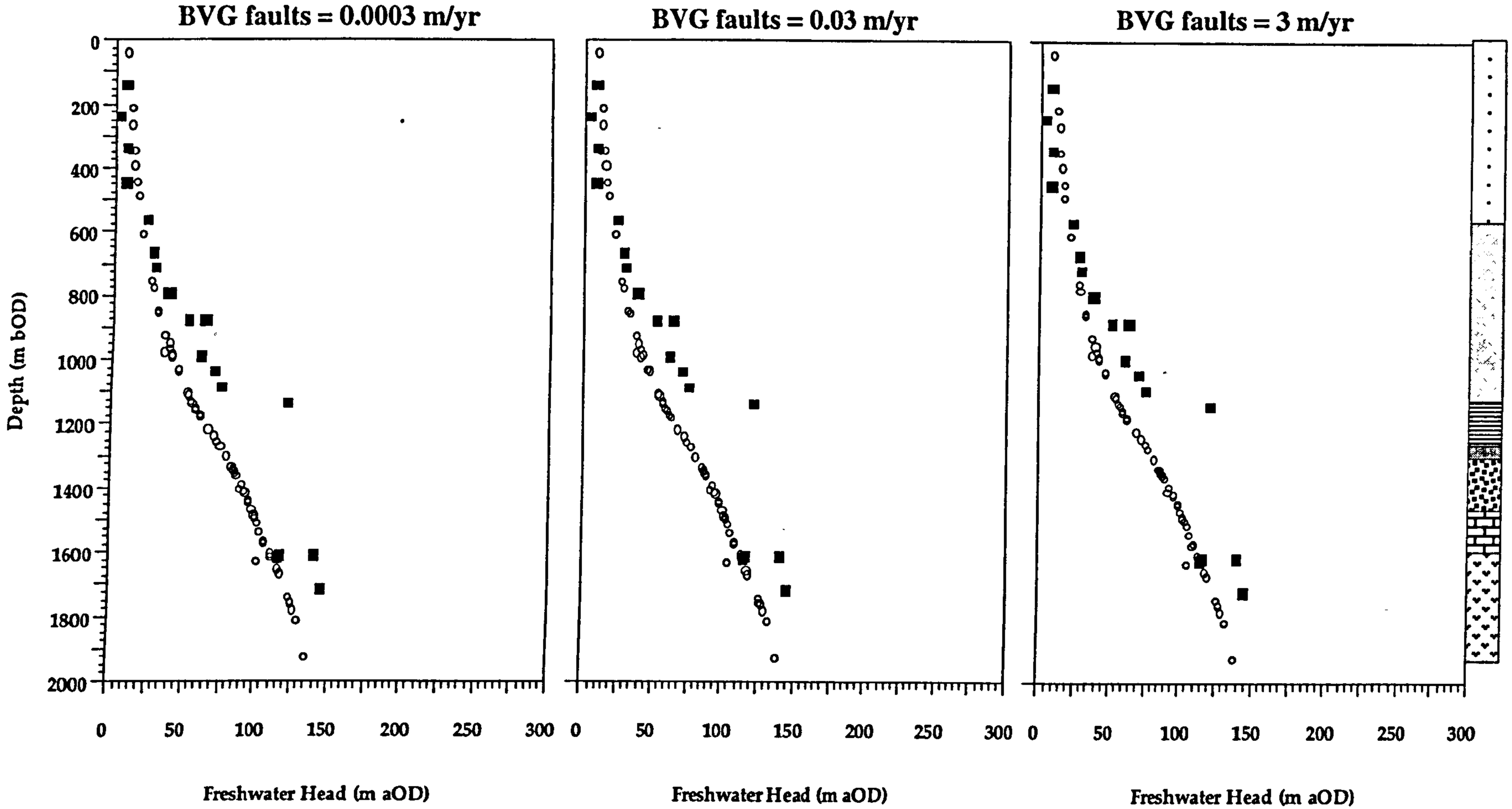

Fig. 3.63 **Comparison between measured and calculated freshwater head in Sellafield BH3.**
BVG hydraulic conductivity set to 1.2 m/yr. Other parameters as those of base case (see Table 3.1a and text). BVG faults hydraulic conductivity ranges from 0.0003 to 3 m/yr. BVG faults hydraulic conductivity variation has no effect on calculated freshwater head.

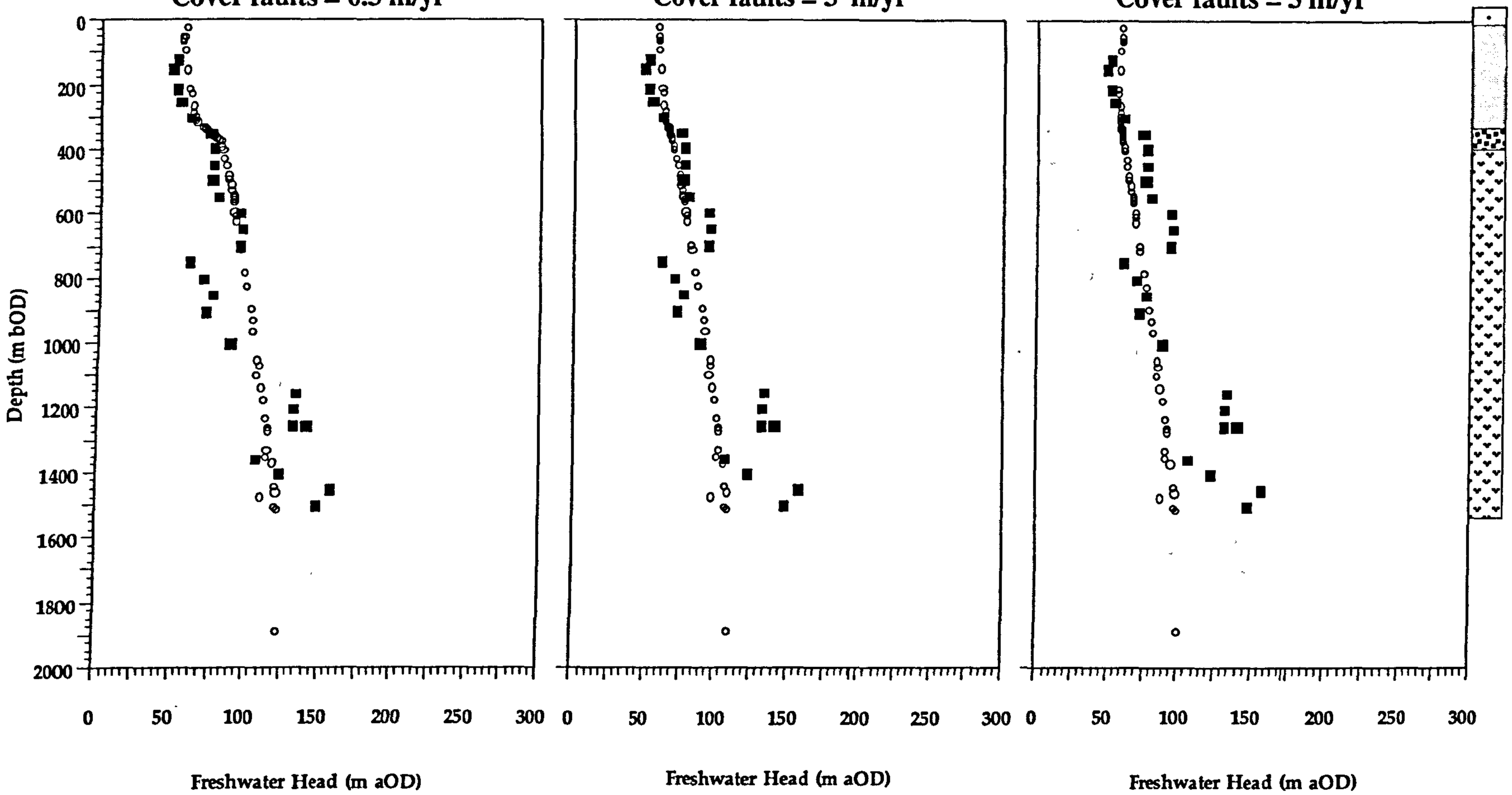

Fig. 3.64 Comparison between measured and calculated freshwater head in Sellafield BH2.
BVG hydraulic conductivity set to 1.2 m/yr. Other parameters as those of base case (see Table 3.1a and text). Cover fault hydraulic conductivity increased to 30 m/yr, equivalent to a "real world" conductivity of 3000 m/yr (see text). Increasing cover fault hydraulic conductivity gives poorer match with measured freshwater head.

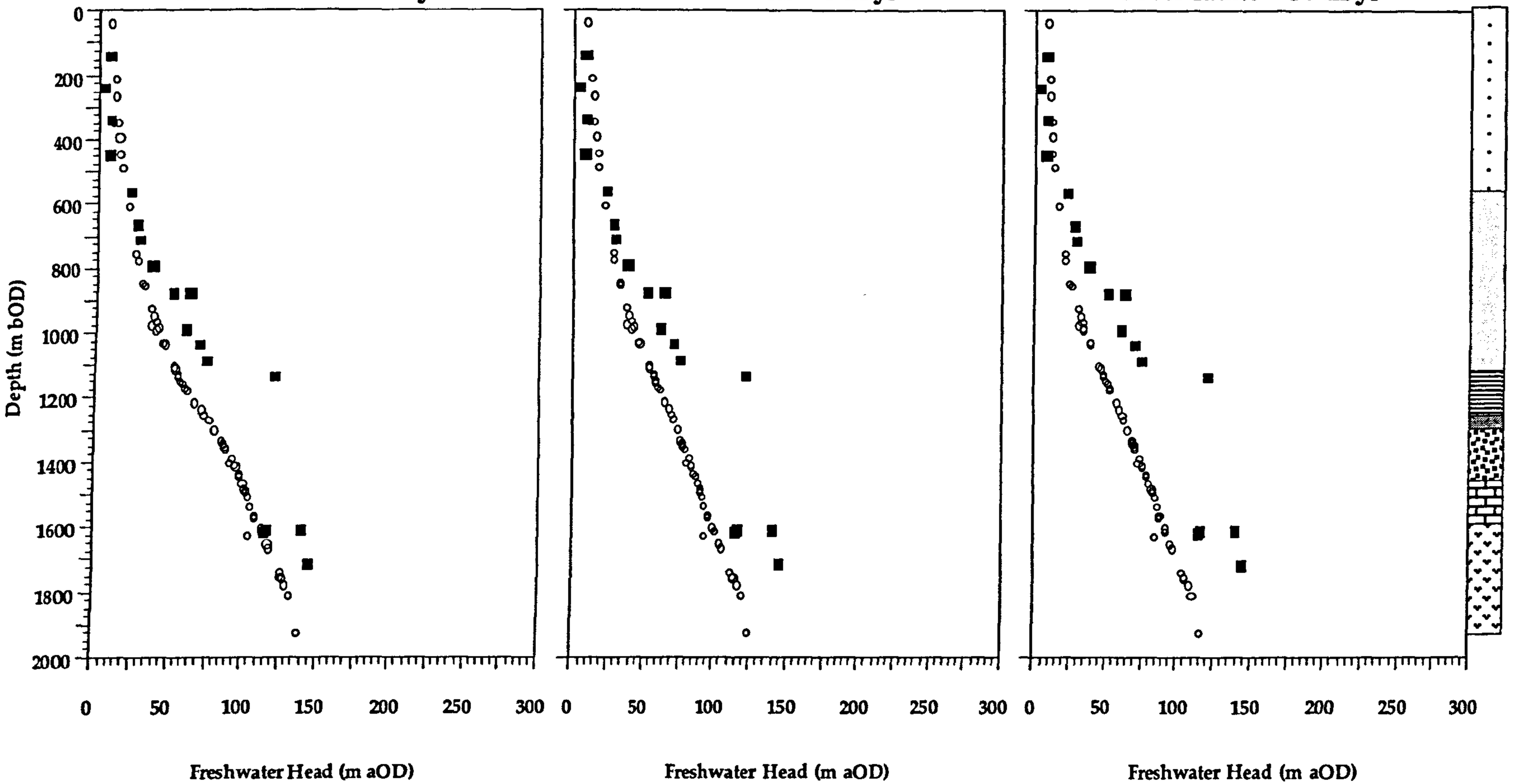

Fig. 3.65 Comparison between measured and calculated freshwater head in Sellafield BH3.
BVG hydraulic conductivity set to 1.2 m/yr. Other parameters as those of base case (see Table 3.1a and text). Cover fault hydraulic conductivity increased to 30 m/yr, equivalent to a "real world" conductivity of 3000 m/yr (see text). Little variation in calculated freshwater head down to 1000 m.

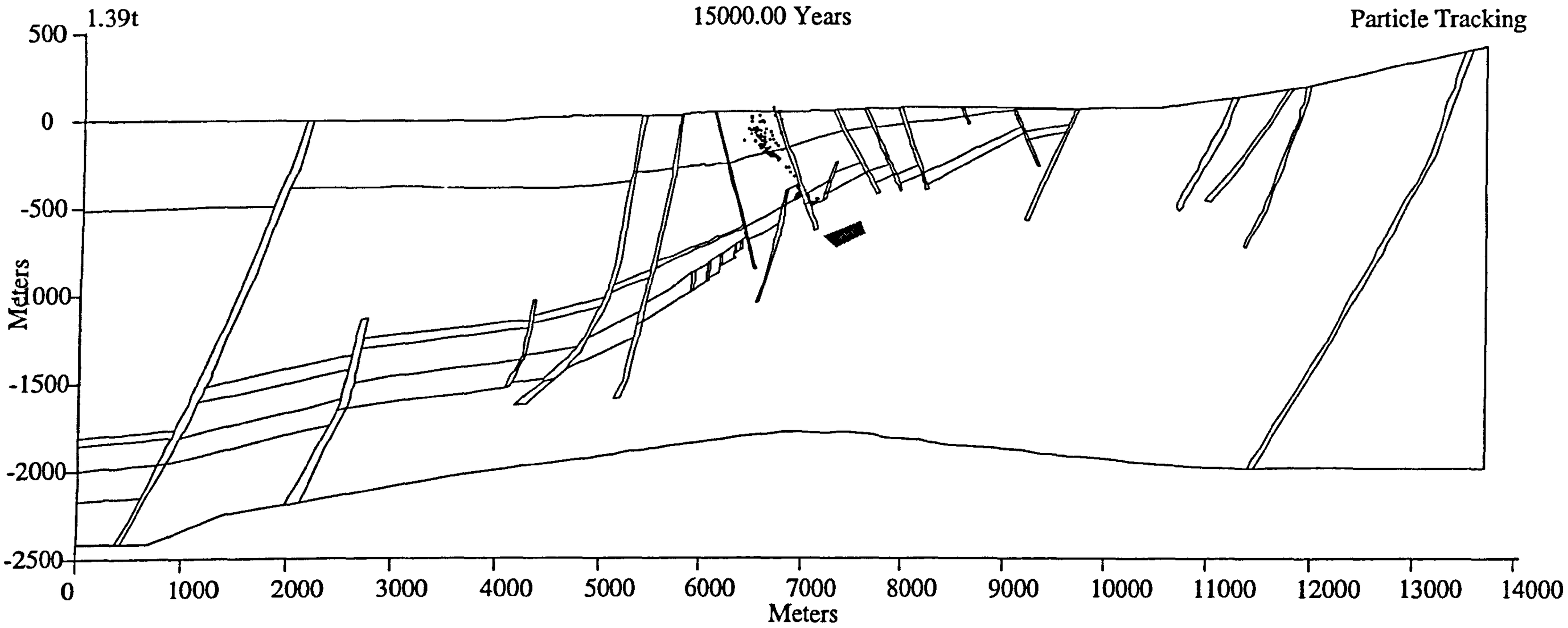

Fig. 3.66 Particle tracking plot showing path of particles of zero mass. Once the steady state flow field is established a number of particles are released from a specific point and tracked through time across the model. Since they have the same buoyancy of the ambient fluid they are passive indicators of the path groundwater would take and the actual time repository fluids would take to reach the surface. Conditions as those of "best fit" hydraulic head; Calder Sst. = 3.00 m/yr; BVG = 1.20E+00 m/yr; all other hydraulic conductivities at base case measured hydraulic conductivity (~median), as in Fig. 3.47. Particles reach surface after only 15,000 years. As this simulation "averages" the particle flow by treating the fractured BVG rock as porous, the true time taken for particles from a repository to reach the surface will be less than 15,000 years.

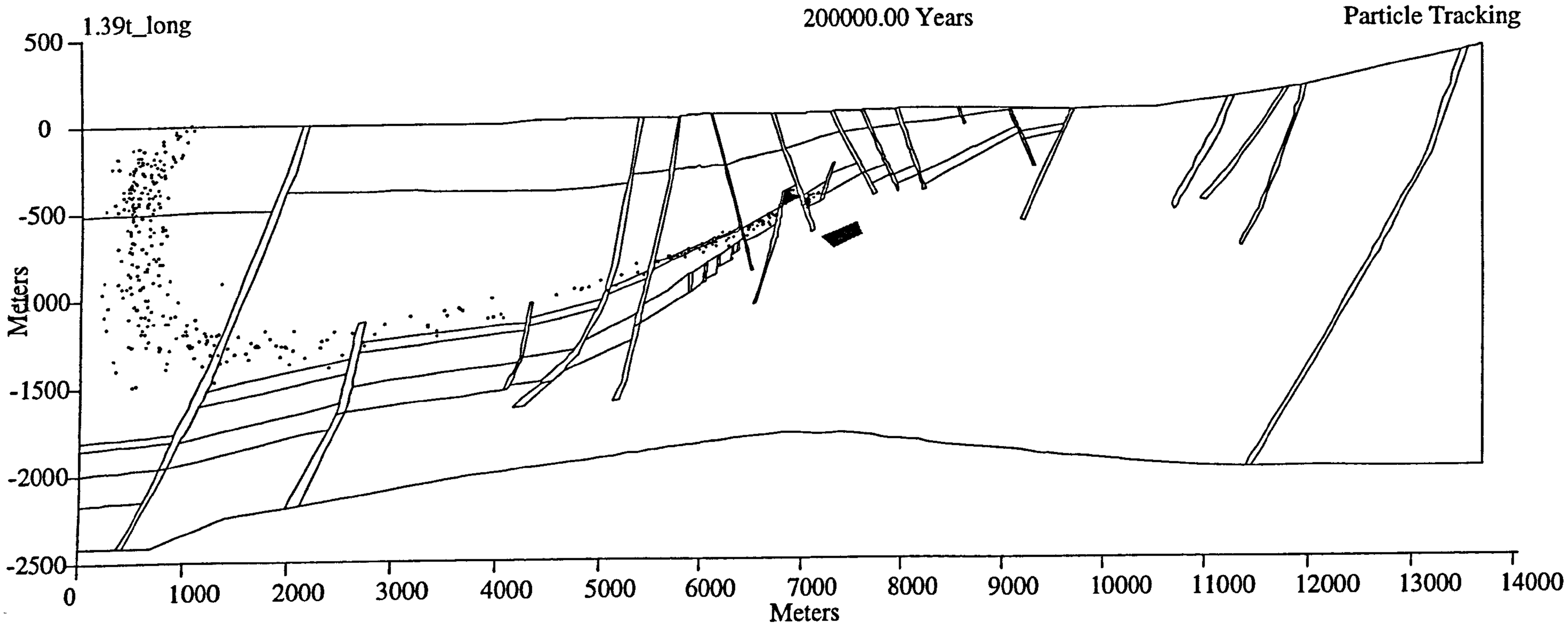

Fig. 3.67 Particle tracking plot showing path of particles of zero mass. Conditions as those of base case; Calder Sst. = 3.00 m/yr; BVG = 1.20E-02 m/yr. This value of BVG permeability is the base case (~median) value, which does not give a good match to measured head data in boreholes. All other hydraulic conductivities set to base case values, as in Fig. 3.47. Particles reach sea bed after 200,000 years.

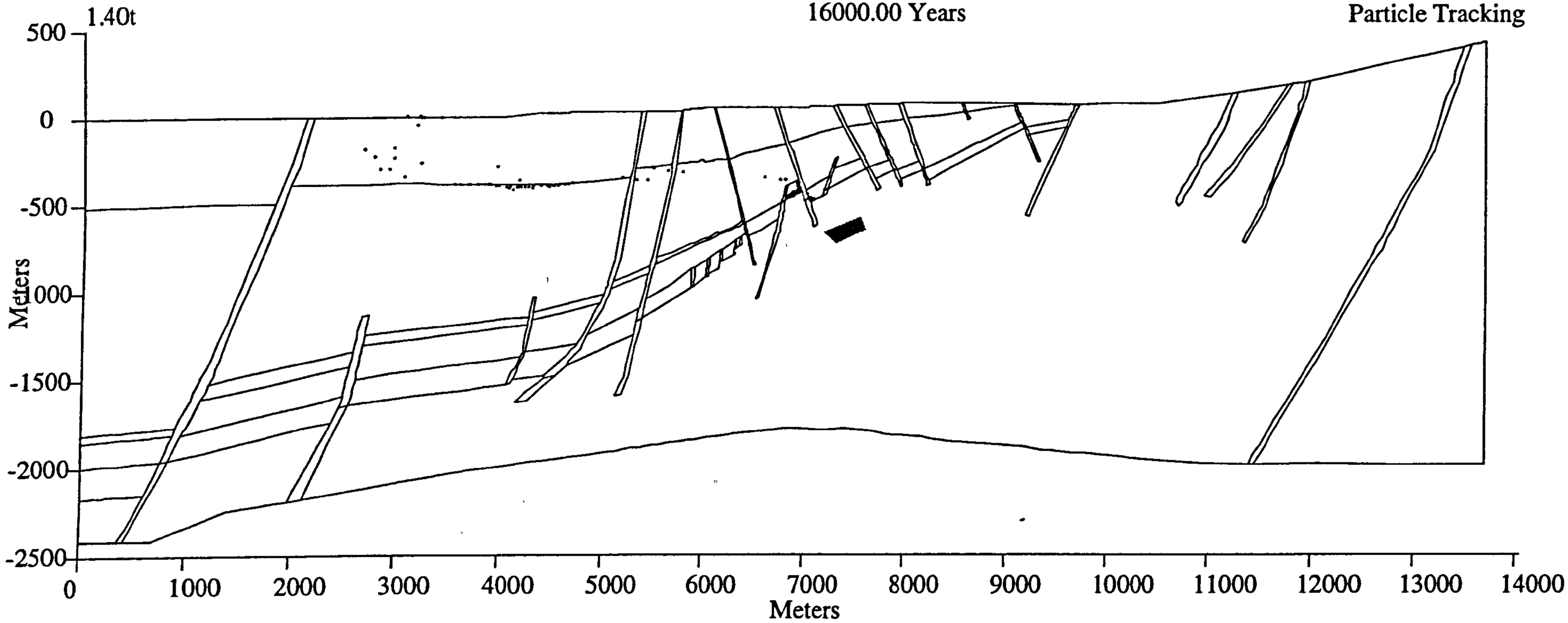

Fig. 3.68 Particle tracking plot showing path of particles of zero mass. Hydraulic conductivities ; Calder Sst. = 30 m/yr; BVG = 1.20E+00 m/yr. All other hydraulic conductivities as in Fig. 3.47. Particles reach sea bed after 16,000 years.

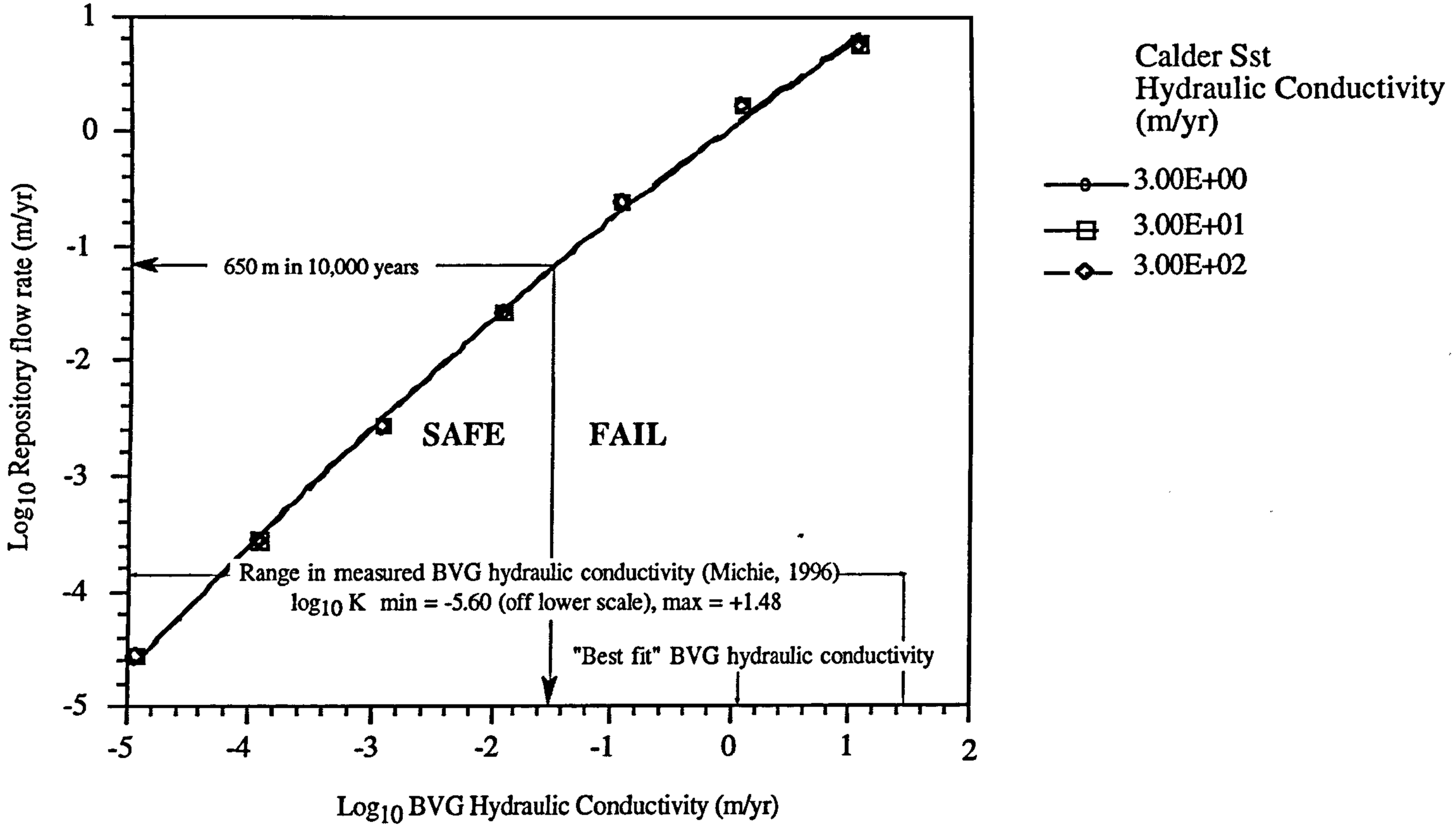

Fig. 3.69 **Graph of $\log_{10}$ repository flow rate vs $\log_{10}$ BVG hydraulic conductivity (log K). Simulations with varying Calder Sst. K superimposed. If BVG hydraulic conductivity > 0.03 m/yr (log K > -1.5) then safety case is failed. BVG maximum measured hydraulic conductivity = 30 m/yr (log K = 1.48), (Michie, 1996), a factor of 1000 times greater than safe/fail boundary. Therefore reasonable for BVG regional hydraulic conductivity to be 0.03 m/yr. BVG hydraulic conductivity producing "best fit" comparison between measured and calculated head falls within fail region (K = 1.2 m/yr, log K = 0.08).**

Chapter 4 Background to geochemical modelling

This small chapter is split into two distinct sections. The first section is both a description of the hydrochemical information required to generate groundwater geochemical models, and a review of the data acquisition methods that are used by UK Nirex Ltd. to generate such data. The code used in this study to model the geochemistry of the BVG groundwaters was the Geochemist's Workbench™ (GWB) (Bethke, 1994). The second section of this small chapter is an overview of the concepts of thermodynamics that are fundamental to geochemical modelling codes such as GWB.

4.1 Hydrogeochemical data

The Sellafield groundwater chemistry indicates the origins of groundwaters and their solutes, helps identify past directions of groundwaters and may provide constraints on the residence times of water and solutes (Nirex, 1993). Water chemical data provide an initial description of the geochemical environment of the proposed repository "far field" (Nirex, 1992b). This natural, far field chemistry will have a direct bearing on the solubility of radionuclides such as uranium (see Chapter 5).

Mineralogical analyses of core and rock cutting samples provide information on the minerals that the in-situ groundwaters would be in contact with (Gillespie & Milodowski, 1994; Strong & Kemp, 1994). These minerals could affect the pH, Eh and elemental concentration of the groundwaters (Metcalfe & Crawford, 1994). As was stated in Chapter 2 the author did **not** gather data from groundwaters at the Sellafield site, **all** data was collected by either UK Nirex Ltd. or their sub-contractors.

4.1.1 Hydrochemical data obtained

To generate a hydrochemical model of a groundwater sample the distribution of the species in the sample have to be calculated. This requires the measurement / calculation of;

- The temperature, pH and redox state of the sample. Care has to be applied to the measurement of the pH and redox state (Plummer *et al.*, 1983). The in situ pH of groundwater samples can be affected by contamination, equilibrium with minerals and, if the sample is from great depth, the degassing of $CO_{2(g)}$ upon sample retrieval (Bond *et al.*, 1995; Bond & Tweed, 1995). The redox state can be derived from measurements of dissolved oxygen, from in-situ measurements of Eh, (the electrode potential relevant to the hydrogen scale, see 4.26)

(Brookins, 1987) or occasionally inferred from the presence or absence of redox sensitive minerals (Lindberg & Runnels, 1984). The latter method has associated problems that are dealt with in Chapter 5.

- The concentration of the major elements; sodium, potassium, calcium, magnesium, chloride, sulphate and total alkalinity (carbonate). In the UK Nirex Ltd. groundwater samples more complete elemental analyses are presented, i.e. all of the above plus trace cations; manganese, strontium, barium, aluminium, silicon, boron and ferrous & ferric iron, trace anions; bromide, iodide, fluoride, sulphide and orthophosphate and redox-sensitive nitrogen species; ammonium, nitrate and nitrite.

- The salinity of the sample, or Total Dissolved Solids (TDS), calculated from the sum of the concentrations of sodium, potassium, calcium, magnesium, chloride, sulphate and total alkalinity.

- Oxygen, hydrogen, carbon, chlorine, radon and helium isotopic analyses of groundwater samples were undertaken by UK Nirex Ltd. (Bath *et al.*, 1996). Such isotopic data provide information regarding the palaeohydrogeology, origin and age of a water sample at a given depth (Faure, 1987). That is, were the groundwaters at the proposed repository depth recharged recently, i.e. within the last 10000 years or are they millions of years old ? If groundwaters in the Proposed Repository Zone (PRZ) are relatively young then this would indicate that PRZ groundwaters are relatively fast moving, which is of obvious importance when determining the safety of the proposed site (Haszeldine, 1996).

4.1.2 Data acquisition and treatment

As well as collecting chemical data from rainfall, rivers, surface springs and shallow boreholes UK Nirex Ltd. have obtained detailed groundwater samples from deep boreholes within the PRZ host rock, the Borrowdale Volcanic Group (BVG) (Nirex, 1992b). Chapter 2 has already detailed the mechanics of the borehole hydrogeological testing methods; Environmental Pressure Measurements (EPM); Full Sector Tests (FST) and Discrete Extraction Tests (DET). Most samples are obtained by DET, performed immediately after drilling a borehole. DET samples provide the most complete and, therefore, useful geochemical information (Nirex, 1992a).

Deep groundwater samples had to be corrected for contamination from the drilling fluid (Nirex, 1992b). The drilling fluid used consisted of a freshwater based

polymer laced with a LiCl tracer maintained at 1000 mg/l so that the degree of invasion could be assessed. This is done by applying linear regression to the analyses of lithium and the constituent of interest, for both the groundwater samples collected during the test and the drilling fluids which may contact the test interval during drilling (Bath *et al.*, 1996).

As mentioned above, the loss of $CO_{2(g)}$ through degassing effects the in-situ estimate of pH. This can be evaluated by using a geochemical simulation code such as GWB to either "titrate" $CO_{2(g)}$ back into the water to a specified end-point or, if carbonate minerals are commonly found lining fractures, allow the samples to be in equilibrium with a mineral such as calcite. The effects of such techniques are dealt with in Chapter 5.

As dealt with in Chapters 1, 2 and 3, the contouring of salinity at depth has enabled UK Nirex Ltd. to construct a spatially varying hydrogeological conceptual model (Black & Brightman, 1996; Littleboy, 1996). This conceptual model formed the basis of the fluid flow modelling presented in Chapter 3, and the BVG samples modelled in the following Chapter (Chapter 5) all fall within the "Hills and Basement", i.e. they have brackish salinities of around 3 equivalent weight %.

4.2 Fundamentals of thermodynamics used in modelling

The GWB speciation/reaction path code relies upon the laws of *equilibrium thermodynamics*; that is, what would a particular system look like if complete equilibrium was attained? The following sections give an overview of the thermodynamic concepts utilised by GWB.

4.2.1 The equilibrium state and equilibrium constant

Fundamental to the description of equilibrium in water is the law of *mass action*. It states that, for a reaction of the generalised type:

$$aA + bB \leftrightarrow cC + dD \qquad 4.1$$

where A, B, C and D represent chemical formulas, *a, b ,c and d* represent coefficients and the double arrow indicates that the reaction is reversible. The distribution at equilibrium between the species on the left (reactants) and right (products) is described by

$$K = \left(\frac{c_C^c \cdot c_D^d}{c_A^a \cdot c_B^b} \right) \qquad 4.2$$

where K is the *equilibrium constant* and c the concentrations of the relevant species raised to a power denoted by its coefficient (Appelo & Postma, 1993). Equilibrium constants are central to both the numerical solution procedure of the Geochemist's Workbench™, (Bethke, 1994) and the determination of the solubility and speciation of important radionuclides such as uranium, therefore it is useful to outline the derivation of these tools for calculating equilibrium states of aqueous solutions.

4.2.2 Chemical potential and Gibbs free energy

A system at equilibrium is characterised by being in a state of minimum energy. A system not at equilibrium can move toward it by releasing energy. For systems at constant temperature *(T)* and pressure *(P)*, energy is measured by the *Gibbs free energy* (G) (Drever, 1982).

If temperature and pressure are fixed, the equilibrium point of a reaction is the point at which the Gibbs free energy is at its minimum, (Fig. 4.1). As with any convex upward function, finding the minimum G is a matter of determining the point at which its derivative vanishes (Bethke, 1996). A way of determining this point is to use a quantity closely related to G, the *chemical potential* (μ) of each species that makes up a phase. The chemical potential :

$$\mu_i = \left(\frac{\partial G}{\partial n_i}\right)_{T,P} \qquad 4.3$$

is the derivative of the species' free energy G with respect to the number of moles (n) of a particular component i being added to the system. Knowing the chemical potential function for each species in a reaction defines the reaction's equilibrium point (Bethke, 1996).

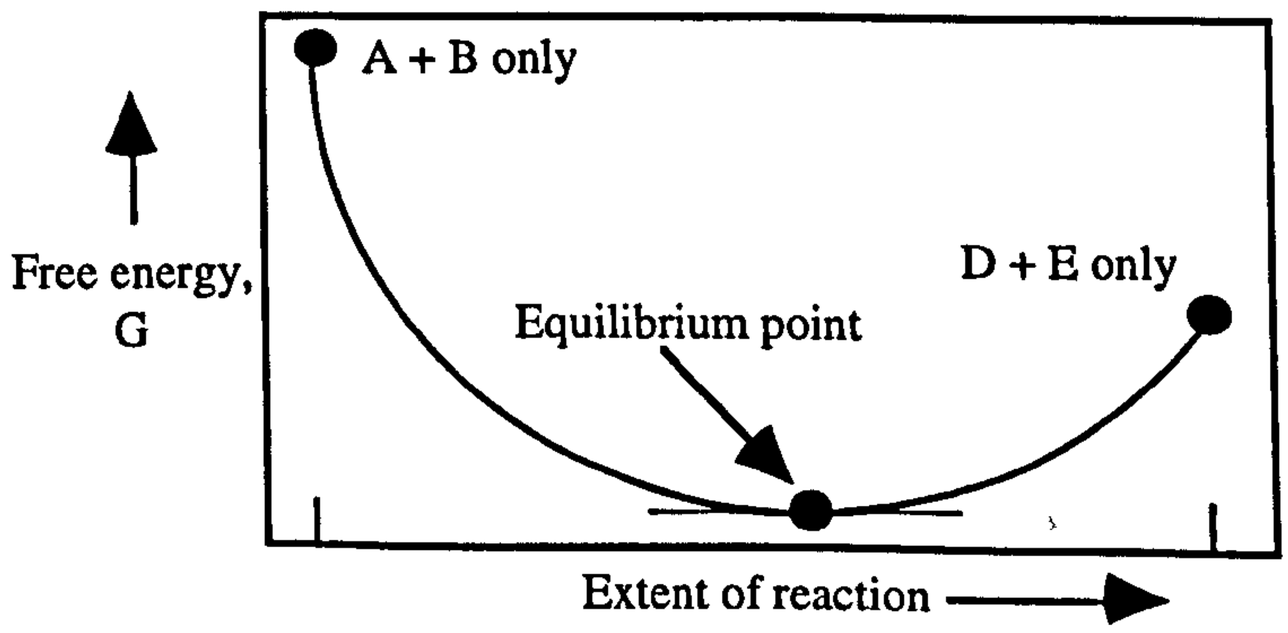

Fig. 4.1 Variation in free energy G with reaction progress for reaction $aA + bB \leftrightarrow cC + dD$. The equilibrium point is the minimum along the curve (after Bethke, 1996).

Considering again Eqn. 4.1, free energy is at a minimum at the point where driving the reaction by a small amount forwards or backwards has no effect on G. From the definition of chemical potential (Eqn. 4.3), the point of minimum G satisfies

$$c\mu_C + d\mu_D - a\mu_A - b\mu_B = 0 \qquad 4.4$$

since c moles of C and d moles of D are produced in the reaction for each a moles of A and b moles of B consumed (Bethke, 1996). The chemical potential (μ_i) of a particular component i can be calculated from

$$\mu_i = \mu_i^\circ + RT \ln a_i \qquad 4.5$$

where μ_i° is the chemical potential constant of component i in its standard state, R is the gas constant (8.3143 $J \cdot mol^{-1} \cdot K^{-1}$), T is the temperature (in Kelvin), and a_i is the *activity* (or *idealised* concentration) of the ith component. *Fugacity* is commonly used in place of activity when dealing with gases (Drever, 1982). The standard potentials μ_i° are tabulated at a standard state: a hypothetical one-molal solution of the species in which the activity and the molality are equal and in which the species properties have been extrapolated to infinite dilution (Nordstrom & Munoz, 1986). This allows activity to follow a molal scale. A species' *molality*, m_i, the number of moles of the species per kilogram of solvent, is related to its activity by

$$a_i = \gamma_i m_i \qquad 4.6$$

The constant of proportionality γ_i is the species' *activity coefficient*, which approaches unity in very dilute solutions (Krauskopf, 1982);

$$\text{i.e. as } \gamma_i \to 1 \quad \text{so} \quad a_i \to m_i \qquad 4.7$$

4.2.3 Activity coefficients

Activity coefficients account for the non-ideality of an aqueous solution. In solutions of ionic species in water there are electrostatic interactions between ions, with the ions ordered in a structure different from pure water (Drever, 1982). The ionic interactions and the ordering of the water both cause the free energy of the real solution to be different from that of the ideal solution and hence, for the activities of both solute and solvent to differ from their concentrations (Appelo & Postma, 1993).

The code used in this modelling study can utilise three methods for estimating activity coefficients; the extended Debye Hückel (B-Dot), Pitzer and Harvie-Moller-

Weare (HMW) methods. The B-Dot equation (extension of Debye Hückel) (Helgeson, 1969) states;

$$\log \gamma_i = -\frac{A z_i^2 \sqrt{I}}{1 + \overset{\circ}{a}_i B\sqrt{I}} + \dot{B} I \qquad 4.8$$

where I is the solution ionic strength, derived from,

$$I = \tfrac{1}{2}\sum m_i z_i^2 \qquad 4.9$$

gives the activity coefficient γ_i of an ion with electrical charge z_i. Variables A, B and $\dot{B}$ are functions of temperature, and the ion size parameter $\overset{\circ}{a}_i$ for each species remains constant. The B-dot equation is accurate in predicting the activities of Na^+ and Cl^- to concentrations up to several molal and of other species up to I = 1M (Bethke, 1996). For higher I the Pitzer and HMW methods are used, (Bethke, 1994).

4.2.4 Gibbs free energy and the equilibrium constant

The equilibrium constant can be derived from the expressions for chemical potential and Gibbs free energy (Nordstrom & Munoz, 1986). The Gibbs free energy per mole of reaction, ΔG_R, is the difference between the Gibbs free energy of the products and that of the reactants:

$$\Delta G_R = G_{products} - G_{reactions} \qquad 4.10$$

which using Eqn. 4.1 can be written in terms of the chemical potential,

$$\Delta G_R = c\mu_C + d\mu_D - a\mu_A - b\mu_B \qquad 4.11$$

Substituting in Eqn. 4.5 produces

$$\begin{aligned}\Delta G_R = {} & c\mu_C^\circ + cRT\ln a_C + d\mu_D^\circ + dRT\ln a_D \\ & - a\mu_A^\circ - aRT\ln a_A - b\mu_B^\circ - bRT\ln a_B\end{aligned} \qquad 4.12$$

rearranging and combining the logarithms into a quotient (Drever, 1982) gives

$$\Delta G_R = c\mu_C^\circ + d\mu_D^\circ - a\mu_A^\circ - b\mu_B^\circ + RT\ln\left(\frac{a_C^c \cdot a_D^d}{a_A^a \cdot a_B^b}\right) \qquad 4.13$$

and as

$$c\mu_C^\circ + d\mu_D^\circ - a\mu_A^\circ - b\mu_B^\circ = \Delta G^\circ \qquad 4.14$$

that is, the *standard free energy* of the reaction, then

$$\Delta G_R = \Delta G^\circ + RT\ln\left(\frac{a_C^c \cdot a_D^d}{a_A^a \cdot a_B^b}\right) \qquad 4.15$$

At equilibrium $\Delta G_R = 0$, therefore

$$\Delta G^\circ = -RT\ln\left(\frac{a_C^c \cdot a_D^d}{a_A^a \cdot a_B^b}\right) \qquad 4.16$$

where the activities are now the particular values for equilibrium between products and reactants (Nordstrom & Munoz, 1986). The quotient, of the familiar mass action form equals the equilibrium constant *K*, thus Eqn. 4.16 can be expressed as

$$\Delta G^\circ = -RT\ln K \quad \text{or} \quad \Delta G^\circ = -2.303RT\log K \qquad 4.17$$

The equilibrium constant K can thus be calculated directly from the equation

$$\log K = -\frac{\Delta G^\circ}{2.303RT} \qquad 4.18$$

once the free energy of reaction is derived (Drever, 1982).

4.2.5 The equilibrium constant and the saturation index (SI)

When an aqueous solution is at saturation equilibrium with a mineral the reaction

$$AB_{(s)} \leftrightarrow A^{x+}_{(aq)} + B^{y-}_{(aq)} \qquad 4.19$$

is at reversible equilibrium. Taking the mineral Calcite ($CaCO_{3(s)}$) as an example;

$$CaCO_{3(s)} \leftrightarrow Ca^{2+}_{(aq)} + CO^{2-}_{3(aq)} \qquad 4.20$$

at equilibrium the mass action expression would apply;

$$K_{eq} = \frac{a_{Ca^{2+}} \cdot a_{CO_3^{2-}}}{a_{CaCO_{3(s)}}} \qquad 4.21$$

Since Calcite would be in it's standard state its activity is unity, thus

$$K_{eq} = a_{Ca^{2+}} \cdot a_{CO_3^{2-}} = K_{sp} \qquad 4.22$$

i.e. the equilibrium constant is equal to the solubility product K_{sp} (Nordstrom & Munoz, 1986). If an aqueous solution is at saturation equilibrium with a mineral then the product of the activities Q should equal the solubility product constant K_{sp}, (Appelo & Postma, 1993);

$$\left(a_{Ca^{2+}} \cdot a_{CO_3^{2-}}\right)_{water} = \left(a_{Ca^{2+}} \cdot a_{CO_3^{2-}}\right)_{equilbrium} = K_{sp} \qquad 4.23$$

or

$$\frac{\left(a_{Ca^{2+}} \cdot a_{CO_3^{2-}}\right)_{water}}{\left(a_{Ca^{2+}} \cdot a_{CO_3^{2-}}\right)_{equilbrium}} = \frac{Q}{K_{sp}} = 1 \qquad 4.24$$

It is more convenient to take the log of the ratio, known as the *saturation index* (*SI*):

$$\mathrm{SI} = \log\left(\frac{Q}{K_{sp}}\right) = 0 \text{ (at equilibrium)} \qquad 4.25$$

From Eqn. 4.25, a mineral at the point of saturation has a SI = 0, an undersaturated mineral has a negative *SI* (mineral tends to dissolve), and a supersaturated mineral has a positive *SI* (mineral tends to precipitate) (Bethke, 1996).

4.2.6 Redox processes

Reduction (red) and oxidation (ox) or redox processes exert an important control on the distribution of species like O_2, Fe^{2+} and UO_2^{2+} (Krauskopf, 1979). The reaction

$$b\mathrm{A}_{red} + b\mathrm{B}_{ox} \leftrightarrow c\mathrm{C}_{ox} + d\mathrm{D}_{red} \qquad 4.26$$

can be written as the half reactions

$$a\mathrm{A}_{red} \rightarrow c\mathrm{C}_{ox} + \mathrm{n}e^- \quad \text{and} \quad d\mathrm{D}_{red} \rightarrow b\mathrm{B}_{ox} + \mathrm{n}e^- \qquad 4.27$$

In terms of Gibbs free energy Eqn 4.26 can be substituted into Eqn. 4.15 (Appelo & Postma, 1993) to give;

$$\Delta G_R = \Delta G^0 + RT\ln\left(\frac{a_{C_{ox}}^c \cdot a_{D_{red}}^d}{a_{A_{red}}^a \cdot a_{B_{ox}}^b}\right) \qquad 4.28$$

Gibbs free energy is related to electrochemical energy by

$$\Delta G = nFE \qquad 4.29$$

where E is the potential (emf) in Volts, n is the number of electrons that the equation is shifting from one kind of atom to another and F is the Faraday constant (96.42 kj/Volt gram equivalent) (Appelo & Postma, 1993). Substitution of Eqn. 4.29 into Eqn. 4.28 produces the *Nernst* equation;

$$E = E^0 + \frac{RT}{nF}\ln\left(\frac{a_{C_{ox}}^c \cdot a_{D_{red}}^d}{a_{A_{red}}^a \cdot a_{B_{ox}}^b}\right) \qquad 4.30$$

In geochemistry the symbol Eh is commonly employed instead of E to designate the hydrogen scale (referred the standard hydrogen electrode) as the basis for electrode potentials. There is no difference in the value between Eh and E (Nordstrom & Munoz, 1986).

The Geochemist's Workbench™ utilises pe; another variable that is frequently used for the redox state of an aqueous solution. The pe, by analogy to pH, is defined as

$$pe = -\log a_{e^-} = \frac{1}{n}\log\frac{Q_{e^-}}{K_{e^-}} \qquad 4.31$$

where n is the number of electrons consumed in the half-cell reaction and Q_{e^-} is the activity product for the half-cell reaction, calculated accounting for each species except the electron (Bethke, 1994). GWB uses a variation on the *Nernst* equation;

$$\mathrm{Eh} = \frac{2.303RT}{\mathrm{nF}}\log\frac{Q_{e^-}}{K_{e^-}} = \frac{2.303RT}{\mathrm{F}}pe \qquad 4.32$$

to determine the Eh value corresponding to any half-cell reaction.

Many natural waters do not achieve redox equilibrium (Lindberg & Runnells, 1984). In this case, no single value of pe or Eh can be used to represent the redox state. Instead, there is a distinct value for each redox couple in the system. Applying the Nernst equation to the reaction,

$$e^- + \tfrac{1}{4}O_{2(aq)} + H^+ \leftrightarrow \tfrac{1}{2}H_2O \qquad 4.33$$

gives a *p*e or Eh representing the hydrolysis of water. Under disequilibrium conditions, this value differs from those calculated from reactions such as

$$8e^- + SO_4^{2-} + 9H^+ \leftrightarrow HS^- + 4H_2O \qquad 4.34$$

and

$$e^- + \underset{goethite}{FeOOH} + 3H^+ \leftrightarrow Fe^{2+} + 2H_2O \qquad 4.35$$

4.2.7 Electroneutrality

One other important aspect of modelling a system is elecroneutrallity. In thermodynamic models charge balance has always to be honoured. If Z_i is the charge on a species component, M_i (the same as the charge on the corresponding basis species) then

$$\sum_i Z_i M_i = 0 \qquad 4.36$$

thus when charged species appear in the basis M_i can be adjusted to retain charge balance.

4.3 References

Appelo, C.A.J. & Postma, D. (1993) *Geochemistry groundwater and pollution.* Balkema, Rotterdam, 536 pp.

Bath, A.H., McCartney, R.A., Richards, H.G., Metcalfe, R. & Crawford, M.B. (1996) Groundwater chemistry of the Sellafield area: a preliminary investigation. *Quarterly Journal of Engineering Geology*, **29**, supplement 1, S39-S57.

Bethke, C.M. (1994) *The Geochemist's Workbench; a users guide to Rxn, Act2, Tact, React and Gtplot.* University of Illinois, Urbana-Champaign, USA, 213 pp.

Bethke, C.M. (1996) *Geochemical reaction modeling.* Oxford University Press, New York, 397 pp.

Black, J.H. & Brightman, M.A. (1996) Conceptual model of hydrogeology of Sellafield. *Quarterly Journal of Engineering Geology*, **29**, supplement 1, S83-S93.

Bond, K.A., Moreton, A.D. & Tweed, C.J. (1995) *Water compositions of relevance to a deep cement-based repository at Sellafield: evaluation using thermodynamic modelling.* Report No. **NSS/R310**, UK Nirex Ltd., Harwell, UK.

Bond, K.A. & Tweed, C.J. (1995) *Groundwater compositions for the Borrowdale Volcanic Group, Boreholes 2, 4 and RCF3 using thermodynamic modelling.* Report No. **NSS/R397**, UK Nirex Ltd., Harwell, UK.

Brookins, D.G. (1987) *Eh-pH diagrams for geochemsitry.* Springer-Verlag, New York, 176 pp.

Drever, J.I. (1982) *The geochemistry of natural waters.* Prentice-Hall, Englewood Cliffs, N.J., 388 pp.

Faure, G. (1987) *Principles of isotope geology.* John Wiley and Sons, New York, 589 pp.

Gillespie, M.R. & Milodowski, A.E. (1994) *The petrology of fractures and fracture mineralisation in Sellafield BH2.* Report No. **CC94S/448/CF-A-C Draft**, British Geological Survey, Keyworth, UK.

Haszeldine, R.S. (1996) Subsurface geology, geochemistry and water flow at a rock characterisation facility (RCF) at Longlands Farm. Proof of evidence. *In:*

Haszeldine, R.S. & Smythe, D.K. (eds) *Radioactive Waste Disposal at Sellafield, UK. Site Selection, geological and engineering problems.* University of Glasgow, Glasgow, UK, 121-164.

Krauskopf, K.B. (1979) *Introduction to geochemistry.* McGraw-Hill Book Company, New York, 617 pp.

Lindberg, R.D. & Runnels, D.D. (1984) Groundwater redox reactions: an analysis of equlibrium state applied to Eh measurements and geochemical modelling. *Science*, **225**, 925-927.

Littleboy, A. (1996) The geology and hydrogeology of the Sellafield area: development of the way forward. *Quarterly Journal of Engineering Geology*, **29**, supplement 1, S95-S104.

Metcalfe, R. & Crawford, M.B. (1994) *Models of water/rock interactions in the Borrowdale Volcanic Group within the potential repository zone at Sellafield.* Report No. **WE/94/26C**, British Geological Survey, Keyworth, UK, Keyworth, UK.

Nirex. (1992a) *The geology and hydrogeology of Sellafield.* Report No. **263**, UK Nirex Ltd., Harwell, UK.

Nirex. (1992b) *Sellafield hydrogeology. Report of the hydrogeology joint interpretation team.* Report No. **268**, UK Nirex Ltd., Harwell, UK.

Nirex. (1993) *The geology and hydrogeology of the Sellafield area: Interim assessment.* Report No. **524 (4 vols)**, UK Nirex Ltd., Harwell, UK.

Nordstrom, D.K. & Munoz, J.L. (1986) *Geochemical thermodynamics.* Blackwell Scientific Publications, Oxford, 477 pp.

Plummer, L.N., Parkhurst, D.L. & Thorstenson, D.C. (1983) The development of reaction models for groundwater systems. *Geochimica et Cosmochimica Acta*, **47**, 665-686.

Strong, G.E. & Kemp, S.J. (1994) *The petrographic, mineralogical and lithogeochemical characteristics of Permo-Triassic rocks from Sellafied BH2.* Report No. **CC93S/358/C-F-B-C**, British Geological Survey, Keyworth, UK.

Chapter 5 Modelling uranium solubility and speciation

McKeown, C. and Haszeldine, R.S.

5.1 Abstract

One of the most important criteria that must be fulfilled by the UK's first repository for Intermediate Level Waste (ILW) at Sellafield in West Cumbria is that the geochemistry of the repository must be able to retain radionuclides for millions of years. As part of a multi-barrier system, radionuclide retention is envisaged to be via engineered physical and chemical barriers, i.e., steel barrels and alkaline cement. The major mass of radioactive material in the repository will be 10^6 kg of uranium, therefore this study focused on the geochemical containment of uranium. Reducing chemical conditions limit uranium solubility, oxidising conditions enhance it. The speciation of uranium in natural waters has been extensively studied, and is reviewed. Thermodynamic data for the most important uranium species were derived from the most recent Nuclear Energy Agency (NEA) review and were used to perform geochemical simulations of uranium speciation, complexation and solubility.

Rock core data provided by UK Nirex Ltd. were reviewed regarding the minerals found to be lining fracture surfaces in contact with present day groundwater. Analyses of in-situ, natural groundwaters in the repository host rock, the Borrowdale Volcanic Group (BVG) were geochemically modelled using the speciation/reaction path code The Geochemist's Workbench (GWB). The in-situ groundwater Eh of +66 mV was shown by calculation to be the most probable Eh. Suggestions by UK Nirex Ltd. that groundwater samples are contaminated by drillpipe chemistry are not supported. These natural groundwaters are not in redox equilibrium, and importantly the chemically reduced iron mineral, pyrite is absent and thus does not enforce a reducing -250 mV Eh, as suggested by UK Nirex Ltd.

Repository cement can be geochemically represented as a mixture of portlandite ($Ca(OH)_2$), Brucite ($Mg(OH)_2$)and Calcite ($CaCO_3$). Simulations with GWB of natural BVG groundwaters interacting with repository cement, produced no change in the +66 mV Eh, but did produce a very alkaline fluid of pH ≈10 at 80°C. Interaction of this water with iron, to simulate steel barrels, produced an alkaline water with Eh ≈ -500 mV. Dissolution of uranium within the "near field" of a repository was simulated by forcing equilibrium of ILW solids with in situ and cement influenced waters. Surprisingly, this was not at all affected by interaction

with steel, and produced a high uranium solubility of $10^{-2.7}$ M. This is some 600 times higher than values used by UK Nirex Ltd. in repository safety case assessments.

Simulations of uranium solubility slightly further from the repository, "the pseudo near field", were performed by using saturation indices to predict the likely uranium solid phase. Uranium concentrations here were closely controlled by Eh; ranging from 10^{-13} M in the presence of steel, to $10^{-2.7}$ with no steel present. Thus the retention of uranium is directly controlled by the durability of the steel barrels. UK Nirex Ltd. have modelled this durability to be 10,000 yr, but this is an overestimate; BVG groundwater is naturally oxidising and will enhance the destruction of the steel barrels. In the "far field" uranium solubility depends on the Eh of the BVG natural groundwater, and is 10^{-12} M if pyrite controls Eh or, more probably, $10^{-5.4}$ if Eh is as measured in-situ.

Variations in thermodynamic data can affect the calculation of uranium solubility, especially at concentrations of less than 10^{-7} M; small variations in equilibrium constants (log K's) can produce uranium solubilities ranging from 10^{-15} to $10^{-8.1}$ M with the same data, and can produce uranium near field concentrations of $10^{-1.4}$ M. The retention of uranium in this particular engineered repository depends entirely on the durability of steel barrels. There is no geochemical containment from the natural water or rock mineralogy. The engineered geochemical containment will fail in substantially less than 10,000 yr. Uranium solubilities in natural BVG groundwater could be around 600 times greater than the $10^{-5.5}$ M used by UK Nirex Ltd. in their safety case simulations.

5.2 Introduction

Britain's first repository for Intermediate Level Waste (ILW) is proposed to be situated 3 km to the east of the British Nuclear Fuels Ltd (BNFL) Sellafield fuel reprocessing plant (THORP) in West Cumbria, north-west England (Fig. 5.1 a, b). The radionuclide uranium forms an important part of the waste streams to be disposed of, in terms of inventoried mass in the waste, around 10^6 kg (Nirex, 1992a; Nirex, 1992b; Nirex, 1992c), longevity of radioactivity, half-life of many millions of years (Weigel, 1986) and potential risk from the repository (Nuclear Energy Agency, 1989).

Although radionuclides such as plutonium, caesium and iodine are important contributors to the radioactive waste inventory, uranium is by far the most abundant and, despite being very complex, its geochemical behaviour is well understood. Therefore this paper solely deals with the results from a geochemical modelling study of the natural and engineered repository groundwater conditions and the effects they might have on the solubility of uranium. No other radionuclides are dealt with in this study.

Hydrochemical data from boreholes have been used to model in-situ pH, Eh, major element concentration and mineral equilibrium. These fluids have been used to model the solubility and speciation of uranium in the chemical conditions immediate to the facility, inside the chemically engineered repository, and in the natural groundwater setting surrounding the repository. By modelling the sensitivity of the system, conclusions can be drawn about the robustness of current models of the repository concept.

As the repository at Sellafield is yet to be built any studies of uranium solubility at the site can only be performed either in laboratory simulations, studies of natural analogues, or by using computer modelling programs. The study reported here approached the problem by taking measured information of natural water and rock mineralogy at the proposed site, and modelling the geochemistry by computer simulation. In common with the many speciation and reaction path codes available to model hydrochemical systems e.g. PHREEQE and EQ3/6 (Parkhurst *et al.*, 1980b; Wolery *et al.*, 1988) the code used in this study; The Geochemist's Workbench™ (GWB) (Bethke, 1994), relies upon the laws of *equilibrium thermodynamics*; that is, what would a particular system look like if complete equilibrium was attained? (see Chapter 4). Although natural systems rarely attain

equilibrium, (Nordstrom & Munoz, 1986) the equilibrium approach is useful as it can often give a good approximation of the real world, and can indicate the reactants and products from the direction in which geochemical reactions proceed (Drever, 1982). The derivation of thermodynamic stability constants (log K's) and their use in determining the redox states of aqueous solutions and the solubility of minerals in such fluids is outlined in Chapter 4.

5.3 Repository concept

When developing repository concepts for the disposal of long-lived radionuclides such as uranium, deep geological emplacement in the "far field" is not enough to guarantee a safety case. Such repositories must also include in their design a number of barriers. These barriers (the "near field") are engineered to prevent or retard the release of radionuclides from the waste into the geosphere and biosphere (Fig. 5.2) (Nirex, 1993b). In common with ILW repository concepts elsewhere (Miller *et al.*, 1994) wastes are to be immobilised in the Sellafield repository, usually in a cementitious material, packaged in concrete or stainless steel/mild steel containers, emplaced in repository vaults and back-filled with hundreds of thousands of cubic metres of cement-based material (Atkinson *et al.*, 1993).

5.3.1 Evolution of pH in the near field

There has been much research into the properties of this backfill (known as Nirex Reference Vault Backfill or NRVB) (Atkinson, 1995; Atkinson *et al.*, 1988a; Atkinson *et al.*, 1988b; Atkinson & Guppy, 1988), a substantial proportion of which will be composed of hydrated, blended Portland cements (Bennet *et al.*, 1992). The detailed constitution of the phases in these cements is complicated but dominantly they are poorly crystalline and in the $CaO-SiO_2-H_2O$ system (Atkinson *et al.*, 1993).

Laboratory and modelling studies of the equilibration of these amorphous calcium silicate hydrogels (CSH) predicts that the pH in the repository setting might increase to 12.5 at 25°C (Atkinson *et al.*, 1987). Due to the heat produced from exothermic cement reaction and radiogenic heating from radionuclide decay, combined with slow heat dispersion by diffusion the temperature in the repository volume is expected to reach a peak of 80°C (Nirex, 1995e). At these temperatures the pH is expected to be around 10.0 (Atkinson *et al.*, 1991). It has been shown to be acceptable to represent the CSH phases in modelling studies by the member minerals portlandite ($Ca(OH)_2$), and the "fictive" solid phase CaH_2SiO_4 described by Berner (Berner, 1987; Bond *et al.*, 1995).

5.3.2 Evolution of Eh in the near field

During construction and operation of the repository oxygen will be introduced and when finally backfilled the cement grout will contain both gaseous and dissolved oxygen in its pores (Nirex, 1995e). This oxygen will cause the aerobic corrosion of the 10^9 moles of iron present in the repository (from mild and stainless steel packaging containers, construction materials and waste inventory) (Naish *et al.*, 1990) by the reaction

$$2Fe + 2H_2O + O_2 \rightarrow 2Fe(OH)_2 \qquad 5.1$$

This mechanism will remove oxygen from the system and it is expected that repository conditions will become anaerobic within 100 years of closure (Atkinson *et al.*, 1993) and that the corrosion of the steel will then proceed by

$$Fe + 2H_2O \rightarrow Fe(OH)_2 + H_2 \uparrow \qquad 5.2$$

with the iron hydroxide produced possibly reacting further to produce magnetite (Fe_3O_4)

$$3Fe(OH)_2 \rightarrow Fe_3O_4 + 2H_2O + H_2 \uparrow \qquad 5.3$$

The overall reaction can be written as

$$3Fe + 4H_2O \rightarrow Fe_3O_4 + 4H_2 \uparrow \qquad 5.4$$

The release of 4 moles of hydrogen for every 3 moles of native iron would control the oxidation state in the repository. Eh is a common measure of the oxidation state of a system, equal to 0.059 x pe at 25°C, where pe is the negative log of the activity of electrons in the system (see Chapter 4 for explanation of activity). The pe should not be interpreted in terms of concentration of electrons, but rather as the *tendency* to release or accept electrons. The theoretical Eh is as low as -780 mV although kinetic constraints may prevent such a low Eh being achieved in the real repository (Haworth & Sharland, 1995).

The main rationale behind this "cement and steel" approach is to provide physical containment in the short term (hundreds of years) and chemical containment over longer time scales (hundreds of thousands of years) (Hooper, 1995a). The reducing ambient conditions produced by the corrosion of the steel and the high pH produced by the dissolution cement are intended to promote precipitation of low solubility U^{4+} oxides/hydroxides and promote sorption.

5.4 Geological and hydrogeological setting

The proposed repository site (Fig. 5.1 a, b) is at least 650 metres below Ordnance Datum (mbOD) within rocks of the Borrowdale Volcanic Group (BVG). This is proposed to give a far field isolation of waste within which near field repository can be engineered (Fig. 5.2). The BVG is a 6000m thickness (regionally) of heavily fractured and folded Ordovician meta-andesites and tuffs. These are unconformably onlapped by 400m of Carboniferous limestones, Permian clastics and evaporites and more than 1500m of Triassic sandstones (Fig. 5.3) (Millward, 1995).

The site area around Sellafield has been subject to a comprehensive series of hydrogeological surveys performed within a suite of drilled, cored and logged deep boreholes (Fig. 5.1b). These have given rise to a conceptual model of the hydrogeology (Nirex, 1995c) (Fig. 5.4), that illustrates the possibility of three distinct hydrological units (Black, 1995);

- Hills and Basement Regime; topographically driven, relatively low flux, saline groundwater within fractured, faulted rocks of the BVG;

- Irish Sea Basin Regime; relatively low flux, hypersaline brines expulsed from the East Irish Sea Basin occurring within fractured BVG, Carboniferous Limestones and Permo-Triassic cover rocks ;

- Coastal Plain Regime; topographically driven, high flux, fresh groundwaters within highly porous and permeable Triassic aquifers.

The proposed repository is to be situated within the so called Hills and Basement Regime, groundwater within which has a salinity of around 2.5 equivalent weight % (Pringle, 1995) and is in direct contact with the whole rock and fracture lining minerals that compose the BVG. These minerals may, or may not, be in equilibrium with the groundwater and may, or may not, have a direct control on parameters such as the Eh, pH and chemical speciation.

5.4.1 Importance of the groundwater

It is essential to develop a good understanding of the groundwater hydrochemistry of the natural groundwater as it is this groundwater that will ultimately enter into the repository volume, "corrode" the backfill, containers and waste, and possibly transport radionuclides into the far field (Metcalfe & Crawford, 1994; Pearson & Scholtis, 1993). The time taken for this entrance and corrosion could be relatively short. The damaged rock zone around an excavated repository can cause altered stress states that induce large new fractures. This could lead to a significant

increase in groundwater flow and decrease the duration of the near field barriers (Nuclear Energy Agency, 1993). Both preferential cracking of the backfill, and voidage due to leaching, decrease the residence time of the repository waters (Atkinson *et al.*, 1993), and thus reduce the effectiveness of the engineered barriers.

The controls of the solubility and speciation of uranium are the ambient redox conditions that any solid phase comes in contact with and the availability of complexing ligands in the aqueous solution. Therefore it is essential that the natural groundwater chemistry be understood as fully as possible (Grenthe, 1991). For the purpose of this study the most useful hydrogeological analyses are those that lie within the Proposed Repository Zone (PRZ) (Fig. 5.1b) and provide detailed information on Eh, pH, temperature and the concentration of ions such as Fe^{+++}/Fe^{++} and SO_4^{--}/HS^-.

Analyses obtained from Discrete Extraction Tests (DETs) from borehole 2, which passes through the PRZ, were used as input to the simulations. These tests pump the groundwater from a packed off interval of interest and samples are either taken in-situ or are pumped to the surface. Chapter two provides more detail on the techniques used in DET sampling and Chapter four reviews the chemical procedures involved in processing the data. Corrections for contamination by formation waters and drilling fluid are applied before tabulation (Nirex, 1995c). A number of Post Drilling Discrete Extraction Tests (PDDET) have also been performed but the data obtained are not as comprehensive as the DETs. Although the DETs in BH2 are performed at a number of depths in all the major geological units encountered, the most relevant to this study are those from the BVG. These are;

DET 7 (1530 mbOD);
DET 8 (950 mbOD);
DET 9 (650 mbOD);
DET 10 (480 mbOD).

and are presented in Table 5.2. All the above analyses (or parts of) were used in this modelling study. DET 9 is obviously the most relevant to the repository (in terms of depth) but has been claimed to be not representative of natural conditions due to being less saline (Metcalfe & Crawford, 1994). Inspection of similar data from Nirex boreholes 3, 4, 5 and 10a (Nirex, 1993a) show that the borehole 2 data are representative of the Hills and Basement (saline water) and Coastal Plain (freshwater) flow regimes.

5.4.2 Whole rock and fracture-lining minerals in the BVG

As mentioned previously, the equilibrium between whole rock and fracture lining minerals that compose the BVG may have an effect on the hydrochemistry and Eh/pH of the groundwaters surrounding the potential repository. The mineralogy of the whole rock BVG is complex but is dominated by pyroxene, plagioclase, ilmenite/magnetite and volcanic glass but these have been extensively altered to chlorite, carbonate/albite, hematite and muscovite (generally further altered to illite) respectively (Beddoe-Stephens & Phillips, 1993). Since these minerals line fractures that permit fluid flow they are in direct contact with the ambient groundwaters and have an important effect upon their hydrochemistry.

The mineralogy of fractures within the BVG and overlying sediments are shown in Table 5.3 (Nirex, 1995b) which summarises the mineralogical episodes (ME1-ME9) and their mineralogical characteristics. The volumes of minerals present within fractures which permit flow of water in the present day, are summarised in Fig. 5.5 (Nirex, 1995b). It is notable that there are minimal amounts of minerals present which indicate a reducing Eh for groundwater during their precipitation. Such minerals indicating geochemically reduced water might include siderite (none present), pyrite or other metallic sulphides (pyrite and sulphides form less than 1% present by volume (Nirex, 1995b).

In contrast, the iron-bearing mineralogy of these "flowing" fractures is dominated by hematite (15%) (Fig. 5.5). This is a mineral which can indicate an "oxidising" Eh in cool temperature groundwater, such as that found here. It must, however, be pointed out that the presence or lack of such minerals is not a clear-cut indicator of the redox of groundwater system. Pyrite can exist in oxidising conditions (Sato, 1992) and hematite can be found in reducing conditions (Hooper, 1995b). Calcite (43% flowing fracture mineral) has well developed euhedral crystals, which are usually interpreted to indicate growth into open fracture voids.

At the Sellafield site detailed investigations into fracture mineralogy have been undertaken at the site of the shafts of the planned rock lab (or RCF) (Nirex, 1995a). Hematite mineralisation is commonly found on fractures and faults, however pyrite is only found as a subordinate mineral on fractures on two occasions, and these are below the proposed repository depth of 650 m (Haszeldine, 1996; Nirex, 1995a). As with fractures at the larger, district scale, fracture zones that have water flowing through at present are linked to mineralisation episodes ME6 and ME9. These appear to have an oxidising mineralogy dominated by calcite, hematite and Fe-oxides. Indeed pervasive or partial hematisation affects 696 m out of 1,365 m (51%)

of the length of the boreholes (Nirex, 1995a). There is no relationship between flow zones and hematisation, so that the extent of hematisation is difficult or impossible to predict and match to present-day water flow (Nirex, 1995a).

Thus it would appear that only a minimal amount of geochemically "reduced" minerals, such as pyrite, occur in the fractures or BVG surrounding them, and that the geochemical history of the BVG and fractures has fundamentally been one dominated by oxidising groundwater. Any pyrite that does occur is found only in "trace" quantities and at greater depth than the projected repository site (Nirex, 1995a) and may be of insufficient volume to constitute a redox buffer (Wogelius, pers comm.). In any event as pyrite can co-exist metastably with more oxidised minerals (Sato, 1992) the presence of pyrite does not automatically indicate a reducing environment.

5.4.3 Significance of the Eh problem

The measurement of the redox state of groundwaters is notoriously difficult (Lindberg & Runnels, 1984). Uranium can exist in more than one oxidation state; the U^{6+} oxidation state complexes easier and is more soluble than the reduced U^{4+}. and therefore may be moved to the surface more easily within groundwater (see section 5.6). If the natural groundwater is oxidising, then greater mobility of uranium in solution would be expected. Eh values of waters in Borehole 2 (Nirex, 1995c) have been measured as very oxidising (+ 350 mV) in the sediments, and only slightly oxidising to mildly reducing (+ 92 to - 119 mV) (Nirex, 1995c)in the BVG (Nirex, 1995c), (Fig. 5.6).

The measured concentration of iron may have been contaminated by the drill string and mud. Modelling performed elsewhere (Metcalfe & Crawford, 1994) suggested that for the Sellafield site a complete 'best estimate' composition of in-situ groundwater was unattainable at present. Consequently several scenarios for the estimate of Eh were presented by Metcalfe & Crawford (1994). Their report details results from the simulation of ambient redox conditions using the speciation and reaction path code EQ3NR/EQ6. In the report, the Eh was derived from either assuming equilibrium with particular minerals or from a single redox pair. Fig. 5.7 (Lindberg & Runnels, 1984) illustrates that for natural waters at temperatures likely at the depth of the proposed repository there is a lack of equilibrium between different redox couples in the same water sample. This is particularly true of the HS^-/SO_4^{2-} couple. Therefore it is probably incorrect to assume that a single redox pair controls the Eh of a solution.

One particular model from Metcalfe & Crawford (1994) has the in-situ groundwater Eh controlled by equilibrium with pyrite (FeS_2) and hematite (Fe_2O_3) giving highly reducing conditions of - 232 mV to - 258 mV. This model was subsequently used in a study, directed by UK Nirex Ltd., that modelled the possible baseline geochemical conditions of the repository groundwaters (the mineral siderite ($FeCO_3$) was also included) (Goldberg *et al.*, 1995).

5.4.4 Redox approach used in study

The approach used in the study reported here was to simulate the effect of all redox couples simultaneously. In GWB the redox state of a solution can be constrained by setting; Eh, pe, or activity of $O_{2(aq)}$ (see Chapter 4 for explanation of activity). An Eh representative of all the redox couples present in the solution can be calculated from the Nernst equation (see Chapter 4). This is termed the equilibrium or bulk Eh. The GWB code also allows interactive coupling or decoupling of redox couples; e.g. decoupling the ferric-ferrous redox couple allows the program to consider that oxidised and reduced iron species may exist in quantities not related to the values entered for Eh.

Whenever there are two or more independent redox couples, the GWB code reports the theoretical oxidation state of each couple, with their corresponding Nernst pe and Eh (Bethke, 1996). Combining such evidence of ranges in Eh with the information regarding fracture lining minerals outlined in section 5.4.2, four modelling scenarios (or cases) were constructed regarding the Eh and equilibrium states of the DET groundwater samples;

- Case *a* Bulk Eh as measured in situ, Fe^{2+} / Fe^{3+} and SO_4^{2-} / HS^- decoupled

For the following cases all redox species are coupled;

- Case *b* Eh as measured in situ;
- Case *c* Eh as measured in situ, fluid in equilibrium with hematite;
- Case *d* Eh controlled by equilibrium with hematite and pyrite; reducing conditions promoted.

5.5 Specific Aims

In many respects the use of computer models as an aid in understanding the safety of radioactive waste repositories is fundamentally flawed: there are almost as many "unknowns" as there are parameters in a given model (Haszeldine & McKeown, 1995). The reduction of these unknowns is of paramount importance if any credence can be attached to a model (Oreskes *et al.*, 1994) therefore the main aims of this

study were to examine *the role of uncertainty* in the values used, and to identify the *critical controls* on the geochemical system.

Other modelling studies have investigated the re-saturation of the backfill with pure water (Goldberg *et al.*, 1995); this is very much a transitory effect and not realistic of the natural conditions. In this study real groundwater analyses were used at all times.

The specific aims of this study were;

- to determine the controls of Eh, pH and speciation of groundwaters in contact with minerals in the whole and fractured BVG;

- to use these groundwater files to determine the solubility and speciation of uranium in the high pH repository environment using two distinct approaches ;

  1) using uranium solid phases other workers presume to be formed from dissolution of the waste;

  2) predicting probable uranium solid phases that may form from waste dissolution, thus checking the likelihood of formation of the above presumed uranium solid phases;

- to predict the uranium solid phases controlling uranium solubility in the far field natural groundwaters, and model their solubility and speciation for a range of Eh and equilibrium states;

- to determine the importance of reliable thermodynamic data in solubility calculations used to assess the safety of a proposed repository.

5.6 Uranium geochemistry : application to radioactive waste disposal

A full review of the large body of work associated with the geochemistry of uranium is beyond the scope of this study; there are many documents giving a broad account of its properties in mineral, fuel and aqueous form (Finch & Ewing, 1992; Harvey, 1995; Janeczek & Ewing, 1992; Weigel, 1986). The complexities of uranium thermodynamics are also dealt with in great detail in a wide variety of papers and reports (Bruno *et al.*, 1987; Bruno *et al.*, 1993; Cross & Ewart, 1990; Fuger, 1992; Grenthe *et al.*, 1992; Langmuir, 1978; Lemire, 1988; Morss, 1986; Pearson & Berner, 1991). As a preface to the modelling study proper it is, however, useful to briefly review the fundamentals of uranium chemistry and this paper draws upon the

above such publications to illustrate the complex nature of uranium solubility and speciation.

5.6.1 Significance of uranium oxidation state

The most important and fundamental property of the actinide element uranium is that it can exist in more than one oxidation state. This has a direct effect on its solubility in aqueous solution (Weigel, 1986). Uranium in aqueous solution is known to exist in oxidation states from U^{2+} to U^{6+}. However only U^{4+} and U^{6+} are significant in nature (Basham & Kemp, 1993). This parity between oxidation state and solubility is reflected in the natural mineralogy of uranium, which is illustrated well in the mechanism of formation of roll front ore bodies (Nash *et al.*, 1981). In oxidising fluids (relatively high Eh) uranium in the hexavalent form (generally agreed to be the uranyl ion UO_2^{2+} (Grenthe *et al.*, 1992)) can complex with a very large number of ligands such as hydroxide, carbonate and sulphate. Such complexes become more soluble in aqueous solution than UO_2^{2+} (Langmuir, 1978; Weigel, 1986). These complexes can be mobilised and transported in groundwater before encountering reducing, low Eh conditions. The reducing conditions encourage the U^{4+} oxidation state to dominate, and the uranium is precipitated from solution (Nash *et al.*, 1981).

The precipitated mineral would most likely be a uranium oxide (Weigel, 1986). As this system also dominates the uranium forms found within ILW (Nirex, 1992b), the study of naturally occurring oxidised uranium minerals provides insights into the probable behaviour of uranium in a repository setting (Finch & Ewing, 1991). The minerals uraninite and pitchblende (both *ideally* UO_2) are the most common uranium minerals in nature (Parks & Pohl, 1988). They are differentiated by their crystal habit; uraninite crystallises in the cubic system (fluorite structure type) and pitchblende is cryptocrystalline and has a colloform or botryoidal habit, reflecting formation at low temperatures, from colloidal suspension (Basham & Kemp, 1993).

In the natural environment both these polymorphs contain uranium essentially in the U^{4+} state, but there is invariably some oxidation to U^{6+}. During this oxidation excess oxygen is incorporated into the structure causing the formation of nonstoichiometric UO_{2+x}, where x is the number of excess interstitial oxygens and is equal to the amount of U^{4+} converted to U^{6+} ($0.00<x<0.25$) (Janeczek & Ewing, 1992), with the theoretical limit to oxidation being $UO_{2.67}$ or U_3O_8. Oxidation beyond $UO_{2.33}$ is not accommodated by the cubic UO_{2+x} structure. Continued oxidation requires crystallisation of orthorhombic U_3O_8. The only anhydrous uranium oxides reported in nature are UO_2, $UO_{2.25}$ and $UO_{2.33}$. $UO_{2.25}$ (or U_4O_9)

is the highest anhydrous oxide that can be expected to be produced from the oxidation of uranium in ILW in the natural environment (Finch & Ewing, 1991).

Other minerals relevant to a repository setting are Schoepite, $UO_2(OH)_2 \cdot H_2O$, (chemically equivalent to $UO_3 \cdot 2H_2O$) and Rutherfordine, $UO_2CO_{3(s)}$. The orthorhombic phase Schoepite is a known corrosion product of uraninite in nature (Torrero *et al.*, 1994) and is generally believed to become unstable with respect to another orthorhombic phase, $UO_2(OH)_2(c,\beta)$ (c = crystalline and β indicates the particular crystalline structure) at temperatures between 40 and 100°C (in contact with liquid water) (Grenthe *et al.*, 1992) or simply through irreversible dehydration (Finch *et al.*, 1992). At standard temperature (25°C) the phase Rutherfordine may become stable with respect to Schoepite if the partial pressure of carbon dioxide (P_{CO_2}) is greater than $10^{-2.2}$ atm (atmospheric P_{CO_2} is $10^{-3.5}$ atm) (Finch & Ewing, 1992).

5.6.2 Thermodynamics and uranium speciation

To model the processes outlined above the thermodynamic database used in the modelling code must have solubility products for the common uranium phases as well as equilibrium constants for :- a) all of the major ionic species common to groundwater and b) the relevant aqueous actinide complexes, for as mentioned, these aqueous actinide species can increase solubility and promote mobilisation and transport. The general thermodynamic database for the version of GWB used in this study was based on an early release of EQ3/6 (Delany & Lundeen, 1990; Wolery, 1992a; Wolery, 1992b). However the thermodynamic data for uranium used in the modelling reported here were, unless otherwise stated, sourced from the recent Nuclear Energy Agency (NEA) assessment (Grenthe *et al.*, 1992). Whilst appreciating that ionic strength, I (a measure of the number of electrical charges in solution, see Chapter 4 for full definition), can affect the speciation and precipitation of uranium (Lemire, 1988; Lemire & Garisto, 1992) all log Ks are quoted relevant to the standard state of $I = 0$, $T = 298.25$ K and $P = 1$ atm.

5.6.3 Uranyl species (U^{6+})

Early studies in uranium solution equilibria indicated that in natural groundwaters the uranyl-phosphate complex would dominate over the range 4<pH<8 (Langmuir, 1978). This is now not believed to be the case unless there are very high concentrations of phosphoric acid (Grenthe *et al.*, 1992). For this reason the aqueous uranium-phosphorous species were not included in this study.

5.6.3.1 Hydroxide species

Although there is some debate over the equilibrium constants, the NEA review (Grenthe *et al.*, 1992) indicates that for the range 4.5<pH<10 the main species at high UO_2^{2+} concentration are $(UO_2)_3(OH)_5^+$, $(UO_2)_4(OH)_7^+$ and $(UO_2)_3(OH)_7^-$ (Fig. 5.8a) with log K's of -15.55, -21.90 and -31.00, respectively. For lower UO_2^{2+} concentrations the speciation is controlled by UO_2^{2+}, $UO_2(OH)_{2(aq)}$ and $UO_2(OH)_{3(aq)}^-$ with log K's of -9.04, -10.3 and -19.20, respectively. There is some disagreement regarding the temperature dependence of the hydrolysis of UO_2^{2+} (Fuger, 1992) but equilibrium constants for temperatures up to 250°C (Plyasunov & Grenthe, 1994) were added to the GWB thermodynamic database. Fig. 5.8b shows the distribution in the speciation of uranium versus pH with a UO_2^{2+} concentration of $1x10^{-5}$ M (moles per litre). As can be seen the species $UO_2(OH)_{2(aq)}$ and $UO_2(OH)_{3(aq)}^-$ dominate over a wide range in pH. With increasing concentrations of UO_2^{2+}(above $1x10^{-3}$ M), (Fig. 5.8a) the distribution would favour $(UO_2)_3(OH)_5^+$, $(UO_2)_4(OH)_7^+$ and $(UO_2)_3(OH)_7^-$.

5.6.3.2 Carbonate and hydroxide-carbonate species

The three main uranyl-carbonate complexes $UO_2CO_{3(aq)}$, $UO_2(CO_3)_2^{2-}$ and $UO_2(CO_3)_3^{4-}$ are well characterised (Fuger, 1992), and have log K's of 9.68, 16.94 and 21.6, respectively. The hydroxycarbonate species $(UO_2)_2CO_3(OH)_3^-$ is also important and has a log K of 19.01 (Grenthe *et al.*, 1992). Fig. 5.9a and Fig. 5.9b show the distribution of uranium species for the system $UO_2^{2+} - CO_3^{2-} - OH^-$. It is interesting to note the relative effects varying the CO_3^{2-} concentration from $2x10^{-3}$M in Fig. 5.9a to $1.5x10^{-4}$ M in Fig. 5.9b has on the distribution of uranium species, i.e. the $UO_2^{2+} - OH^-$ species becomes more dominant at higher pH as CO_3^{2-} concentration is lowered. The implications of this effect will be discussed later in the results section, (5.9)

5.6.3.3 Sulphate species

Although of less importance than the hydroxide, carbonate and hydroxycarbonate species, the sulphur complexes UO_2SO_4 and $UO_2(SO_4)_2^{2-}$ (log Ks of 3.15 and 4.14, respectively) also play a minor role in solubility studies (Grenthe & Lagerman, 1993).

5.6.4 Uranous species (U^{4+})

The solubility of U^{4+} oxide, either as stoichiometric, crystalline UO_2 or a more amorphous material ("amorphous" or "hydrous oxide" or "hydroxide") has been studied extensively and the log K's display a very wide scatter (Fuger, 1993; Rai *et*

al., 1990). The difficulty in properly identifying the starting material is compounded by the ease by which U^{4+} oxidises to U^{6+} and becomes more soluble; leading to erroneously high equilibrium solubility values. It is generally agreed that $U(OH)_4$ is the most important species encountered in alkaline media in equilibrium with UO_2 (whether crystalline, "amorphous" or "hydrated") (Fuger, 1993). The disagreement lies in the equilibrium constant assigned to it. In their 1990 paper , Rai *et al.* dealt with the solubility of $UO_2 \cdot xH_2O$(am) (am = amorphous) and provided a log K of -12. Results from their paper have been used as a basis for other modelling studies of uranium solubility at Sellafield (Baston *et al.*, 1993; Cross *et al.*, 1995).

The NEA review gives log K as -4.7 and notes that the results of the Rai study imply a ΔG^{o} $U(OH)_4$ that is approximately 40 kJ mol^{-1} more positive than the NEA value and very low equilibrium uranium concentrations of 10^{-14} M in non-complexing aqueous solutions with 4<pH<12 over crystalline UO_2 (Grenthe, 1991). Table 5.1 shows the log K's for uranous species used throughout this study; note that an "intermediate" value of log K $U(OH)_4$ = -8.53 is given in the GWB thermodynamic database. Previously believed to be the dominant species above pH 12 (Langmuir, 1978), it is now felt that there is little evidence for the formation of $U(OH)_5^-$ (Parks, Stanford University, pers. comm.; Wolery, Lawrence Livermore National Laboratory, pers comm.; Fuger, 1992; Fuger, 1993; Grenthe *et al.*, 1992). The equilibrium constants for the U^{4+} hydrolysis species are generally regarded to be very little affected by temperature (Grenthe, 1991; Grenthe *et al.*, 1992).

5.6.4.1 Comment on thermodynamic database used in study

All of the species' log K's from the thermodynamic database used in this study are listed in Table 5.1 including their errors (corresponding to the 95% confidence limit). It is important to note that log K's for some uranyl species were not used, e.g. $UO_2(OH)_{2(aq)}$, $UO_2(OH)_{3(aq)}^-$ and $(UO_2)_3(OH)_4^{2+}$ as they were not included in the GWB thermodynamic database. The relevance of their omission or inclusion will be discussed later (Section 5.9.5).

5.6.5 Stability fields of solid phases

Knowing which phase would be most thermodynamically stable in the repository setting is essential in determining the solubility (or concentration) of uranium in aqueous solution. For example the concentration of uranium in solution if uraninite is the solubility controlling stable phase would be several orders of magnitude lower than if Schoepite was the dominant phase. As shown in section 5.6.3 distribution

diagrams are a useful way of illustrating species variation with respect to uranium concentration and pH. Another type of figure that is useful is the redox potential vs. pH diagram (either shown as pe/pH or Eh/pH).

The significance of a solutions' redox state on uranium solubility is depicted in Fig. 5.10a and Fig. 5.10b. Fig. 5.10a shows the predominance of uranium speciation in the UO_2^{2+} / U^{4+} hydroxide system. As mentioned above pe is another way of expressing the redox state of a solution. Although Eh is the most common way of dealing with redox reactions, the advantage of using pe in modelling studies is that it simplifies the algebra of redox reactions to become similar to other mass action expressions (see Chapter 4).

At reducing pe $U(OH)_{4(aq)}$ is the dominant species and, therefore, the solubility of uranium would be very low. If solid phases are included at the low pe, uraninite is the dominant stable phase and the solubility of uranium very low. Whereas at oxidising pe, uranium concentration can be as much as 10^{-5} M and still exist in solution before schoepite becomes the dominant stable phase at pH < 9.2. If carbonate is included in the system the speciation is not dominated by uranyl hydroxide species but uranyl carbonate and polymeric uranyl hydroxycarbonate species (Fig. 5.11 a, b). Comparison of Fig. 5.11b with Fig. 5.10b shows the stabilising effect of carbonate on the solution species of uranium due to the formation of stable aqueous complexes (Grenthe *et al.*, 1992).

5.7 Method

5.7.1 Outline of speciation and reaction path code

Geochemical speciation and reaction path codes have a long history of use in a wide variety of geological problems (Nuclear Energy Agency, 1993; Plummer *et al.*, 1983; Wolery, 1992b). The many Radioactive Waste Management bodies investigating the possibility of subterranean disposal (UK NIREX, US DOE, Swedish SKB, Swiss NAGRA, etc.) have been driving forces in code development and elicitation of relevant chemical data e.g. thermodynamic solubility products of radionuclide solid phases and species (Grenthe *et al.*, 1992).

They are also responsible for verification and testing of the thermodynamic databases (Baston *et al.*, 1993) and modelling codes by comparison between separate codes (Bruno *et al.*, 1993) with laboratory experiments (Valsami-Jones & Ragnarsdottir, 1995) and so-called Natural Analogue studies (Bruno *et al.*, 1990; Nordstrom *et al.*, 1990).

5.7.2 The Geochemist's Workbench™

In this study, the computer code Geochemist's Workbench™ (GWB) has been used to simulate both speciation and reaction path geochemical reactions. GWB is a collection of interactive software tools for manipulating chemical reactions (**Rxn**) calculating stability diagrams with regard to Eh/pH (**Act2**) and activity/temperature (**Tact**). The **React** program is the code used to determine equilibrium states of natural waters and trace reaction processes. An outline of the fundamentals of thermodynamics utilised by GWB is provided in Chapter 4. Greater details on GWB are provided in the users guide for the code (Bethke, 1994) and texts utilising the program (Bethke, 1996).

5.7.3 Structure of the model

Any geochemical system can be described by a set of chemical components; these are the basic "ingredients" required to define the composition of the overall system as well as the individual species that make up the system. Often termed the master species (Parkhurst *et al.*, 1980a) these *basis species* are used by GWB to construct reactions for the 617 minerals and 551 secondary species in the thermodynamic database (Bethke, 1994).

If the system is not adequately described by the original basis, secondary species appropriate to a system can be *swapped* in and their concentrations set. Eh, temperature and pH can also be set at this stage (Bethke, 1994). This swapping continues during the course of a reaction path if, for example, a mineral dissolves: the software must alter the basis to match the new mineral assemblage before continuing. GWB utilises transformation matrixes to perform basis swaps and the corresponding alteration of equilibrium constants (Bethke, 1996).

A set of governing equations can be derived to describe a system, incorporating the independent reactions between species, minerals and gases and evolving mass action equations for the corresponding reaction. Mass balance equations then have to be derived for each chemical component of the system. By substituting the mass action equations into the mass balance equations a set of governing equations can be derived, one for each chemical component. These non-linear equations can be solved directly for the system's equilibrium state by use of Newton Raphson iteration (Bethke, 1996).

5.8 Experimental technique

Since it is accepted by the author that there has been much work done in modelling the *mineral* equilibrium (as opposed to *redox*-equilibrium) state of the natural

groundwaters of the BVG (Bond *et al.*, 1995; Bond & Tweed, 1995; Metcalfe & Crawford, 1994), this study is not primarily concerned with reproducing such results; the main purpose is to present results of modelling uranium solubility in the far and near field of the repository.

When simulating the solubility of uranium in the conditions within, near, and far from a repository it is essential that a robust understanding of the in-situ geochemical conditions be established. Fig. 5.12 illustrates the physical stages that need to be simulated and understood, essentially;

1) The natural in-situ groundwaters;
2) the interaction of the groundwaters with cement backfill;
3) the interaction of the high pH repository fluids with the steel barrels;
4) the simulation of the solubility of uranium in all three of the above stages.

Each of the above stages was modelled using in-situ analyses from Discrete Extraction Tests (DETs) 7, 8, 9 and 10 from Borehole 2. Since the Eh of the natural groundwater is important to the repository geochemistry, all of the above stages and DETs were modelled with the four methods of determining Eh outlined in section 5.4.4, i.e.;

- Case *a* Bulk Eh as measured in situ, Fe^{2+} / Fe^{3+} and SO_4^{2-} / HS^- decoupled

For the following cases all redox species are coupled;

- Case *b* Eh as measured in situ;
- Case *c* Eh as measured in situ, fluid in equilibrium with hematite;
- Case *d* Eh controlled by equilibrium with hematite and pyrite; reducing conditions promoted.

5.8.1 In-situ groundwater (Stage 1 on Fig. 5.12)

The analyses of natural water in borehole 2 used to model uranium solubility (Stage 1 on Fig. 5.12) were altered to include only the important and relevant ions as this greatly simplifies the output. The following ions were not included; Al^{+++}, Ba^{++}, Br^-, I^-, F^-, NO_3^-, NO_2^- and HPO_4^-, (Table 5.4). As outlined in the previous sections none of these ions are important complexing agents for uranium at the pH in the far or near field and are of little importance as regards redox. The most important information remains; the Eh, pH and concentration of HCO_3^-, SO_4^{--}, HS^- and ferric/ferrous iron. Geochemical simulations were performed on the DET samples 7, 8, 9 and 10 for the four methods of calculating Eh denoted by case names *a, b, c, d.*

5.8.2 Groundwater plus backfill (Stage 2 on Fig. 5.12)

As outlined in section 5.3.1 the near field environment would be dominated by the high pH conditions promoted by the planned dissolution of cement containers, engineered cavern structures and the hydrated, blended, Portland cement backfill (Stage 2 on Fig. 5.12) (Bennet *et al.*, 1992). Section 5.3.1 also illustrated that the phases in this backfill (known as Nirex Reference Vault Backfill or NRVB) are poorly crystalline and in the $CaO-SiO_2-H_2O$ (CSH) system (Atkinson *et al.*, 1993). These CSH phases are commonly represented as portlandite ($Ca(OH)_2$) and the "Berner" solid phase CaH_2SiO_4 (see section 5.3.1).

Modelling of the dissolution of portlandite and CaH_2SiO_4 by BVG groundwaters (Bond *et al.*, 1995; Bond & Tweed, 1995) has shown that essentially all the magnesium is precipitated as brucite ($Mg(OH)_2$) and all the carbonate is precipitated as calcite ($CaCO_3$), thus it is acceptable to use a simplified representation of NRVB consisting of portlandite with the precipitation of brucite and calcite included. Such an approach has been used in other studies (Goldberg *et al.*, 1995). Simulations of the equilibration of groundwaters with simplified NRVB was performed on the DET samples 7, 8, 9 and 10 for the four methods of calculating Eh denoted by case names *a, b, c* and *d*. Simulations were performed over a range in temperatures.

5.8.3 Groundwater plus steel (Stage 3 on Fig. 512)

Section 5.4.2 indicated that the interaction of groundwater with the large amount of iron present in the repository (Stage 3 on Fig. 5.12) will cause a release of hydrogen gas and a large reduction of the redox potential (theoretically to as low as - 780 mV). Modelling of this process was performed by reacting to equilibrium the portlandite/calcite/brucite equilibrated groundwaters with native iron, according to the equation

$$Fe \leftrightarrow Fe^{2+} + 2e^- \qquad 5.5$$

which, under the promoted reducing conditions will follow equation 5.3;

$$3Fe(OH)_2 \rightarrow Fe_3O_4 + 2H_2O + H_2\uparrow \qquad 5.3$$

and release hydrogen gas. Simulations of the equilibration of NRVB-equilibrated water with native iron was performed on the DET samples 7, 8, 9 and 10 for the four methods of calculating Eh. As these simulations will have markedly different Eh from those of simply equilibrating with NRVB they are denoted by case names *a'*, *b'*, *c'* and *d'*. The simulations were performed over a range in temperatures.

5.8.4 Groundwater plus uranium (Stage 4 on Fig. 5.12)

In the near-field, the main source of uranium (Stage 4 on Fig. 5.12) is from spent fuel and depleted uranium which is expected to be in the form of uranium metal, oxides and hydroxides (Goldberg *et al.*, 1995; Nirex, 1992a; Nirex, 1992b; Nirex, 1992c). U^{6+} solid phases are likely to be present from aerobic oxidation of pre-encapsulated waste, together with the presence of U^{6+} in depleted uranium materials. From experimental studies (Baston *et al.*, 1993; Cross *et al.*, 1995) this solid phase is believed to be possibly $UO_2(OH)_2(c,\beta)$, where c = crystalline and β indicates the particular crystalline structure. The U^{4+} oxide is likely to be formed from the oxidation of uranium metal on contact with the near field groundwater. Previous laboratory studies (Buchan *et al.*, 1990) have indicated that this early precipitated oxide is expected to be poorly crystalline and have the formula $UO_2(am)$, where am = amorphous.

5.8.4.1 General technique of determining uranium solubility

When a solution is in equilibrium, i.e. saturated, with a uranium solid phase, then the solubility of that phase (i.e. the concentration of uranium in the solution saturated with the phase) can be calculated from the mass action equation (see Chapter 4). The GWB code can be used to determine the solubility by *swapping* the solid phase into the basis species (see Section 5.7.1) and setting a *free* mass of the solid phase (Bethke, 1994). The fluid is then in equilibrium with this solubility controlling solid phase and the uranium concentration can be calculated.

Two approaches were used to model the solubility and speciation of uranium in the repository; the "near field" and the "pseudo near field". Both of these approaches utilise the above "swap and set" technique. The difference between them is that in the "near field" approach simulations were performed using the solid phases that were derived from published laboratory experiments. These solid phases are *forced* to be the solubility limiting solid phases in the repository fluids regardless of the geochemistry of these fluids. This was termed method one. In the "pseudo near field" approach the most likely solubility controlling solid phases that might exist have to be determined from the fluid geochemistry before uranium solubility calculations can be performed. This was termed method two.

5.8.4.2 The "near-field" : Method one

As mentioned previously, the near field environment represents the engineered pH and Eh conditions of the repository. In the context of this chapter, the "near-field" represents both the physical repository environment and the method that may be used to simulate the solubility of uranium. This method builds upon the assumption

outlined above that we know the mineral form uranium would have in the portlandite-equilibrated high pH conditions of the repository.

Laboratory experiments performed elsewhere (Baston *et al.*, 1993; Cross *et al.*, 1995) have indicated that U^{4+} and U^{6+} might exist as $UO_2(am)$ and $UO_2(OH)_2(c,\beta)$, respectively. These minerals can be "forced" to be the solubility controlling stable phases in GWB by swapping them for the basis species U^{4+} and UO_2^{2+} respectively and, following the method outlined in section 5.8.4.1, setting a free mass of each phase. This effectively maintains a constant "supply" of the mineral phase to the fluid. This method has been used in studies of uranium solubility undertaken elsewhere (Baston *et al.*, 1993; Goldberg *et al.*, 1995).

5.8.4.3 The "pseudo near field"" : Method two

The term "pseudo-near-field" relates to a technique used in this study to determine uranium solubility. It is not meant to represent an actual physical environment. It represents the evolution of the repository environment; where uranium would be in solution prior to the formation of solubility controlling solid phases. Therefore it is not automatically assumed that uranium would definitely exist as $UO_2(am)$ and $UO_2(OH)_2(c,\beta)$. This method enables the determination of the solubility controlling solid phases that may be most likely to form in the high pH repository conditions.

For this method the solid phases were determined by the equilibrium state of the ambient fluids. By gradually increasing uranium concentration in repeated runs, the saturation indices of solids which may potentially precipitate can be used to determine the solubility limiting phases (i.e. most thermodynamically stable), (see Chapter 4 for explanation of saturation indices). This method has been used in similar studies of uranium solubility in natural analogues (Bruno *et al.*, 1990) and repository groundwaters (Tyrer *et al.*, 1995).

Uranium solubility calculations can then be performed by swapping the solid phases in GWB for the uranium basis species and, following the method outlined in section 5.8.4.1, setting a free mass of each phase. This effectively maintains a constant "supply" of the mineral phase to the fluid. Simulations were performed over a wide range of Eh and temperatures to determine the likely concentration and speciation of uranium associated with the chosen solid phase. This method is also meant as a check, to ensure that the solubility controlling solid phases assumed in method one are suitable for the Eh, pH and temperature conditions of the repository.

5.8.4.4 Simulations performed

For both the "near" and "pseudo-near" fields, simulations were performed using the groundwater samples modelled previously. Uranium solubility was determined for the DET samples 7, 8, 9 and 10, equilibrated with simplified NRVB, again using the four methods of calculating Eh denoted by case names *a, b, c* and *d*. Simulations were performed over a range in temperatures;

- without the effects of steel dissolution (cases *a, b, c* and *d*);
- with the effects of steel dissolution (cases *a'*, *b'*, *c'* and *d'*).

By varying the temperature and Eh of the simulations the aqueous speciation and concentration of uranium was calculated as a function of these controlling parameters.

Method two was also used to calculate the concentration and speciation of uranium in the far-field, i.e. the naturally occurring groundwater conditions for DET 7, 8, 9 and 10 for the four equilibrium states (cases *a, b, c* and *d*).

5.9 Results

5.9.1 Modelling natural groundwater equilibrium without uranium

Before simulating the solubility of uranium in the repository conditions it is essential that a good understanding of the in-situ groundwater geochemistry be established. Therefore simulations were undertaken on the groundwater samples from DET 7, 8 9 and 10 from borehole 2. As detailed in section 5.8 there has been a large body of work undertaken to determine that the groundwaters in the BVG in the repository zone are in equilibrium with the volumetrically abundant *major* minerals in the matrix and fractured BVG outlined in section 5.4.2, and that there are many uncertainties in estimating the in-situ pH and Eh (Metcalfe & Crawford, 1994; Nirex, 1995c). Hematite and calcite, commonly found as fracture lining minerals, have a large influence on the Eh and pH of the fluid in equilibrium with them.

All the DET measured water samples and outcomes of all cases modelled in this study were oversaturated with respect to hematite. This suggests that the groundwaters would precipitate this mineral if complete equilibrium were attained. The deeper samples modelled (DET 7 & 8) were oversaturated with respect to calcite whereas DET 9 & 10 are undersaturated with respect to calcite. The deeper DET samples have an apparently increased pH, perhaps due to degassing of CO_2 (Bond & Tweed, 1995). Calcite is a very important fracture lining mineral at these depths and is reasonably reactive. Consequently other modelling studies have

assumed that all the DET samples are in equilibrium with this carbonate mineral (Bond *et al.*, 1995; Bond & Tweed, 1995; Metcalfe & Crawford, 1994). In the GWB study detailed here using this $CO_{2(g)}$/calcite equilibrium affects the pH. The pH of DET 7 and DET 8 falls, and the pH of DET 9 and DET 10 increases (Tables 5.4 and 5.5).

5.9.1.1 The natural groundwater (Stage 1 on Fig. 5.12)

For DETs 7, 8 , 9 and 10 when Eh is set to the in-situ measured value, with no correction for any iron or mud reaction effects, and redox disequilibrium permitted (case *a* on Fig. 5.12), the Fe^{3+}/Fe^{2+} iron couple predicts a Nernst Eh of between + 130 mV and + 399 mV (Table 5.5). This is much lower than that predicted for the iron couple in other modelling studies (+ 782 mV for DET 8 (Nirex, 1995c) therefore contamination with Fe^{3+} from the drill string may not be as prevalent as purported.

The Nernst Eh from the sulphur couple modelled alone was calculated to be between - 261 mV and - 136 mV (Table 5.5), these values are broadly similar to those found in other studies (Nirex, 1995c). However the concentration of HS^- in DET 8, 9 and 10 is at, or below, the detection limits (0.1 mg/l) of the analytical technique employed by the field team measuring elemental concentrations (Nirex, 1992d). Therefore extreme caution should be attached to using the Eh calculated from the sulphur couple as a robust basis for decisions concerning groundwater Eh The bulk Eh was + 66 mV (Table 5.5). This is as measured in situ and is considered to be the most probable natural condition.

The Nernst Ehs vary over a large range of values, therefore it would be inappropriate to constrain Eh of the fluid by selecting a single Eh value. However in a bid to scope out the relative effects on further models of uranium solubility such an experiment was performed. There is abundant hematite lining fractures that allow water flow. Therefore simulations were performed where Fe concentration was controlled by equilibrium with hematite, (case *b* on Fig. 5.12).

The Eh of the fluids was calculated at between + 46 mV and + 90 mV, (Table 5.5). To scope the effect of pyrite equilibrium with groundwaters the fluids were equilibrated with both pyrite and hematite (case *c* on Fig. 5.12). The Eh of the fluids was calculated at between - 240 mV and - 104 mV, (Table 5.5) which is very similar to the sulphur couple range determined elsewhere (Metcalfe & Crawford, 1994).

The observed lack of pyrite in fractures (found by analyses of borehole core (Nirex, 1995b)) at the depths relevant to the repository has already been mentioned. However in the current study it was thought to be relevant to model a wide range of scenarios. Since pyrite is a reduced mineral its formation is explicitly linked to the presence of reduced sulphur (HS^-) in the groundwaters. The simulations performed assume that HS^- is actually present in the water samples. As mentioned HS^- was measured in the DET porewaters to be at, or less than detection limits.

If these measurements are spurious pyrite precipitation can truly only be simulated by assuming that pyrite is a common mineral in equilibrium with the fluid. However if the HS^- concentrations were used in the redox disequilibrium simulations (case *a* on Fig. 5.12) pyrite was a mineral predicted to precipitate. Therefore these redox disequilibrium case *a* models simulate the situation where hematite is the dominant iron mineral in equilibrium with the groundwaters, but pyrite precipitation *could* occur without dominating the redox state of the fluid (Sato, 1992).

5.9.1.2 Equilibrium with cement (Stage 2 on Fig. 5.12)

When the groundwaters are equilibrated with portlandite, calcite and brucite (to simulate the reaction with NRVB) the pH increases in all the DET samples to as much as 12.7 (Table 5.6). This is due to the reaction with portlandite. For simulations where the Eh is determined by methods denoted by *a*, *b*, *c* and *d* (see Fig. 5.12) the Eh remains at the original constrained value: nothing is being altered to cause the bulk Eh to change.

The fluid composition after equilibration with portlandite was dominated by the fall in carbonate and magnesium concentrations (buffered by calcite and brucite, respectively) and the increase in pH due to equilibration with portlandite. As can be seen in Table 5.6 the pH of the fluid was related to temperature (derived from the geothermal gradient), with the lowest pH of 11.7 in the deepest sample, DET 7. The pH drop with increasing temperature resulted from the negative enthalpy (ΔH) of the pH-buffering reaction;

$$Ca(OH)_{2(s)} + 2H^+ \leftrightarrow Ca^{2+} + 2H_2O \qquad 5.6$$

Increasing the temperature in this exothermic reaction favoured the formation of the reactants, thus producing H^+ ions and reducing the pH. This temperature dependence was reinforced when the thermal pulse from heat generated by the radioactive waste was taken into account. When temperature is increased to 80°C the pH falls to around 11.0 (Table 5.6). As mentioned previously, when the

portlandite equilibrated groundwaters are reacted with steel in the form of native iron, the release of hydrogen gas corresponds with a large reduction in the Eh. For all these steel equilibrated cases *a'*, *b' c'* and *d'* the Eh of the fluid universally falls to less than - 500 mV.

5.9.2 Modelling uranium solubility : the "near field"

As outlined in section 5.8.4.1 the "near field" environment is that where the uranium solid phases are "known" to be $UO_2(am)$ and $UO_2(OH)_2(c,\beta)$. This was modelled using method 1, that is, the solutions are "forced" to be in equilibrium with these uranium solubility controlling solid phases. This resulted in high concentrations of $10^{-3.5}$, $10^{-3.2}$, $10^{-2.8}$ and $10^{-2.7}$ moles of uranium in the portlandite-equilibrated fluids DET 7, 8, 9 and 10, respectively (Fig. 5.13 and Table 5.7). Uranium exists almost exclusively as the U^{6+} anionic species $(UO_2)_3(OH)_7^-$ with a very minor contribution by the U^{4+} species $U(OH)_4$ (Table 5.7).

These high calculated concentrations were fixed regardless of the equilibrium state of the original groundwater sample (cases *a, b, c* and *d*) or interactions with steel (cases *a', b', c'* and *d'*). These values are around two orders of magnitude higher than those of similar uranium solubility studies (Baston *et al.*, 1993; Cross *et al.*, 1995; Goldberg *et al.*, 1995).

5.9.2.1 Temperature effects

As mentioned in section 5.9.1.1, in general, the four DET fluid analyses are broadly geochemically similar; the main difference being the temperature of the fluid sample, and thus the pH. This temperature/pH relationship was further heightened when the fluid temperatures were increased to 80°C to simulate heat generation by the radioactive waste; in all DET samples the pH fell to around 10.7 (Table 5.7). The aqueous speciation was dominated by the equilibrium between $UO_2(OH)_2(c,\beta)$ and $(UO_2)_3(OH)_7^-$. Inspection of the equilibrium constants for the reaction,

$$3UO_2(OH)_2(c,\beta) + H_2O \leftrightarrow (UO_2)_3(OH)_7^- + H^+ \qquad 5.7$$

suggests that an increase in temperature could cause a slight increase in uranium solubility but the opposite occurred; uranium concentration fell to around 10^{-4} M for all DETs and redox cases (Table 5.7 and Fig. 5.14). The reason for this decrease in concentration relates directly to Portlandite dissolution as shown in equation 5.6. Equation 5.6 showed that as temperature increases the pH of the solution in equilibrium with portlandite would fall.

This pH fall would result in an increase in the concentration of H^+ ions in solution. This would have a direct effect on the equilibrium state of the uranium mineral $UO_2(OH)_2(c,\beta)$. From the mass action equation derived from equation 5.7 the following relationship can be derived.

$$a_{(UO_2)_3(OH)_7^-} \cdot a_{H^+} = K_{eq} \qquad 5.8$$

where

$a_{UO_2(OH)_2(c,\beta)}$ and a_{H_2O} (both = unity)

To remain at equilibrium an increase in the activity of H^+ will cause a decrease in the activity of $(UO_2)_3(OH)_7^-$, and hence its concentration. Therefore the solubility of $UO_2(OH)_2(c,\beta)$ decreased with increasing temperature.

As mentioned in section 5.6.3.2 the uranyl carbonate species $UO_2(CO_3)_2^{2-}$ and $UO_2(CO_3)_3^{4-}$ and uranyl-hydroxy-carbonate species $(UO_2)_2CO_3(OH)_3^-$ are common to the Eh / pH / uranium concentrations that are dealt with in this paper. However, as mentioned above, for simulations of the high pH repository fluids, HCO_3^- concentration was controlled by equilibrium with calcite and, as a result, was too low for these species to predominate. This is clearly illustrated in Fig. 5.9b.

The U^{4+} species also contributed to the uranium concentration. The equilibrium between the U^{4+} solid phase $UO_2(am)$ and species $U(OH)_4$ proceeded according to the reaction;

$$UO_2(am) + 2H_2O \leftrightarrow U(OH)_4 \qquad 5.9$$

regardless of pH change. Temperature increase caused an increase in the concentration of $U(OH)_4$ and thus the solubility of uranium, but this increase was masked by the fall in U^{6+} concentration.

5.9.3 Modelling uranium solubility : the "pseudo near field"

As outlined in section 5.8.4.1, the term "pseudo-near-field" relates to the technique that is used to determine uranium solubility. This enables the most likely solid phase forming in the high pH repository conditions to be determined. The uranium solubility controlling solid phase was determined using method two, that is, the uranium concentration was increased until the saturation indices indicated the suitable uranium solubility limiting phase was reached (see Chapter 4 for explanation of saturation indices). The following results indicate that the solubility of uranium in the "pseudo-near-field" was affected strongly by the temperature and equilibrium state of the groundwater. In addition, the reducing condition produced

by steel equilibration was found to play a major role in the choice of the uranium solubility limiting solid phase and the subsequent calculations of aqueous speciation.

5.9.3.1 Solubility limiting solid phases

As mentioned in section 5.6.1 $UO_2(OH)_2(c,\beta)$ is unstable with respect to the solid phase schoepite at around 53°C. Therefore when method two was used in non-reducing conditions up to 53°C, schoepite was chosen as the solubility limiting stable phase. $UO_2(OH)_2(c,\beta)$ was chosen for temperatures above 53°C. In reducing conditions the fully crystalline form of UO_2 (uraninite) was chosen as the solubility limiting phase. Whether kinetic barriers would allow such a crystalline phase to form will not be discussed here, thermodynamically this was the solid phase predicted from the saturation indexes of the analyses used.

5.9.3.2 Effects of groundwater redox and sample used

For the in-situ temperatures, simulations were performed on all DET samples for the Eh methods denoted by cases *a, b* and *c* (see Fig. 5.12). These simulations resulted in approximately the same concentration of uranium as the near field simulations. For DET samples 7, 8, 9 and 10 at in-situ temperatures, the uranium concentration was calculated at $10^{-3.5}$, $10^{-3.1}$, $10^{-2.7}$, $10^{-2.7}$ M, respectively (Fig. 5.15, Table 5.8), again there was a trend associated with temperature (Fig. 5.15, Table 5.8) with the shallowest sample (DET 10) having the higher uranium concentration. $(UO_2)_3(OH)_7^-$ again dominates the speciation (Table 5.8) with the equilibrium reaction between this species and schoepite given by;

$$\underset{schoepite}{UO_2(OH)_2 \cdot H_2O} \leftrightarrow H^+ + 2H_2O + (UO_2)_3(OH)_7^- \qquad 5.10$$

For the simulation where redox is determined from equilibrium with pyrite and hematite (case *d* on Fig. 5.12) the reducing conditions (Table 5.5) suggested that uraninite be selected as the uranium solubility limiting solid phase. This produced a much lower concentration of uranium of around 10^{-13} M (Fig. 5.15, Table 5.8). Simulations of high pH fluids interacted with steel (cases *a'*, *b' c'* and *d'* on Fig. 5.12) also produced reducing conditions (Table 5.6). Uraninite was selected as the stable phase and uranium concentration calculated at 10^{-13} M (Fig. 5.15, Table 5.8). In all these simulations of high pH reducing conditions the uranium speciation was dominated by $U(OH)_4$ (Fig. 5.15, Table 5.8). As in the case of UO_2(am) the equilibrium reaction between uraninite and $U(OH)_4$;

$$\underset{uraninite}{UO_2} + 2H_2O \leftrightarrow U(OH)_4 \qquad 5.11$$

was unaffected by temperature induced pH change. The $U(OH)_4$ concentration was approximately 10^{-13} M for all cases and DETs. The reducing Eh (Table 5.5) of case *d* was a direct result of the equilibrium with pyrite and hematite, in the other four cases interactions with steel caused the low Eh (Table 5.6).

5.9.3.3 Effect of temperature

As in the near field case the concentration of U^{6+} species fell with the decrease in pH associated with a temperature increase. For cases *a*, *b* and *c* in DET samples 7, 8, 9 and 10 the uranium concentration decreased from $10^{-3.5}$, $10^{-3.1}$, $10^{-2.7}$, $10^{-2.7}$ M, respectively to approximately 10^{-4} M (Fig. 5.16, Table 5.8). For cases *d*, *a'*, *b'*, *c'* and *d'* the uranium concentration only rises to a maximum of approximately 10^{-12} M.

5.9.3.4 Effects of other solid phases

It has been shown that the "near-field" environment was generally unaffected by Eh and temperature; uranium concentration remaining relatively high (approximately 10^{-3} M). The "pseudo-near field" environment appeared to more sensitive to the redox state of both the natural groundwater and that induced by interactions with steel. Work published by Goldberg *et al.* (1995) suggested that any iron in the in-situ groundwater would precipitate out as amorphous oxides in the high pH repository conditions and that manganese from both the groundwater and steel would also form solid phases.

To scope this effect the solid phases $Fe(OH)_3$ and hausmannite, (Mn_3O_4) were used at non-reducing conditions. Under reducing conditions $Fe(OH)_3$ and the amorphous phase $Mn(OH)_2$(am) were used (this phase being more stable under reducing conditions). Surprisingly inclusion of these mineral phases had no effect on the equilibrium state of the portlandite equilibrated groundwaters or on the calculated uranium concentrations (which were identical to those reported in Table 5.8).

5.9.3.5 Effects of steel

To illustrate the importance of the steel-induced low Eh conditions to the "pseudo near-field", each DET was allowed to increase its Eh to a maximum of + 400 mV (thus ensuring that fully oxidising conditions are reached) with the pH highly alkaline. Method two was used to select the likely uranium solubility controlling stable phase. As can be seen in Fig. 5.17, uraninite was the likely stable phase at very reducing Eh. Beyond an Eh of - 300 mV for all the DET samples the concentration of uranium in solution began to increase, with U_4O_9(c) (where c = crystalline) the dominant stable phase.

This increase steadily continued until $U_3O_8(c,\alpha)$ (c = crystalline and α indicates the particular crystalline structure) became the dominant stable phase for all DETs at approximately - 175 mV. The maximum uranium concentration of approximately 10^{-3} M was reached around - 110 mV when schoepite became the stable phase. Thus the low Eh effect of steel has a critical effect on uranium solubility; once steel is consumed the solubility increased from approximately 10^{-13} M to around 10^{-3} M.

5.9.4 Modelling uranium solubility ; the far field

As can be seen from section 5.9.3.5 above, it is only the steel barrels which limit uranium solubility. This effect will cease if steel is oxidised by ambient groundwater. This oxidation of steel and eventual increase in Eh would obviously be prevented if the far-field groundwaters were as reducing as the "near" and "pseudo-near field". There would be no "gradient" between the reducing and oxidising conditions of the far field and near fields. However it appears that the equilibrium state of the natural groundwater, as outlined in sections 5.4 and 5.9.1 is oxidising. Therefore it is likely that, over time, the steel buffer will be consumed and uranium concentration in the near field will increase to 10^{-3} M.

5.9.4.1 Uranium in the far field

To determine if the far-field groundwater conditions would be effective at keeping uranium concentrations low in solution, the concentration of uranium in the far field was calculated for the in-situ pHs, Ehs and temperature of each DET without the effects of the cement or steel barriers. Method two was used to determine the likely solubility controlling solid phase of uranium (see Fig. 5.12 and section 5.8.4.3). As can be seen in Fig. 5.18, the choice of stable phase used was dependent upon the Eh of the groundwater solution. For the relatively oxidising cases *a*, *b* and *c* (Fig. 5.12 and Table 5.5) $U_4O_9(c)$was the stable phase selected, but for the reducing pyrite/hematite equilibrated case *d*, (Fig. 5.12 and Table 5.5) uraninite was the stable phase.

As can be seen in Fig. 5.18 for the field pH models the uranium concentration was between 10^{-9} and $10^{-3.4}$ M for the $U_4O_9(c)$equilibrated cases (*a*, *b* and *c*) and approximately 10^{-12} M for the uraninite equilibrated case *d*. pH measured in the field increased with depth (apart from DET 8 having a higher pH than DET 7) (Tables 5.2 and 5.4). When using the field pH in the simulations this increase caused an increase in uranium concentrations in solution; according to the equations;

$$U_4O_9(c) + 12HCO_3^- \leftrightarrow 10H^+ + H_2O + 4UO_2(CO_3)_3^{4-} + 4e^- \quad 5.12$$

$$U_4O_9(c) + 8HCO_3^- \leftrightarrow 6H^+ + H_2O + 4UO_2(CO_3)_2^{2-} + 6e^- \quad 5.13$$

In equations 5.12 and 5.13 $U_4O_9(c)$ dissociates to give $UO_2(CO_3)_3^{4-}$ and $4UO_2(CO_3)_2^{2-}$, respectively. The hydrogen ion is on the same side of the equation as the dissolved species (as in equation 5.7). Therefore, the higher the pH the lower the H^+ ion concentration and, from the mass action equation, the concentration of uranyl-carbonate would be higher. Therefore the lowest pH in DET 10 resulted in the lowest uranium concentration of approximately 10^{-9} M.

As mentioned previously, the natural groundwaters in the BVG are in contact with an enormous quantity of the reactive mineral calcite, so identical models were run with this mineral in equilibrium with the groundwaters. The results indicated that the increase in pH with increase in depth is not apparent when the groundwaters are in equilibrium with calcite; the pH decreased with depth (apart from, again, DET 8 being now lower than DET 7).

However, although DET 10 has the highest pH, it does not automatically have the highest uranium concentration. This was due to a lower concentration of the carbonate ligand in the in-situ sample (Tables 5.2 and 5.4). This resulted, from the mass action equation, in decreasing the uranyl-carbonate in solution which subsequently lowered the uranium concentration. The uranium concentration remains relatively constant at approximately 10^{-6} M, around three orders of magnitude less than the near field values. It is important to note that the maximum uranium concentration ($10^{-5.4}$ M) was calculated for the DET 9 groundwater sample. This water sample was taken from the depth of the potential repository and thus the water that would contact the repository would provide the greatest "far field" uranium concentrations.

5.9.4.2 Effects of fracture-lining minerals

The efficacy of the fracture lining minerals, calcite, hematite and illite in reducing uranium concentration were also investigated. These minerals were found to have no effect on the concentration of uranium in the far field of any of the DET samples regardless of the method of determining Eh or the method of modelling uranium solubility. Similar results were obtained for "near field" and "pseudo near field" simulations. In common with section 5.9.3, it was though to be unnecessary to include such non-results in tables or figures. The only mineral that had ANY effect on the uranium concentration in solution was pyrite; lowering the Eh and causing a reduction in uranium concentration. The presence of pyrite in the BVG is conjectural and so open to debate. Pyrite only occurs in the deepest sampled fractures, it would therefore seem unlikely that uranium would be geochemically

retained by such fractures as uranium saturated water will flow upwards from the proposed repository (see Chapter 3).

5.9.5 Effects of database variation

It has been mentioned previously that the uranium solid phase and species equilibrium constants are, with the exception of $U(OH)_4$, all sourced from the 1992 Nuclear Energy Agency (NEA) review of uranium chemical thermodynamics (Grenthe *et al*, 1992). In order to assess the importance of variations in thermodynamic data, uranium solubility calculations were performed using log K's from other databases.

5.9.5.1 Uranyl species

The thermodynamic database used with the Geochemist's Workbench™ (GWB) (Bethke, 1994) does not include uranium species that might play an important role in the problems modelled in this paper, i.e. $UO_2(OH)_{2(aq)}$, $UO_2(OH)_3^-$ and $UO_2(OH)_4^{2-}$. GWB also uses a lower log K value for $U(OH)_4$; -8.53 (Bethke, 1994) (Table 5.1) compared to the -4.7 value published elsewhere (Grenthe, *et al.*, 1992). To determine the significance of these omissions and variations, simulations were performed with $UO_2(OH)_{2(aq)}$, $UO_2(OH)_3^-$ and $UO_2(OH)_4^{2-}$ included at their NEA values of -10.3, -19.2 and -33, respectively.

Using DET 9 case *a* (where redox disequilibrium was permitted, see Fig. 5.12), the high pH, cement-equilibrated fluids were simulated without and with the effects of steel (cases a and a' on Fig. 5.12). Using method two to determine the likely uranium solubility solid phase schoepite was selected as the stable phase for case *a* and uraninite for case *a'*.

For DET 9 case *a*, as can be seen in Fig. 5.19a, the uranium in solution at high pH is divided between the anionic uranyl hydroxide species $(UO_2)_3(OH)_7^-$, $UO_2(OH)_4^{2-}$ and $UO_2(OH)_3^-$, with the latter species dominating. The uranium concentration in solution is significantly increased to $10^{-1.4}$ M. Thus variations in thermodynamic data could significantly affect the solubility of uranium in solution.

5.9.5.2 Other uranium solubility studies

Experimental studies have been undertaken elsewhere to determine the likely solid uranium phases in the high pH repository fluids (Baston *et al.*, 1993; Cross *et al.*, 1995; Goldberg *et al.*, 1995). These studies have also attempted to simulate the uranium solubility via geochemical speciation codes.

1 Baston *et al.*, (1993) determined from laboratory experiments that the most likely stable phases of U^{6+} and U^{4+} in a mixture of cement and distilled water, would be $UO_2(OH)_2(c,\beta)$ and $UO_2(am)$, respectively. Using method one (see Fig. 5.12) they calculated the solubility of these solid phases in a solution of pH 13 with both reducing and oxidising Eh conditions. Baston modified the thermodynamic database to provide a better fit of theoretical data with laboratory data; $UO_2(OH)_3^-$ was removed and the log K's of $(UO_2)_3(OH)_7^-$, and $UO_2(OH)_4^{2-}$ were adjusted. Using these new, adjusted log K's Baston calculated the uranium solubility in high pH repository fluids to be $10^{-4.5}$ M.

2 The study by Cross *et al.* (1995) is effectively an expanded version of the Baston study. Cross performed simulations on a wide variety of radionuclides. Simulations were undertaken to determine the solubility of uranium in solutions where cement was equilibrated with samples of actual groundwater to produce solutions with pH 12.39 and Eh between -400 mV and -100 mV. The Cross study also incorporated the above modifications to the thermodynamic database. $UO_2(OH)_2(c,\beta)$ and $UO_2(am)$ were again chosen as the stable phases. Using method one (see Fig. 5.12) the uranium solubility was calculated to be $10^{-5.1}$ M.

3 Goldberg *et al.*(1995) details the results of simulations of the solubility of a wide number of radionuclides in repository fluids of pH 12.43 and Eh -400 mV. Using the altered database mentioned above, and $UO_2(OH)_2(c,\beta)$ and $UO_2(am)$ as the stable phases they calculated uranium solubility to be $10^{-4.9}$ M.

Given the variations in pH between studies, and that pH is an important factor in the calculation of uranium solubility (see section 5.9.2.1), the calculated uranium solubilities detailed above are all very similar. They are similar to the $10^{-5.5}$ M value of uranium solubility used in UK Nirex Ltd. safety case assessments (Nirex, 1995d). The uranium solubility used in the UK Nirex Ltd database is approximately 600 times less than the uranium solubility calculated for the near field in section 5.9.2.

The above three UK Nirex Ltd. sponsored solubility studies illustrate the importance of the thermodynamic data (i.e. log K's) used to determine uranium solubility. If certain species are ignored or their log K's altered, then this can cause the calculated uranium concentration to be lowered. Conversely if species such as $(UO_2)_3(OH)_7^-$ were assigned log K's derived from internationally approved thermodynamic data then the calculated uranium concentration may have been higher in the above three UK Nirex Ltd. sponsored studies.

5.9.5.3 Significance of variations in log K

The equilibrium constants in the database used in this study (Table 5.1) have, in general, errors of ± 5 %. The equilibrium constants (section 5.9.5.2) for the major anionic polymeric uranyl hydroxide complexes used in the other studies, (Baston *et al.*, 1993; Cross *et al.*, 1995; Goldberg *et al.*, 1995), fall within the 95 % confidence limits of the NEA values, i.e. they are not significantly different. Thus a small variation in the log K's of the most important uranyl species could cause a significant variation in the calculation of uranium solubility. Such variations in uranium concentration due to log K variation are very common in modelling studies yet are often not included in safety assessments papers relating to risk from radioactive waste repositories (Goldberg *et al.*, 1995).

5.9.5.4 Uranous species

To determine the effects variations in uranous log K's might have on uranium solubility, simulations were performed with varying log K's of $U(OH)_4$ and $U(OH)_5^-$ (although as discussed in section 5.6.4, there is little evidence for the formation of $U(OH)_5^-$ at high pH conditions). The high pH, cement-equilibrated DET 9 sample, with redox disequilibrium permitted and steel interactions included (case a' on Fig. 5.12), was used. Using method two (see Fig. 5.12) uraninite was selected as the uranium solubility controlling solid phase. The uranium in solution was calculated to have a maximum concentration of $10^{-8.1}$ M, with the more soluble $U(OH)_5^-$ as the dominant species (Fig. 5.19b). This is higher than that calculated in section 5.9.3.5. The log K used for $U(OH)_5^-$ was -16.5 (Grenthe, *et al.*, 1992) according to the equation

$$U^{4+} + 5H_2O \leftrightarrow U(OH)_5^- + 5H^+ \qquad 5.14$$

If this species is suppressed (as was the case in previous sections), in keeping with the arguments offered in section 5.6.4, then $U(OH)_4$ becomes the dominant species. If the various values of log K's used in recent publications are used; -12 (Rai *et al.*, 1990), -8.53 (Bethke, 1994) and the NEA log K of -4.53 (Grenthe, *et al.*, 1992) the concentration of $U(OH)_4$ is found to vary widely (Fig. 5.19b) with the NEA log K giving the highest uranium concentration of $10^{-8.1}$ M.

5.9.6 Discussion of results

Since DET 9 is from 650 mbOD it is reasonable to propose that it is the best approximation of the in-situ groundwater geochemistry around the potential repository. This being the case, Fig. 5.20 summarise the most probable geochemical

scenarios for the main stages of modelling, both of the natural groundwater conditions and those of the high pH near field.

As discussed in the previous sections, there is more than one way to calculate Eh. The Eh calculated from the sulphate/sulphide couple was reducing, ~-200 mV. This is a similar value to that calculated from equilibrium with pyrite. Since the quantity of in-situ sulphide measured was probably spurious, and there was no pyrite found in fractures at the depth of the repository, such a reducing Eh would be unlikely. The Eh calculated from the ratio of the ferric/ferrous species was ~+300 mV which is very oxidising. UK Nirex Ltd. also used the ferric/ferrous couple to derive Eh. They rejected such high Eh values, maintaining that degradation (in effect, oxidation) of the steel drill pipe would lead to artificially high values of Eh.

This is disingenuous as the retention of radioactivity within the repository relies upon the fact that the steel barrels will degrade to produce highly reducing conditions. Surely, if the steel pipe had any effect it would be to lower the Eh of the natural groundwater ? If this were the case, this might explain why the Eh of the in-situ BVG groundwaters was +66 mV. Thus, in order to encompass such wide ranges in Eh, the most probable natural groundwater condition is that shown as *A* on Fig. 5.20, i.e. redox disequilibrium permitted, T = 23°C, pH 7.2 and Eh = +66 mV, (slightly oxidising and falling between the iron and sulphur Eh).

When DET 9 was equilibrated with portlandite, calcite and brucite the most likely scenario was for the resultant 23°C fluid to have pH of 12.7 and, since redox disequilibrium was still likely the Eh was +66 mV (*B*) on Fig. 5.20. When this fluid was equilibrated with steel barrels (*C* on Fig. 5.20) the most likely scenario was for the bulk Eh to fall to -700 mV. The uranium minerals $UO_2(OH)_2(c,\beta)$ and $UO_2(am)$ produced a uranium concentration of $10^{-3.8}$ M, at 80°C.

The likely uranium minerals found in the repository can also be derived by thermodynamic stability (*D* on Fig. 5.20; derived by simulating the likelihood of mineral precipitation). When steel-induced reducing conditions are prevalent, the most probable uranium mineral, uraninite, produced a very low uranium concentration of 10^{-12} M at 80°C. When the steel barrels are consumed this concentration could be much higher, 10^{-4} M, at 80°C.

Using fluids sampled at the depth of the potential repository (DET 9) the uranium solubility calculated for the near field was as high as $10^{-2.7}$ M (at 23°C). Using the same sample to model the "far field" environment the uranium solubility was

calculated as $10^{-5.4}$ M. Thus the uranium concentration in the repository is around 500 times greater than that of the natural BVG groundwater. Such a difference would greatly enhance the diffusion gradient between the repository near field and the waters surrounding it and might cause earlier uranium release to the BVG groundwaters.

All of the above results show that the uranium concentration in a potential repository simulated using a state-of-the-art geochemical speciation/reaction path code are, in general, two orders of magnitude higher than those derived by UK Nirex Ltd.. Such high values of uranium solubility have implications for the safety of a potential repository at Sellafield.

5.10 Summary, conclusions and implications

5.10.1 Summary

A review of the solid phases and speciation of uranium at low temperatures indicated that this element can exist in many valency states but that the tetravalent and hexavalent states are most common in the near-surface. The hexavalent state is commonly complexed with free ligands, becoming more soluble and more easily transported in moving groundwater. Thermodynamic information relevant to uranium speciation, complexation and solid phase formation was presented to illustrate the importance of thermodynamic data to modelling studies performed as part of nuclear waste repository safety case assessments.

The proposed repository concept at Sellafield was outlined; the maintenance of high pH, (hydroxide buffered) and low Eh (iron buffered) ambient groundwater conditions are intended to act as a near field barrier to uranium release to the geosphere. The natural groundwater setting at Sellafield was briefly reviewed and the rapid and upward flow of water through the PRZ identified. Evidence for possible equilibrium between fracture lining minerals in the BVG and the groundwaters were outlined.

The lack of any geochemically reduced iron minerals in the fractures and the abundance of oxidised iron minerals probably indicates that the natural groundwaters are oxidising and would favour the transport but not retention of a redox sensitive element such as uranium. Eh is difficult to measure in situ with confidence, yet is a critical parameter controlling the solubility. It is possible to use a redox disequilibrium approach to model the natural groundwater conditions at Sellafield. Real measurements of discrete extraction test (DET) water samples from Sellafield borehole 2 from a range of depths in the Borrowdale Volcanic Group

(BVG) host rock were modelled using the speciation/reaction path geochemical modelling code The Geochemist's Workbench™.

A redox disequilibrium approach was used to delineate the possible range in predicted Nernst Eh derived from the measured species concentrations of single redox couples (Table 5.5). This found that the Eh could be similar to that measured in-situ, i.e. between +46 and +92 mV. Therefore simulation case *a*, with Eh +66 mV was preferred for the far field simulations. Simulating the equilibrium between the natural groundwaters and carbonate minerals in veins resulted in pH variation with depth coincident with that measured in situ.

Nirex repository vault backfill cement (NRVB) can be represented as portlandite, calcite and brucite. The modelling of the interactions between these mineral phases and in-situ groundwater compositions was performed to determine the likely water compositions of high pH near-field groundwaters. GWB was utilised to determine the likely composition of the near-field water for a range of depths and temperatures likely in repository heated to 80°C by waste. The pH of all DET samples increased to as much as 12.7. The *bulk* Eh of the redox decoupled samples (i.e. simulation case *a*) remained at its input value (all DETs < 92 mV), but samples that were forced to be in equilibrium with pyrite had Eh values of approximately -500 mV. Simulation case *a* is again the preferred result, Eh = +66 mV. Further modelling of the interactions of high pH waters with native iron illustrated that this interaction controls the release of hydrogen gas and that the hydrogen produces a very negative Eh of -700 mV in the fluids for all case modelled.

Modelling was performed to determine the concentration of uranium in the repository "near field", i.e. when the uranium solid phases, $UO_2(OH)_2(c,\beta)$ and $UO_2(am)$ and forced to be in equilibrium with the high pH repository fluids. The above, predicted hydroxide and amorphous oxide phases resulted in uranium concentrations of between $10^{-3.5}$ and $10^{-2.7}$ M, with the speciation dominated by the polymeric anionic uranyl hydroxide species $(UO_2)_3(OH)_7^-$. These concentrations were around two orders of magnitude higher than previous modelling studies undertaken by UK Nirex Ltd.. These high values of uranium solubility were relatively constant over the range in sample depths studied but were decreased by increases in temperature, i.e., $10^{-2.8}$ M at 23°C to $10^{-3.9}$ M at 80°C. This was due to an enforced change in the concentration of the hydrogen ion in solution. Surprisingly the highly reducing conditions produced by the interaction of repository fluids with steel caused no discernible lowering of the uranium concentration in solution.

Modelling was performed for the "pseudo near field", i.e., when the solid phases controlling solubility were deduced by simulating precipitation. The variation in the methods used to determine the natural groundwater redox caused a variation in the predicted stable phase, speciation and solubility. For the measured in-situ Eh (the preferred model) the solubility controlling stable phase was predicted to be Schoepite, a hydrated uranyl hydroxide mineral ($UO_2(OH)_2 \cdot H_2O$). When this was used as the stable phase the uranium solubility ranged from $10^{-3.5}$ to $10^{-2.7}$ M; a similar range to that determined for the "near field" when equilibrium with the expected solid phase was enforced. A similar trend of reduced solubility with temperature increase was produced; $10^{-2.7}$ M at 23°C to $10^{-4.1}$ M at 80°C.

Further modelling of the "pseudo near field" investigated the reducing groundwater conditions produced by reaction of high pH cement-equilibrated waters with iron (representing steel). The highly reducing conditions produced (< -500 mV) resulted in the use of a uranous solid (Uraninite; UO_2) as the solubility controlling uranium solid phase. The speciation was wholly dominated by a uranous hydroxide complex ($U(OH)_4$) producing a uranium concentration of ~10^{-13} M at 23°C with a minor increase in solubility to ~10^{-12} M as the temperature was increased to 80°C. The inclusion of manganese and iron solid phases had no effect on the outcome of the models.

Similar uranium concentrations of ~10^{-13} to ~10^{-12} M were calculated for simulations where repository cement minerals were reacted with groundwaters that were in equilibrium with pyrite. As pyrite was not a common fracture lining mineral and would not dominate the Eh of natural groundwaters, this scenario was considered to be unlikely. The removal of the reducing effects of the steel were modelled in simulations where Eh was allowed to increase to 400 mV. The maximum solubility of uranium (10^{-3} M) was reached when pH was alkaline (~12) and Eh still relatively reducing (~-100 mV).

Modelling the solubility of uranium "far-field" natural groundwaters showed that the method used to determine the Eh of the groundwaters has a direct control on the stable phase used to determine the solubility and speciation of uranium. When Eh was controlled by equilibrium with very infrequently occurring reduced iron minerals, (not likely), the uranium concentration was very low (10^{-12} M).

For all other cases when the Eh was that measured in-situ, (most probable) or when controlled by equilibrium with oxidised iron minerals, or when redox disequilibrium was permitted, or when the abundant mineral calcite was in equilibrium with the

waters, the uranium concentration in solution was approximately 10^{-6} M (Fig. 5.18). Fracture lining minerals within the BVG (other than pyrite) have no effect on the concentration of uranium in solution.

The thermodynamic data used to model uranium speciation vary considerably between databases. For the uranyl species, inclusion of monomeric anionic uranyl hydroxide species in this study resulted in very high concentrations of uranium in solution ($10^{-1.4}$ M). Uranium solubility studies undertaken elsewhere (Baston *et al.*, 1993; Cross *et al.*, 1995; Goldberg *et al.*, 1995) used a modified thermodynamic database to provide a better fit to laboratory experiments.

Values of "near field" uranium solubility of $10^{-5.5}$ M have been used by UK Nirex Ltd. in safety case assessment studies. This uranium concentration is similar to those calculated in the study presented here for the "far field", but is around 600 times less than those calculated for the "near field".

Variations in the GWB thermodynamic data for uranous species caused both an increase and a decrease in the calculated uranium solubility (10^{-15} M to $10^{-8.1}$ M). It would be useful if safety case assessment studies included comments relating to the variability of thermodynamic data for the uranium species and phases.

5.10.2 Conclusions

- A robust attempt was made to determine the redox state of the naturally occurring groundwater in the BVG at the proposed repository site, and to determine the solubility and speciation of uranium in the near field, pseudo near field and far field.

- Simulations of natural BVG groundwater accord with measured Eh (~+66 mV) suggesting redox disequilibrium, not controlled by pyrite. Contamination of natural fluids by steel drill pipe appears to have only a minor effect.

- BVG groundwater interacting with NRVB cement does not affect Eh but produces pH 10 at 80°C.

- Simulations of the repository near field setting show that, regardless of which method was used to determine the groundwater redox, when the uranium solid phases are prescribed, i.e. waste/porewater equilibrium is enforced, the uranium concentration in solution is as high as $10^{-2.7}$ M. This is appreciably higher than other studies performed by UK Nirex contractors on the same site, with the same

data and with similar computer codes, $10^{-4.5}$ M (Baston *et al.*, 1993), $10^{-5.1}$ M (Cross *et al.*, 1995), $10^{-4.9}$ M (Goldberg *et al.*, 1995).

- The modelling in this study was performed using the NEA international standard database (Grenthe *et al.*, 1992). By contrast UK Nirex Ltd. used their own corporate values based on a limited suite of laboratory experiments (Baston *et al.*, 1993). Small variations in the Log K's of the most important uranyl species produced significant increases in uranium solubility in the pseudo near field close to the steel barrels. Uranium solubility was calculated at 10^{-15} M using Nirex data and $10^{-8.1}$ M when NEA data used. This sensitivity to variations in equilibrium constants should be taken into account when using uranium solubilities in further studies relating to safety case assessment.

- Simulations of the "pseudo near field" showed equilibrium of repository fluids with steel promoted highly reducing conditions, and suggested a uranous solubility controlling solid phase with a low solubility (10^{-13} M). If these iron effects were not included then the uranium solubility was found to be significantly higher ($10^{-2.7}$ M). Thus the durability through time of the steel barrels buffer is critical. One report has estimated this to be 10,000 years (Naish *et al.*, 1995).

- The Naish *et al* (1995) UK Nirex Ltd. report assumed that no oxygen would be present in the repository system. If the natural BVG groundwater is oxidising (as hypothesised in the study presented here) anaerobic conditions would not be maintained and the durability of the steel containers would be greatly lessened. Uranium would also be retained in the near field if the oxidation state of the natural groundwater was reducing. This could occur if the groundwater was in equilibrium with reduced iron minerals, or Eh was controlled by a natural sulphur redox couple, as shown by the simulations of natural Eh. The presence of both the reduced iron minerals and reduced sulphur species claimed by Nirex are spurious. Thus the 10,000 yr duration of reducing Eh is likely to be a very considerable overestimate.

- In the far field environment the most likely stable uranium phase was predicted to be a mixed valence, more oxidised form of uranium dioxide (U_4O_9). Commonly termed pitchblende, this mineral is common to the natural environment. Uranium solubility was calculated to be relatively high (maximum of $10^{-5.4}$ M), regardless of interactions with natural minerals, observed in core to line fractures in the BVG.

- In simple terms, if the uranium solid phases are prescribed (i.e., if equilibrium is enforced), the uranium solubility is 10^{-3} M. Taking a very conservative view, if the uranium solid phases are unknown, then uranium solubility could be as low as 10^{-13} M. This would be controlled by the geochemical buffering from the slow oxidation of the steel barrels enclosing the waste. The natural groundwater is relatively oxidising (+46 < Eh +92 mV) so the natural tendency will be for the steel barrels to be oxidised. Studies published by UK Nirex Ltd. estimate that the steel barrels would be consumed after 10, 000 years. Given the oxidising nature of the natural groundwater this is likely to be a considerable overestimate. After this, the concentration of uranium in the high pH fluids emanating from the repository would be 10^{-3} M. This is some 600 times higher than the uranium solubility value used by UK Nirex Ltd. when calculating their safety case (Nirex, 1995d).

Acknowledgements

Chris McKeown was funded by the Greenpeace Environmental Trust. The GWB code was hired from the University of Illinois. UK Nirex Ltd. are thanked for providing data. The authors wish to thank Allan Hall, University of Glasgow; Gordon Macleod, University of Newcastle; Craig Bethke and Amy Berger, University of Illinois; Ian Ridley, United States Geological Survey and Randy Cygan, Sandia National Laboratories for their advice and comments during this research project.

5.11 References

Atkinson, A. (1995) *Buffering of pH in an inhomogenous repository.* Report No. **NSS/R287**, UK Nirex Ltd., Harwell, UK.

Atkinson, A., Everitt, N.M. & Guppy, R. (1988a) *Evolution of pH in a radwaste repository: experimental simulations of cement leaching.* Report No. **DoE/RW/89-025 Part 1**, Department of Environment, London, UK.

Atkinson, A., Everitt, N.M. & Guppy, R. (1988b) *Evolution of pH in a radwaste repository: internal reactions between concrete constituents.* Report No. **DoE/RW/89-025 Part 2**, Department of Environment, London, UK.

Atkinson, A. & Guppy, R.M. (1988) *Evolution of pH in a radwaste repository: leaching of modified cements and reactions in groundwater.* Report No. **DoE/RW/89-025 Part 3**, Department of Environment, London, UK.

Atkinson, A., Hearne, A.J. & Knights, C.F. (1987) *Aqueous chemistry and thermodynamic modelling of CaO-SiO_2-H_2O gels.* Report No. **AERE-R12548**, AEA Technology, Harwell.

Atkinson, A., Hearne, J.A. & Knights, C.F. (1991) *Aqueous geochemistry and thermodynamic modelling of CaO-SiO_2-H_2O gels.* Report No. **AEA-D&R-0153**, AEA Technology, Harwell.

Atkinson, A., Williams, S.J. & Wisbey, S.J. (1993) *NSARP reference document : the near field : January 1992.* Report No. **NSS/G117**, UK Nirex Ltd., Harwell, UK.

Basham, I.R. & Kemp, S.J. (1993) *A review of natural uranium and thorium minerals.* Report No. **DOE/HMIP/RR/94/007**, Her Majesty's Inspectorate of Pollution, London, UK.

Baston, G.M.N., Brownsword, M., Cross, J.E., Hobley, J., Moreton, A.D., Smith-Briggs, J.L & Thomason, H.P. (1993) *The solubility of uranium in cementitous near-field chemical conditions.* Report No. **NSS/R222**, UK Nirex Ltd., Harwell, UK.

Beddoe-Stephens, B. & Phillips, E.R. (1993) *The petrology of the Borrowdale Volcanic Group within Sellafield borehole No. 2.* Report No. **CC92S/193/CF-1-A**, British Geological Survey, Keyworth, UK.

Bennet, D.G., Read, D., Atkins, M. & Glasser, F.P. (1992) A thermodynamic model for blended cements. II: Cement hydrate phases; thermodynamic models and modelling studies. *Journal of Nuclear Materials*, **190**, 315-325.

Berner, U. (1987) *Radionuclide speciation in the porewater of hydrated cement II.* Report No. **EIR Report TM-45-87-10**, Swiss Federal Institute for Reactor Research, Wurenlinger, Switzerland.

Bethke, C.M. (1994) *The Geochemist's Workbench; a users guide to Rxn, Act2, Tact, React and Gtplot.* University of Illinois, Urbana-Champaign, USA, 213 pp.

Black, J.H. (1995) The hydrogeology of the Sellafield area, The geological disposal of radioactive waste, Royal Lancaster Hotel, London, IBC Technical Services Ltd, Gilmoora House, 57-61 Mortimer St., London.

Bond, K.A., Moreton, A.D. & Tweed, C.J. (1995) *Water compositions of relevance to a deep cement-based repository at Sellafield: evaluation using thermodynamic modelling.* Report No. **NSS/R310**, UK Nirex Ltd., Harwell, UK.

Bond, K.A. & Tweed, C.J. (1995) *Groundwater compositions for the Borrowdale Volcanic Group, Boreholes 2, 4 and RCF3 using thermodynamic modelling.* Report No. **NSS/R397**, UK Nirex Ltd., Harwell, UK.

Bruno, J., Casas, I., Lagerman, B. & Muñoz, M. (1987) The determination of the solubility of amorphous $UO_{2(s)}$ and the mononuclear hydrolysis constants of uranium (IV) at 25°C. *In:* Materials Research Society (eds) *Scientific basis for nuclear waste management X.* 84, Materials Research Society, Boston, Massachusetts, USA, 153-160.

Bruno, J., Crawford, M., Fabriol, R., Jamet, P., Lang, H., Read, D., Tweed, C. & Warwick, P. (1993) *Status review of CHEMVAL2 technical areas, June 1992.* Report No. **DoE/HMIP/RR/93.014**, Her Majesty's Inspectorate of Pollution, London, UK.

Bruno, J., Cross, J.E., Eikenberg, J., McKinley, I.G., Read, D., Sandino, A. & Sellin, P. (1990) *Testing of geochemical models in the Poço de Caldas analogue study.* Report No. **NTB 90-29**, Nagra, Wettingen, Switzerland.

Buchan, A.B., Ewart, F.T., Hobely, J., Ormerod, G.J., Smith-Briggs, J.L. & Thomason, H.P. (1990) *Solubility limiting solid phases of uranium.* Report No. **AEA D&R 0032**, Her Majesty's Inspectorate of Pollution, London, UK.

Cross, J.E. & Ewart, FT. (1990) *HATCHES - a thermodynamic database management system.* Report No. **NSS/R212**, UK Nirex Ltd., Harwell, UK.

Cross, J.E., Moreton, A.D. & Tweed, C.J. (1995) *Thermodynamic modelling of radioactive waste disposal: assessment of near-field solubility.* Report No. **NSS/R311**, UK Nirex Ltd., Harwell, UK.

Delany, J.M. & Lundeen, S.R. (1990) *The LLNL thermochemical database.* Report No. **UCRL-21658**, Lawrence Livermore National Laboratory, Livermore, California.

Drever, J.I. (1982) *The geochemistry of natural waters.* Prentice-Hall, Englewood Cliffs, N.J., 388 pp.

Finch, R.J. & Ewing, R.C. (1991) Alteration of natural UO_2 under oxidising conditions from Shinkolobwe, Katanga, Zaire: a natural analogue for the corrosion of spent fuel. *Radiochimica Acta*, **52/53**, 395-401.

Finch, R.J. & Ewing, R.C. (1992) The corrosion of uraninite under oxidising conditions. *Journal of Nuclear Materials*, **190**, 133-16.

Finch, R.J., Miller, M. & Ewing, R.C. (1992) Weathering of natural uranyl oxide hydrates: Schoepite polytypes and dehydration effects. *Radiochimica Acta*, **58/59**, 433-443.

Fuger, J. (1992) Thermodynamic properties of actinide aqueous species relevant to geochemical problems. *Radiochimica Acta*, **58/59**, 81-91.

Fuger, J. (1993) Problems in the thermodynamics of the actinides in relation with the back-end of the nuclear fuel cycle. *Journal of Nuclear Materials*, **201**, 3-14.

Goldberg, J.E., Gould, L.J., Heath, T.G., Thompson, A.M. & Tweed, C.J. (1995) *Development of a methodology for modelling the redox chemistry and predicting the redox potential of the near field of a cementitous radioactive waste repository.* Report No. **NSS/R398**, UK Nirex Ltd., Harwell, UK.

Grenthe, I. (1991) Thermodynamics in migration chemistry. *Radiochimica Acta*, **52/53**, 425-432.

Grenthe, I., Fuger, J., Lemire, R.J., Muller, A.B., Nguyen-Trung, C. & Wanner, H. (1992) *Chemical thermodynamics of Uranium.* Chemical thermodynamics, **1**, Elsevier, Amsterdam, The Netherlands, 715 pp.

Grenthe, I. & Lagerman, B. (1993) Ternary metal complexes 2. The U(VI) - SO_4^{2-} - OH^- system. *Radiochimica Acta*, **61**, 169-176.

Harvey, B.R. (1995) Speciation of radionuclides. *In:* Ure, A.M. & Davidson, C.M. (eds) *Chemical speciation in the environment.* Blackie Acadamic and professional, Glasgow, 276-306.

Haszeldine, R.S. (1996) Subsurface geology, geochemistry and water flow at a rock characterisation facility (RCF) at Longlands Farm. Proof of evidence. *In:* Haszeldine, R.S. & Smythe, D.K. (eds) *Radioactive Waste Disposal at Sellafield, UK. Site Selection, geological and engineering problems.* University of Glasgow, Glasgow, UK, 121-164.

Haszeldine, R.S. & McKeown, C. (1995) A model approach to radioactive waste disposal at Sellafield. *Terra Nova*, **7**, 1, 87-96.

Haworth, A. & Sharland, S.M. (1995) *The evolution of the Eh in the pore water of a radioactive waste repository.* Report No. **NSS/R308**, UK Nirex Ltd., Harwell, UK.

Hooper, A. (1995a) The Nirex repository concept, The geological disposal of radioactive waste, Royal Lancaster Hotel, London, IBC Technical Services Ltd, Gilmoora House, 57-61 Mortimer St., London.

Hooper, A. (1995b) *Supplementary proof of evidence. Repository performance.* RCF planning Enquiry, **PE/NRX/15/S1**, UK Nirex Ltd., Harwell, UK, Cleator Moor, Cumbria, 171 pp.

Janeczek, J. & Ewing, R.C. (1992) Structural formula of uraninite. *Journal of Nuclear Materials*, **190**, 128-132.

Langmuir, D. (1978) Uranium-solution mineral equilibria at low temperatures with applications to sedimentary ore deposits. *Geochimica et Cosmochimica Acta*, **42**, 547-569.

Lemire, R.J. (1988) *Effects of high ionic strength groundwaters on calculated equilibrium concentrations in the uranium-water system.* Report No. **AECL-9549**, Atomic Energy of Canada Ltd.

Lindberg, R.D. & Runnels, D.D. (1984) Groundwater redox reactions: an analysis of equlibrium state applied to Eh measurements and geochemical modelling. *Science*, **225**, 925-927.

Metcalfe, R. & Crawford, M.B. (1994) *Models of water/rock interactions in the Borrowdale Volcanic Group within the potential repository zone at Sellafield.* Report No. **WE/94/26C**, British Geological Survey, Keyworth, UK, Keyworth, UK.

Miller, W., Alexander, R., Chapman, N., McKinley, I. & Smellie, J. (1994) *Natural analogue studies in the geological disposal of radioactive wastes.* Report No. **NTB 93-03**, Nagra, Wettingen, Switzerland.

Millward, D. (1995) The geological environment of the Potential Repository Zone at Sellafield, Cumbria, The geological disposal of radioactive waste, Royal Lancaster Hotel, London, IBC Technical Services Ltd, Gilmoora House, 57-61 Mortimer St., London.

Morss, L.R. (1986) Thermodynamic Properties. *In:* Katz, J.J., Seaborg, G.T. & Morss, L.R. (eds) *The chemistry of the actinide elements.* **2**, Chapman & Hall, London, 1278-1360.

Naish, C.C., Balkwill, P.H., O'Brien, T.M., Taylor, K.J. & Marsh, G.P. (1990) *The anaerobic corrosion of carbon steel in concrete.* Report No. **NSS/R273**, UK Nirex Ltd., Harwell, UK.

Naish, C.C., Blackwood, D.J., Taylor, K.J. & Thomas, M.I. (1995) *The anaerobic corrosion of stainless steels in simulated repository backfill environments.* Report No. **NSS/R307**, UK Nirex Ltd., Harwell, UK.

Nash, J.T., Grainger, H.C. & Adams, S.S. (1981) Geology and concepts of genesis of important types of uranium deposit. *Economic Geology 75th Anniversary Volume*, 63-116.

Nirex. (1992a) *The 1991 UK radioactive waste inventory.* Report No. **284**, UK Nirex Ltd., Harwell, UK.

Nirex. (1992b) *The physical and chemical characteristics of UK radioactive wastes.* Report No. **286**, UK Nirex Ltd., Harwell, UK.

Nirex. (1992c) *The radionuclide content of UK radioactive wastes.* Report No. **285**, UK Nirex Ltd., Harwell, UK.

Nirex. (1992d) *Sellafield hydrogeology. Report of the hydrogeology joint interpretation team.* Report No. **268**, UK Nirex Ltd., Harwell, UK.

Nirex. (1993a) *The geology and hydrogeology of the Sellafield area: Interim assessment.* Report No. **524 (4 vols)**, UK Nirex Ltd., Harwell, UK.

Nirex. (1993b) *Scientific update 1993 : Nirex deep waste repository project.* Report No. **525**, UK Nirex Ltd., Harwell, UK.

Nirex. (1995a) *The 3D geology and hydrogeology of the RCF south shaft location, summary report.* Report No. **S/95/007**, UK Nirex Ltd., Harwell, UK.

Nirex. (1995b) *The flow zone characterisation of the RCF area : summary report.* Report No. **S/95/006**, UK Nirex Ltd., Harwell, UK.

Nirex. (1995c) *The hydrochemistry of Sellafield, 1995 update.* Report No. **S/95/008**, UK Nirex Ltd., Harwell, UK.

Nirex. (1995d) *Nirex 95: A Preliminary analysis of the groundwater pathway for a deep repository at Sellafield.* Report No. **S/95/012 (3vols)**, UK Nirex Ltd., Harwell, UK.

Nirex. (1995e) *Post-closure performance assessment, near-field evolution.* Report No. **S/95/009**, UK Nirex Ltd., Harwell, UK.

Nordstrom, D.K. & Munoz, J.L. (1986) *Geochemical thermodynamics*. Blackwell Scientific Publications, Oxford, 477 pp.

Nordstrom, D.K., Puigdomènech, I. & McNutt, R.H. (1990) *Geochemical modelling of water-rock interactions at the Osamu Utsumi mine and Morro do Ferro analogue sites, Poço de Caldas, Brazil.* Report No. **NTB 90-24**, Nagra, Wettingen, Switzerland.

Nuclear Energy Agency. (1989) *Safety assessment of radioactive waste repositories.* Organisation for Economic Co-operation and Development, Paris, France, 250 pp.

Nuclear Energy Agency. (1993) *The status of near-field modelling*. Organisation for Economic Co-operation and Development, Paris, France, 289 pp.

Oreskes, N., Shrader-Frechette, K. & Belitz, K. (1994) Verification, validation and confirmation of numerical models in the earth sciences. *Science*, **263**, 641-646.

Parkhurst, D.L., Thorstenson, D.C. & Plummer, LN. (1980a) *PHREEQE-a computer program for geochemical calculations.* Report No. **80-96**, U.S. Geological Survey, Reston, USA.

Parkhurst, D.L., Thorstenson, D.C. & Plummer, L.N. (1980b) *PHREEQE - a computer program for geochemical calculations.* Report No. **Report 80-96**, USGS Water-Resources Investigations.

Parks, G.A. & Pohl, D.C. (1988) Hydrothermal solubility of uraninite. *Geochimica et Cosmochimica Acta*, **52**, 863-875.

Pearson, F.J. & Berner, U. (1991) *Nagra thermochemical database I: Core data.* Report No. **NTB 91-17**, Nagra, Wettingen, Switzerland.

Pearson, F.J. & Scholtis, A. (1993) *Chemistry of reference waters of the crysalline basement of northern Switzerland for safety assessment studies.* Report No. **NTB 93-07**, Nagra, Wettingen, Switzerland.

Plummer, L.N., Parkhurst, D.L. & Thorstenson, D.C. (1983) The development of reaction models for groundwater systems. *Geochimica et Cosmochimica Acta*, **47**, 665-686.

Plyasunov, A.V. & Grenthe, I. (1994) The temperature dependence of stability constants for the formation of polynuclear cationic stability constants. *Geochimica et Cosmochimica Acta*, **58**, 17, 3561-3582.

Pringle, A. (1995) *Relationships between hydraulic and chemical characteristics of Sellafield groundwaters.* Report No. **95524360/208**, Golders Associates, Nottingham, UK.

Rai, D.R., Felmy, A.R. & Ryan, J.L. (1990) Uranium (IV) hydrolysis constants and solubility product of $UO_2 \cdot x\ H_2O$(am). *Inorganic Chemistry*, **29**, 260-264.

Sato, M. (1992) Persistency field Eh-pH diagrams for sulfides and their application to supergene oxidation and enrichment of sulfide ore bodies. *Geochimica et Cosmochimica Acta*, **56**, 3133-3156.

Torrero, M.E., Casas, I., de Pablo, J., Sandino, M.C.A. & Grambow, B. (1994) A comparison between unirradiated and Schoepite solubilities in 1 M NaCl medium. *Radiochimica Acta*, **66/67**, 29-35.

Tyrer, M., Bennet, D.G., Read, D. & Yunus, I. (1995) *Near field and chemical transport modelling.* Report No. **TR-Z2-9**, Her Majesty's Inspectorate of Pollution, London, UK.

Valsami-Jones, E. & Ragnarsdottir, K.V. (1995) Solubility of uranium oxide and calcium uranate in pure water and $Ca(OH)_2^-$ bearing solutions. *Geochimica et Cosmochimica Acta*, (submitted).

Weigel, F. (1986) Uranium. *In:* Katz, J.J., Seaborg, G.T. & Morss, L.R. (eds) *The chemistry of the actinide elements.* **1**, Chapman & Hall, London, 169-442.

Wolery, T.J. (1992a) *EQ3NR, a computer program for geochemical aqueous speciation-solubility calculations: theoretical manual, user's guide, and related documentation (Version 7.0).* Report No. **UCRL-MA-110662-PT-III**, Lawrence Livermore National Laboratory.

Wolery, T.J. (1992b) *EQ6, a computer program for reaction path modeling of aqueous geochemical systems: theoretical manual, user's guide, and related documentation (Version 7.0).* Report No. **UCRL-MA-110662-PT-IV**, Lawrence Livermore National Laboratory.

Wolery, T.J., Jackson, K.J., Bourcier, W.L., Bruton, C.J., Viani, E., Knauss, K. & Delany, J.M. (1988) Current status of the EQ3/6 software package for geochemical modeling. *In:* Melchior, D. & Bassett, R.L. (eds) *Cemical modeling of aqueous systems II.* American Chemical Society, Washington DC, USA, 104-116.

Species	log K (error)	Reaction
UO_2^{2+}	-9.04 ±0.04	$U^{4+} + 2H_2O \leftrightarrow UO_2^{2+} + 4H^+ + 2e^-$
		Hydrolyis reactions refer to ;
UO_2OH^+	-5.20 ±0.30	$m(UO_2^{2+}) + nH_2O_{(l)} \leftrightarrow (UO_2)_m(OH)_n^{2m-n} + nH^+$
$(UO_2)_2(OH)_2^{2+}$	-5.62 ±0.04	"
$(UO_2)_3(OH)_4^{2+}$	-11.90 ±0.30	"
$(UO_2)_3(OH)_5^+$	-15.55 ±0.12	"
$(UO_2)_3(OH)_7^-$	-31.00 ±2.00	"
$(UO_2)_4(OH)_7^+$	-21.90 ±1.00	"
		Complexation reactions refer to ;
UO_2CO_3	16.94 ±0.12	$m(UO_2^{2+}) + nL \leftrightarrow (UO_2)_m(L)_n^{2m-n}$ (L= Ligand)
$UO_2(CO_3)_2^{2-}$	16.94 ±0.12	"
$UO_2(CO_3)_3^{4-}$	21.60 ±0.05	"
UO_2SO_4	3.15 ±0.05	"
$UO_2(SO_4)_2^{2-}$	4.14 ±0.07	"
$(UO_2)_2CO_3(OH)_3^-$	19.01 ±0.50	$CO_2(g) + 4H_2O + 2UO_2^{2+} \leftrightarrow (UO_2)_2CO_3(OH)_3^- + 5H^+$
U^{4+}	9.04 ±0.04	$UO_2^{2+} + 4H^+ + 2e^- \leftrightarrow U^{4+} + 2H_2O$
$U(OH)_4$	-8.53	$U^{4+} + 4H_2O \leftrightarrow U(OH)_4 + 4H^+$

Solid Phase	LogK_{SP}	Reaction
Uraninite	+ 27.67	$UO_{2(cr)} + 2H^+ + \frac{1}{2}O_{2(g)} \leftrightarrow UO_2^{2+} + H_2O$
$UO_{2(am)}$	+ 0.11	$UO_{2(am)} + 4H^+ \leftrightarrow U^{4+} + 2H_2O$
$U_4O_{9(c)}$	- 45.69	$U_4O_{9(c)} + 16H^+ \leftrightarrow 8H_2O + \frac{1}{2}O_{2(g)} + 4U^{4+}$
$U_3O_{8(c,\alpha)}$	- 62.51	$U_3O_{8(c,\alpha)} + 12H^+ \leftrightarrow 6H_2O + O_{2(g)} + 3U^{4+}$
Schoepite	+ 4.85	$UO_2(OH)_2 \cdot H_2O + 2H^+ \leftrightarrow 3H_2O + UO_2^{2+}$
$UO_2(OH)_{2(c,\beta)}$	+ 4.95	$UO_2(OH)_{2(c,\beta)} + 2H^+ \leftrightarrow 2H_2O + UO_2^{2+}$

Table 5.1 **Equilibrium constants and solubility products for main uranium species and solid phases relevant to this study. Majority of values taken from latest Nuclear Energy Agency database (Grenthe *et al.*, 1992), see text for exceptions. In general errors are ± 5 %.**

Sample mbOD	DET 7 1522-1537	DET 8 946-961	DET 9 646-656	DET 10 478-488
T °C	45.00	32.00	23.00	21.00
pH (field)	7.14	7.85	6.52	6.25
Eh (V)	0.092	0.090	0.066	0.046
mg/l				
Na^+	9120.00	8530.00	7500.00	8000.00
K^+	187.00	151.00	95.80	102.00
Ca^{++}	1490.00	1080.00	484.00	685.00
Mg^{++}	136.00	150.00	62.00	82.30
Mn^{++}	1.88	1.31	0.91	0.86
Sr^{++}	32.50	25.7	11.60	15.4
Al^{+++}	0.02	0.01	0.02	0.02
Ba^{++}	0.29	0.13	0.24	0.14
Fe^{++}	2.30	2.10	2.10	2.00
Fe^{+++}	5.14	6.64	2.80	2.25
SiO_2^-	10.60	16.60	4.84	4.38
Cl^-	17400.00	15700.00	12600.00	13000.00
SO_4^{--}	1130.00	1210.00	962.00	1060.00
HS^-	<0.10	<0.10	0.16	0.13
Br^-	30.3	25.90	22.10	23.60
I^-	0.15	0.13	0.12	0.12
F^-	2.61	2.20	2.66	2.34
NO_3^-	0.22	0.24	2.52	0.20
NO_2^-	0.02	0.01	0.02	0.04
HPO_4^-	0.05	0.08	0.05	0.04
HCO_3^- alkalinity	68.10	204.00	197.00	85.9
TDS calculated	29600.00	27000.00	21900.00	23000.00

Table 5.2 **Geochemical data from Sellafield borehole 2 Discrete Extraction Tests (DETs). mbOD = metres below Ordnance Datum.**

Mineralising Episode		Principal associated minerals	Dominant type of mineralisation
ME1		K-feldspar/adularia ± quartz, ± chlorite, ± albite, ± hematite	Silicate
ME2		Quartz ± epidote, ± calcite, ± chlorite, ± apatite, ± K-feldspar, ± albite, ± sericite, ± hematite	Silicate (& carbonate)
ME3		Pyrite, ± traces of chalcopyrite, arsenopyrite, marcasite, galena, sphalerite, Bi-Se sulphosalts and quartz	Sulphide (& silicate ?)
ME4		Anhydrite, ± barite, ± fluorite, ± hematite, ± quartz, ± siderite (?), ± K-feldspar	Sulphate
ME5		Albite, ± K-feldspar, kaolinite, illite, ± hematite	Silicate
ME6	[a]	*Early ME6a* : ferroan/manganoan carbonate now replaced completely by specular hematite and calcite with abundant inclusions of Fe- and Mn-oxides. *Late ME6a* : calcite and hematite	Carbonate
	[b]	Dolomite, ferroan dolomite, ankerite, ± siderite, ± quartz, ± anhydrite, ± ferroan calcite	± sulphate
	[c]	Calcite (usually ferroan), ± barite, ± fluorite, ± hematite, ± pyrite, ± sphalerite, ± galena	± sulphide
ME7		Illitic clay and hematite	Silicate & oxide
ME8		Mn- and Fe-oxides/oxyhydroxides	Oxide
ME9		Calcite, ± pyrite, ± anhydrite, ± gypsum	Carbonate ± sulphate ± sulphide

Table 5.3 **Summary of the principal mineralisation episodes in the Sellafield Boreholes, (after Nirex, 1995b).**

Sample mbOD	DET 7 1522-1537	DET 8 946-961	DET 9 646-656	DET 10 478-488
T °C	45.00	32.00	23.00	21.00
pH(field)	7.14	7.85	6.52	6.25
pH(calcite)	6.90	6.78	7.20	7.40
Eh (V)	0.092	0.090	0.066	0.046
mg/l				
Na^+	9120.00	8530.00	7500.00	8000.00
K^+	187.00	151.00	95.80	102.00
Ca^{++}	1490.00	1080.00	484.00	685.00
Mg^{++}	136.00	150.00	62.00	82.30
Mn^{++}	1.88	1.31	0.91	0.86
Sr^{++}	32.50	25.7	11.60	15.4
Fe^{++}	2.30	2.10	2.10	2.00
Fe^{+++}	5.14	6.64	2.80	2.25
SiO_2^-	10.60	16.60	4.84	4.38
Cl^-	17400.00	15700.00	12600.00	13000.00
SO_4^{--}	1130.00	1210.00	962.00	1060.00
HS^-	<0.10	<0.10	0.16	0.13
HCO_3^- alkalinity	68.10	204.00	197.00	85.9
TDS calculated	28275.00	25556.00	21900.00	23000.00

Table 5.4 **Major element geochemical data excerpted from Sellafield borehole 2 discrete extraction tests (DETs) data shown in Table 5.2.**

DET	Case	T°C	pH		Eh (V)		Eh (Field pH) (redox couples)		Eh (Calcite pH) (redox couples)	
			Field	Calcite	Field	Calcite	Fe^{2+}/Fe^{3+}	SO_4^{2-}/HS^-	Fe^{2+}/Fe^{3+}	SO_4^{2-}/HS^-
7	a	45	7.14	6.90	+ 0.092	+ 0.092	+ 0.206	- 0.226	+ 0.250	- 0.209
	b		7.14	6.90	+ 0.092	+ 0.092	N/A	N/A	N/A	N/A
	c		7.14	6.90	+ 0.092	+ 0.092	N/A	N/A	N/A	N/A
	d		7.14	6.90	- 0.205	- 0.186	N/A	N/A	N/A	N/A
8	a	32	7.85	6.78	+ 0.090	+ 0.090	+ 0.131	- 0.261	+ 0.319	- 0.185
	b		7.85	6.78	+ 0.090	+ 0.090	N/A	N/A	N/A	N/A
	c		7.85	6.78	+ 0.090	+ 0.090	N/A	N/A	N/A	N/A
	d		7.85	6.78	- 0.240	- 0.158	N/A	N/A	N/A	N/A
9	a	23	6.52	7.20	+ 0.066	+ 0.066	+ 0.360	-0.159	+ 0.252	- 0.207
	b		6.52	7.20	+ 0.066	+ 0.066	N/A	N/A	N/A	N/A
	c		6.52	7.20	+ 0.066	+ 0.066	N/A	N/A	N/A	N/A
	d		6.52	7.20	- 0.127	- 0.178	N/A	N/A	N/A	N/A
10	a	21	6.25	7.40	+ 0.046	+ 0.046	+ 0.399	- 0.136	+ 0.217	- 0.219
	b		6.25	7.40	+ 0.046	+ 0.046	N/A	N/A	N/A	N/A
	c		6.25	7.40	+ 0.046	+ 0.046	N/A	N/A	N/A	N/A
	d		6.25	7.40	- 0.104	- 0.192	N/A	N/A	N/A	N/A

Table 5.5 **Table showing pH and Eh variation due to determining method used. pH value taken from field measurement or from equilibrating with calcite via GWB. Cases a, b, c and d relate to the equilibrium state of the fluid constrained in GWB;**

a Bulk Eh as measured in situ (+ 0.046 < Eh < + 0.090 V)
Redox species Fe^{3+} / Fe^{2+} and SO_4^{2-} / HS^- decoupled.
Fluid can precipitate hematite (Fe_2O_3) and pyrite (FeS_2)
Fe^{3+} / Fe^{2+} couple -> + 0.131 < Nernst Eh < + 0.399
SO_4^{2-} / HS^- -> - 0.261 < Nernst Eh < - 0.136

The Eh measured by electrode always fell between Nernst Eh calculated for iron and sulphur redox couples. Since the Nernst Eh values varied over a maximum range of more than 0.5 V the DET fluids are unlikely to be in redox equilibrium.

To scope the importance of the equilibrium state the in-situ groundwaters were run with the Eh constrained to that measured in situ with no redox disequilibrium permitted;

b Eh as measured in situ (+ 0.046 < Eh < + 0.090 V), all redox species coupled.

and with equilibrium enforced with the common fracture lining mineral, hematite (Fe_2O_3);

c Eh as measured in situ (+ 0.046 < Eh < + 0.090 V), enforced equilibrium with hematite all redox species coupled.

Equilibrium with hematite (Fe_2O_3) and pyrite (FeS_2) was enforced to simulate fluid in contact with both minerals, although pyrite is only found in trace amounts in fracture linings (see text);

d Eh reducing (- 0.240 < Eh < - 0.104 V); enforced equilibrium with pyrite and hematite.

DET		T	pH	Eh (V)	DET		T	pH	Eh (V)
7	a	45	11.7	+ 0.092	7	a'	45	11.7	< - 0.700
	b		11.7	+ 0.092		b'		11.7	< - 0.500
	c		11.7	+ 0.092		c'		11.7	< - 0.500
	d		11.7	< -0.500		d'		11.7	< - 0.500
7	a	60	11.2	+ 0.092	7	a'	60	11.2	< - 0.700
	b		11.2	+ 0.092		b'		11.2	< - 0.500
	c		11.2	+ 0.092		c'		11.2	< - 0.500
	d		11.2	< -0.500		d'		11.2	< - 0.500
7	a	80	10.7	+ 0.092	7	a'	80	10.7	< - 0.700
	b		10.7	+ 0.092		b'		10.7	< - 0.500
	c		10.7	+ 0.092		c'		10.7	< - 0.500
	d		10.7	< -0.500		d'		10.7	< - 0.500
8	a	32	12.2	+ 0.090	7	a'	32	12.2	< - 0.700
	b		12.2	+ 0.090		b'		12.2	< - 0.500
	c		12.2	+ 0.090		c'		12.2	< - 0.500
	d		12.2	< -0.500		d'		12.2	< - 0.500
8	a	60	11.3	+ 0.090	7	a'	60	11.3	< - 0.700
	b		11.3	+ 0.090		b'		11.3	< - 0.500
	c		11.3	+ 0.090		c'		11.3	< - 0.500
	d		11.3	< -0.500		d'		11.3	< - 0.500
8	a	80	10.8	+ 0.090	7	a'	80	10.8	< - 0.700
	b		10.8	+ 0.090		b'		10.8	< - 0.500
	c		10.8	+ 0.090		c'		10.8	< - 0.500
	d		10.8	< -0.500		d'		10.8	< - 0.500
9	a	23	12.7	+ 0.066	9	a'	23	12.7	< - 0.700
	b		12.7	+ 0.066		b'		12.7	< - 0.500
	c		12.7	+ 0.066		c'		12.7	< - 0.500
	d		12.7	< -0.500		d'		12.7	< - 0.500
9	a	60	11.5	+ 0.066	9	a'	60	11.5	< - 0.700
	b		11.5	+ 0.066		b'		11.5	< - 0.500
	c		11.5	+ 0.066		c'		11.5	< - 0.500
	d		11.5	< -0.500		d'		11.5	< - 0.500
9	a	80	11.0	+ 0.066	9	a'	80	11.0	< - 0.700
	b		11.0	+ 0.066		b'		11.0	< - 0.500
	c		11.0	+ 0.066		c'		11.0	< - 0.500
	d		11.0	< -0.500		d'		11.0	< - 0.500
10	a	21	12.7	+ 0.046	10	a'	21	12.7	< - 0.700
	b		12.7	+ 0.046		b'		12.7	< - 0.500
	c		12.7	+ 0.046		c'		12.7	< - 0.500
	d		12.7	< -0.500		d'		12.7	< - 0.500
10	a	60	11.4	+ 0.046	10	a'	60	11.4	< - 0.700
	b		11.4	+ 0.046		b'		11.4	< - 0.500
	c		11.4	+ 0.046		c'		11.4	< - 0.500
	d		11.4	< -0.500		d'		11.4	< - 0.500
10	a	80	11.0	+ 0.046	10	a'	80	11.0	< - 0.700
	b		11.0	+ 0.046		b'		11.0	< - 0.500
	c		11.0	+ 0.046		c'		11.0	< - 0.500
	d		11.0	< -0.500		d'		11.0	< - 0.500

Table 5.6 **Eh and pH of near field groundwater, i.e.; DET analyses equilibrated with portlandite, calcite and brucite allowed to precipitate. Relationship between temperature and pH shown by hottest, deepest samples having lowest pH and, as heat pulse increases temperature to 80°C, pH falls to as low as 10.7.**

Effects on Eh of equilibrium state of water analyses and interactions with steel also shown. Water files taken from DET 7, 8, 9 & 10. Cases a,b,c,d as described in text and previous tables. Cases a'b'c'd' represent near-field groundwaters equilibrated with steel (in the from of native iron).

DET for all cases	T (°C)	pH	Solubility controlling solid phases	U concentration (M)	Species	%
7	45	11.7	$UO_2(OH)_{2(c,\beta)}$ $UO_{2(am)}$	3.38×10^{-4}	$(UO_2)_3(OH)_7^-$	> 99.9
					$U(OH)_4$	< 0.1
	60	11.2	"	1.75×10^{-4}	$(UO_2)_3(OH)_7^-$	> 99.9
					$U(OH)_4$	< 0.1
	80	10.7	"	9.05×10^{-5}	$(UO_2)_3(OH)_7^-$	> 99.9
					$U(OH)_4$	< 0.1
8	32	12.2	$UO_2(OH)_{2(c,\beta)}$ $UO_{2(am)}$	7.00×10^{-4}	$(UO_2)_3(OH)_7^-$	> 99.9
					$U(OH)_4$	< 0.1
	60	11.3	"	1.96×10^{-4}	$(UO_2)_3(OH)_7^-$	> 99.9
					$U(OH)_4$	< 0.1
	80	10.8	"	8.81×10^{-5}	$(UO_2)_3(OH)_7^-$	> 99.9
					$U(OH)_4$	< 0.1
9	23	12.7	$UO_2(OH)_{2(c,\beta)}$ $UO_{2(am)}$	1.70×10^{-3}	$(UO_2)_3(OH)_7^-$	> 99.9
					$U(OH)_4$	< 0.1
	60	11.5	"	3.29×10^{-4}	$(UO_2)_3(OH)_7^-$	> 99.9
					$U(OH)_4$	< 0.1
	80	11.0	"	1.38×10^{-4}	$(UO_2)_3(OH)_7^-$	> 99.9
					$U(OH)_4$	< 0.1
10	21	12.7	$UO_2(OH)_{2(c,\beta)}$ $UO_{2(am)}$	1.90×10^{-3}	$(UO_2)_3(OH)_7^-$	> 99.9
					$U(OH)_4$	< 0.1
	60	11.4	"	4.00×10^{-4}	$(UO_2)_3(OH)_7^-$	> 99.9
					$U(OH)_4$	< 0.1
	80	11.0	"	1.23×10^{-4}	$(UO_2)_3(OH)_7^-$	> 99.9
					$U(OH)_4$	< 0.1

Table 5.7 **Uranium concentration in near-field groundwater, i.e DET analyses equilibrated with portlandite and calcite and bructite allowed to precipitate. Method one used to determine uranium solubility , i.e. for all cases a,b,c,d,a',b',c',d' equilibrium enforced with the U^{6+} and U^{4+} solid phases $UO_2(OH)_{2(c,\beta)}$ and $UO_{2(am)}$. Water files taken from DETs 7, 8, 9 & 10. Cases a,b,c,d,a',b',c',d' as described in text and previous tables.**

DET a,b,c	T (°C)	pH	Solubility controlling solid phases	U concentration (M)	Species	%
7	45	11.7	Schoepite	2.78×10^{-4}	$(UO_2)_3(OH)_7^-$	> 99.9
	60	11.2	$UO_2(OH)_{2(c,\beta)}$	1.13×10^{-4}	$(UO_2)_3(OH)_7^-$	> 99.9
	80	10.7	$UO_2(OH)_{2(c,\beta)}$	2.97×10^{-5}	$(UO_2)_3(OH)_7^-$	> 99.9
8	32	12.2	Schoepite	7.40×10^{-4}	$(UO_2)_3(OH)_7^-$	> 99.9
	60	11.3	$UO_2(OH)_{2(c,\beta)}$	1.57×10^{-4}	$(UO_2)_3(OH)_7^-$	> 99.9
	80	10.8	$UO_2(OH)_{2(c,\beta)}$	4.00×10^{-4}	$(UO_2)_3(OH)_7^-$	> 99.9
9	23	12.7	Schoepite	1.88×10^{-3}	$(UO_2)_3(OH)_7^-$	> 99.9
	60	11.5	$UO_2(OH)_{2(c,\beta)}$	1.98×10^{-4}	$(UO_2)_3(OH)_7^-$	> 99.9
	80	11.0	$UO_2(OH)_{2(c,\beta)}$	7.93×10^{-5}	$(UO_2)_3(OH)_7^-$	> 99.9
10	21	12.7	Schoepite	1.81×10^{-3}	$(UO_2)_3(OH)_7^-$	> 99.9
	60	11.4	$UO_2(OH)_{2(c,\beta)}$	1.96×10^{-4}	$(UO_2)_3(OH)_7^-$	> 99.9
	80	11.0	$UO_2(OH)_{2(c,\beta)}$	4.03×10^{-5}	$(UO_2)_3(OH)_7^-$	> 99.9

DET d,a',b'c',d'	T (°C)	pH	Solubility controlling solid phases	U concentration (M)	Species	%
7	45	11.7	Uraninite	1.34×10^{-13}	$U(OH)_4$	100.0
	60	11.2	"	2.30×10^{-13}	$U(OH)_4$	100.0
	80	10.7	"	5.56×10^{-13}	$U(OH)_4$	100.0
8	32	12.2	Uraninite	8.34×10^{-14}	$U(OH)_4$	100.0
	60	11.3	"	2.41×10^{-13}	$U(OH)_4$	100.0
	80	10.8	"	5.58×10^{-13}	$U(OH)_4$	100.0
9	23	12.7	Uraninite	6.13×10^{-14}	$U(OH)_4$	100.0
	60	11.5	"	5.60×10^{-13}	$U(OH)_4$	100.0
	80	11.0	"	9.05×10^{-13}	$U(OH)_4$	100.0
10	21	12.7	Uraninite	5.74×10^{-14}	$U(OH)_4$	100.0
	60	11.4	"	2.41×10^{-13}	$U(OH)_4$	100.0
	80	11.0	"	5.60×10^{-13}	$U(OH)_4$	100.0

Table 5.8 **Uranium concentration in pseudo near-field groundwater, i.e DET analyses equilibrated with portlandite, calcite and bructite allowed to precipitate. Method two used to determine uranium solubility, i.e.; uranium concentration increased until Saturation Index (SI) indicated solid phase formation. This phase then used as solubility controlling stable phase. For all a,b,c solubility controlling phases were schoepite ($UO_2(OH)_2 \cdot H_2O_{(s)}$) below 53°C and $UO_2(OH)_{2(c,\beta)}$ above 53°C. For all d,a',b',c',d' cases solubility controlling stable phase was uraninite (UO_2). Water files taken from DETs 7, 8, 9 & 10. Cases a,b,c,d,a',b',c',d' as described in text and previous tables.**

DET (& case)	Solubility controlling solid phase	U conc at "field" pH (M)	Species	%	U conc at "Calcite" pH (M)	Species	%
7 (a,b,c)	U_4O_9(c)	1.882×10^{-6}	$UO_2(CO_3)_3^{4-}$	51.5	5.923×10^{-7}	$UO_2(CO_3)_2^{2-}$	62.0
			$UO_2(CO_3)_2^{2-}$	48.0		$UO_2(CO_3)_3^{4-}$	37.0
			UO_2CO_3	0.5		UO_2CO_3	1.0
7 (d)	Uraninite	1.563×10^{-13}	$U(OH)_4$	100.0	1.698×10^{-13}	$U(OH)_4$	100.0
8 (a,b,c)	U_4O_9(c)	3.780×10^{-4}	$UO_2(CO_3)_3^{4-}$	94.5	2.424×10^{-6}	$UO_2(CO_3)_3^{4-}$	64.0
			$UO_2(CO_3)_2^{2-}$	5.0		$UO_2(CO_3)_2^{2-}$	35.0
			UO_2CO_3	0.5		UO_2CO_3	1.0
8 (d)	Uraninite	2.291×10^{-13}	$U(OH)_4$	100.0	1.690×10^{-13}	$U(OH)_4$	100.0
9 (a,b,c)	U_4O_9(c)	6.633×10^{-8}	$UO_2(CO_3)_2^{2-}$	51.0	4.061×10^{-6}	$UO_2(CO_3)_3^{4-}$	85.0
			$UO_2(CO_3)_3^{4-}$	46.5		$UO_2(CO_3)_2^{2-}$	14.0
			UO_2CO_3	2.5		UO_2CO_3	1.0
9 (d)	Uraninite	1.582×10^{-13}	$U(OH)_4$	100.0	1.214×10^{-13}	$U(OH)_4$	100.0
10 (a,b,c)	U_4O_9(c)	8.384×10^{-10}	$UO_2(CO_3)_2^{2-}$	66.0	5.483×10^{-7}	$UO_2(CO_3)_3^{4-}$	84.0
			UO_2CO_3	18.0		$UO_2(CO_3)_2^{2-}$	15.0
			$UO_2(CO_3)_3^{4-}$	16.0		UO_2CO_3	1.0
10 (d)	Uraninite	1.369×10^{-13}	$U(OH)_4$	100.0	6.992×10^{-14}	$U(OH)_4$	100.0

Table 5.9 Uranium concentration in far-field groundwater for 4 equilibrium states, and two methods of constraining pH; either from field analyses or by equilibrating fluid with calcite. Method two was used to determine uranium solubility , i.e. uranium concentration increased until Saturation Index (SI) indicated solid phase formation. This phase then used as solubility controlling stable phase. For all a,b and c cases the solubility controlling stable phase was U_4O_9(c). For all d cases the solubility controlling stable phase was uraninite (UO_2). Water files taken from DET 7, 8, 9 & 10. Cases a, b, c & d as described in text and previous tables.

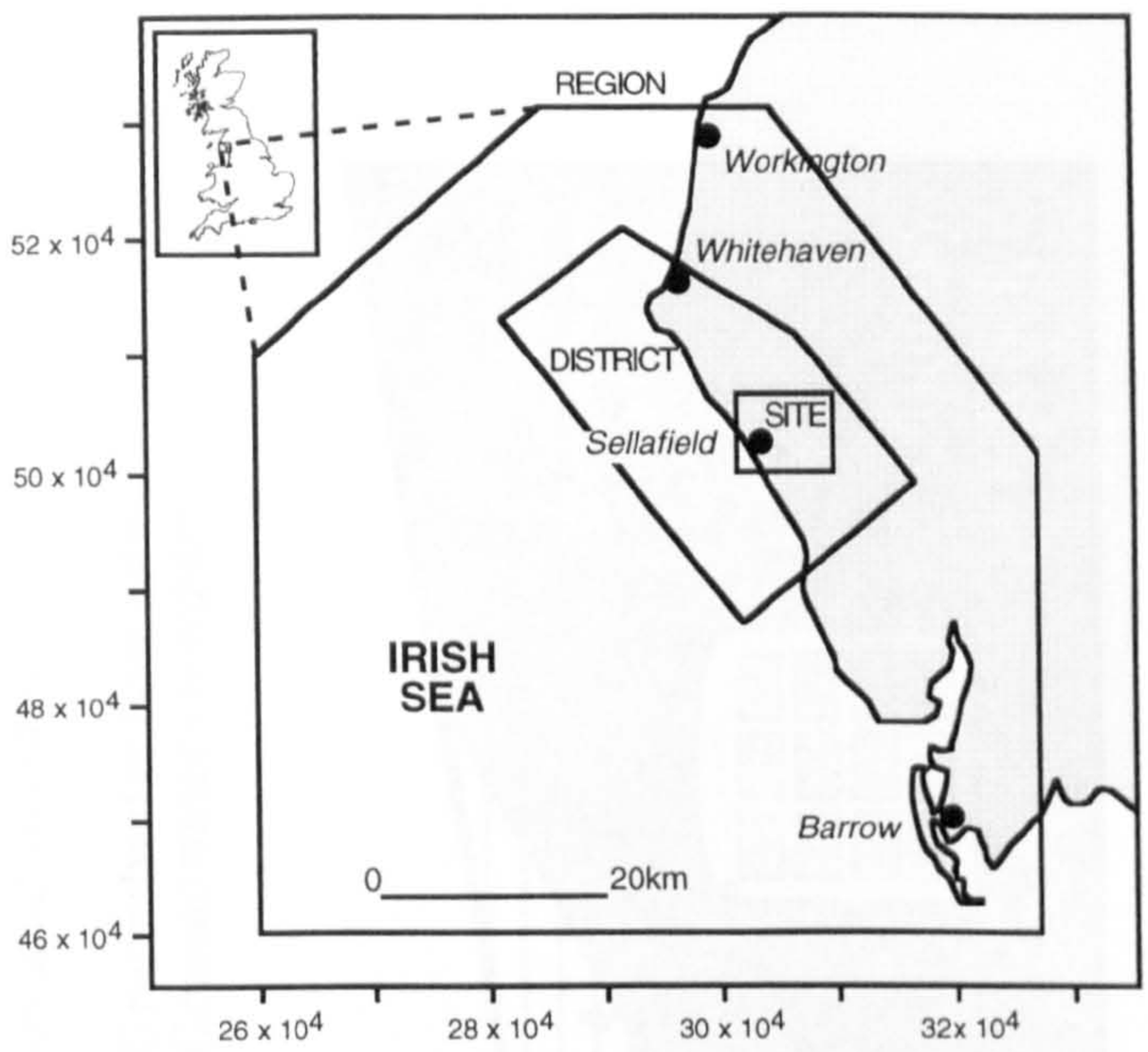

Fig. 5.1a **Region, District and Site definitions (after Michie & Bowden, 1994).**

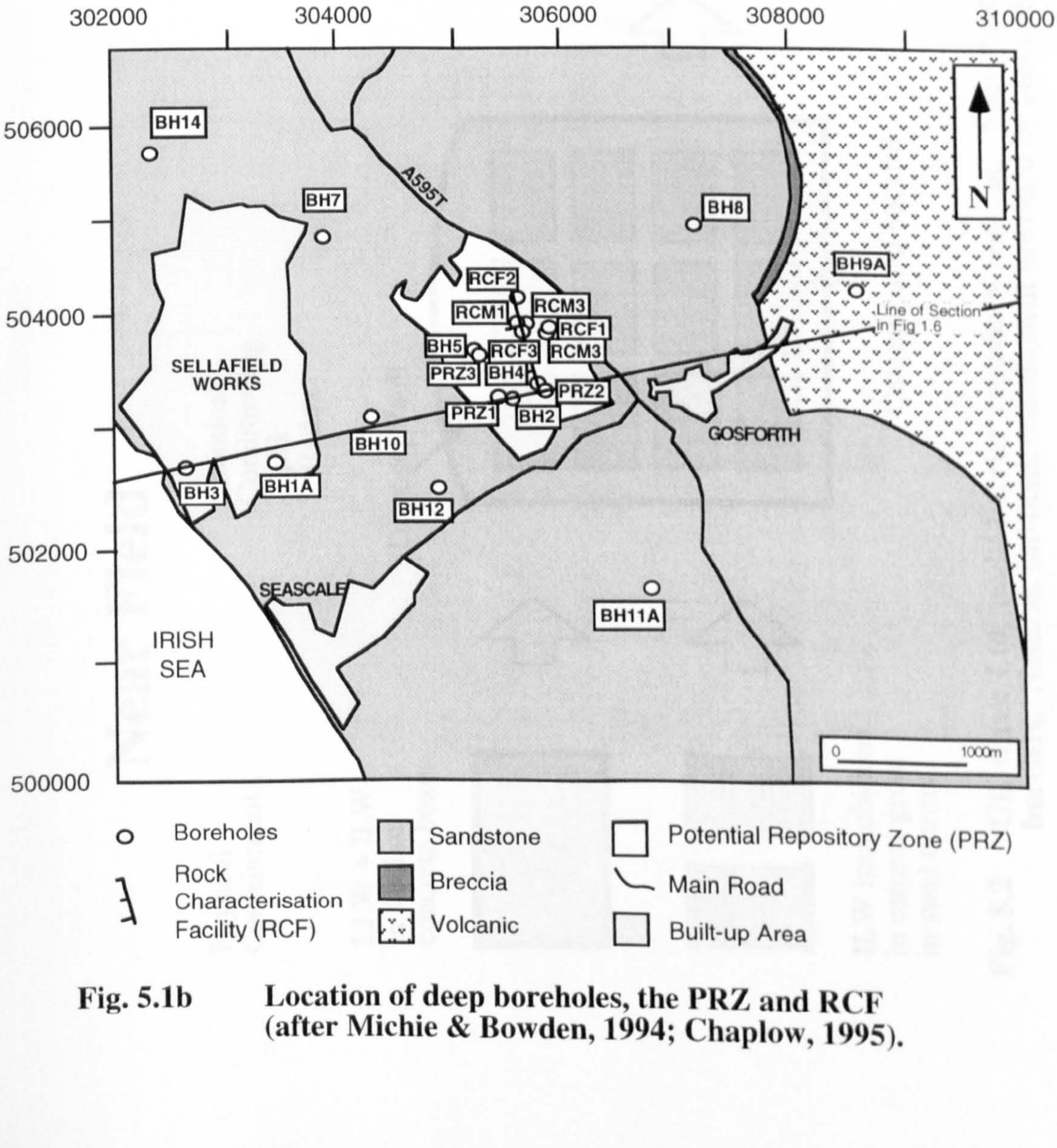

Fig. 5.1b **Location of deep boreholes, the PRZ and RCF (after Michie & Bowden, 1994; Chaplow, 1995).**

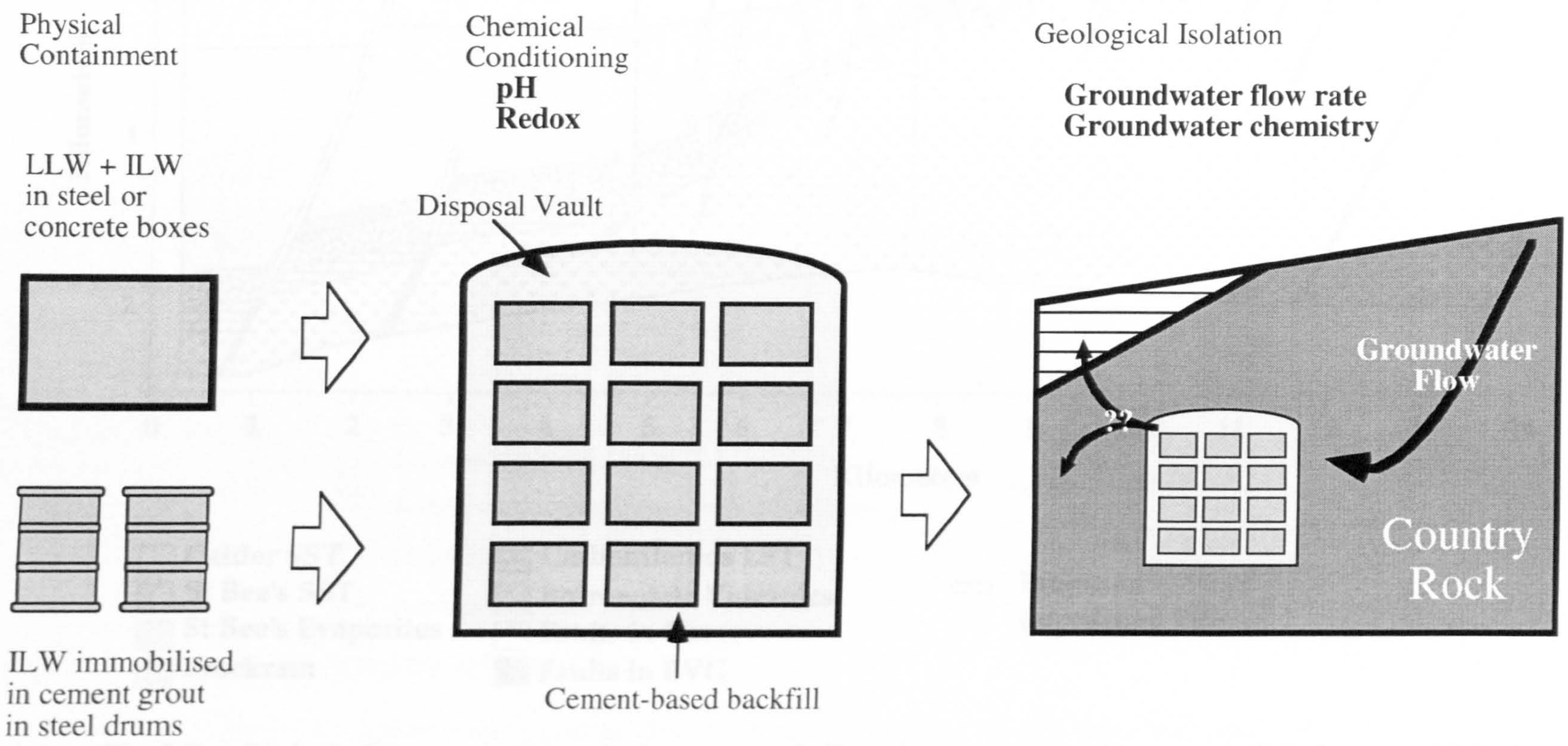

Fig. 5.2 UK Nirex Ltd. multi-barrier repository concept. Near field engineered to provide physical and chemical barriers. Natural, far-field, containment provided by geological setting (after Holmes, 1995; Hooper, 1995).

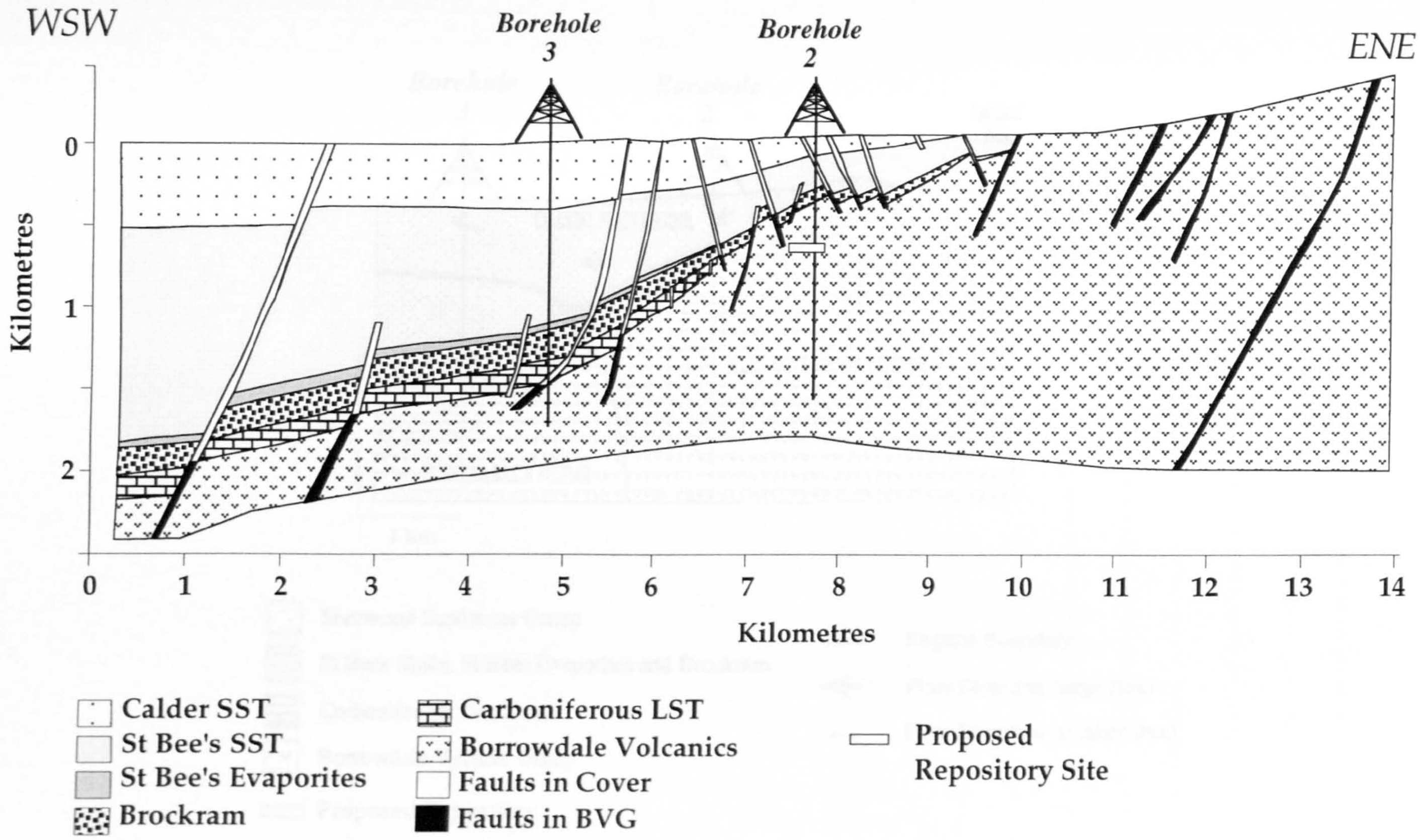

Fig. 5.3 Geological cross section of the proposed Repository site at 650m, compiled from published information (Nirex, 1992b; Nirex, 1993b; Nirex, 1993d) and extended W and E using publicly available geological information (Taylor et al 1971). Rocks of the Borrowdale Volcanic Group (BVG) rise to 1,000m elevation in the Lake District, and fall westwards to lie well below sea level. This elevation provides a topographical drive for meteoric water flow through any fracture or matrix conductivity in the BVG. Carboniferous to Triassic sediments onlap the BVG, and provide a series of matrix and fracture permeable aquifers.

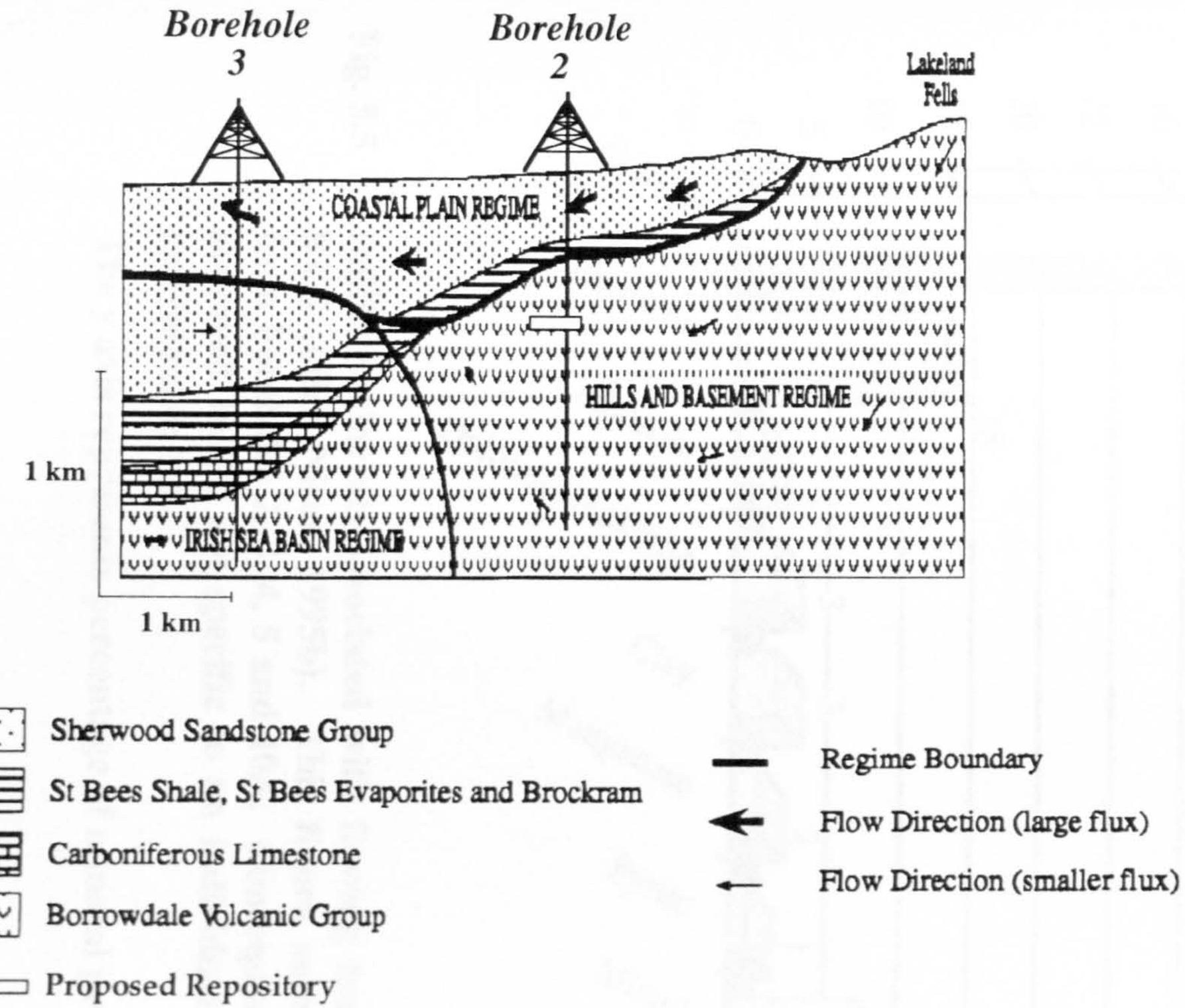

Fig. 5.4 Nirex conceptual model of the hydrogeology of the Sellafield area (after Black, 1995). The divisions coincide largely with the distribution of salinity Groundwaters in the Irish Sea Basin regime are predominantly basin-derived brines; in the Hills and Basement Regime, saline; in the Coastal Plain Regime, fresh. Scale same as Fig. 5.3.

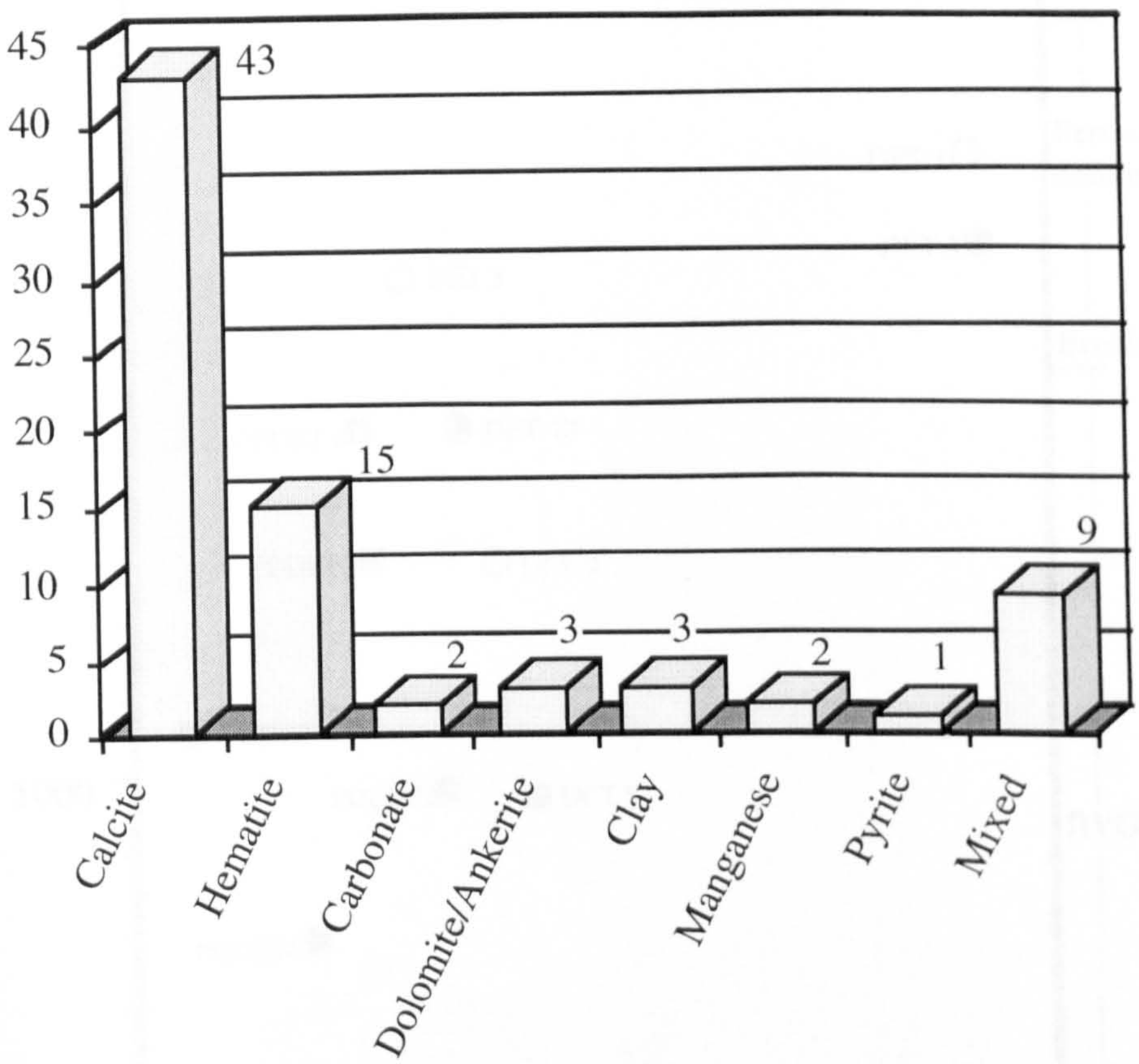

Fig. 5.5 **Infilling minerals associated with flowing fractures in the BVG (after Nirex, 1995b). This figure summarises data from boreholes 2, 3, 4, 5 and 10A. Consequently these are averaged values not specific to an individual borehole, or individual depth.**

The y axis represents percentage of mineral present.

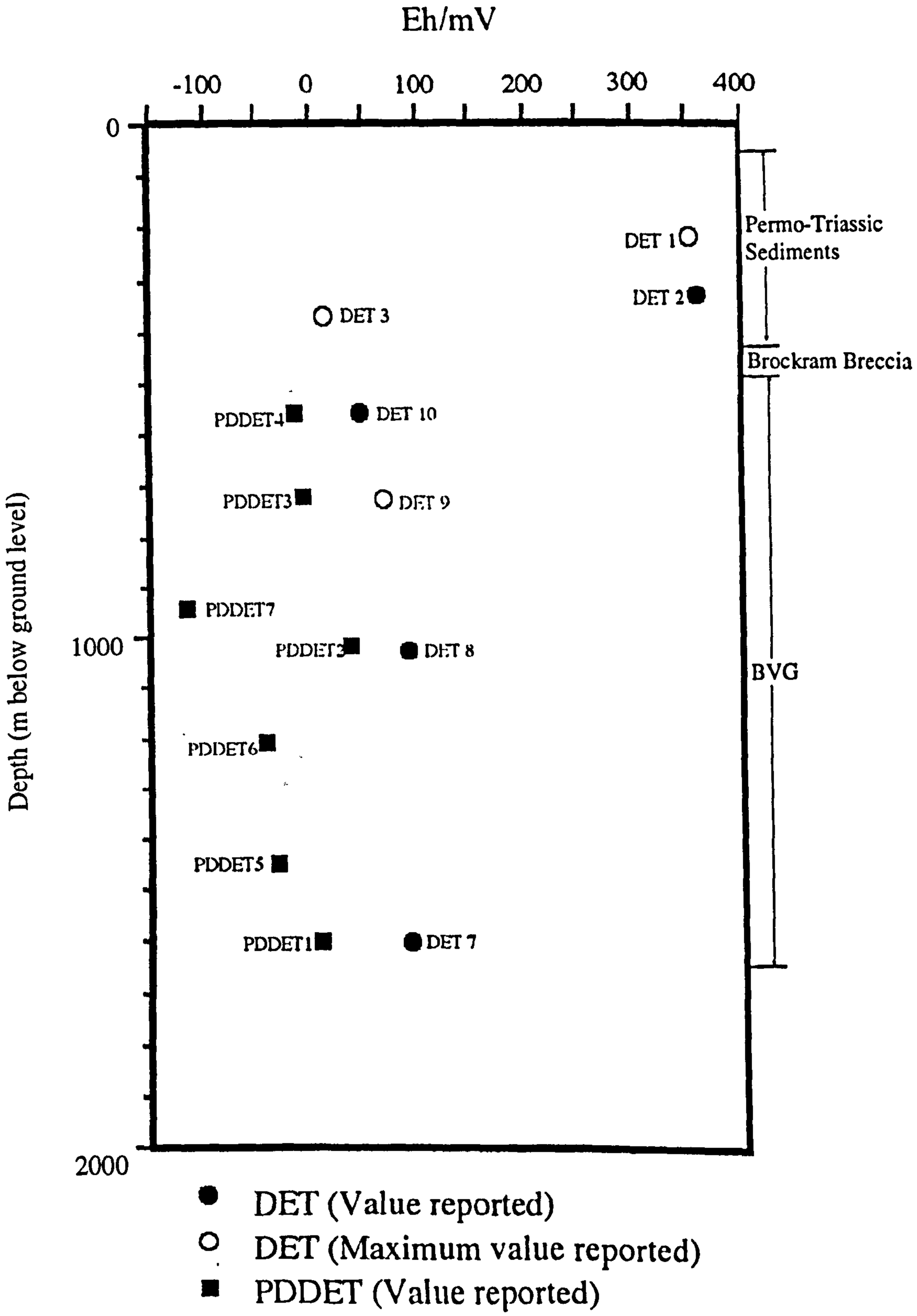

Fig. 5.6 Plot of depth vs Eh of samples taken from extraction tests in borehole 2 (after Nirex, 1995c).

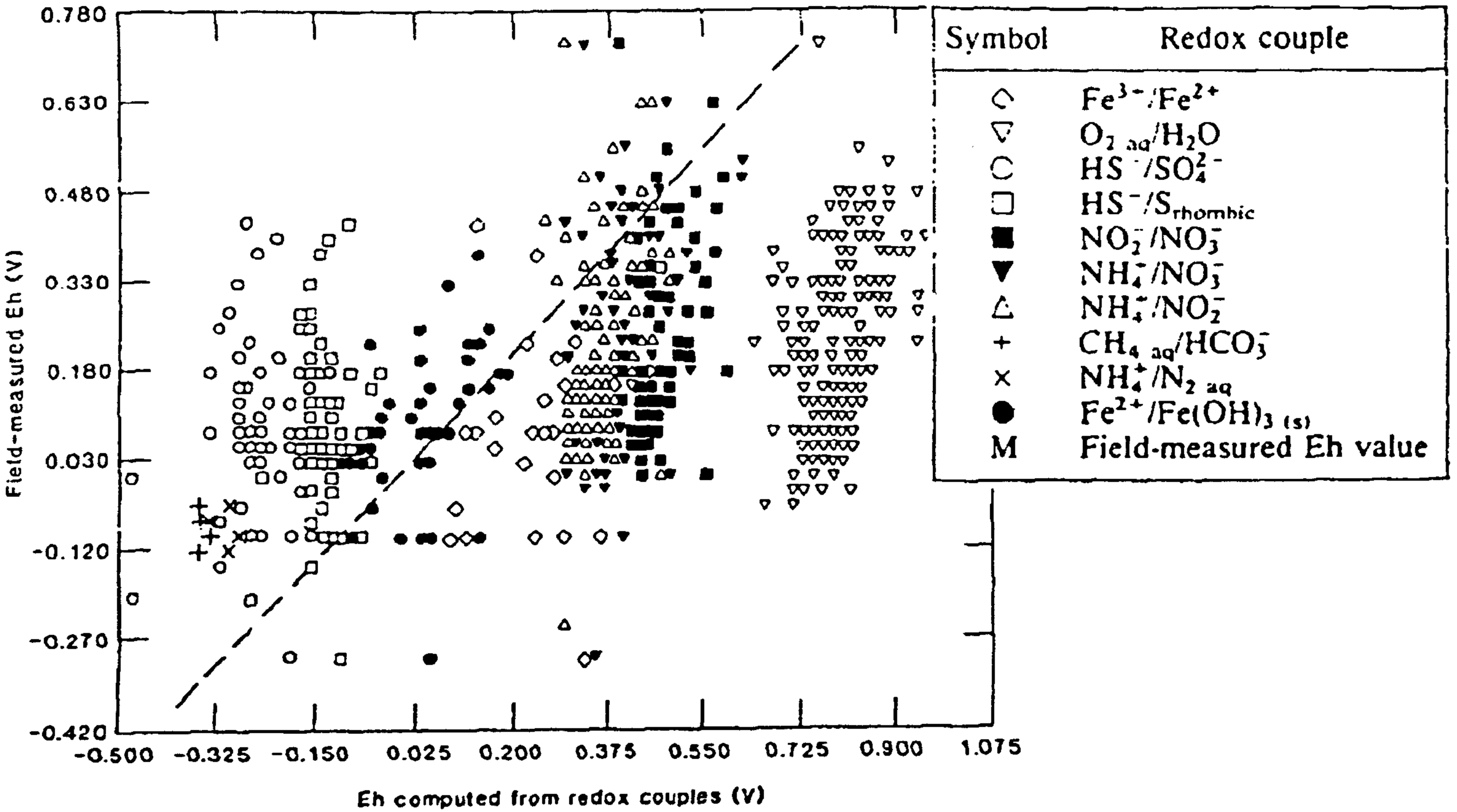

Fig. 5.7 **Comparison of groundwater field Eh measurements with potentials calculated for individual redox species (after Lindberg and Runnels, 1984).**

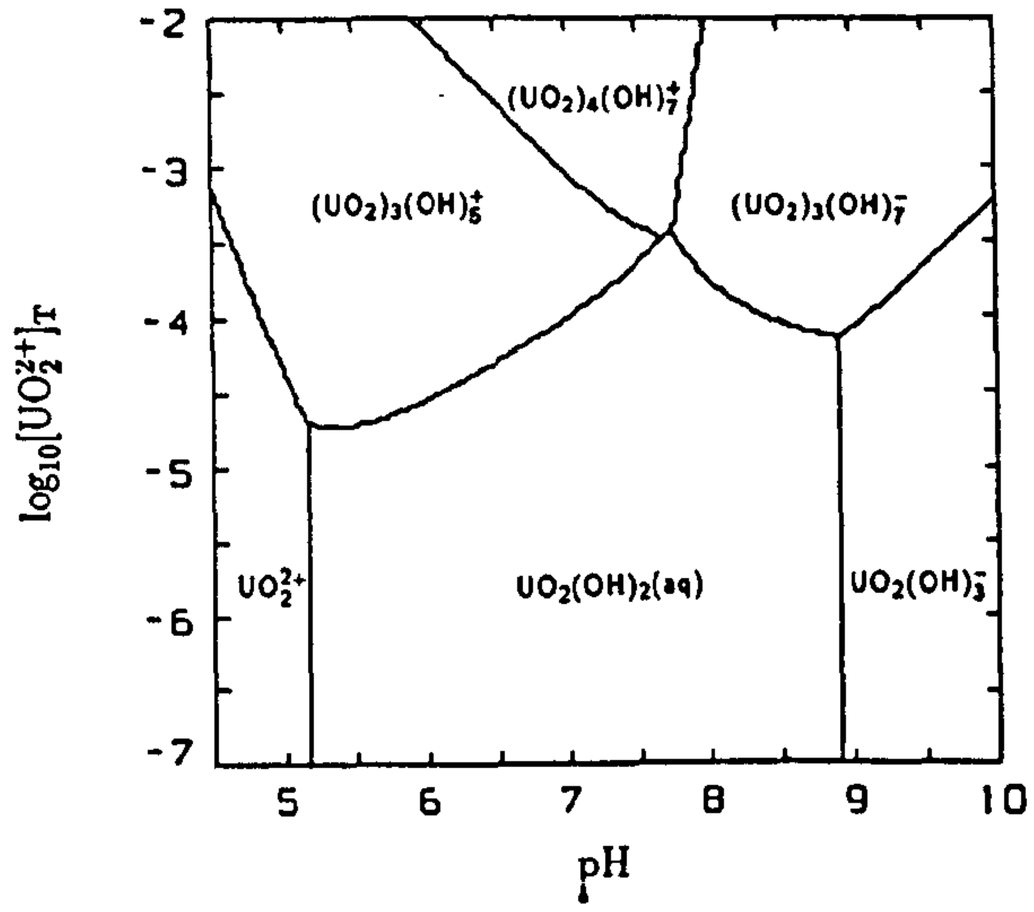

Fig. 5.8a **Predominance diagram of the UO_2^{2+} hydroxide system at 25 °C in the range 4.5 < pH < 10 (after Grenthe et al, 1992).**

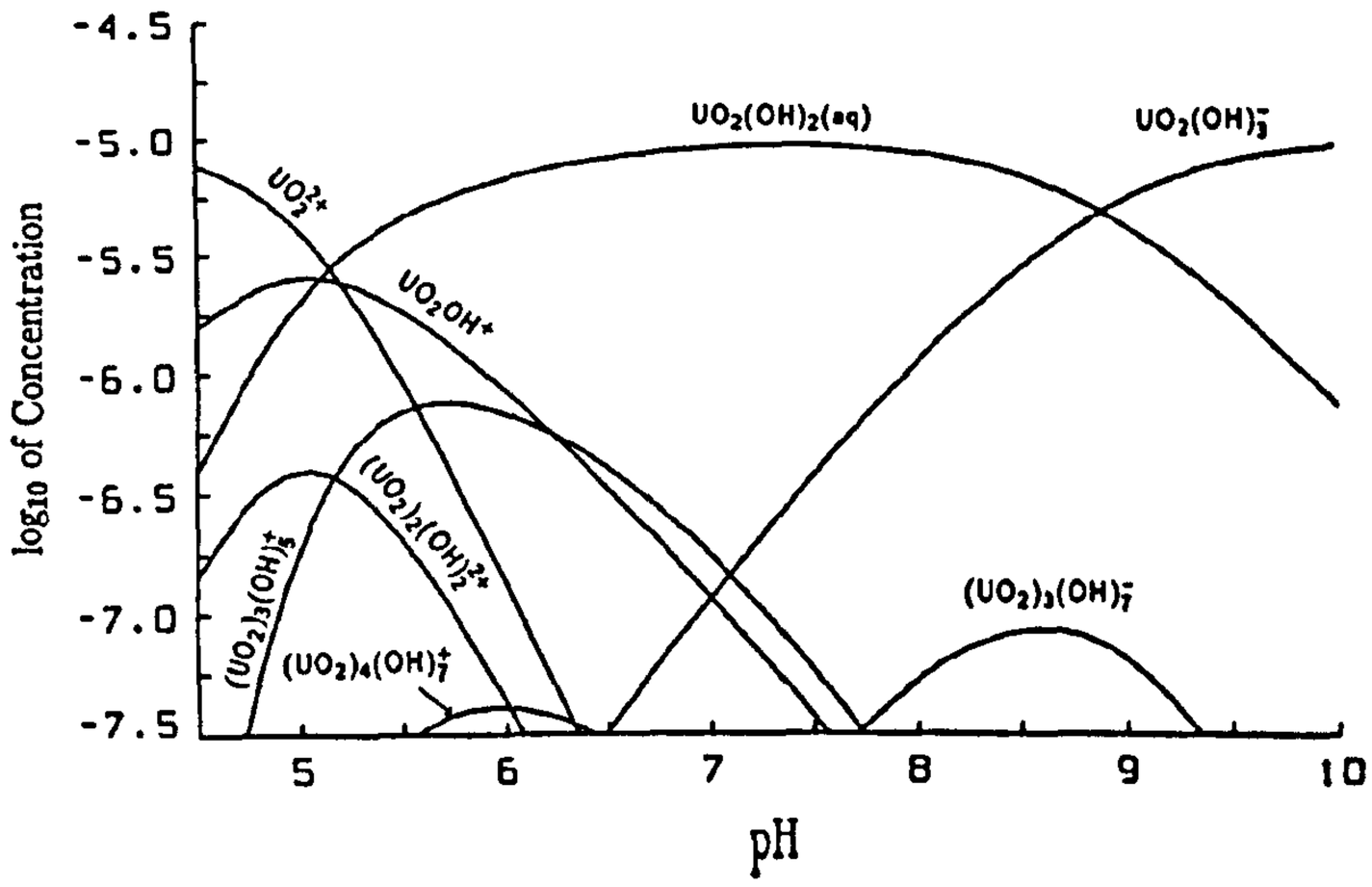

Fig. 5.8b **Distribution diagram of the UO_2^{2+} hydroxide system at 25 °C in the range 4.5 < pH < 10 (after Grenthe et al, 1992). $[UO_2^{2+}] = 1x10^{-5}$ M**

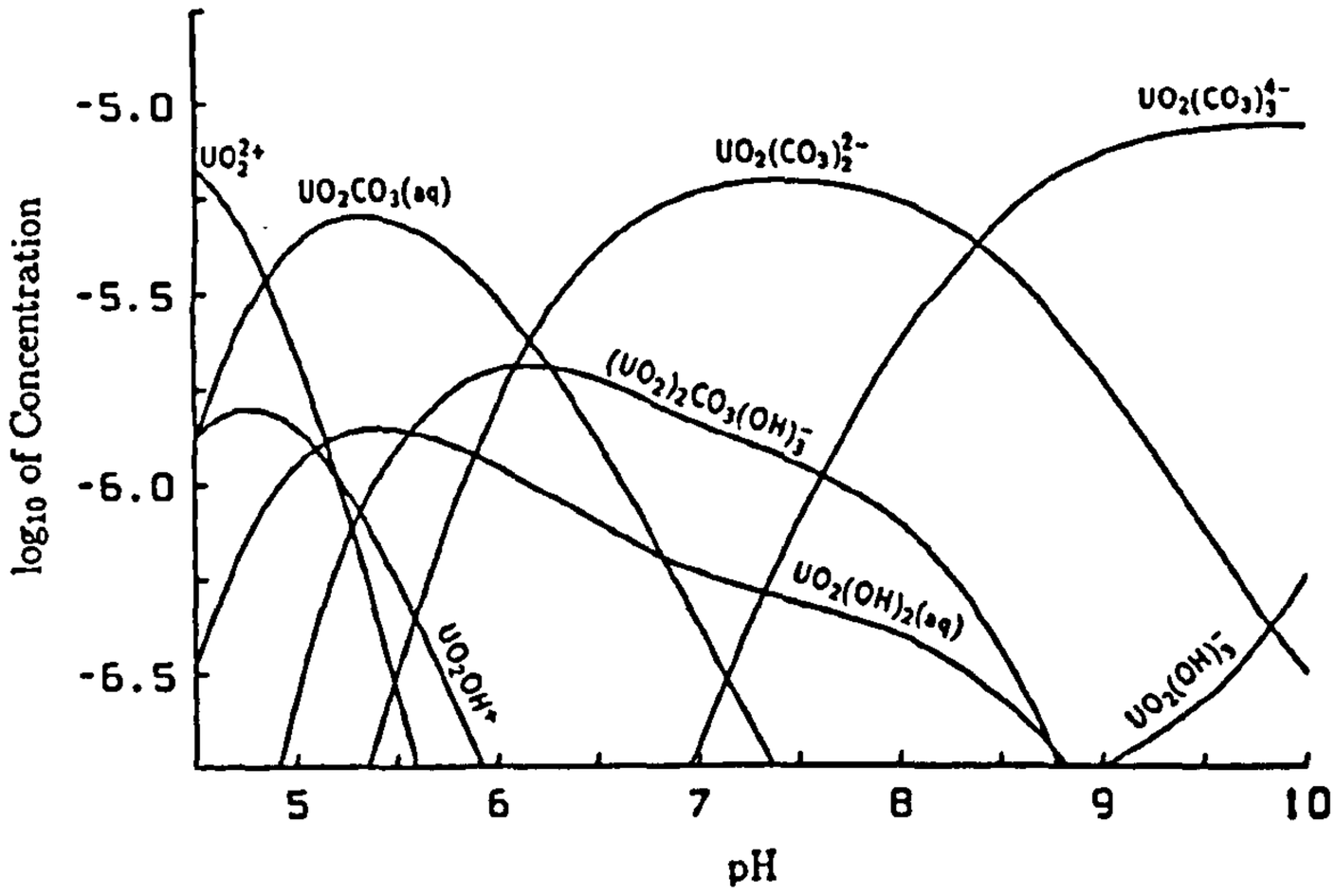

Fig. 5.9a **Distribution diagram of the UO_2^{2+} hydroxide-carbonate system at 25 °C in the range 4.5 < pH < 10 (after Grenthe et al, 1992).**

$[UO_2^{2+}] = 1x10^{-5}$ M

$[CO_3^{2-}] = 2x10^{-3}$ M

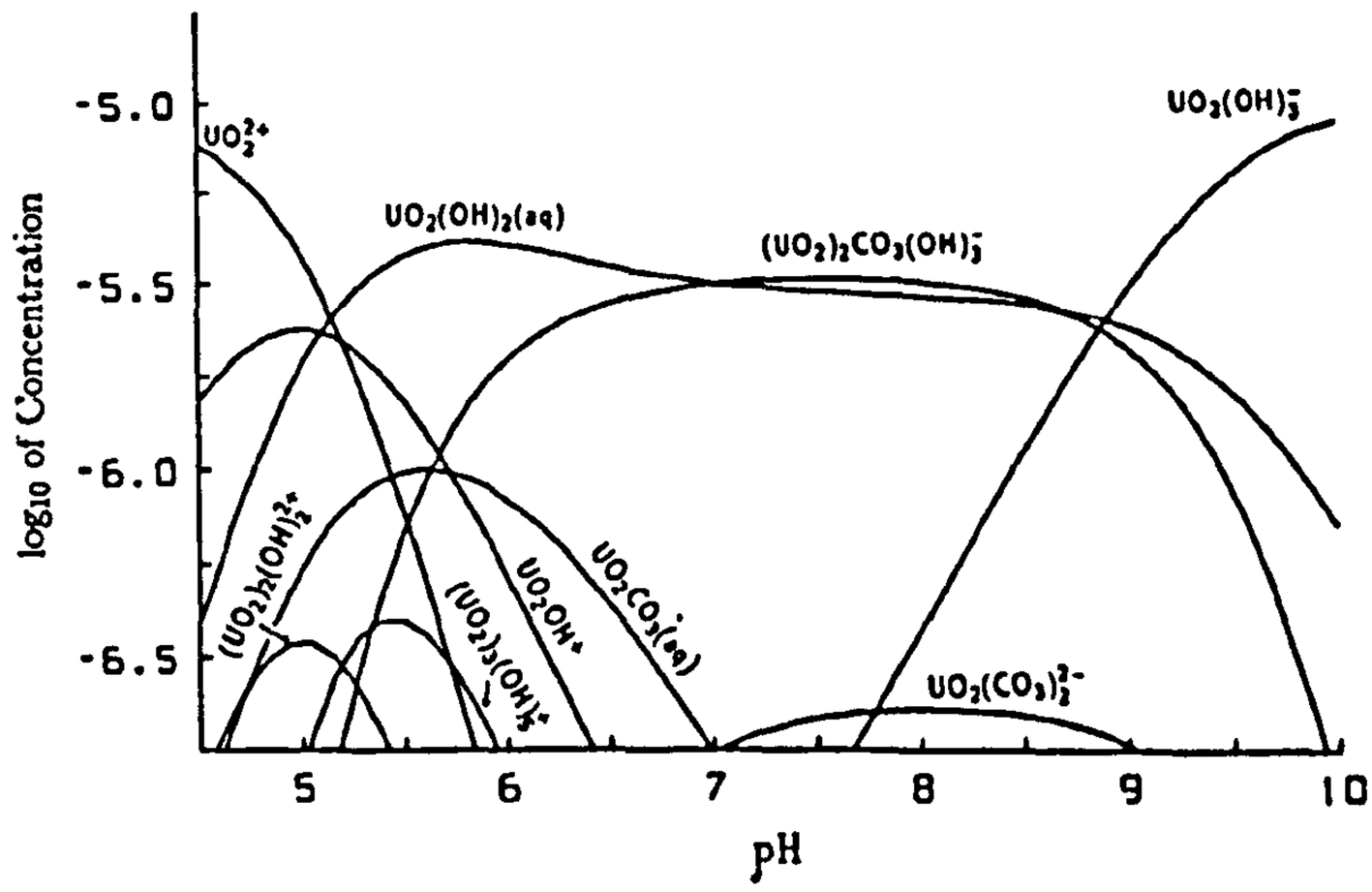

Fig. 5.9b **Distribution diagram of the UO_2^{2+} hydroxide-carbonate system at 25 °C in the range 4.5 < pH < 10 (after Grenthe et al, 1992).**

$[UO_2^{2+}] = 1.0x10^{-5}$ M

$[CO_3^{2-}] = 1.5x10^{-4}$ M

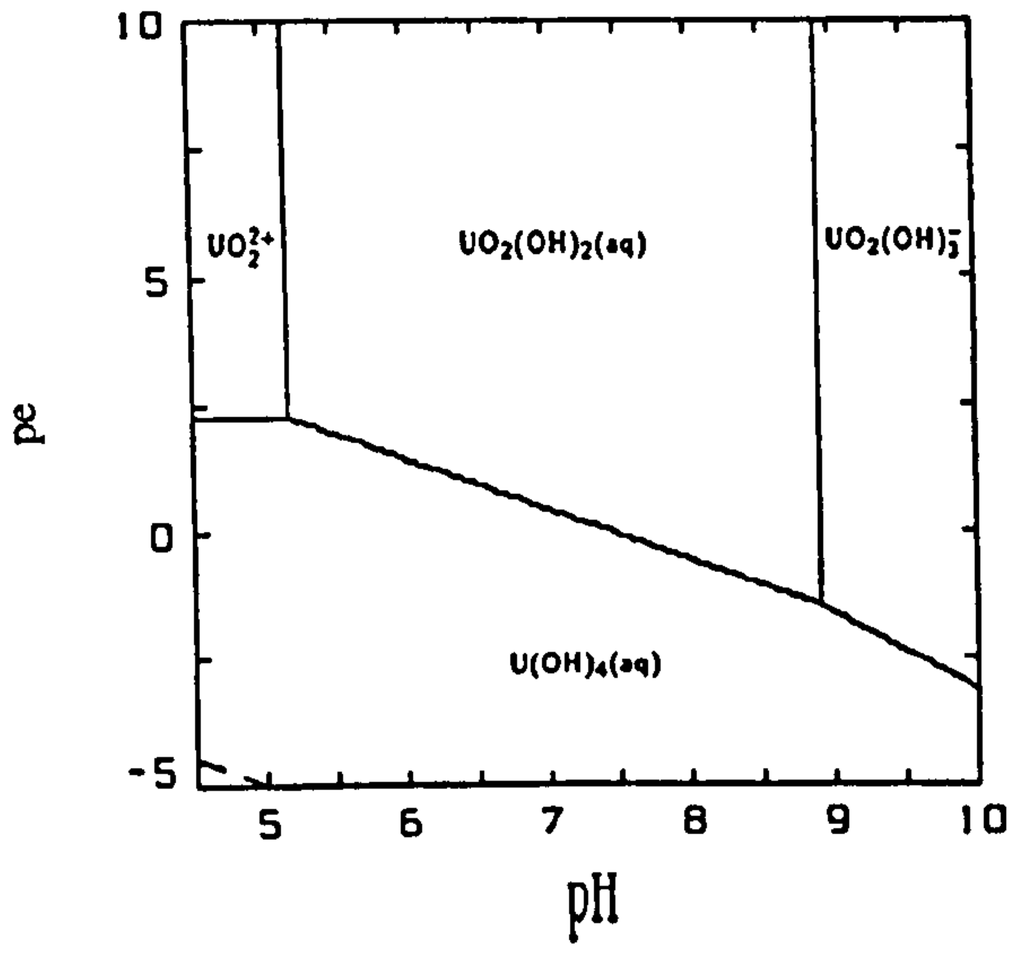

Fig. 5.10a **Predominance diagram of the UO_2^{2+} / U^{4+} hydroxide system at 25°C in the range 4.5 < pH < 10 as a function of the redox potential, (after Grenthe et al, 1992).**
$[UO_2^{2+}]$ = $1x10^{-5}$ M

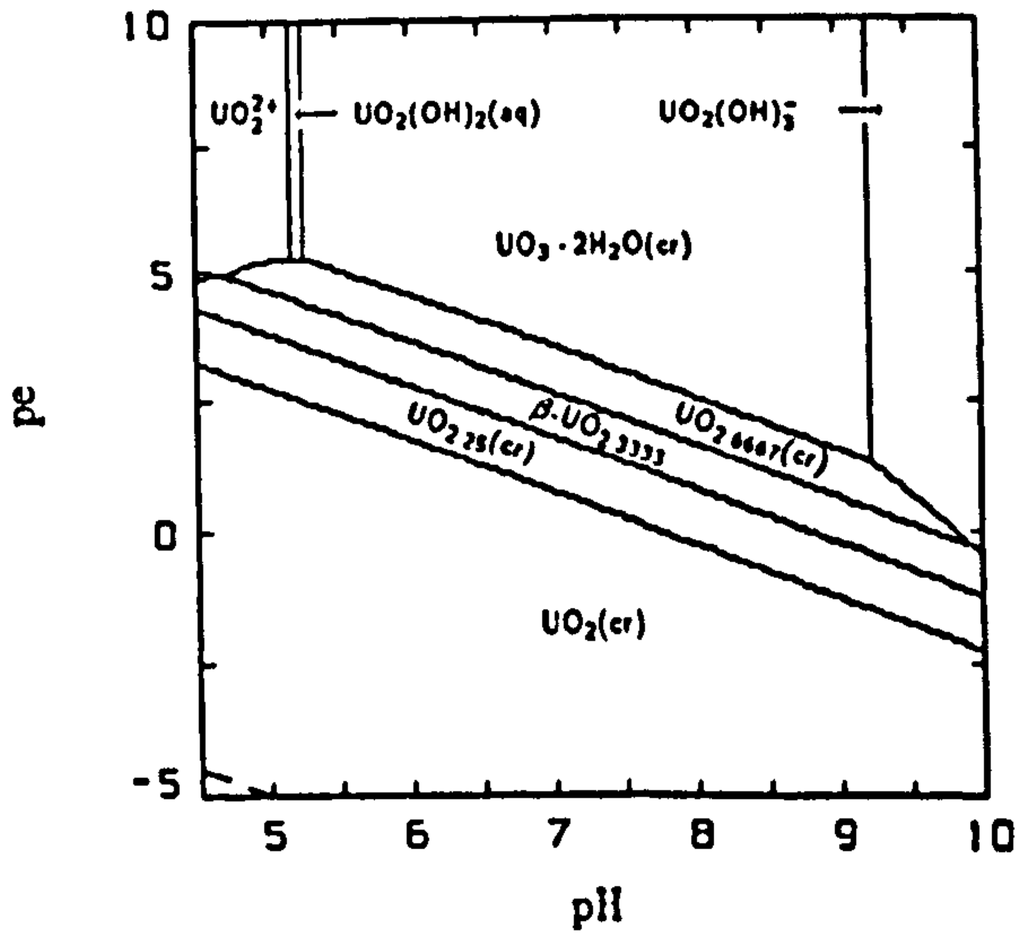

Fig. 5.10b **Solubility and predominance diagram of the UO_2^{2+} / U^{4+} hydroxide system at 25°C in the range 4.5 < pH < 10 as a function of the redox potential if solid phases are allowed to precipitate. Solubility limiting phases are indicated. Schoetite is $UO_3 \cdot 2H_2O$ (cr), uraninite is UO_2 (cr). (after Grenthe et al, 1992).**
$[UO_2^{2+}]$ = $1x10^{-5}$ M

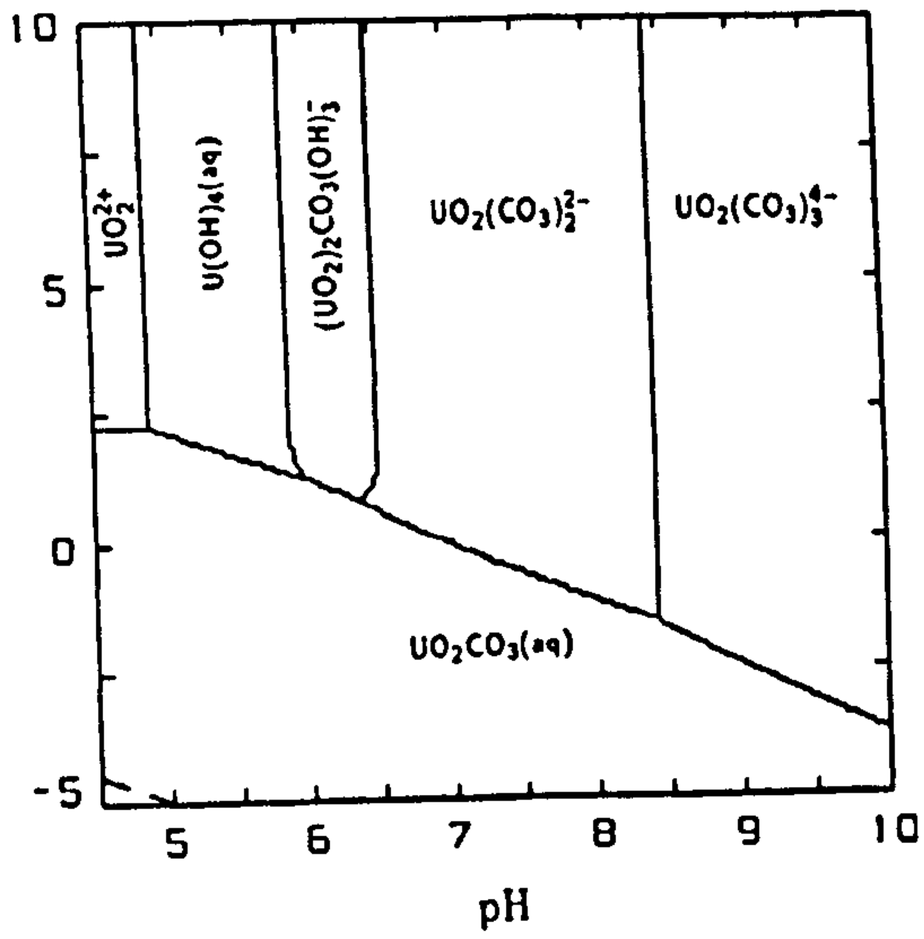

Fig. 5.11a **Predominance diagram of the UO_2^{2+} / U^{4+} hydroxide-carbonate system at 25°C in the range 4.5 < pH < 10 as a function of the redox potential, (after Grenthe et al, 1992).**
$[UO_2^{2+}]$ = $1x10^{-5}$ M
$[CO_3^{2-}]$ = $2x10^{-3}$ M

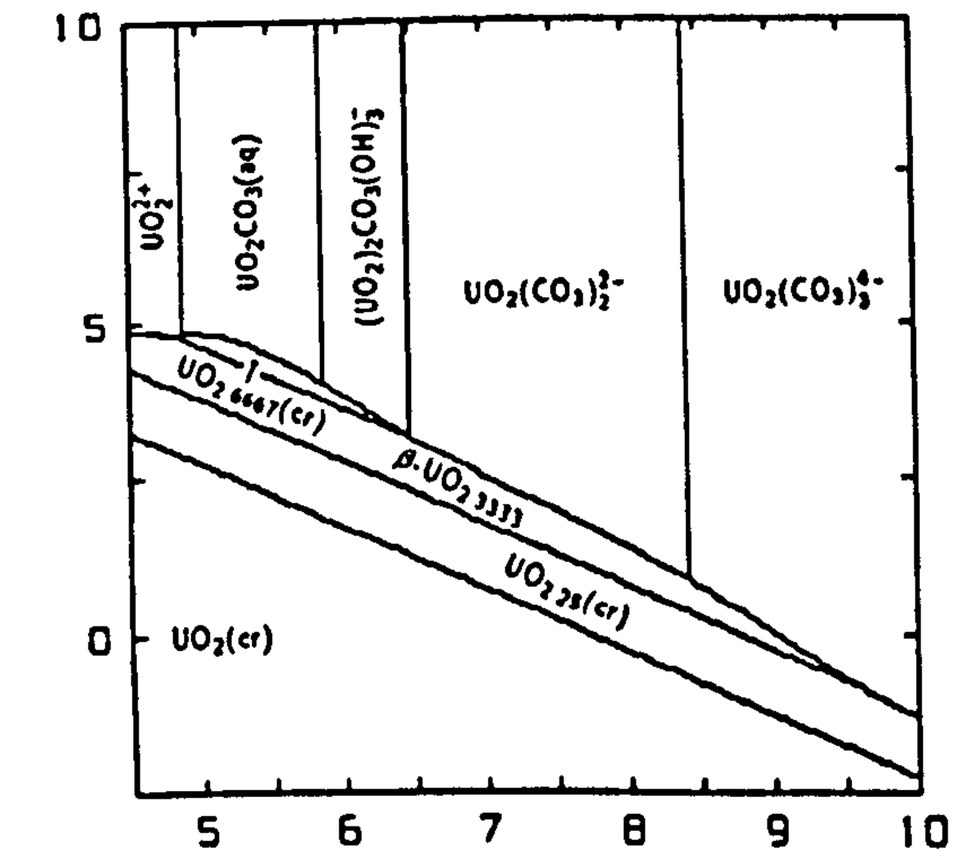

Fig. 5.11b **Solubility and predominance diagram of the UO_2^{2+} / U^{4+} hydroxide-carbonate system at 25°C in the range 4.5 < pH < 10 as a function of the redox potential if solid phases are allowed to precipitate. Solubility limiting phases are indicated. Schoepite is $UO_3 \cdot 2H_2O$ (cr), uraninite is UO_2 (cr).**
(after Grenthe et al, 1992).
$[UO_2^{2+}]$ = $1x10^{-5}$ M
$[CO_3^{2-}]$ = $2x10^{-3}$ M

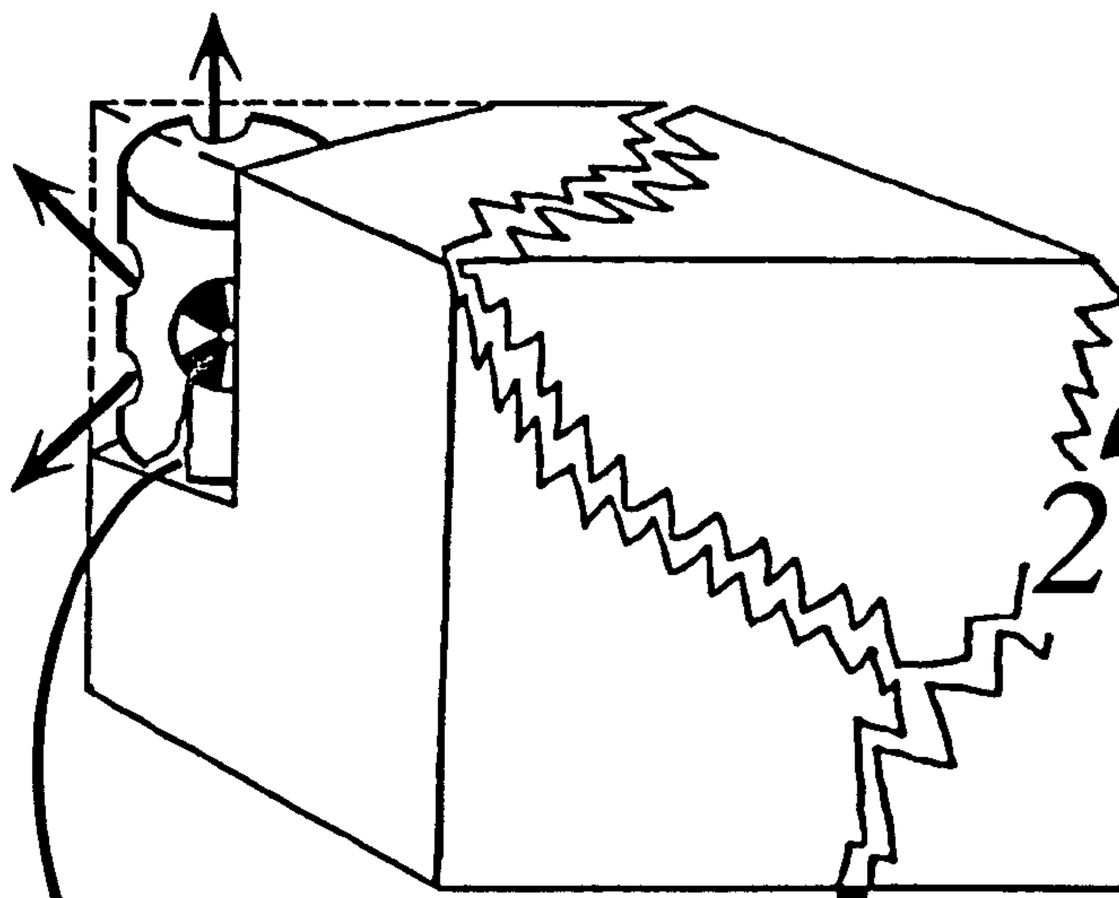

1

Natural groundwater conditions
Modelled using Borehole 2 Discrete Extraction Tests (DETs) 7, 8, 9 & 10, (Table 5.4). Redox determined by four methods, (Table 5.5):
a Eh as measured + redox disequilibrium (see text)
b Eh as measured
c Equilibrium with Hematite
d Equilbrium with Hematite & Pyrite

2

Groundwater samples reacted with cement
(portlandite, brucite & calcite) for all DET and Eh methods, (Table 5.6). Case names relate to method used to calculate Eh : *a, b, c, d*
Resultant fluids either reacted with steel -> (3) or
used to calculate uranium solubility -> (4).

3

High pH samples reacted with steel
in the form of iron for all DET and Eh methods (Table 5.6).
Case names relate to method used to calculate Eh :
a,' b,' c', d'
' denotes high pH fluid reacted with steel.
Resultant fluids used to determine uranium solubility -> (4)

Emergent fluids carry uranium

4

Uranium solubility calculated using two methods ;

Method one Uranium solubility controlling stable phases assumed. Equilibrium with fluid enforced

Method two Solubility controlling stable phases determined from saturation indices of minerals (see text and Appendix).

"NEAR FIELD"
Method one used to determine uranium solubility. Uranium solid phases selected: $UO_2(OH)_2$ (c,β) and UO_2(am) (see text). Simulations of all DETs and Eh cases (Table 5.7);

Without Steel	With Steel
a, b, c, d	*a', b', c', d'*

"PSEUDO NEAR FIELD"
Method two used to determine uranium solubility for all DETs and Eh cases (Table 5.8);

Without Steel	With Steel
a, b, c, d	*a', b', c', d'*

"FAR FIELD"
Method two used to determine uranium solubility for all DETs and Eh cases (Table 5.9);

No Steel
a, b, c, d

Fig. 5.12

Simplified stages in modelling concept

1 The natural groundwater is modelled without uranium;
2 The interaction with cement is modelled;
3 The interaction with the steel barrels is modelled;
4 Uranium solubility is modelled by two methods, see box 4.

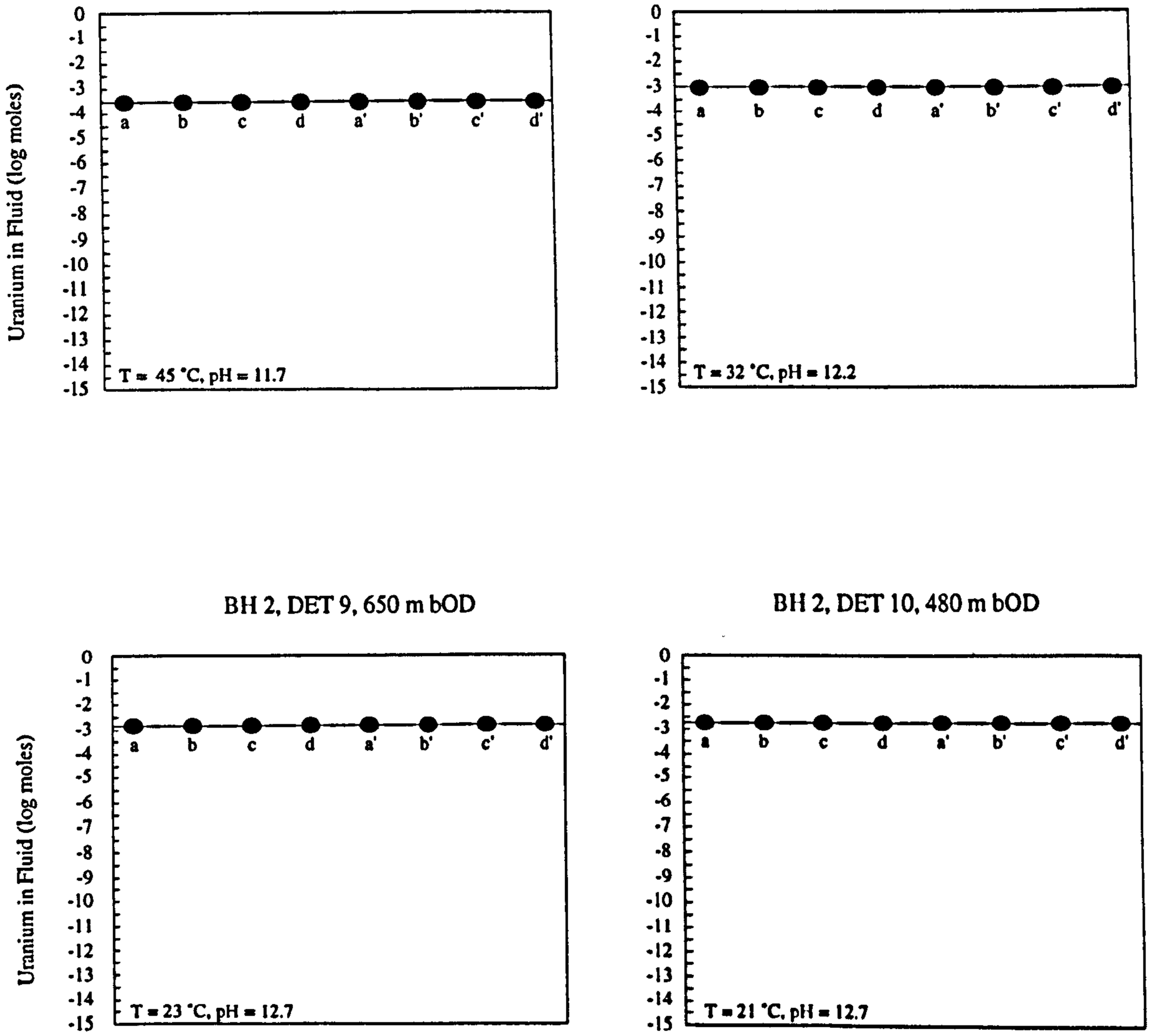

Fig 5.13 Uranium concentration in near-field groundwater for 4 equilibrium states, using method one to determine uranium solubility :

Enforced equilibrium with $UO_2(OH_2)$ (c,β) and UO_2 (am)

All analyses equilibrated with porlandite ($Ca(OH)_2$), with Calcite ($CaCO_3$) and Brucite ($Mg(OH)_2$) allowed to precipitate.
Detailed redox information of cases a,b,c,d,a',b',c',d' in table 5.6. Speciation and numerical breakdown in table 5.7.

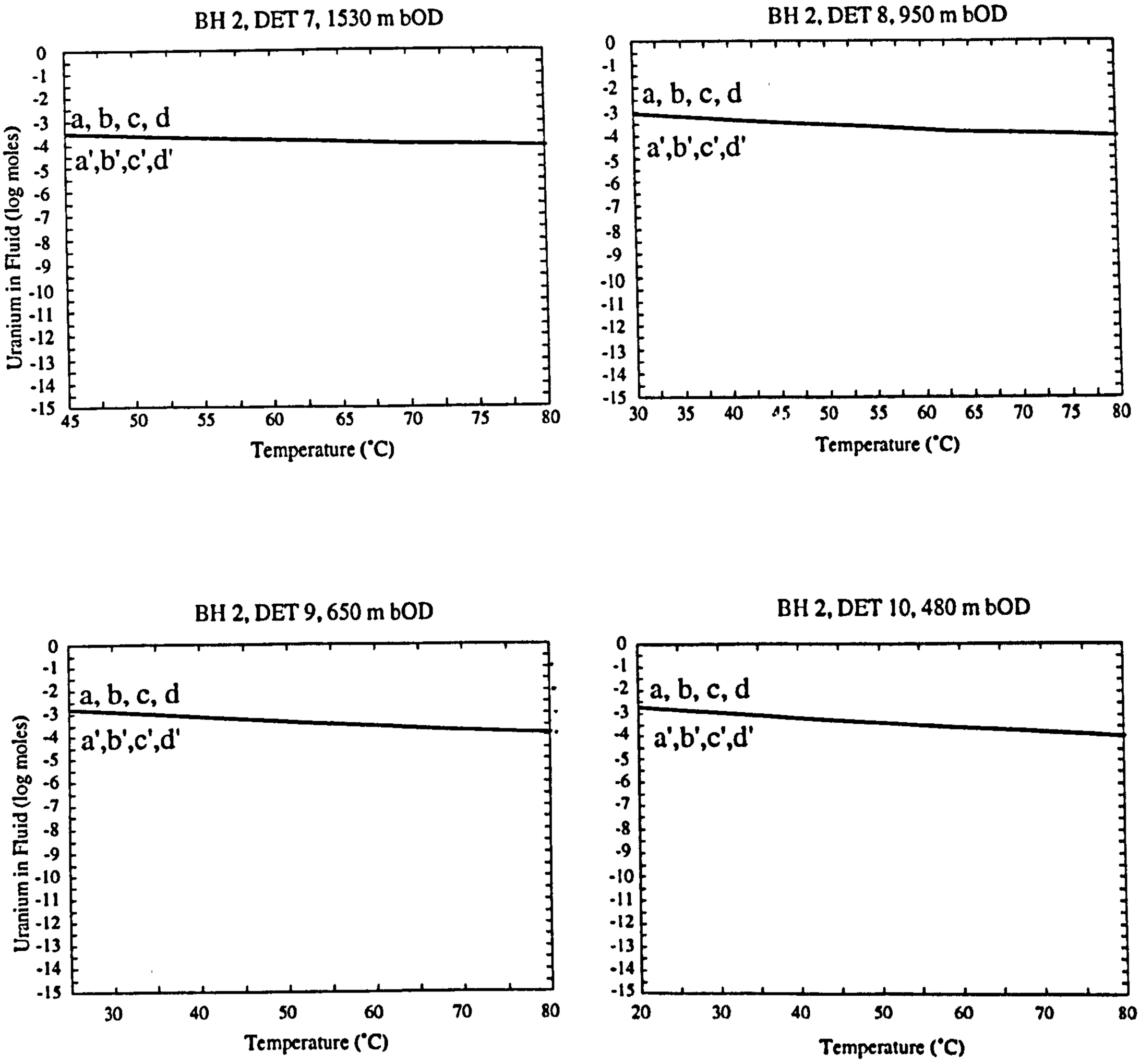

Fig. 5.14 Uranium concentration in near-field groundwater versus temperature for 4 equilibrium states, using method one to determine uranium solubility :

Enforced equilibrium with $UO_2(OH_2)$ (c,β) and UO_2 (am)

All analyses equilibrated with porlandite ($Ca(OH)_2$), with Calcite ($CaCO_3$) and Brucite ($Mg(OH)_2$) allowed to precipitate.

Detailed redox information of cases a,b,c,d,a',b',c',d' in table 5.6. Speciation and numerical breakdown in table 5.7.

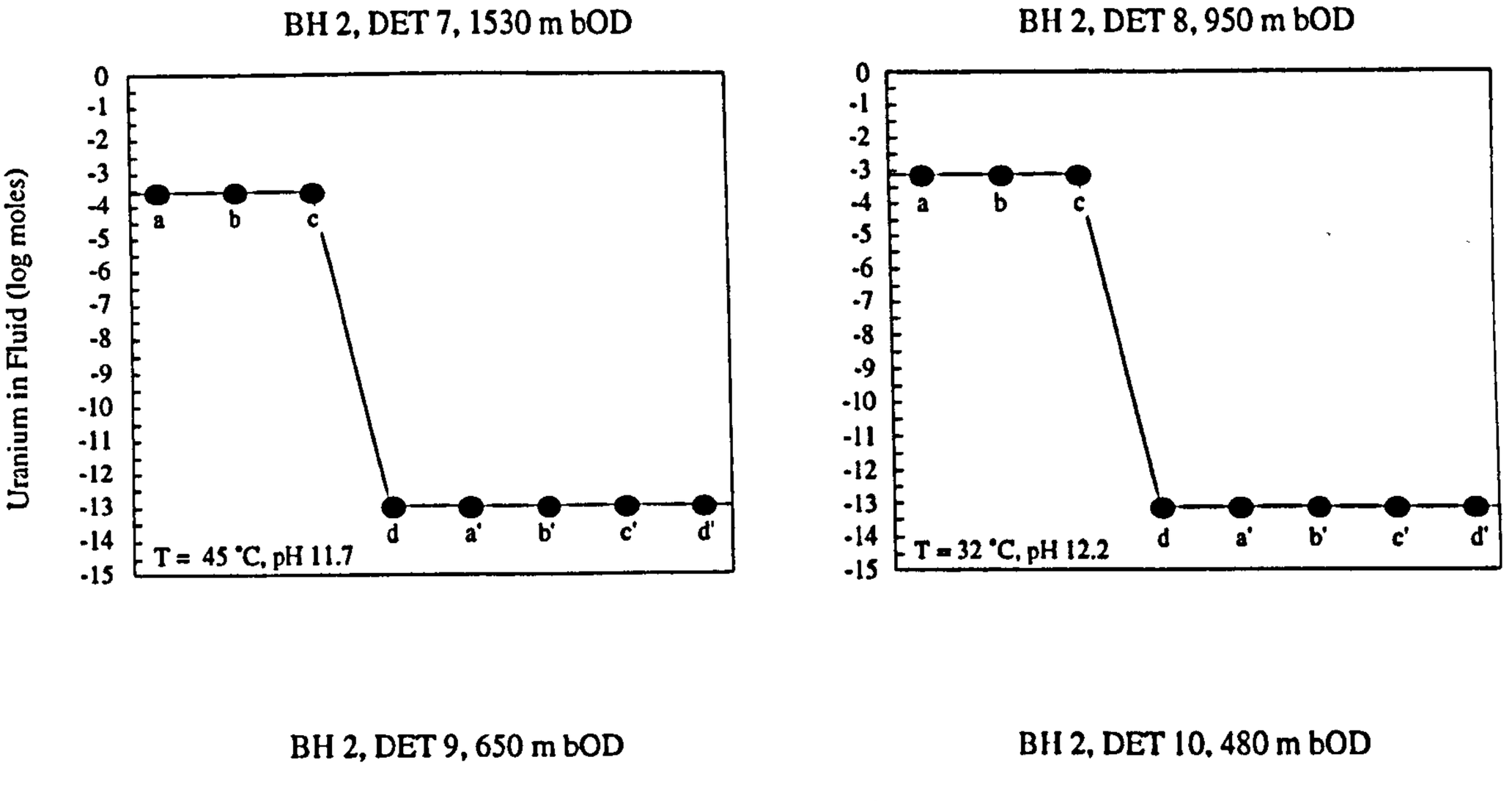

Fig 5.15 Uranium concentration in pseudo-near-field groundwater for 4 equilibrium states, and including interactions with steel using method two to determine uranium solubility :

Uranium concentration increased until Saturation Index (SI) indicates solid phase formation. This phase then used as solubility controlling stable phase.

For all a,b and c the solubility controlling stable phases were schoepite ($UO_2(OH_2) \cdot H_2O$) below 53°C and $UO_2(OH_2)$ (c,β) above 53°C. For all d cases the solubility controlling stable phase was uraninite (UO_2). For all a',b',c',d' cases the solubility controlling stable phase was uraninite.

Detailed redox information for cases a,b,c,d,a',b',c',d' given in table 5.6 and speciation and numerical breakdown in table 5.8.

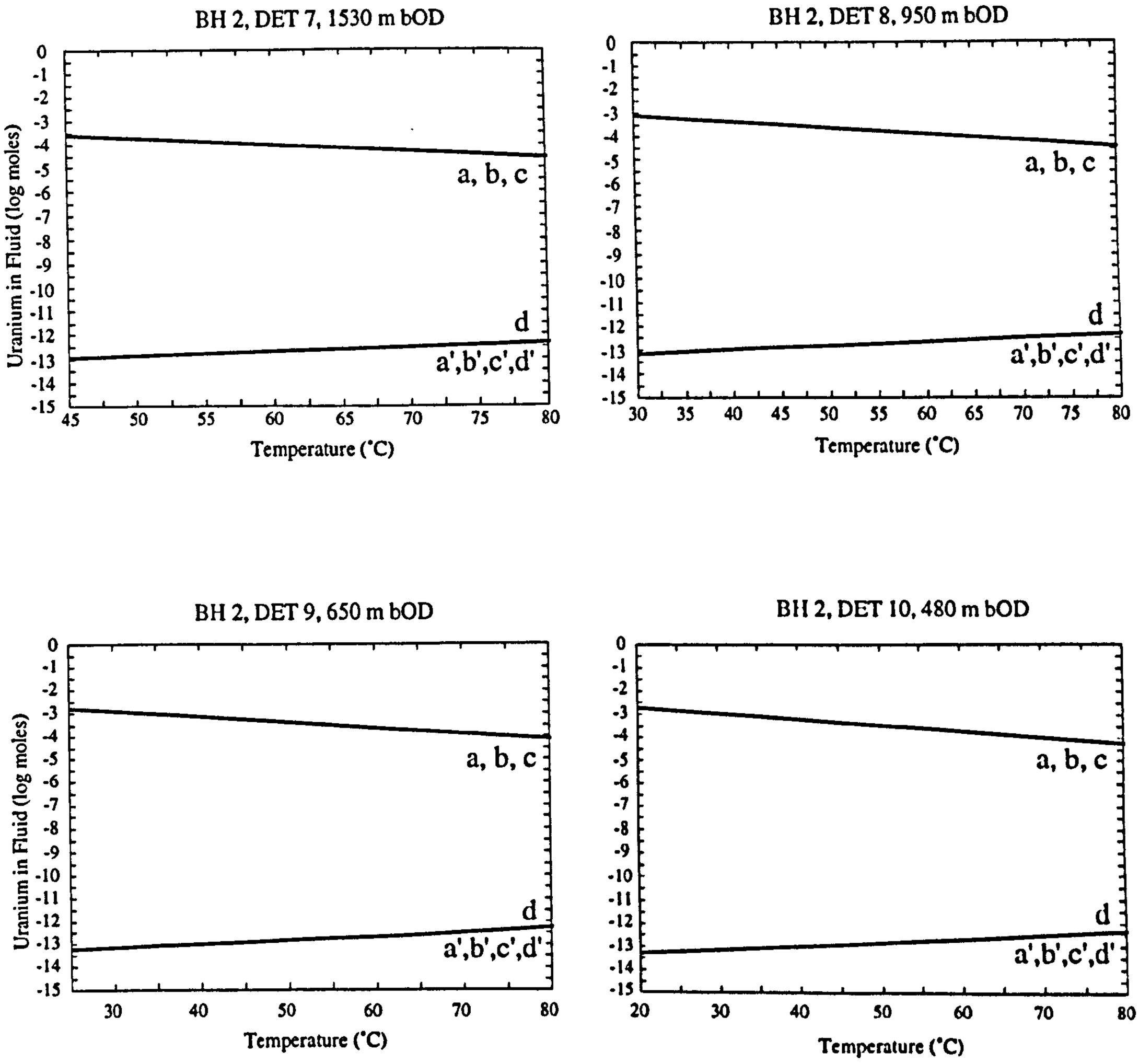

Fig. 5.16 Uranium concentration in pseudo-near-field groundwater versus temperature for 4 equilibrium states, and including interactions with steel using method two to determine uranium solubility :

Uranium concentration increased until Saturation Index (SI) indicates solid phase formation. This phase then used as solubility controlling stable phase.

For all a,b and c the solubility controlling stable phases were
schoepite ($UO_2(OH_2) \cdot H_2O$) below 53°C and $UO_2(OH_2)$ (c,β) above 53°C.
For all d cases the solubility controlling stable phase was uraninite (UO_2).
For all a',b',c',d' cases the solubility controlling stable phase was uraninite.

Detailed redox information for cases a,b,c,d,a',b',c',d' given in table 5.6 and speciation and numerical breakdown in table 5.8.

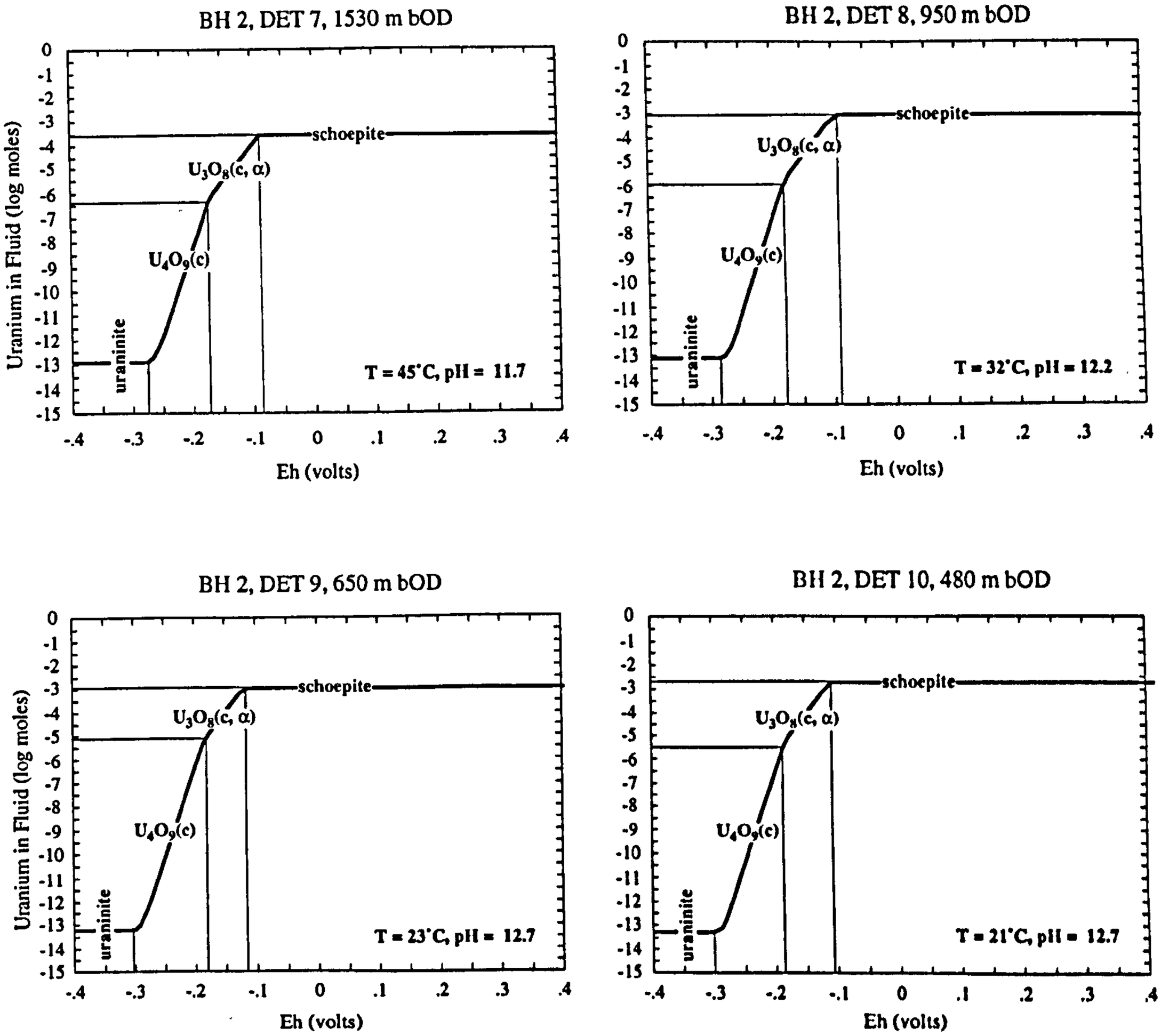

Fig. 5.17 Uranium concentration in pseudo-near-field groundwater versus Eh; modelling effect of steel degradation and subsequent Eh increase. Using method two to determine uranium solubility :

Uranium concentration increased until Saturation Index (SI) indicates solid phase formation. This phase then used as solubility controlling stable phase.

Solubility controlling stable phases were : uraninite (UO_2, U_4O_9(c), U_3O_8(c,α) and schoepite ($UO_2(OH_2) \cdot H_2O$).

All analyses equilibrated with porlandite ($Ca(OH)_2$), with Calcite ($CaCO_3$) and Brucite ($Mg(OH)_2$) allowed to precipitate. All cases equilibrated with native iron (Fe) before Eh increased to +0.4 V.
Water files taken from DET 7, 8, 9 & 10.

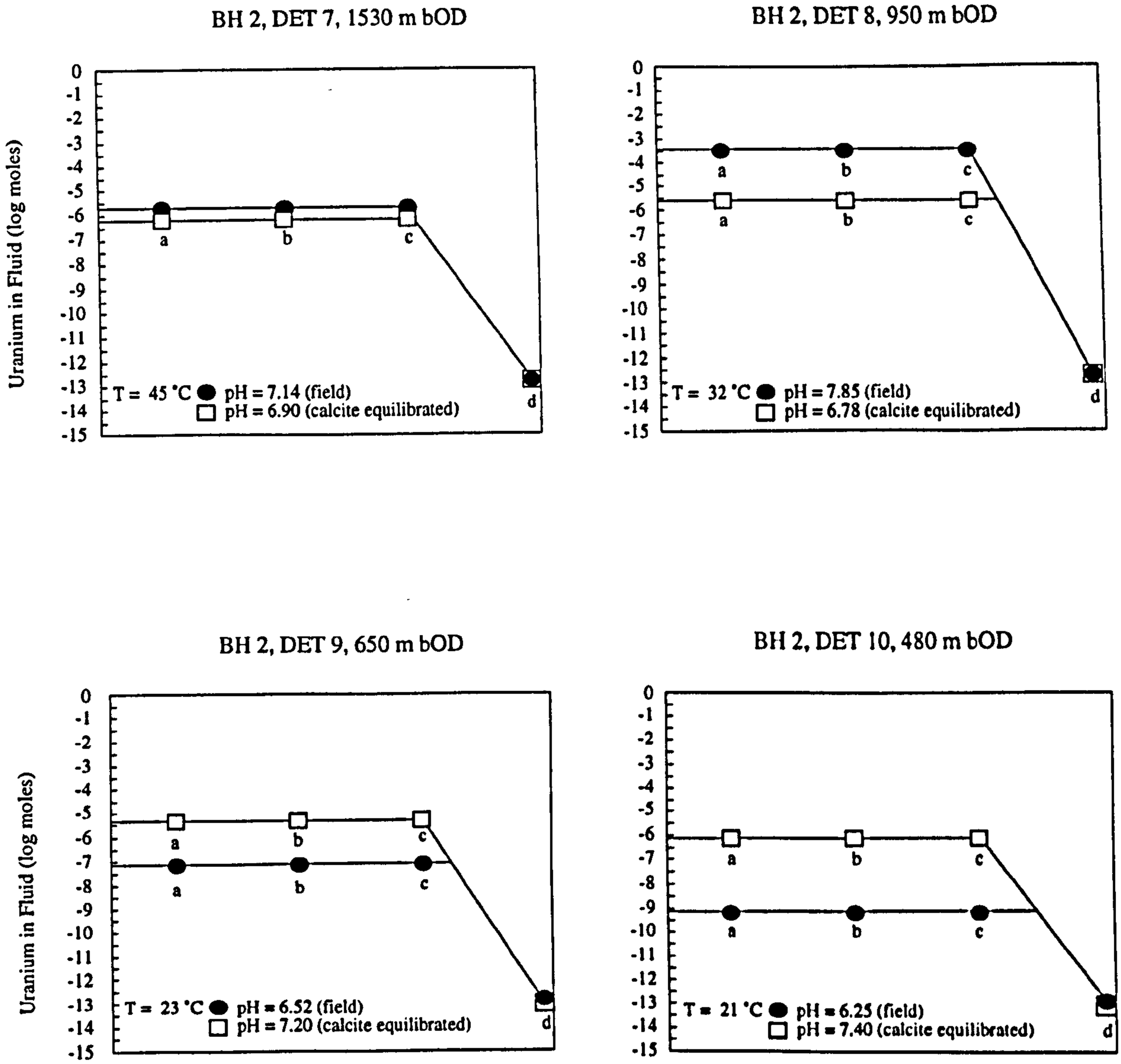

Fig. 5.18 **Uranium concentration in far-field groundwater for 4 equilibrium states, and two methods of constraining pH; either from field analyses or by equilibrating fluid with calcite. Method two was used to determine uranium solubility , i.e. uranium concentration increased until Saturation Index (SI) indicated solid phase formation. This phase then used as solubility controlling stable phase. For all a,b and c cases the solubility controlling stable phase was U4O9(c) For all d cases the solubility controlling stable phase was uraninite (UO2). Water files taken from DET 7, 8, 9 & 10. Cases a, b, c & d as described in text and previous tables.**

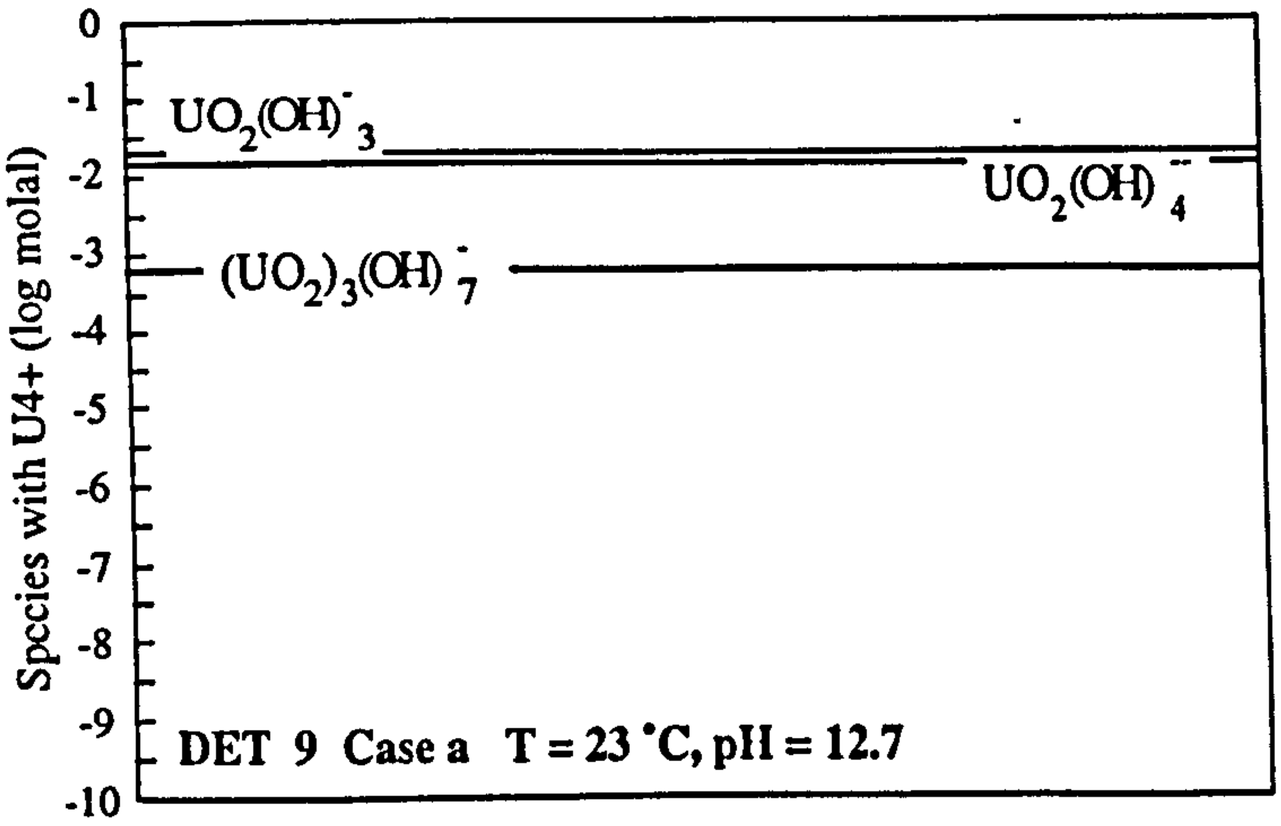

Fig. 5.19a Uranium speciation in pseudo-near-field groundwater for equilibrium state case a, including anionic uranyl hydroxide species omitted from GWB database. Fluid in equilibrium with schoepite ($UO_2(OH_2) \cdot H_2O$), total uranium concentration = $10^{-1.4}$ M.

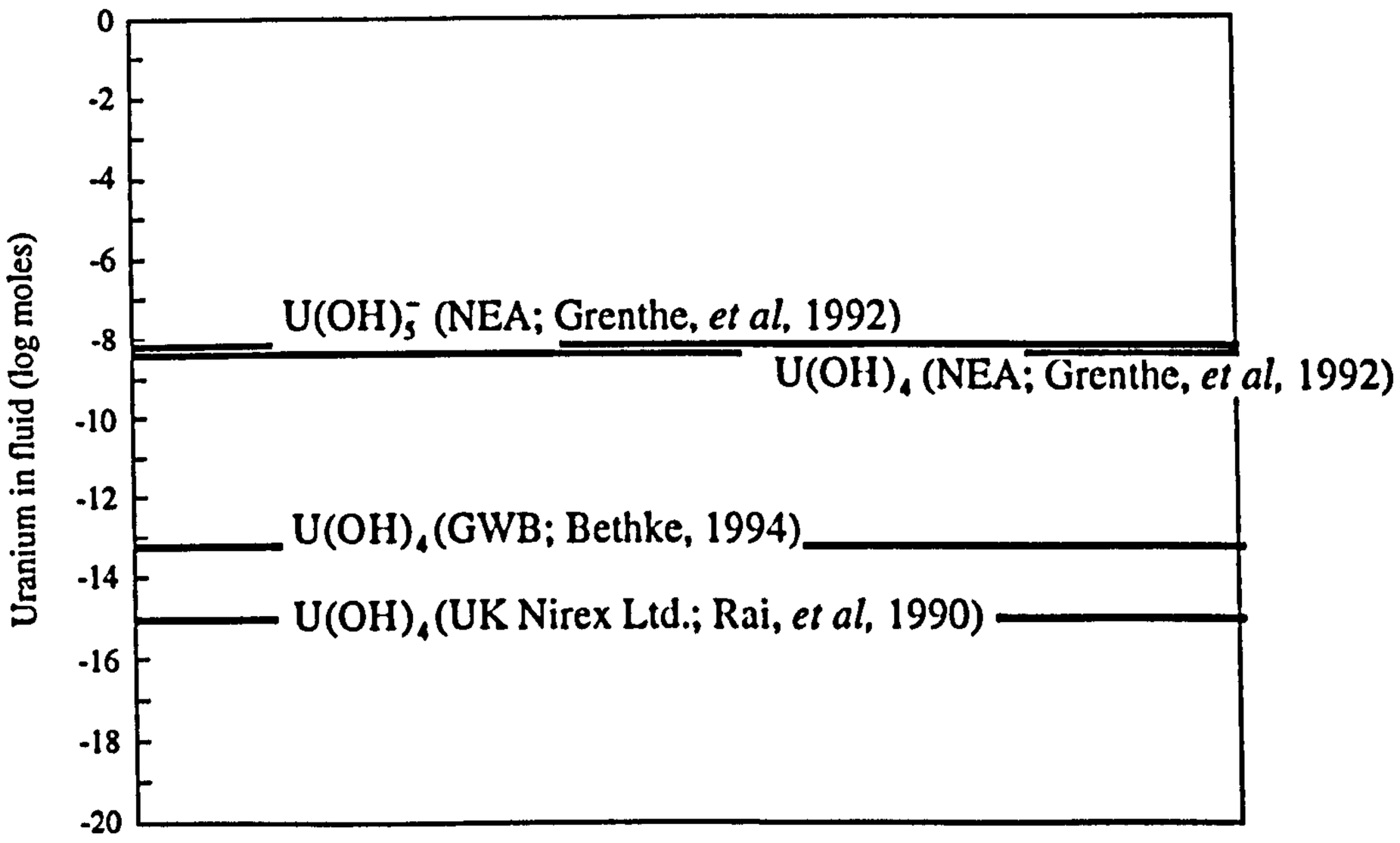

Fig. 5.19b Uranium speciation in pseudo-near-field groundwater for equilibrium state case *a'*, showing variation in uranium concentration due to variability in thermodynamic equilibrium constants used. Fluid in equilibrium with uraninite (UO_2).

UK Nirex Ltd.	Log K for $U(OH)_4$	= -12.00 (Rai, *et al*, 1990)
GWB	Log K for $U(OH)_4$	= - 8.53 (Bethke, 1994)
NEA	Log K for $U(OH)_4$	= - 4.53 (Grenthe, *et al* , 1992)
NEA	Log K for $U(OH)^-_5$	= -16.50 (Grenthe, *et al* , 1992)

When U^{4+} forms 100% of the species in solution variations in log K can cause increase in uranium solubility from 10^{-15} M to $10^{-8.1}$ M. If U^{6+} species are dominant such an increase would have insignificant contribution to overall uranium concentration.

A

Natural BVG groundwater

Case *a* DET 9, 23°C, pH 7.2, Eh +66 mV
redox disequilibrium allowed

B

BVG groundwater reacted with cement

Case *a* DET 9, 23°C, pH 12.7, Eh +66 mV
redox disequilibrium allowed

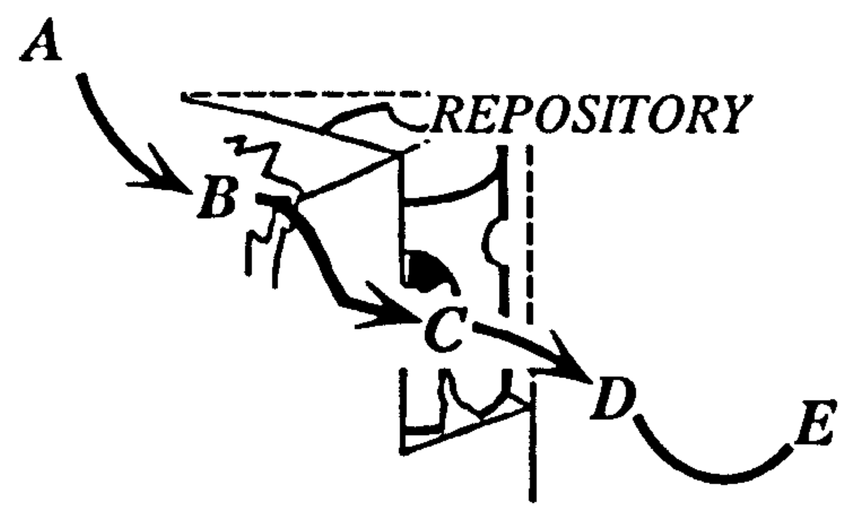

C

"Near Field"
BVG groundwater reacted with cement, steel barrels and uranium

Case *a'* DET 9, 80°C, pH 11, Eh -700 mV
redox disequilibrium allowed
uranium = $10^{-3.8}$ M

E

"Far field"

Case *a* DET 9, 23°C, pH 7.2, Eh +66 mV
redox disequilibrium allowed
uranium = $10^{-5.4}$ M

D

"Pseudo near field" Escaping uranium BVG groundwater reacted with cement, with and without steel barrels and uranium at 80°C

With steel Case *a'* DET 9, 80°C, pH 11, Eh -700 mV
redox disequilibrium allowed
uranium = 10^{-12} M

No Steel Case *a* DET 9, 80°C, pH 11, Eh +66 mV
redox disequilibrium allowed
uranium = 10^{-4} M

Fig. 5.20 **Summary of geochemical stages modelled, showing most probable scenarios for each stage. All stages are likely to display redox disequilibrium. pH ranged from 7.2 in the natural groundwater to 12.7 in the repository near field. Far field Eh was +66 mV. Near field Eh ranged from +66 mV to -700 mV, when interaction with steel was included. Steel-equilibrated, low Eh, "pseudo near field" scenarios provided the lowest uranium concentration of 10^{-12} M. Maximum uranium concentration at 80°C was $10^{-3.8}$ M in the high pH repository near field. Far field uranium concentration was $10^{-5.4}$ M. Variations in thermodynamic log K could increase calculated uranium concentration to $10^{-1.4}$ M (see text).**

Chapter 6 Conclusions, implications and further work

6.1 Conclusions

6.1.1 Review of aims

Before drawing some overall conclusions and indicating potential future work it is useful to review the research aims that were outlined in Chapter One. At the outset of this research study it was intended that the project would serve as an independent check on the potential strengths and failings of the currently proposed models of subsurface groundwater conditions at the potential site of the radioactive Intermediate Level Waste (ILW) repository proposed for Longlands Farm, adjacent to Sellafield in Cumbria.

To achieve this it was intended that published hydrogeological data would be used to construct mathematical models of groundwater movement that could be simulated numerically via a finite element, steady state fluid flow code, OILGEN (Garven, 1989). It was intended that the study would delineate the controlling parameters of fluid movement in the far-field, Potential Repository Zone (PRZ) and surface environments and determine the sensitivity of this natural groundwater system to perturbations. Calculation of possible rates of groundwater return were intended to allow elucidation of simple safety cases.

The geochemical properties of the in-situ repository groundwaters would be numerically modelled via a thermodynamic speciation/reaction path code, The Geochemist's Workbench™ (GWB) (Bethke, 1994), to determine the controls of groundwater chemistry by modelling geochemical fluid/rock interactions and redox states. Modelling the solubility of relevant radionuclides would allow a simple safety case to be presented.

6.1.2 Conclusions from fluid flow simulations

Both simple and complex numerical simulations of groundwater movement in the Sellafield area indicated that flow is dominantly topographically driven; descending from the 1000 m upland areas of the Lake District through the heavily faulted and fractured Borrowdale Volcanic Group (BVG) repository host rock before trending upward through the potential repository site at 650 mbOD. The faulted and fractured nature of the BVG contributed to the relatively fast rate of fluid return, as did the highly saline groundwaters found at depth to the west of the repository site.

Two decoupled, but connected, aquifer systems were shown to exist:- in the Calder Sandstone and in the BVG. Comparison of measured and calculated freshwater

hydraulic head enabled models which do not match in-situ measurements to be rejected. This process of calibration indicated that the best simulation is one where the BVG permeability was 1.2 m/yr (Fig. 6.1). This regional permeability when used in transient mass transport simulations, indicated that emergent repository fluids could return to the surface within 15,000 years. Safety case calculations indicated that the regional permeability of the BVG might be 1000 times too permeable to be simply declared safe (Fig. 6.2).

6.1.3 Conclusions from geochemical modelling

The most probable scenarios to be found in the natural and engineered geochemical environments at Sellafield are illustrated on Fig. 6.3. Simulations of natural BVG groundwater indicated that redox disequilibrium was prevalent, and the most probable Eh was relatively oxidising (+46 < Eh +92 mV). The Eh of the natural groundwater was not controlled by a sulphur redox couple or equilibrium with reduced iron minerals.

In the artificially engineered repository "near field", depending on the method used to determine solubility, uranium concentration was calculated to be as low as 10^{-13} M and as high as $10^{-2.7}$ M. This maximum value was around 600 times the laboratory-derived value used in UK Nirex Ltd. safety assessment studies.

Oxidising natural groundwaters will be entrained into the repository and will destroy the steel barriers engineered to retain uranium. UK Nirex Ltd. estimated that the steel barrels would last 10, 000 years. However, such calculations assumed a chemically reducing environment. Given the oxidising nature of the natural groundwater this is likely to be a considerable overestimate. Uranium concentration in the "far field", rock distant from the repository, was calculated to be to be as high as $10^{-5.4}$ M.

6.1.3 Overall conclusions

The results from the simulations of fluid flow in thesis have shown, that given the present understanding of the regional, and local, hydrogeology at Sellafield;

- the proposed repository at 650m bOD is in a poor position where flow directions in the BVG are towards the surface, and will need to be counteracted;
- the BVG might be 1000 times more permeable than a simple safety threshold
- radioactive material released from a repository could reach the surface in less than 15,000 years;

- natural groundwater conditions in the BVG are oxidising; this will promote the rapid degradation of the steel repository barriers engineered to retain uranium;

- the solubility of uranium in the high pH repository "near field" is high; a maximum of 600 times greater than the value currently used in simulations of repository safety. Uranium solubility in the "far-field" would also be significant.

6.2 Implications

The modelling in this thesis utilised the data obtained from one of the most comprehensive, and expensive, suites of geological and hydrogeological investigations ever undertaken in the UK. The simulations have shown that given the current understanding of the site's geology, hydrogeology and hydrochemistry there is no scientifically sound reason for selecting Sellafield in Cumbria as the site of the final resting place for radioactive waste that will be lethal for millions of years.

The Sellafield site is geologically complex, the natural water flow is upwards and rapid, the natural geochemical environment is unsuitably oxidising and the engineered barriers would be destroyed relatively quickly. Uranium solubility was shown to be much higher than that assumed in assessments of the site's safety. Therefore, the results presented in this thesis indicate that;

- a great deal more non-intrusive data gathering, simulation and evaluation should be undertaken before any decision be made regarding the building of the underground rock laboratory or the repository itself;

- improved hydrogeological data might provide information that could explain the high hydraulic heads at depth in the BVG and could provide direct measurements of regional permeability;

- more accurate estimates of uranium solubility need to be used in repository safety case assessments, the ambiguities resulting from differing thermodynamic databases need to be resolved;

- if a safety case cannot be successfully achieved after all of the extra data gathering, simulation and interpretation, the Sellafield site should be deemed unsuitable and UK Nirex Ltd. should direct their interests elsewhere.

6.3 Further work

Work outlined elsewhere (Chapter 5) demonstrates that it was possible to use simple geochemical speciation and reaction path simulation codes to develop an understanding of the geochemistry of the groundwaters in the Sellafield area. The effects of the in-situ fluids upon repository conditions and solubility of radionuclides was also presented.

Further work that would be pertinent to this study would be the development of coupled fluid flow and reaction transport simulations of the regional groundwater regime of the site to assess the retardation effects of the fractures in the geological formations both in terms of chemical interactions of unpolluted groundwater and the possible retention of radionuclides. Such work is the next step in many studies of groundwater movement (Lichtner, 1985; Lichtner, 1993; Raffensperger & Garven, 1995; Steefel & Lasaga, 1994; Yeh & Tripathi, 1989) and could provide essential information relevant to a safety case assessment

Further 2-D fluid flow simulations could look at larger scales of groundwater flow, (hundreds rather than tens of kilometres). This would be useful in elucidating if the boundary conditions to the model described above have an effect on the flow i.e.; would extending the depth of the model alter the flow path; would extending the western extent alter the particle path and would extending the eastern extent provide greater hydraulic gradients as the higher Lakeland Hills are included.

Simulations of flow through fractures, rather than average matrix permeability, may be appropriate, although this could prove unfeasible in terms of constraints on measured input data and computing ability.

6.4 References

Bethke, C.M. (1994) *The Geochemist's Workbench; a users guide to Rxn, Act2, Tact, React and Gtplot.* University of Illinois, Urbana-Champaign, USA, 213 pp.

Garven, G. (1989) A hydrogeologic model for the formation of the giant oil sands deposits of the Western Canadian sedimentary basin. *American Journal of Science*, **289**, 105-166.

Lichtner, P.C. (1985) Continuum model for simultaneous chemical reactions and mass transport in hydrothermal systems. *Geochimica et Cosmochimica Acta*, **49**, 779-800.

Lichtner, P.C. (1993) Scaling properties of time-space kinetic mass transport equations and the local equilibrium unit. *American Journal of Science*, **293**, 4, 257-296.

Raffensperger, J.P. & Garven, G. (1995) The formation of unconformity-type uranium deposits. 2 Coupled hydrochemical modeling. *American Journal of Science*, **295**, 639-696.

Steefel, C.I. & Lasaga, A.C. (1994) A coupled model for transport of multiple chemical species and kinetic precipitation/dissolution reactions with applications to reactive flow in single phase hydrothermal systems. *American Journal of Science*, **294**, 5, 529-592.

Yeh, G.T. & Tripathi, VS. (1989) A critical evaluation of recent developments in the hydrogeochemical transport models of reactive multichemical components. *Water Resources Research*, **25**, 1, 93-108.

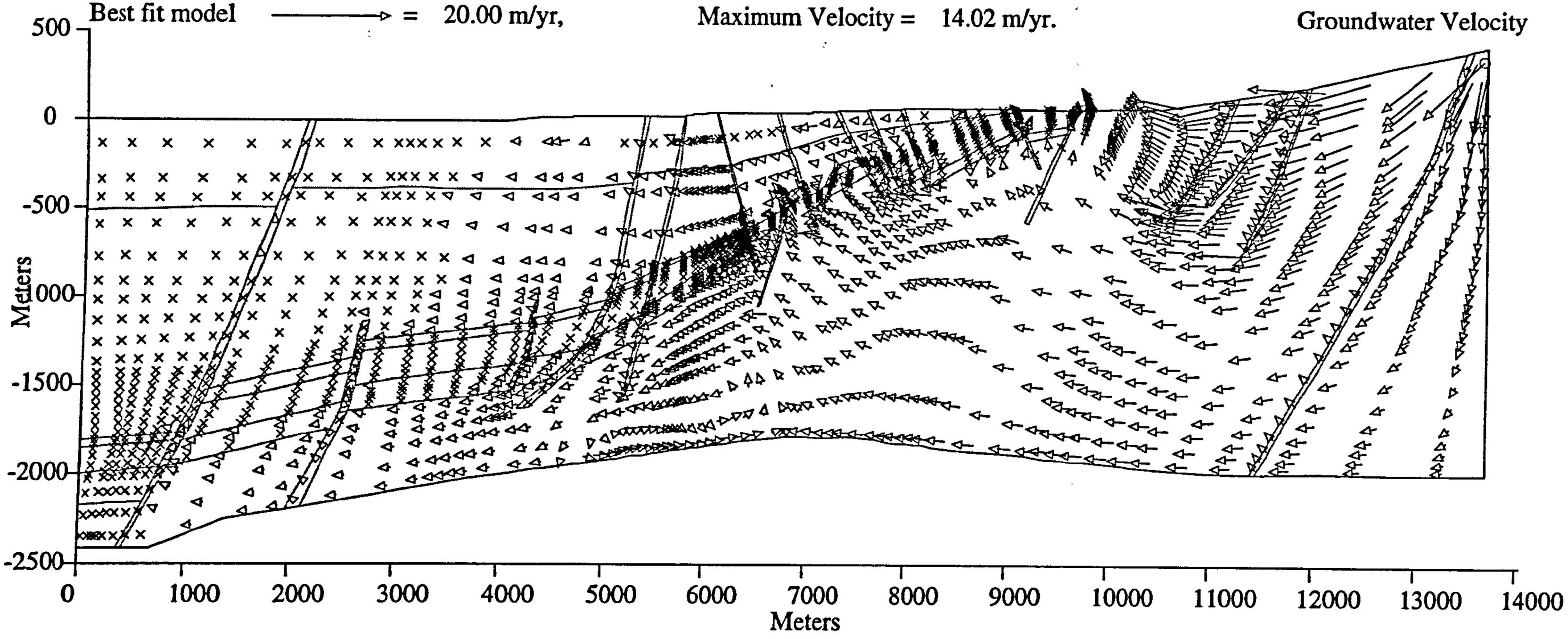

Fig. 6.1 Comparisons of calculated and measured hydraulic head provided a "best fit" regional permeability value of 1.20E+00 m/yr. When the BVG hydraulic conductivity was set to this value the flow rate is relatively rapid, with the maximum in the BVG. Topographically driven groundwater from upland areas travels downwards in the BVG before ascending, via the potential repository, towards the surface. Brines at depth to the west of the repository cause upward deflection of groundwater. If BVG regional permeability = 1.20E+00 m/yr radioactive material could reach the surface in less than 15,000 years.

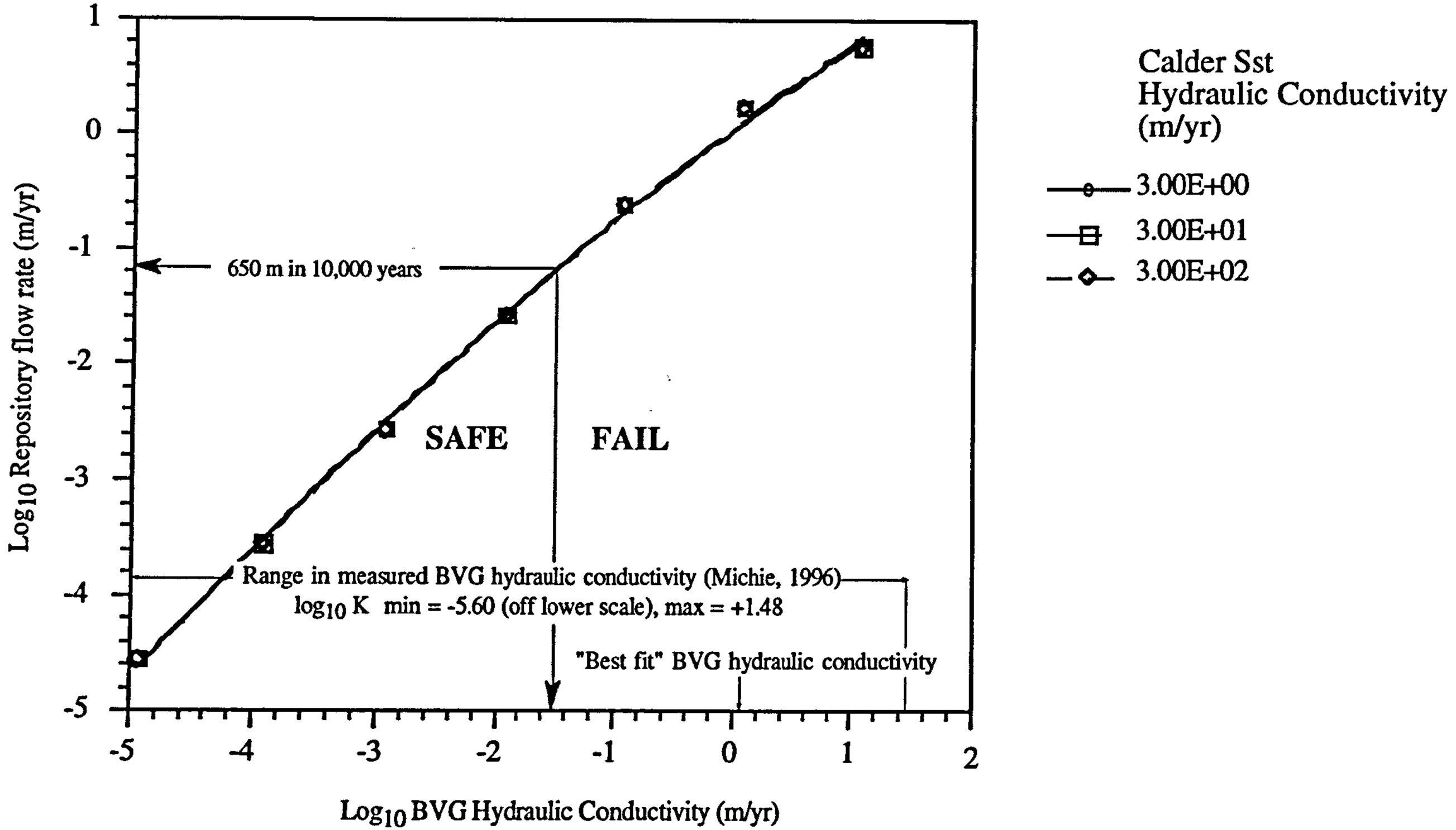

Fig. 6.2 **Graph of $\log_{10}$ repository flow rate vs $\log_{10}$ BVG hydraulic conductivity (log K). Simulations with varying Calder Sst. K superimposed. If BVG hydraulic conductivity > 0.03 m/yr (log K > -1.5) then safety case is failed. BVG maximum measured hydraulic conductivity = 30 m/yr (log K = 1.48), (Michie, 1996), a factor of 1000 times greater than safe/fail boundary. Therefore reasonable for BVG regional hydraulic conductivity to be 0.03 m/yr. BVG hydraulic conductivity producing "best fit" comparison between measured and calculated head falls within fail region (K = 1.2 m/yr, log K = 0.08).**

A

Natural BVG groundwater

Case *a* DET 9, 23°C, pH 7.2, Eh +66 mV
redox disequilibrium allowed

B

BVG groundwater reacted with cement

Case *a* DET 9, 23°C, pH 12.7, Eh +66 mV
redox disequilibrium allowed

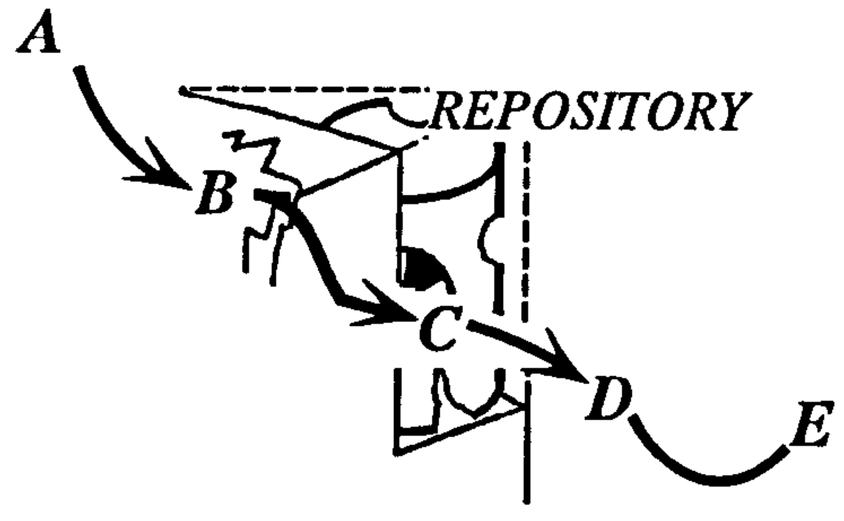

C

"Near Field"
BVG groundwater reacted with cement, steel barrels and uranium

Case *a'* DET 9, 80°C, pH 11, Eh -700 mV
redox disequilibrium allowed
uranium = $10^{-3.8}$ M

E

"Far field"

Case *a* DET 9, 23°C, pH 7.2, Eh +66 mV
redox disequilibrium allowed
uranium = $10^{-5.4}$ M

D

"Pseudo near field" Escaping uranium BVG groundwater reacted with cement, with and without steel barrels and uranium at 80°C

With steel Case *a'* DET 9, 80°C, pH 11, Eh -700 mV
redox disequilibrium allowed
uranium = 10^{-12} M

No Steel Case *a* DET 9, 80°C, pH 11, Eh +66 mV
redox disequilibrium allowed
uranium = 10^{-4} M

Fig. 6.3 **Summary of geochemical stages modelled, showing most probable scenarios for each stage. All stages are likely to display redox disequilibrium. pH ranged from 7.2 in the natural groundwater to 12.7 in the repository near field. Far field Eh was +66 mV. Near field Eh ranged from +66 mV to -700 mV, when interaction with steel was included. Steel-equilibrated, low Eh, "pseudo near field" scenarios provided the lowest uranium concentration of 10^{-12} M. Maximum uranium concentration at 80°C was $10^{-3.8}$ M in the high pH repository near field. Far field uranium concentration was $10^{-5.4}$ M. Variations in thermodynamic log K could increase calculated uranium concentration to $10^{-1.4}$ M (see text).**

EARTHWORKS

A model approach to radioactive waste disposal at Sellafield

R. S. Haszeldine* and C. McKeown
Department of Geology and Applied Geology, University of Glasgow, Glasgow G12 8QQ, Scotland, UK

ABSTRACT

One of the great environmental problems of our age is the safe disposal of radioactive waste for geological time periods. Britain is currently investigating a potential site for underground burial of waste, near the Sellafield nuclear plant. Future leakage of radionuclides depends greatly on subsurface water flows; these must be understood from the past, to predict hydrogeology 10^4–10^5 years into the future. We have taken information from the present-day, published by the government company Nirex, and used a finite-element steady-state fluid flow computer code to examine water flows in the subsurface. We find that flow directions at the planned Repository are persistently upwards, and that geologically significant flow rates could occur. Flow rates are particularly sensitive to uncertainties of rock permeability (conductivity) measurements made from site investigation boreholes. The hydrogeology at this site needs longer term investigation before a confident and credible prediction can be made.

Terra Nova, **7**, 87–95, 1995.

INTRODUCTION

When choosing a suitable Repository site, the pattern and rate of underground water flow must be both predictable, and safe for geologically long times into the future. The diverse geological factors affecting such predictions, and some of their difficulties of measurement and forecasting have been reviewed by Chapman (1994). At the Sellafield site (Fig. 1), an aquifer of Calder Sandstone is at and below sea-level and unconformable onto 1000 m crystalline hills of the Borrowdale Volcanic Group (BVG). Nirex plan to site their nuclear waste Repository at 650 m below sea-level (Fig. 2) in a unit of the BVG which is unconformably overlain by sediments (Nirex, 1993b). This is a variant of a long-recognized proposal for underground disposal (Bredehoeft and Maini, 1981), which implicitly relies upon the adequate present-day description and reliable forecasting of the subsurface hydrogeological conditions. The geology and hydrogeological investigations of this Sellafield site are summarized by Nirex (1992, 1993a, 1993b), who recognized the possibility that the regional flow pathways surrounding the proposed Repository would be directed upwards (Nirex 1993b, fig. 13). Similar views have also been reached by ERM (1993), RWMAC (1994), and Royal Society (1994). However, none of these studies have published simulations to support their work, or attempted to quantify the flow rates and pathways involved. In 1992 when we commenced our own work, our intuitive expectation for subsurface water flows at this Sellafield site, was that meteoric water flow, driven by gravity, would move westwards through the proposed Repository site and possibly return upwards towards the surface. We have taken published data and used a finite-element computer code to: (i) *confirm* our expectation; (ii) obtain a *visualization* of the flow directions and patterns; (iii) obtain an indication of flow pattern *robustness*; (iv) examine the *sensitivity* of flow magnitudes to changes in conductivity. Examine the discharge *pathways* taken by water after contact with a Repository. Absolute flow magnitudes cannot be proved, verified, or validated by such single models (Konikow and Bredehoeft, 1992; Oreskes *et al.*, 1994). However, we see value in producing pictorial representations of flow directions which persist throughout the measured range of present-day permeabilities, and value in producing a numerical safety target which can be compared to field measurements.

APPROACH

At this site, there are good data on rock stratigraphy and geometry. However, there are many poorly known factors, such as hydraulic conductivity anisotropy, fault conductivity, and particularly the regional-scale conductivity of the BVG away from the boreholes. We know from borehole (B/H) data that the BVG has a fracture conductivity, some 10^2 greater than

*Correspondence—Tel: +44/ 141339 8855; fax: + 44 141330 4817; E-mail: rsh@geology.glasgow.ac.uk

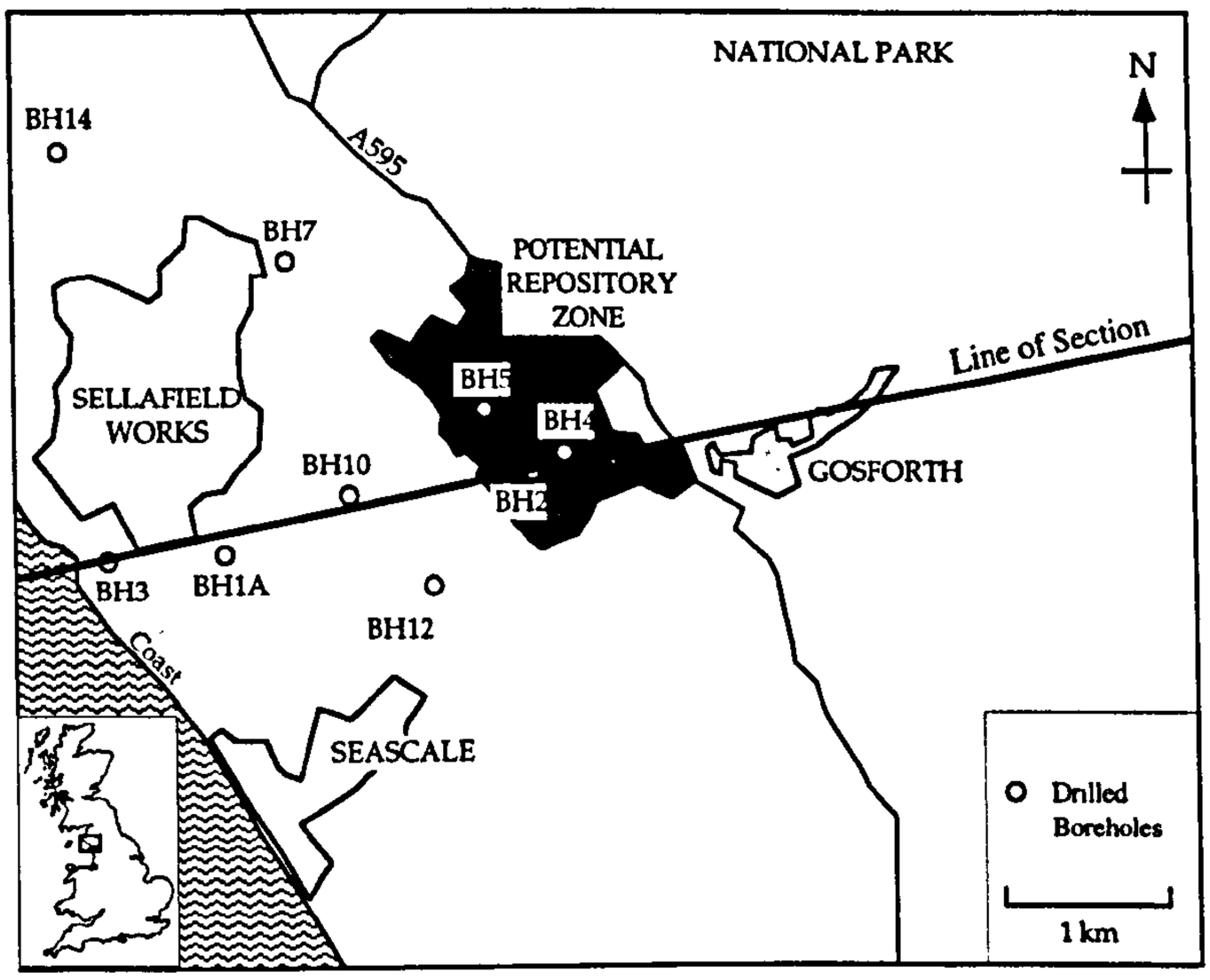

Fig. 1. *Location map of Sellafield on coastline of NW England. Locations shown for Nirex site investigation boreholes (Nirex, 1992, 1993a) Line of section in Fig. 2 starts SW of B/H 3, passes through it and B/H 2, and finishes NE on the 1000 m hills of BVG meta-volcanics.*

matrix conductivity (Nirex, 1992, 1993a,b), as do most crystalline rocks (Clauser, 1992) For the purposes of our modelling, we note from borehole measurements (Nirex, 1992, 1993a,b) that fluid flow in the BVG is controlled by fractures, which have a spacing of 50–100 m vertically. This is at least one fracture per finite element of our mesh, so that this can be treated as a matrix conductivity (Neumann, 1990).

Our approach then becomes one of testing sensitivity to different variables, by means of undertaking a series of experiments with the computer model. Before each simulation, we can vary one numerical attribute of the model. Running the model enables us to see if the result has changed from the previous experiments. If the result has not changed significantly, then that particular attribute was not important. If the result has changed, then it is important to measure that attribute as accurately as possible in the real world.

MODELLING

A geological cross-section was selected, to run SW–NE through the Repository, passing through site investigation boreholes 3 and 2, and close to B/H 1, 10, 4 (Fig. 1). This section has been extended by us both seaward and landward (Fig. 2), using public geological and topographical information Taylor *et al.* (1971). Similar sections were used by Nirex (1992, 1993a,b). The section was converted to a series of rows and columns, forming a finite element mesh of 2100 quadrilaterals (Fig. 2b), whose spatial co-ordinates were entered into a Silicon Graphics personal Iris computer workstation. The simulation code used was OILGEN, written by Grant Garven and described in detail elsewhere (Garven and Freeze, 1984; Garven, 1989). This is a generic code, formulated to study water movement in large sedimentary basins over geological time spans. The code uses a finite element mesh to iteratively solve equations of flow, based on Darcy's Law of single phase, steady-state fluid flow through a porous medium. Fluid pressure, temperature, and concentration (salinity) are coupled equations. Vector flows are calculated as average linear velocities, which are constant over individual elements, but discontinuous across element boundaries. The lower boundary of the model is impermeable to fluid flow, but allows a constant geothermal input. The upper (land) surface is the topography, so that flow can pass up or down through this. The topographically derived head of pressure is the major driving force for flow, although density induced flows are also permitted. Lithological boundaries within the mesh have no special qualities, and flow simply crosses between elements of different porosity and permeability. The lateral (vertical) boundaries to the section are impermeable to fluid flow. The code iterates until convergence of temperature change reaches less than 1 °C. Output from the code is a numerical data tabulation, which can be interrogated for each node. A graphics code displays the information visually. We have used measured data from site investigation boreholes (Table 1). Our hydraulic conductivity units are ma^{-1}, and we have simplified to ignore any variations in conductivity due to water salinity. The Repository was considered as normal BVG rock, with no additional conductivity or heat production, our assumptions will tend to reduce the circulation of water. During our modelling, the BVG conductivity range was found to be an important control of fluid flow, consequently we simulated BVG data 100 × greater and 10 × less than that actually measured, to give a wider context for interpretation. Initially, five suites of experiments were run, each time varying only one attribute of the model: salinity, fault conductivity, conductivity anisotropy of the matrix, Calder Sandstone conductivity, BVG conductivity. The last two attributes proved to be the most sensitive, so that a further 32 experiments were run to investigate their variation.

The measured salinity framework was found to be a crucial attribute. A brine 'pluton' in the lower west of the section forces westward-directed flows upwards towards the surface. The position of brine is reasonably well established from B/H data, so that all subsequent experiments were run including a brine 'pluton'. Fault conductivity was examined separately

for faults cutting sediments, and for faults cutting the BVG. Changing fault conductivities for all measured values produced an insignificant change in flow through the Repository.

Subsequent models used 3.0×10^{-1} ma^{-1} for sediments, and $1.3 \times 10^{+0}$ ma^{-1} for the BVG. Anisotropy was examined by changing the BVG horizontal:vertical conductivity from 5 to 1. Surprisingly, flow through the Repository was little affected. This suggests that the direction and rate of flow in the BVG is not controlled by the shape of our finite-element cells, and that the cross-sectional area of the BVG is so large that fracture orientation may have little importance in the real world. Subsequent models used a BVG anisotropy of 5.

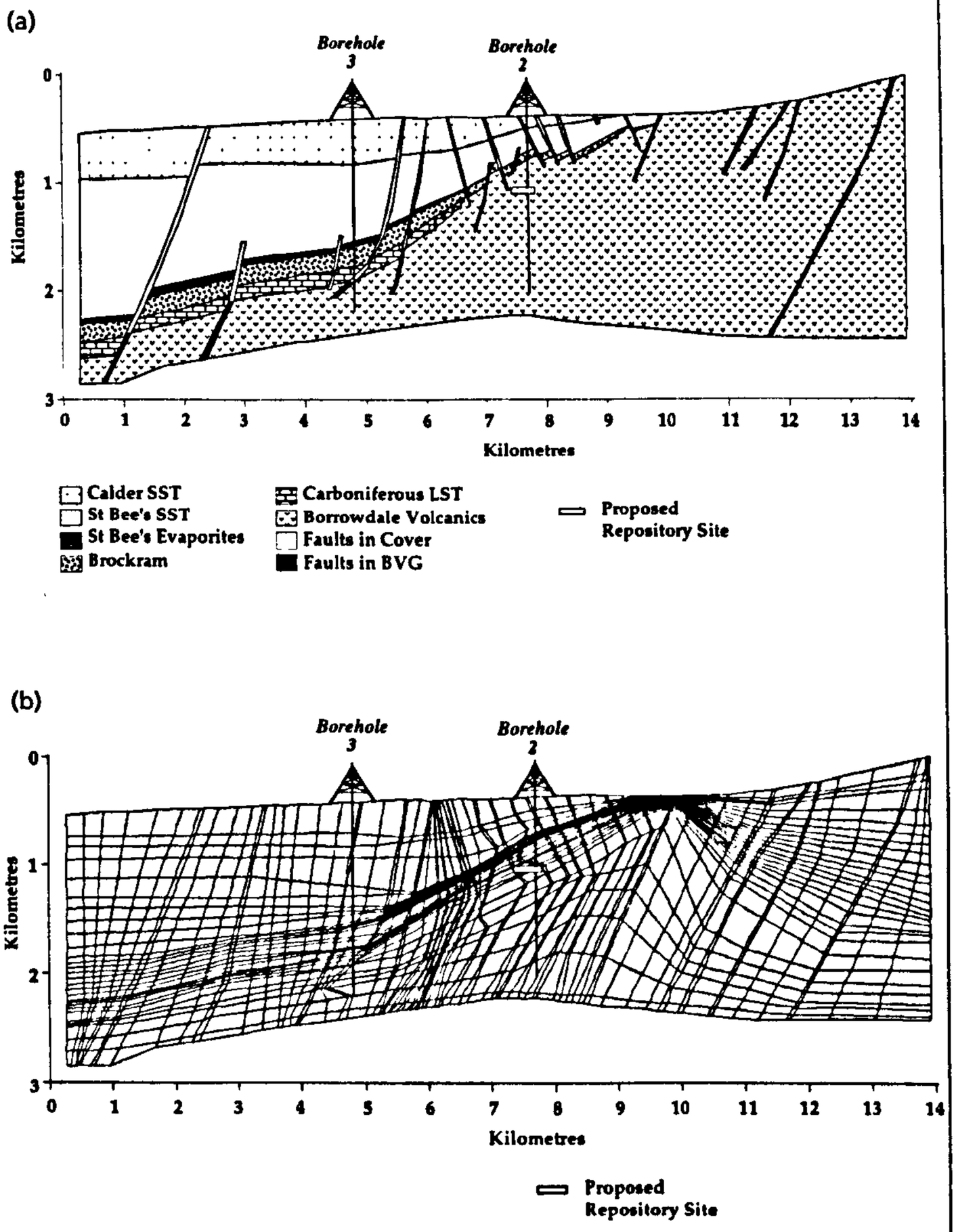

Fig. 2. *(a) Geological cross-section of the proposed Repository site at 650 m, compiled from published information by Nirex (1992, 1993a), and extended SW and NE using publically available geological information (Taylor* et al., *1971). Line of section is similar to that shown in Fig. 1. The crystalline meta-volcanics of the Borrowdale Volcanic Group rise to 1000 m elevation in the Lake District, and fall westwards to lie well below sea-level. This elevation provides a topographical drive for meteoric water flow through any fracture or matrix conductivity in the BVG. Carboniferous to Triassic sediments onlap the BVG, and provide a series of matrix and fracture permeable aquifers. (b) Finite element mesh derived from Fig. 2a, and used in fluid flow simulations to give an accurate representation of the geology. Each element of the mesh can have discrete physical properties. Each lithology is a distinct hydro-stratigraphical unit, with identical porosity and conductivity values throughout. There are no barriers to flow between units.*

Graphical outputs visually illustrate the results of selected modelling experiments (Figs 3, 4). Each section mimics the stratigraphy, rock geometry and faults in the area. The different rock layers or faults are assigned different porosity and conductivity attributes, uniform to each rock type. Faults were treated by modelling artificially wide quadrilaterals, but with correspondingly reduced conductivity. Consequently, the measured area: conductivity relationship remains intact. For example, a real fault 10 m wide, 1 ma^{-1} conductivity, is modelled as 100 m wide, 10^{-1} ma^{-1} conductivity. BVG anisotropy (horizontal:vertical conductivity) was set at 5 for all experiments. Specific salinity values were taken from B/H 2 (saline 2%), and B/H 3 (brine 20%). These were entered as a linear vertical gradient of $\%NaCl.m^{-1}$ from a datum point measured in metres from the base of the section. To accommodate lateral variations of salinity, the code was modified to enable data files of salinities to be assigned to specific nodes on the finite element mesh. The overall salinity pattern was to mimic a 'pluton' of brine salinity in the lower left of the section, as derived from field measurements in B/H 3, 1, 10, 12, 5, 2, 4 (Nirex, 1992, 1993a). The groundwater directions are displayed by arrows, and it is important to note that fluid velocity is proportional to the length of the arrow of the fastest velocity on that particular plot, i.e. each different plot has a different arrow length scale. Crosses indicate that flow is less than 1% of the maximum for that plot, so that water could still be moving, but relatively slowly.

RESULTS: FLOW PATTERNS AND RATES

Calder Sandstone conductivity was

Table 1. Numerical values of hydraulic conductivity and porosity used during the modelling experiments for different rock units, taken from Nirex (1992, 1993a) Anisotropy values were chosen by us, with background information from Nirex. Measured conductivity units of ms^{-1} were converted to ma^{-1}, through multiplying 31×10^6. Permeability in milli Darcies shown to enable easy comparison with oil industry data sets (3.28 mD = approx. 1 ma^{-1}).

Stratigraphic Unit	Hydraulic Conductivity K (ma^{-1})	Intrinsic Permeability k(milli Darcies)	Porosity ϕ (%)	Anisotropy ($K_{horiz}/K_{vertical}$)
Calder Sandstone	$3.0 \times 10^{+0}-3.0 \times 10^{+2}$ (log mean) (log mean)	$1.0 \times 10^{+1}-1.0 \times 10^{+3}$	20	10
St Bee's Sandstone	4.2×10^{-1} (log mean)	$1.4 \times 10^{+0}$	12	30
St Bee's Evaporites	1.6×10^{-3} (log mean)	5.2×10^{-3}	1	100
Brockram	9.46×10^{-4} (log mean)	3.1×10^{-3}	8	100
Carboniferous Limestone	1.5×10^{-1} (log mean)	4.9×10^{-1}	1	50
Borrowdale Volcanics	$1.2 \times 10^{-4}-1.2 \times 10^{+0}$	$4.0 \times 10^{-4}-4.0 \times 10^{+0}$	1	5
Faults in cover sequence	$3.0 \times 10^{+2}$ (log mean)	$1.0 \times 10^{+3}$	20	1
Faults in Borrowdale Volcanic Group	$1.2 \times 10^{+0}$	$4.0 \times 10^{+0}$	20	1

varied from $3.0 \times 10^{+1} - 3.0 \times 10^{+2}$ ma^{-1}, whilst keeping BVG conductivity constant. Flow rates in the sandstone related directly to conductivity, although patterns remained similar (Fig. 3a,b). Surprisingly, in each case, the flow through the Repository remained constant. This important result indicates that the Calder Sandstone and BVG aquifers are de-coupled.

BVG conductivity was varied from $1.2 \times 10^{-5}-1.2 \times 10^{+2}$ ma^{-1}, holding the Calder Sandstone conductivity constant for four cases from $3.0 \times 10^{+0}-3.0 \times 10^{+2}$ ma^{-1}. In these 32 experiments, flow rate through the Repository is directly related to BVG conductivity. Absolute flow rate in the Calder Sandstone is not affected, but becomes visually less important on Fig. 4a,b. The pattern of flow direction remains similar in all cases, with upward flow at the 650–1000 m bOD depth proposed for the Repository, westwards horizontal flow beneath 1500 m, and westwards downwards flow in the BVG beneath the present coastline.

Our modelling suggests that, for any value of Calder Sandstone conductivity, flow through the Repository is unaffected. Thus the only contribution of this sandstone aquifer to Repository safety is the possible seaward transport and dispersion of any waters + radionuclides migrating upwards from the Repository through the BVG. Flow in the Repository relates directly to BVG conductivity, and the pattern of flow is persistently upwards, through several decade values of BVG conductivity experiments. These flow patterns imply that water from the Repository could eventually reach the surface as springs in the BVG outcrop, or by dispersion within the Calder Sandstone. Hence the proposed Repository position will need to engineer against natural groundwater flow, rather than be assisted by it.

The relationship of water flow to BVG conductivity can be expressed graphically. The results from 8 decades of BVG conductivity fall in a systematic pattern, with all Calder Sandstone conductivity results superimposed (Fig. 5). From this, we can make a simple safety case calculation. We assume that it is unacceptable for water from the Repository, 1000 m bOD, to return to the surface within 10, 000 years. Arithmetically, such a flow rate is 10^{-1} ma^{-1}. Using Fig. 5, this flow rate equates to a regional BVG conductivity of 3×10^{-2} ma^{-1}. If measured BVG conductivities exceed this value, then the hydrogeological safety of a 1000 m Repository must be doubted. Superimposed on Fig. 5 are the BVG conductivities measured by Nirex (1992, 1993a,b) in boreholes at 400–1900 m bOD. It is apparent that measured values are 40 times too large to be simply declared 'safe'. Only one connective fracture is needed to supply a radioactive warm spring to the surface, so that modelling the statistical distribution of fractures is unlikely to give sufficient confidence (Nirex 1993a). Further site investigation work needs to be directed towards establishing the long-term water flow rates in these locally measured fractures, so obtaining a more reliable assessment of regional BVG connectivity. Perhaps the most reliable way of achieving this confidence in engineering terms is to

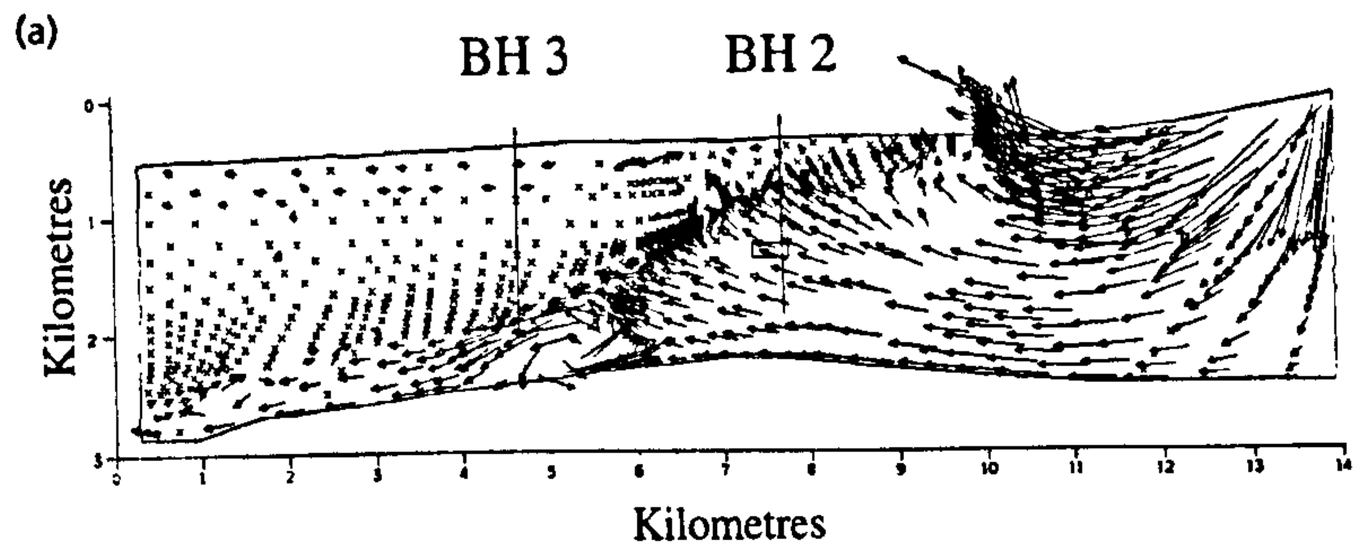

Fig. 3. *(a) Selected modelling experiment, to illustrate patterns of water flow directions. Calder Sandstone low conductivity (3 ma^{-1}), BVG conductivity 1.2 ma^{-1}. Flow through repository 1.1 ma^{-1}. Repository shown at 1000 m, see text for explanation. (b) Selected modelling experiment, to illustrate patterns of water flow directions. Calder Sandstone high conductivity (300 ma^{-1}), BVG conductivity 1.2 ma^{-1}. Flow through repository 1.1 ma^{-1}. Repository shown at 1000 m, see text for explanation.*

use boreholes to undertake *in-situ* flow tests, of many years duration, before any underground excavations are made to disturb the long-term flow pattern. Even so, this will only investigate the present-day conductivities and flows. This in itself gives no guide to the long-term forecasting of flow rates during future climate changes, or tectonically induced changes of conductivity. However, stable isotopic and noble gas data on present-day waters in these B/H (Nirex, 1993a) suggests that some BVG water may have recharged during a glaciation. This raises the possibility that the extra loading, topographical head and fracturing provided by an ice sheet could have induced much more rapid and extensive flows in the recent geological past, and could do so again in the geologically short-term future.

PARTICLE TRACKING

As a visual guide to the degree of physical containment that the BVG and overlying sediments may afford, we have undertaken a suite of particle tracking experiments (Figs 6, 7). We ignore any effects of enhanced flow due to thermal buoyancy of water from a warm Repository, or vertical leakoff of H_2, CH_4 and CO_2 gases generated from the Repository (Chapman, 1994). These particle tracking displays all assume that no chemical interaction of radionuclides with surrounding rock occurs, but simply monitor the progress of 'water particles' released from the Repository at an arbitrary Time = 0 (Garven, 1989). Such water could conceivably be carrying dissolved radionuclides. These particles have the same density and temperature as the surrounding water, so that they are passive indicators of water flow paths and dispersion, and do not have any inherent buoyancy or capillarity effects. These simulations have utilized two values of BVG regional conductivity of 1.2×10^{0} ma^{-1} and 1.2×10^{-2} ma^{-1} (3.8×10^{-8} and 3.8×10^{-10} ms^{-1}). These are about a factor of 10 above and below our own proposed 'safety target'. The upper value of BVG conductivity is the maximum measured value (Nirex, 1993a), the lower conductivity value is identical to the modal regional conductivity interpreted by Nirex (1993a,b) from their measurements and simulations. Fluid flow through porous media, or through fractures, usually moves preferentially along the highest conductivity conduits, rather than uniformly through the whole anisotropic medium. Consequently, our 'average' modelling will tend to underestimate maximum flow rates. All other conditions are as for the experiment illustrated in Fig. 3a. The OILGEN code is run iteratively to achieve these tracking simulations, with a time step of just 3 years for each iteration. This ensures that a tracer particle does not jump between finite element cells. Five hundred tracking particles were 'released' at one time. Particle dispersion along aquifers was set to be 1 m laterally in 10 m forward flow, with 10% of this for transverse flow components.

Figure 6a and b show simulations with a Repository zone at 650 m (Nirex, 1993b; RWMAC 1994). It is apparent (Fig. 6a) that with high measured permeabilities, water from the Repository zone could reach the surface within 10, 000 years. Breakthrough of water from the BVG to overlying

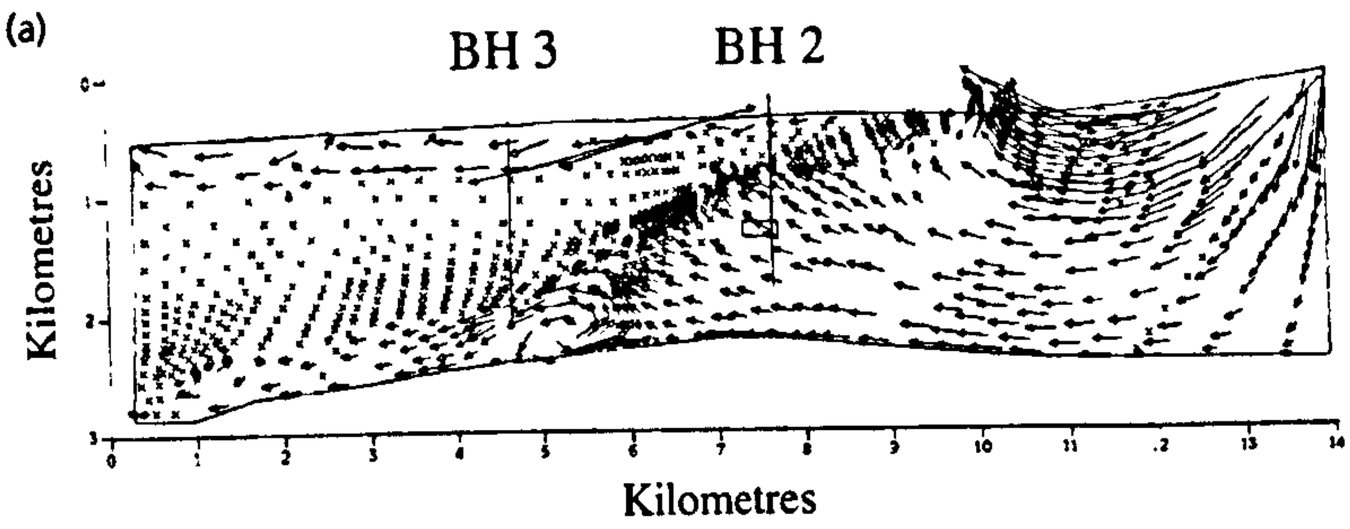

Fig. 4. *(a) Selected modelling experiment, to illustrate patterns of water flow directions. BVG conductivity (1.2 ma^{-1}), Calder Sandstone medium conductivity 30 ma^{-1}. Flow through repository 1.1 ma^{-1}. Repository shown at 1000 m, see text for explanation. (b) Selected modelling experiment, to illustrate patterns of water flow directions. BVG high conductivity (120 ma^{-1}), Calder Sandstone medium conductivity 30 ma^{-1}. Flow through repository 19 ma^{-1}. Repository shown at 1000 m, see text for explanation.*

sediments occurs predominantly via the Fleming Hall fault zone, but also via minor faults to its east. Breakthrough is very sensitive to the existence of such faults which focus flow, but not to their absolute values of conductivity. In Fig. 6b, it is apparent that a lower conductivity for the BVG has resulted in much longer containment of water. Repository water does not even leave the BVG until 50, 000 years after release (not shown), and takes 200, 000 years from its release until reaching the surface, having moved laterally through the St Bees Sandstone aquifer at 400 m depth then into the Calder Sandstone before discharging onto the present-day sea bed. Experiments in Fig. 7a, b investigate the potential benefit of placing the Repository deeper than currently proposed by Nirex, at 1000 m. With the high BVG conductivity, only a slight delay is found in the return of water towards the surface, with an arrival time of 15, 000 years (Fig. 7a), which is not very different to 10, 000 years in Fig. 6a. With the low BVG conductivity (Fig. 7b), flow from the Repository is much better contained, taking 300, 000 years to reach the surface after release. In this case, the water leaves the BVG slightly further west than Fig. 6b, but again flows laterally through the St Bees Sandstone some 400 m below the surface before discharging at the sea bed 4 km west of the experiment shown in Fig. 6b. From these experiments we conclude that both physical containment and discharge paths of water from the Repository are very sensitive to the conductivity of BVG rock surrounding the Repository. With the upper range of measured BVG permeabilities, any overlying sediments provide very little physical barrier or dispersion to flow. Once water from the Repository has entered the Calder Sandstone, dispersion ensures its transport to the surface. Other experiments (not shown) suggest that this is especially so with rapid lateral flows in the Sandstone. Thus the regional BVG conductivity is crucial. It is difficult to measure or estimate regional BVG conductivity in connected fractures with sufficient certainty (Nirex, 1993a). Consequently, at this Repository site, containment of radionuclides would need to be dependent upon the estimated certainty of chemical blocking from engineered barriers, or by chemical retardation from rock-water interaction. Any increase in BVG vertical conductivity either from engineering the Repository, or from gas leakoff from the waste (Chapman, 1994), would have a critically bad effect.

It is particularly instructive to contrast these deterministic results of our particle tracking experiments with the very different results obtained from Nirex's probabilistic modelling (RWMAC, 1994; Fig. 2). The Nirex model suggests that flow of water from the Repository will ascend into the fresh meteoric water in Carboniferous–Triassic sediments, and will then descend westwards into the higher density brines of the Irish Sea 'brine pluton'. Our modelling contradicts this. Different models with different assumptions produce different results, perhaps illustrating a lack of descriptive and predictive confidence.

CONCLUSIONS

1 Modelling experiments show that two decoupled, but connected, aquifer systems exist: in the Calder Sandstone

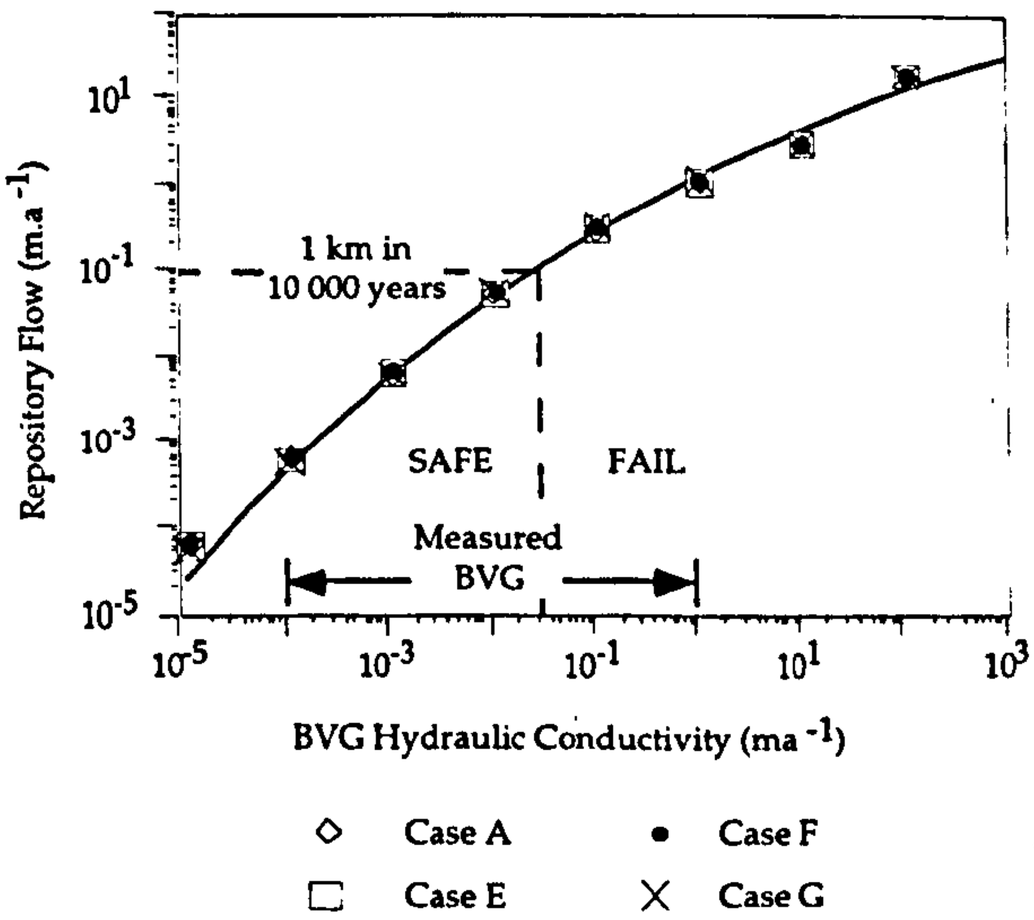

Fig. 5. *(left) Graph of Repository flow against BVG conductivity. This shows the range of values tested in 32 different experiments; the measured range of BVG conductivities was extended by 10^2 upwards and 10^{-1} downwards, to give a greater context for interpretation. Varying the conductivity of the Calder Sandstone has no effect on flow through the Repository, and symbols for 4 different extreme cases (A–G) are superimposed. By contrast, variation in the BVG conductivity produces a very systematic change in modelled water flow through the Repository. A simple safety case has been superimposed, to assume that no water should return to the surface within 10, 000 yr. This would occur if flows were 10^{-1} ma^{-1} or faster (vertical axis). Using this model-derived graph, such flows would result if BVG conductivity was 3×10^{-2} ma^{-1} or greater (1×10^{-9} ms^{-1}). Some 35% of BVG fractures measured in Nirex boreholes at the proposed Repository depth of 650 m exceed this conductivity (Nirex, 1992, 1993a, b). Thus the measured range of fracture conductivities, superimposed on the horizontal axis, mainly fall in the 'Safe' sector, but 35% of fractures fall in the 'Fail' sector, and are up to 40 times too permeable.*

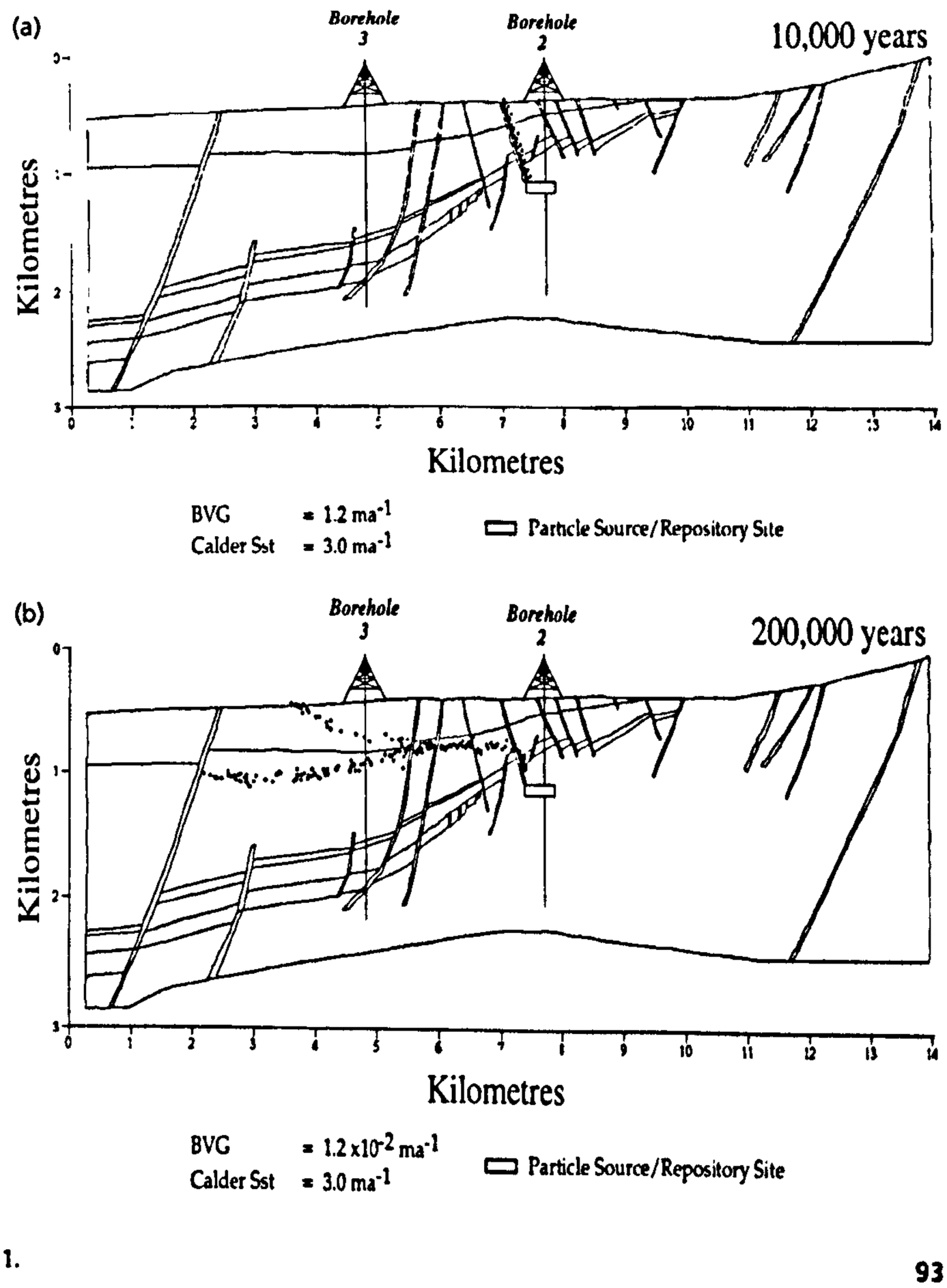

Fig. 6. *(right) (a) Particle tracking diagram showing positions of water tracked from the 650 m deep Repository. BVG conductivity is the maximum measured in site investigation boreholes, 1.2 ma^{-1} (3.8 × 10^{-8} ms^{-1}). The Calder Sandstone set to low conductivity, 3 ma^{-1}. Water from the Repository reaches the surface by 10, 000 yr after release, and 50% of particles released reach the surface by 30, 000 yr. Experiments not shown indicate that increasing the conductivity of the Calder Sandstone to 30 or 300 ma^{-1} reduces the time for particles to reach the surface. (b) Particle tracking diagram showing positions of water tracked from a 650 m Repository. Conditions as for Fig. 6a, but BVG conductivity reduced to 1.2×10^{-2} ma^{-1} (3.8×10^{-10} ms^{-1}). This is the modal value proposed by Nirex (1993a), but some 40% of all BVG measured fractures exceed this (Nirex 1993b, fig. 10a). This produces a marked difference from Fig. 6a, water from the Repository is still within the BVG 50, 000 yr after release, and does not reach the sea bed until 200, 000 yr after release.*

and in the Borrowdale Volcanic Group. Modelled flow rates within the BVG are directly dependent on BVG conductivity. Flow conductivities measured in boreholes are 40 × too great to be acceptable.

2 The proposed repository at 650–1000 m is in a poor position where flow directions in the BVG are towards the surface, and will need to be

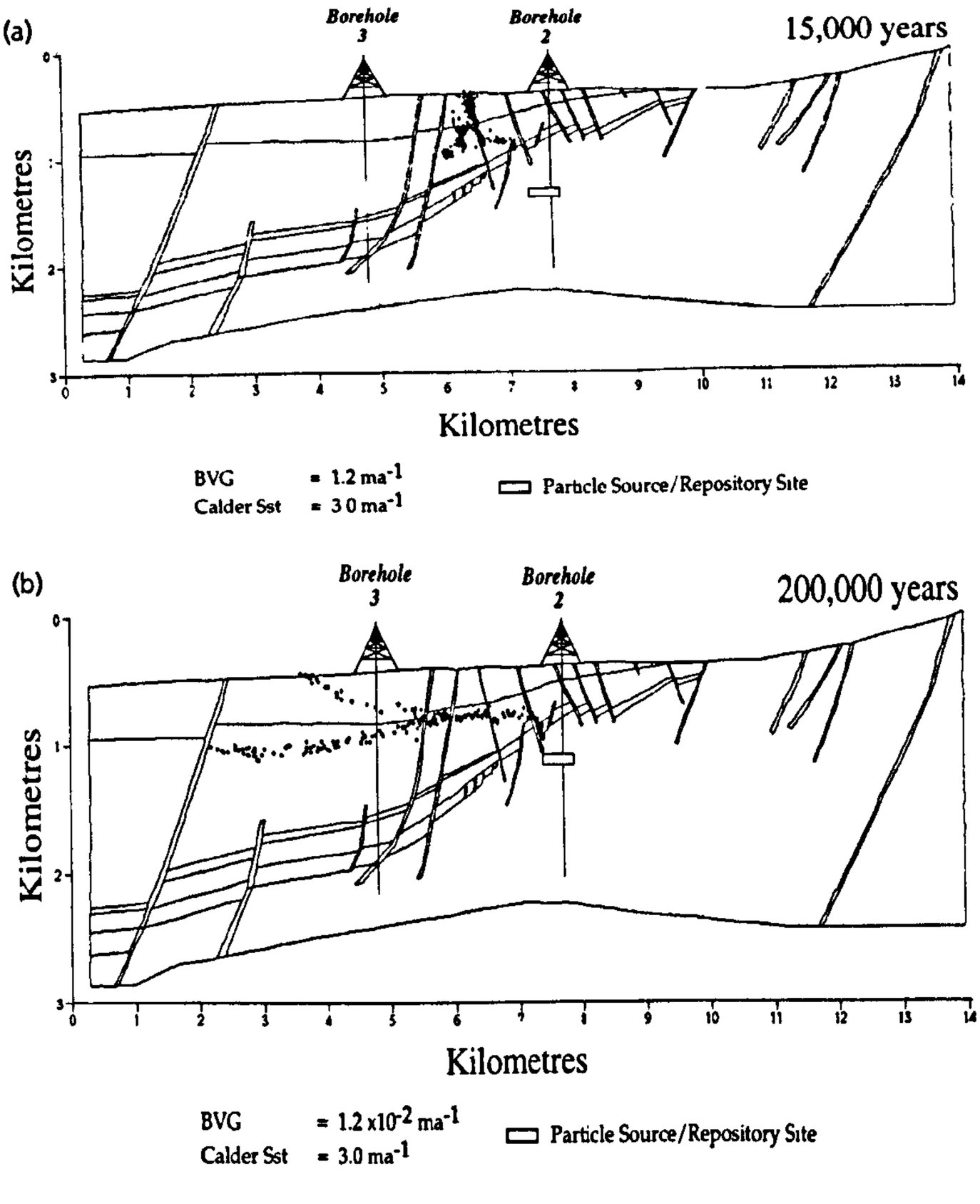

Fig. 7. *(a) Particle tacking diagram showing positions of water tracked from a putative 1000 m Repository. All other conditions as Fig. 6a. Water from the Repository Zone has reached the surface after 15, 000 yr, and 50% of particles released reach the surface by 30, 000 yr. Simply placing the Repository deeper in permeable BVG rock does not help. (b) Particle tracking diagram showing positions of water tracked from a putative 1000 m deep Repository. All other conditions as Fig. 6b, i.e. BVG conductivity 1.2 × 10^{-2} ma^{-1} (3.8 × 10^{-10} ms^{-1}). Results are similar to Fig. 6b. In this case water from the Repository Zone does not reach the surface until about 300, 000 yr after release. Another major difference is that water leaves the BVG slightly further west, again moving horizontally through the St Bees Sandstone some 400 m beneath the surface and up to the sea bed. Thus it is critical to demonstrate that all present and future regional conductivity in the BVG is substantially less than 3 × 10^{-2} ma^{-1} (Fig. 5).*

counteracted. Better sites for a Repository would seek positions where water flow directions are downwards, seawards, or static, such as 2000 m beneath the present coastline. However, engineering costs may be prohibitive.

3 Simulated tracking of water particles released from the Repository zone shows that radionuclides could return to the surface within 10, 000–30, 000 years, if regional conductivity of the BVG was equivalent to its highest measured value of 1.2 ma^{-1}. We assume that no chemical retardation occurs within the engineered Repository, or within the overlying rock.

4 Further site investigation work must establish that *all* BVG fractures have a large-scale regional conductivity *less than* 3 × 10^{-2} ma^{-1}. The most direct way of measuring this is by water flow tests in boreholes, lasting many years, before any excavations are made. Consideration should be given to climatically induced changes in subsurface conductivity and water flow patterns from the past, and in the future.

ACKNOWLEDGEMENTS

C McK. was funded by the Greenpeace Environmental Trust. The OILGEN code was kindly provided to RSH by Grant Garven (Johns Hopkins University). G. Couples provided an improved graphical interface. G. Bowes assisted with re-coding salinity, A Mullis helped modify the graphics output. We thank J. D. Bredehoeft for a helpful review.

REFERENCES

Bredehoeft J.D. and Maini T. (1981) Strategy for radioactive waste disposal in crystalline rocks, *Science*, **213**, 293–296.

Chapman N.A. (1994) The geologists dilemma: predicting the future behaviour of buried radioactive wastes, *Terra Nova*, **6**, 5–19.

Clauser C. (1992) Permeability of crystalline rocks, *Trans. Am. Geophys. Un.*, **73**, 233–238.

ERM (1993) *Summary of Radioactive Waste Disposal Policy and Environmental Issues affecting Cumbria.* Report ITA/9 to Cumbria County Council. Environmental Resources Management, Oxford.

Garven G. (1989) A hydrogeologic model for the formation of the giant oil sands deposits of the Western Canada sedimentary basin, *Am. J. Sci.*, **289**, 105–166.

Garven G. and Freeze R.A. (1984) Theoretical analysis of the role of groundwater flow in the genesis of stratabound ore deposits: 1 mathematical and numerical model, *Am. J. Sci.*, **284**, 1085–1124.

Konikow L.F. and Bredehoeft J.D. (1992) Ground-water models cannot be validated, *Adv. Water Resources*, **15**, 75–83.

Neumann S.P. (1990) Universal scaling of

hydraulic conductivities and dispersivities in geological media. *Water Resour. Res.*, **26**, 1749–1758.

NIREX (1992) *The Geology and Hydrogeology of Sellafield*. Report 263, UK Nirex Ltd, Harwell, UK.

NIREX (1993a) *The Geology and Hydrogeology of the Sellafield area: Interim assessment*. Report 524 (4 vols), UK Nirex Ltd, Harwell, UK.

NIREX (1993b) *Scientific update 1993: Nirex deep water repository project*. Report 525, UK Nirex Ltd, Harwell, UK.

Oreskes N., Shrader-Frechette K. and Belitz K. (1994) Verification, validation and confirmation of numerical models in the earth sciences, *Science*, **263**, 641–646.

Royal Society (1994) *Disposal of Radioactive Wastes in Deep Repositories*. The Royal Society, London, 194 pp.

RWMAC (1994) *Fourteenth Annual Report of the Radioactive Waste Management Advisory Committee*. HMSO, London 60 pp.

Taylor, B.J., Burgess I.C., Land D.H., Mills D.A.C., Smith D.B. and Warren P.T. (1971) *Geology of Northern England*. HMSO, London, 121 pp.

Manuscript received 5 July 1994; revision accepted 23 December 1994

